

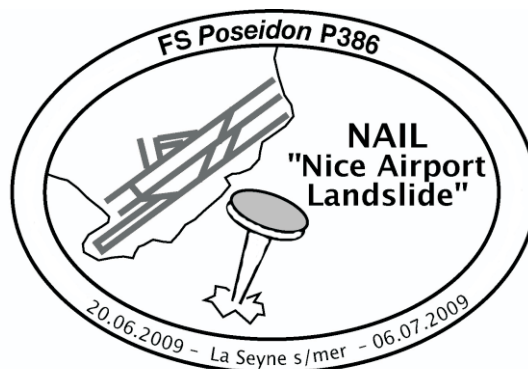
# BERICHTE

aus dem Fachbereich Geowissenschaften  
der Universität Bremen

No. 271

Kopf, A., R. Apprioual, J. Blandin, J.-P. Brulport, P. Crassous, T. Fleischmann,  
A. Förster, G. Guyader, S. Hammerschmidt, P. Henry, R. Jacinto Silva, J. Legrand,  
A. Mayer, S. Pape, P. Pelleau, P. Pichavant, T. Pichler, R. Price, M. Seydel,  
S. Stegmann, K. Weber

**REPORT AND PRELIMINARY RESULTS OF POSEIDON CRUISE P386:  
NAIL (Nice Airport Landslide),  
La Seyne sur Mer, 20.06.2009 – La Seyne sur Mer, 06.07.2009.**



The "Berichte aus dem Fachbereich Geowissenschaften" are produced at irregular intervals by the Department of Geosciences, Bremen University.

They serve for the publication of experimental works, Ph.D.-theses and scientific contributions made by members of the department.

Reports can be ordered from:

Monika Bachur

DFG-Forschungszentrum MARUM

Universität Bremen

Postfach 330 440

**D 28334 BREMEN**

Phone: (49) 421 218-65516

Fax: (49) 421 218-65515

e-mail: MBachur@uni-bremen.de

Citation:

Kopf, A. and cruise participants

Report and preliminary results of R/V POSEIDON Cruise P386: NAIL (Nice Airport Landslide),

La Seyne sur Mer, 20.06.2009 – La Seyne sur Mer, 06.07.2009

Berichte, Fachbereich Geowissenschaften, Universität Bremen, No. 271, 161 pages. Bremen, 2009.

**ISSN 0931-0800**

## Table of Contents

Preface	4
Participants <i>RV Poseidon</i> and participating institutions	5
Group photographs	6
1. Abstract	7
2. Introduction	8
3. Geological background	11
4. Scientific rationale and State-of-the-art	23
5. Logistical approach	32
6. Methods	34
6.1. Long term tests of acoustic modems for subsea observatories	34
6.2. Sediment traps, ADCP and current meters	35
6.3. Shallow water methodology	38
6.3.1. Echosounder	38
6.3.2. Underwater video surveys (ROV, scuba dives)	38
6.3.3. <i>In situ</i> temperature measurements	39
6.3.4. <i>In situ</i> CPT testing	41
6.3.5. Piezometer deployments	43
6.3.6. Gravity coring and sediment description	45
6.3.7. Physical properties	49
6.3.8. Pore water geochemistry	52
6.3.9. <i>In situ</i> Radon measurements	54
7. Preliminary Results	57
7.1. Long term tests of acoustic modems for subsea observatories	57
7.2. Sediment traps, ADCP and current meters in the Var Canyon	60
7.3. Nice Airport landslide	61
7.3.1. Echosounder	61
7.3.2. Underwater video surveys (ROV, scuba dives)	62
7.3.3. <i>In situ</i> temperature measurements	64
7.3.4. <i>In situ</i> CPT testing	65
7.3.5. Piezometer deployments	69
7.3.6. Gravity coring and sediment description	79
7.3.7. Physical properties	86
7.3.8. Pore water geochemistry	88
7.3.9. <i>In situ</i> Radon measurements	97
8. References	101
9. Acknowledgements	109
10. Appendices	110
10.1. Station list	111
10.2. Lithologs and core photographs	127
10.3. MSCL results	CD

## Preface

The expedition P386 *NAIL* (Nice Airport Landslide) aims to shed light on the controls of slope failure and submarine landslide processes at the Ligurian Margin in the proximity of the Nice international airport, southern France. The cruise was a follow-up project of two earlier expeditions in the same area (Kopf et al., 2008; Sultan et al., 2008) and put special focus on deepening the knowledge regarding the causes of the 1979 Nice airport landslide and tsunami, acquire crucial geological data and materials for the recently submitted IODP (Integrated Ocean Drilling Program) drilling proposal 748-full (Stegmann et al., 2009), and test state-of-the-art technology for long-term monitoring and data transmission. The latter is loosely related to the EU real-time network of excellence *ESONET* (European Seafloor Observatory Network).

Among the methods utilised during *Poseidon* Leg P386 were echosounding to complement existing bathymetric charts, *in situ* measurements to characterize the natural state of the potentially metastable slope, seafloor sampling and place long-term instruments to study sedimentological phenomena and further evaluate the performance of acoustic data transmission systems. The regional goals were restricted to a small area south of Nice as well as the adjacent Var Canyon in the Baye des Anges, where mass wasting at various scales is observed. The research during and after cruise P386 serves to test key hypotheses concerning the trigger mechanisms of the mass wasting, which include ground water charging of slope sediments, high excess pore pressures, creep and plastic shear in sensitive clay horizons, vertical loading owing to anthropogenic construction, and regional seismicity.

The majority of the efforts during P386 were dedicated to the failed shallow slope near the Nice airport in water depths between 15 to 50 mbsl (meters below sea level). In addition, the moderately deep Var Canyon was instrumented to quantify the amount of material ending up in this system once sediment gets entrained by the river Var or remobilised from the shallow slope. Finally, one deep-water location further southeast was revisited for the long-term test of acoustic data communication devices.

Logistically, cruise P386 was split into two halves because of the number and size of seagoing equipment (4 moorings, large Borel buoy, 2 long-term piezometers). In addition, a second vessel (*Poseidon III*) operated in the same study area for part of Leg B; it hosted research scuba divers and devices to study groundwater seepage along the slope.



### **Personnel aboard R/V *Poseidon***

1. Kopf, Achim	P386-A, B	MARUM Univ. HB
2. Apprioual, Ronan	P386-B	IFREMER
3. Blandin, Jerome	P386-A	IFREMER
4. Brulport, Jean-Pierre	P386-A	IFREMER
5. Crassous, Philippe	P386-A	IFREMER
6. Fleischmann, T	P386B	MARUM Univ. HB
7. Förster, Annika	P386-A, B	MARUM Univ. HB
8. Guyader, Gerard	P386-A	IFREMER
9. Hammerschmidt, Sebastian	P386-B	Univ. HB
10. Henry, Pierre	P386-A	CEREGE
11. Jacinto Silva, Ricardo	P386-A	IFREMER
12. Legrand, Julien	P386 -A	IFREMER
13. Mayer, Adriano	P386 -B	CEREGE
14. Pape, Silvana	P386 -B	Univ. HB
15. Pelleau, Pascal	P386 -B	IFREMER
16. Pichavant, Pascal	P386 -A, B	IFREMER
17. Pichler, Thomas	P386 -B	Univ. HB
18. Price, Roy	P386 -B	MARUM Univ. HB
19. Seydel, Michael	P386 -B	Univ. HB
20. Stegmann, Sylvie	P386-A, B	IFREMER
21. Weber, Kai	P386-B	MARUM Univ. HB

### **Participating institutions**

DFG-Research Centre MARUM  
University Bremen  
Leobener Strasse  
28359 Bremen --- GERMANY

University of Bremen  
Klagenfurter Strasse  
28359 Bremen --- GERMANY

IFREMER  
B.P. 70  
29280 Plouzané --- FRANCE

CEREGE  
B.P. 80  
13545 Aix-en-Provence --- FRANCE

## Group photographs



**Leg A science party (L-R):** Stegmann, S., Kopf, A., Blandin, J., Crassous, P., Jacinto Silva, R., Förster, A., Pichavant, P., Guyader, G., Henry, P., Legrand, J., Brulport, J.-P.



**Leg A science party (L-R):** Hammerschmidt, S., Fleischmann, T., Pape, S., Pichavant, P., Pelleau, P., Förster, A., Weber, K., Stegmann, S., Kopf, A., Mayer, A., Apprioual, R.



***Poseidon III* science party (L-R):** Seydel, M., Price, R., Pichler, T.

## Abstract

Cruise P386 “NAIL” with R/V *Poseidon* studied the western Ligurian Margin off Southern France, and area in the northeastern part of the western Mediterranean Sea characterized by its active tectonism and frequent mass wasting. The region near the Var estuary close to the city of Nice is particularly suited for landslide research because it represents a natural laboratory where it is possible to study a series of trigger processes of geological and anthropogenic origin. The aim of this MARUM expedition was to:

- i. Study the Nice airport landslide and adjacent stable slope in 15-50 m water depth;
- ii. Deploy a number of mooring stations to study sedimentological processes in the deeper slope (200-1500 m water depth) in the Var Canyon; and
- iii. Set up a long-term seafloor unit and adjacent buoy to test the performance of data communication systems for marine applications such as observatories.

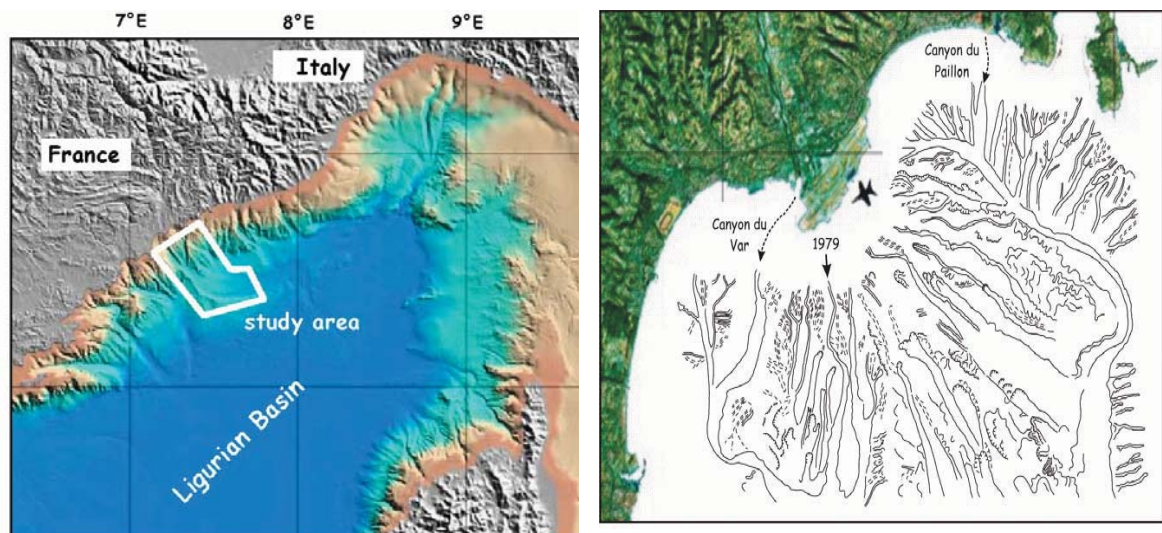
Accordingly, the wealth of initial results include the successful deployment of several moorings as well as the communication system with the buoy. Data will be retrieved once the instruments get recovered in early 2010, so no scientific conclusions can be drawn from these portions of the cruise. In contrast, a large number of results is already available from the sampling and measurements south of the airport of Nice. From the gravity cores taken in or adjacent to the headwall of the landslide, the majority showed extremely freshened pore water composition (usually in 0.6 – 3.4 m depths) related to groundwater charging at deep levels. Although ROV surveying in this area showed pockmark-type seafloor roughness, bottom water sampling by research scuba divers failed to attest freshened water at the seafloor. Cores further showed evidence for catastrophic emplacement of sediment packages which were tentatively related to the 1979 slide/tsunami event. In several cores, steep normal faults with mm-displacement further support active deformation in the recent past. Results from 65 cone penetration tests (CPT) showed variable penetration depth (max. 3.5 m sub-seafloor) and oftentimes excess pore pressure increase during the 30-60 mins. “dissipation” period.

In addition to the above, gravity coring as well as CPT testing was undertaken at all 9 positions proposed for mission-specific drilling (IODP proposal 748-full). Also, 11 cores were taken but left unsplit because of the necessity for post-cruise geotechnical testing. Those cores originate both from the Nice Airport landslide and its vicinity, but also from the deeper landslide complexes sampled in 2007 during cruise M73/1.



## 2. Introduction

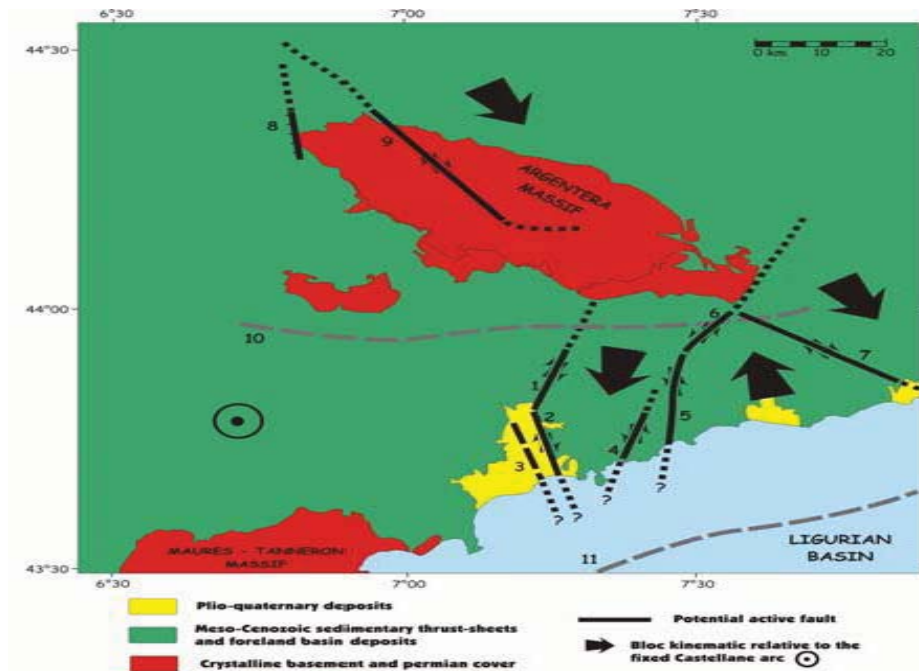
Based on the fact that 60% of the Earth's population live within the frontal 50 km of the coast, considerable scientific and economic efforts are undertaken to shed light on the processes shaping ocean margins. One of the most prominent of these phenomena are submarine landslides, which often coincide with earthquake activity and other geohazards. Given the highly dynamic setting and complexity of collision zones in the Mediterranean Sea, many processes are still poorly understood. Among the shortcomings in understanding collision zones, the temporal variation of deep-seated processes as well as their manifestations at shallower levels is an emerging key question. As a consequence, scientific research has to focus on long-term measurements of key physical parameters that drive landsliding. In Europe, the EIU Network of Excellence *ESONET* has identified a total of 203 data end-users in 11 countries with a wide-spread need for data monitoring of the solid earth beneath the sea, the interface between the solid earth and sea, and the water column. The University of Bremen (Germany) and IFREMER Brest (France) have joined forces on a multi-disciplinary level to work at the Ligurian Margin within *ESONET* and the Integrated Ocean Drilling Program (IODP).



**Fig. 1:** (a) Bathymetric map of the Ligurian Sea and surrounding land masses; (b) Structural/geomorphic map of the study area at the Var estuary and canyon.

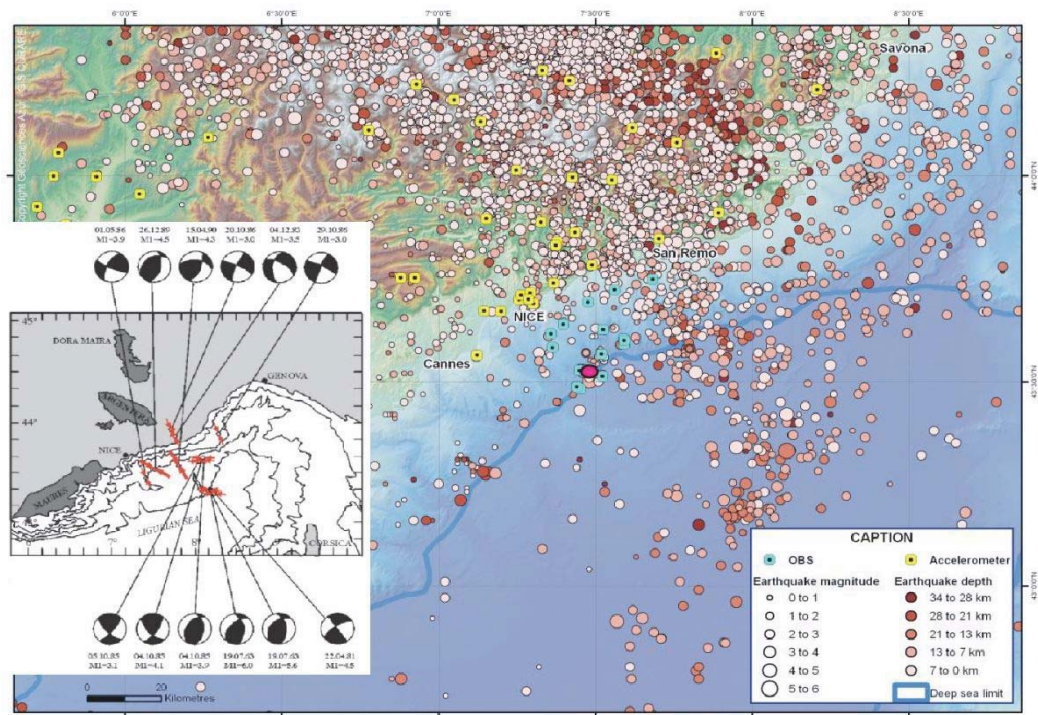
Several programmes and national as well as international initiatives dedicated considerable parts of their efforts towards submarine landslides. The ‘The Deep-Sea Frontier’ initiative (<http://ec.europa.eu/research/environment/pdf/deepseefrontier.pdf>), as well as its successor program DS<sup>3</sup>F (‘Deep Sea & Sub-Sea-floor Frontiers’; cf. Kopf, 2009)

by the EC have dedicated work packages concerning geohazards. Also, the IUGS-UNESCO IGCP511 project “Submarine Mass Movements and their Consequences” enters its 5<sup>th</sup> year with annual meetings and either books or special issues of journals resulting from the conferences (e.g. Solheim, 2006; Lykousis et al., 2007; Mosher et al., 2009). One of those meetings, held as an ESF Magellan workshop in Barcelona (<http://www.geohazards.no/IGCP511/>; Camerlenghi et al., 2007), was co-sponsored by ECORD and set the spotlight on scientific ocean drilling. The proposal *MEDSLIDES* (Camerlenghi et al.; initially a pre-proposal to IODP in 2007, followed by a full proposal in 2008) was a major outcome here and spans the Eastern and Western Mediterranean including the Israel continental slope, Nile deep-sea fan, Gela Basin, Ebro Margin, Eivissa channel, and the Herodotus, Ionian and Balearic abyssal plains. In addition an IODP-sponsored workshop on Geohazard drilling followed in Portland, Oregon in 2007 (see <http://www.nsfmargins.org/Publications/Newsletters/Newsletter.html>). A year later, another ESF Magellan workshop on “Drilling seismic hazards in European Geosystems” was held in Luleå, Sweden (Ask et al., 2008). Among other things, an APL concerning mass wasting events in the forearc to the Nankai Trough subduction system, Japan (proposal #738-APL; Strasser et al., 2008) and a mission-specific drilling proposal at the Nice slope (proposal #748-full; Stegmann et al., 2009) resulted as a direct consequence of that workshop.



**Fig. 2:** Tectonic map of the area showing major faults and direction of movement. See text and cross section in Figure 4.

In general, the understanding of the temporal variations in geohazards is essential for many geoscientific research disciplines as well as mankind as a whole. Especially early warning networks for EQs and tsunamis have further become a major societal interest. The Ligurian margin is well suited for such a project because of its proximity, well known morphological and tectonic setting (Figs. 1-2), regional seismicity and landsliding (Figs. 3-4), and the wealth of existing data in the region. Cruise P386 aimed to broaden the data base in the area and install a number of long-term moorings to collect time series data offshore southern France.



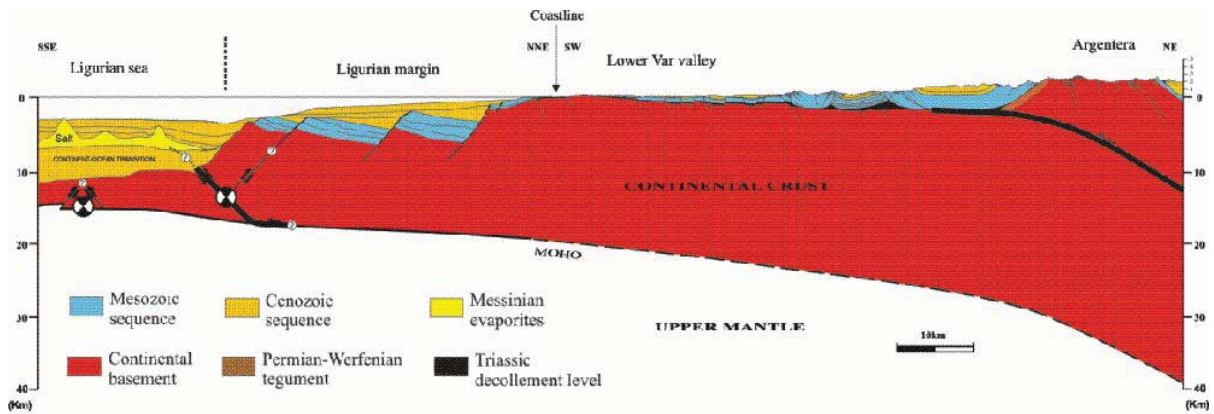
**Fig. 3:** History of seismic events in distribution in the southern Alps and Ligurian Sea, and focal mechanisms of  $M_w > 3$  earthquakes on the Ligurian Margin between 1960-2001 (from Henry et al., 2005, proposal 685-full).



### 3. Geological background

#### *General Overview*

The geological setting in the Ligurian Basin is that of a tectonically active and unstable margin. Much of the morphology on- and offshore as well as the main tectonic lineaments, their direction of movement and seismicity is illustrated in map view (Figs. 1-3) and SW-NE cross section (Fig. 4). Most of the sediment is received from the erosion of the Alps in the north (Fig. 1; see Mulder et al., 1998). Tectonic deformation rates are small, however, a background seismic activity is present, with the largest earthquakes occurring offshore (M~6 in 1887, and M 6.3 in 1963; see also Fig. 3). This activity may be explained by compression on the rim of the Alpine belt, which is now collapsing at least in the French-Italian part (Fig. 4). However, the active offshore fault network, consisting of both compressional and extensional structures, is incompletely understood (see Migeon et al., 2006).



**Fig. 4:** Schematic cross section through the study area in SW-NE direction. Earthquakes are most abundant on the deep-seated crustal faults in the SW.

The Ligurian margin has a very narrow (or absent) continental shelf of ~2-3km width and a steep continental slope with a mean gradient of ca. 11° (Cochonat et al., 1993). The margin is fed with material from several small mountain-supplied rivers (Var, Paillon and Roya rivers) that experience semi-annual violent flash floods owing to snowmelt and convective rainfall (spring and fall). During floods, suspended sediment concentration can reach tens of kg/m<sup>3</sup>, resulting in hyperpycnal flows (Mulder et al., 1998). High and episodic sediment supply at the mouth of these rivers, cause deposition of thick under-consolidated deposits of variable grain size on the upper slope. In the Var canyon, the most relevant of the three river systems mentioned above, three types of seafloor failures are observed: (1) superficial slumping, which occurs in area of low slope angles in the upper slope, (2) Canyon-wall

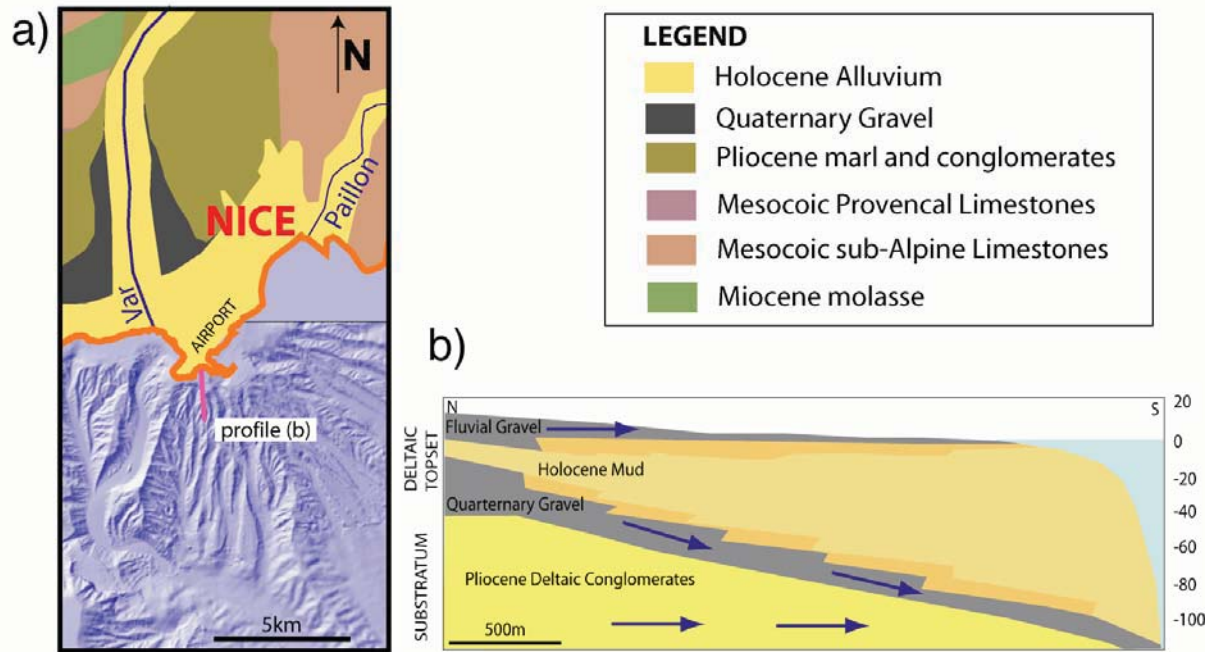
gullyng by undercutting currents and debris flows at the canyon wall, and (3) deep-seated failures characterised by pronounced headwalls at higher slope gradients and often unknown flow paths of the slid material (Klaucke and Cochonat, 1999; Klaucke et al., 2000). Adjacent to the Var estuary failures initiate on the upper slope, at less than 200 m of water depth, with scarps typically being approximately 100 m wide and mobilized volumes are less than 0,07 km<sup>3</sup> (Migeon et al., 2006). Failure may either be catastrophic, or a successive strain accumulation from creeping via folding, slumping to mass wasting and deposition of debrites, turbidites, and landslide bodies.

### *The Nice Slope*

The very narrow or absent continental margin off Nice (Fig. 5a), situated in the Baie des Anges and bounded by the prominent Cap d'Antibes Ridge (W) and Cap Ferrat Ridge (E), is characterized by a very steep slope characterized by deep erosion and canyoning with maximum slope angles of 27° along the side-walls of the canyons (Pautot 1981). The Var and Paillon canyons represent the most important erosive features, which are both linked to the fluvial systems, the latter being a negligible contributor of terrigenous supply at present (Klaucke et al., 2000). During the Messinian salinity crises, the Var paleo-canyon was shaped and filled during the Early Pliocene transgression and prograded in the Mid-Pliocene as a steep delta to the slope break, which corresponds to the modern coastline (Clauzon et al. 1990). Quaternary sedimentary sequences of the Var river mouth show a tripartite stack of facies (Dubar & Anthony 1995). The oldest Quaternary deposits are made of clast-supported gravel with a matrix of sand, silt and clay (Fig. 5b). A thick wedge of Holocene fine-grained, shallow-marine and estuarine-deltaic sediments interbedded with river flood-plain paludal sediments is related to the postglacial marine transgression, whereas an upper fluvial channel gravel prograded a Gilbert-type fan delta recently. From a hydro-geological point of view these sedimentary sequences act as an aquifer system with pathways for conductive flow of meltwater or rainwater in the delta (see below). In the Var delta system, highly permeable strata (Pliocene substratum, Quaternary sandy gravel; see Fig. 5b) is confined by low-permeability muds (Anthony & Julian, 1997). Following their model the aquifer layer drains seaward at various levels down to a water depth of ~140m (Fig. 5b). Geochemical analyses in the upstream part of the Var (Guglielmi & Mudry, 1996), offshore in the water column overlying the Nice Slope (Guglielmi & Prieur, 1997), and piezometric measurements in the Nice slope sediment (Sultan et al. 2008) support the aquifer model and demonstrate a direct relationship between high discharge (flood) events (about 200 m<sup>3</sup>/s),



flow through the alluvial aquifer (Guglielmi & Mudry, 1996) and the occurrence of fresh water discharge into the sea (Guglielmi & Prieur, 1997). Regarding the superficial sediments of the uppermost Nice continental slope, major portions are unstable due to the underconsolidated state of the sediment owing to rapid deposition (Klaucke & Cochonat, 1999). This material has also been imaged during recent geophysical surveys (see Fig. 7 and Stegmann et al., 2009).



**Fig. 5:** Geology of the Nice area on-shore and the Nice slope off-shore compiled from previous workers (modified after Dubar & Anthony 1995 and Anthony & Julian 1997). (a) Map illustrating the different lithologies related to the evolution of the Var delta from the Pliocene to present; (b) schematic cross-section through the Var delta deposits in N-S-direction south of the Nice airport (see [a] for location).

### *The 1979 Nice Airport catastrophe*

The abovementioned Nice Airport Landslide (*NAIL*, also the namesake of cruise P386) occurred on October 16<sup>th</sup>, 1979 on the Var prodelta of the Nice Slope (Figs. 5a, 6a). The *NAIL* area is surrounded by smooth, but narrow shelf with water depth ranging between 0m and 15m at the headwall. An embankment of the extended airport construction collapsed into the sea (Fig. 6a) and generated a tsunami wave of 2-3 m (Gennessieux et al., 1980). Based on bathymetry data the volume of failed material was estimated  $\sim 8.7 \times 10^6 \text{ m}^3$  (Assier-Rzadkiewicz et al., 2000), which was mobilized and transformed into a debris flow cutting two submarine cables tens of kilometres away from the sliding area (Hugot, 2000). The path of the failed mass is clearly expressed on the upper slope by a 4.5 km-long gully with depths between 25m and 40m (see Fig. 6a, arrows; Mulder et al. 1998). The airport was damaged (Fig. 6b), the tsunami affected the nearby village of Antibes (Fig. 6c), and the

former embankment was transported to more than 1000 m depth into the Var canyon (Fig. 6d).



**Fig. 6:** Location and transport pathway of the Nice Airport Landslide (NAIL) on Oct 16, 1979.

(a) The trace and velocity of the mobilised material running down the Nice Slope southward into the Var Canyon, and then redirected towards the West and then South again (data from Dan, 2007). Panels (b) and (c) are newspaper clipping from the Nice Matin the day after the event, illustrating the damage to the airport, here inspected by airport police (b) and the effect the tsunami had in the village of Antibes (c). In the course of detailed mapping of the seafloor in 1986, ROV dives discovered blocks having originated from the fill used for the failed harbor construction that got transported to the deeper part of the slope (d). Positions for panels b through d is given in Fig. (a).

Shortly after the accident, a detailed investigation of the bathymetry was started (Pautot, 1981) and several studies aimed to characterize the trigger mechanism(s). Reduction of sedimentary strength due to an earthquake can be excluded for this event, as no anomalous seismic signal was recorded. The MIP (MIP, 1981) proposed retrogressive failure, which initiated at the slope and then retrogressively reached the NAIL area. On the other hand, the tsunami wave following the slide lowered the sea level by  $\sim 2.5\text{m}$ , which resulted in static liquefaction of the overloaded slope (e.g. Seed, 1988). Both scenarios were tested by numerical modelling and the retrogressive failure mechanism was excluded as this kind of failure could not have provided the energy to generate the observed tsunami wave (Assier-Rzadkiewicz et al. 2000). Slope stability assessment under static conditions demonstrated a Factor of Safety (FS)  $> 1.$ , which in case of sealevel lowering of  $2.5\text{m}$  decreases, but remains

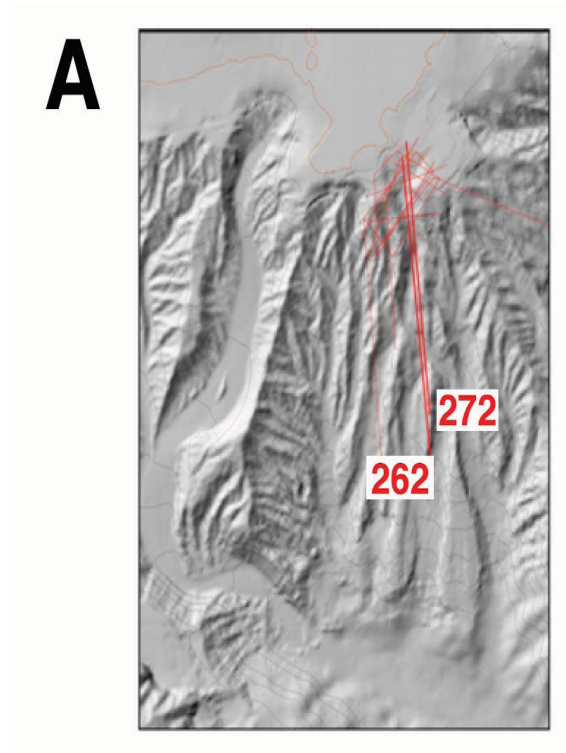
>1 (Sultan et al., 2001). Unfortunately, the landfill operations preceding the airport extension, where 11 million tons of material at water depth of 25m and distances of up to 300m offshore had been additionally put on the slope six month prior to the failure (see details in De la Tullaye, 1989), were not considered in the study. Furthermore, the effect of overpressuring was disregarded, although the landslide occurred after several days of heavy rain (25cm in 4 days). Given that both the extra loading and episodic rainfall events (see <http://www.hydro.cea.fr>) remain crucial factors destabilizing the present-day slope, they were into consideration during recent studies (see Kopf et al., 2008; Sultan et al., 2008; Stegmann et al., 2009, below).

### ***Previous work by participant group/institutions***

Over the previous decade, the working groups at IFREMER Brest, CEREGE and MARUM Bremen contributed tremendously to the understanding of landslide processes in general (e.g. Sultan et al., 2004, 2007, 2008; Stegmann et al., 2007; Kopf et al., 2006, 2007, 2008, 2009), and the Ligurian Margin in particular. At the Nice slope, the most fundamental data set on is a hydrological model and set of questions and hypotheses is based upon is a grid of high-resolution MCS data with good penetration (>150 mbsf) acquired during M73/1 cruise in 2007 (see Fig. 7; and Kopf et al., 2008 for methodology and specifications). An example profile crossing the NAIL scar in N-S-direction is shown in Figure 7b to illustrate the overall geological situation and main lithological units.

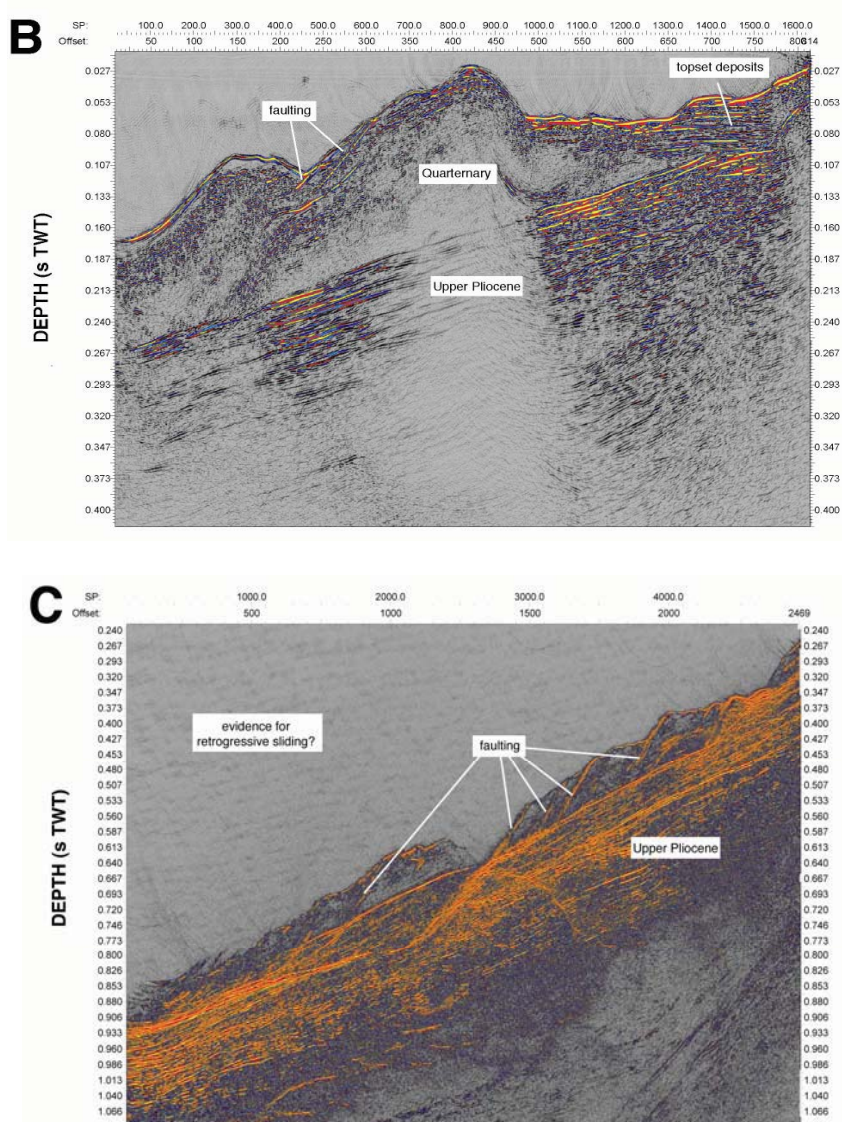
The typical lithological succession on the Nice continental slope consists of three main units: **(a)** Along some profiles, lenses or homogeneous carpets of seismically transparent, ~10 m-thick “mobile layers” are found (Unit A). These have been identified earlier (Dan, 2007) and may represent modern spill-over deposits from snowmelt floods, recently mobilized material with a higher mobility (debris flow type or fluidized units). **(b)** Below the transparent series, parallel layered Quaternary deposits of variable thickness (a few m to ~50 m, Unit B) are probably Var delta sediments with various facies (clay, silt, sand and even gravel layers with components exceeding 10 cm in diameter; see cross-section in Fig. 5b). On the Nice shelf, those deposits are perfectly horizontal and in places show discordant contact to the inclined sand package. Closer to the shelf edge, prograding and aggrading delta deposits (i.e. topset to foreset beds) show tilting of the layers towards the Ligurian basin, possibly indicating deposition during a sealevel rise. Presumably, some of the uppermost layers may represent floodplain deposits, because the Var river mouth migrated westward over time (Sage, 1976). Inside the NAIL scar as well as in some locations down-

slope, the Holocene units lacks coherent internal layering and is hence difficult to interpret. While the surface topography may suggest displacement of some of these sequences (potentially from mass movement and sliding), other incoherent units lie topographically exposed and cannot result from downslope transport. **(c)** A S-dipping, well-stratified coherent package (Unit C) of sand/gravel or otherwise reflective, competent lithology, with its upper ~80 meters showing higher amplitude reflections (Fig. 7b). Its surface and contact to the overburden is predominantly smooth (in particular towards the deeper basin), but rough in places close to the coast. Nearshore, the top of the unit is interpreted as a former land surface during sea level low-stand. When compared to earlier work, this succession is presumably Upper Pliocene in age (see Savoye et al., 1993, their Fig. 12) and typically contains puddingstones, marls, sand and gravel (Guglielmi & Mudry, 1996). In a second seismic profile, the cascading normal faults in the mid-slope suggest that portions of the slope may have indeed been mobilised in a retrogressive manner (Fig. 7c).



**Fig. 7:** (a) map with track chart offshore Nice from expedition M73/1 (Kopf et al., 2008), including N-S trending MCS lines 262 (b) and 272 (c) through the study area. Please note topset strata in line 262 (right) and possible evidence for retrogressive failure in line 272.

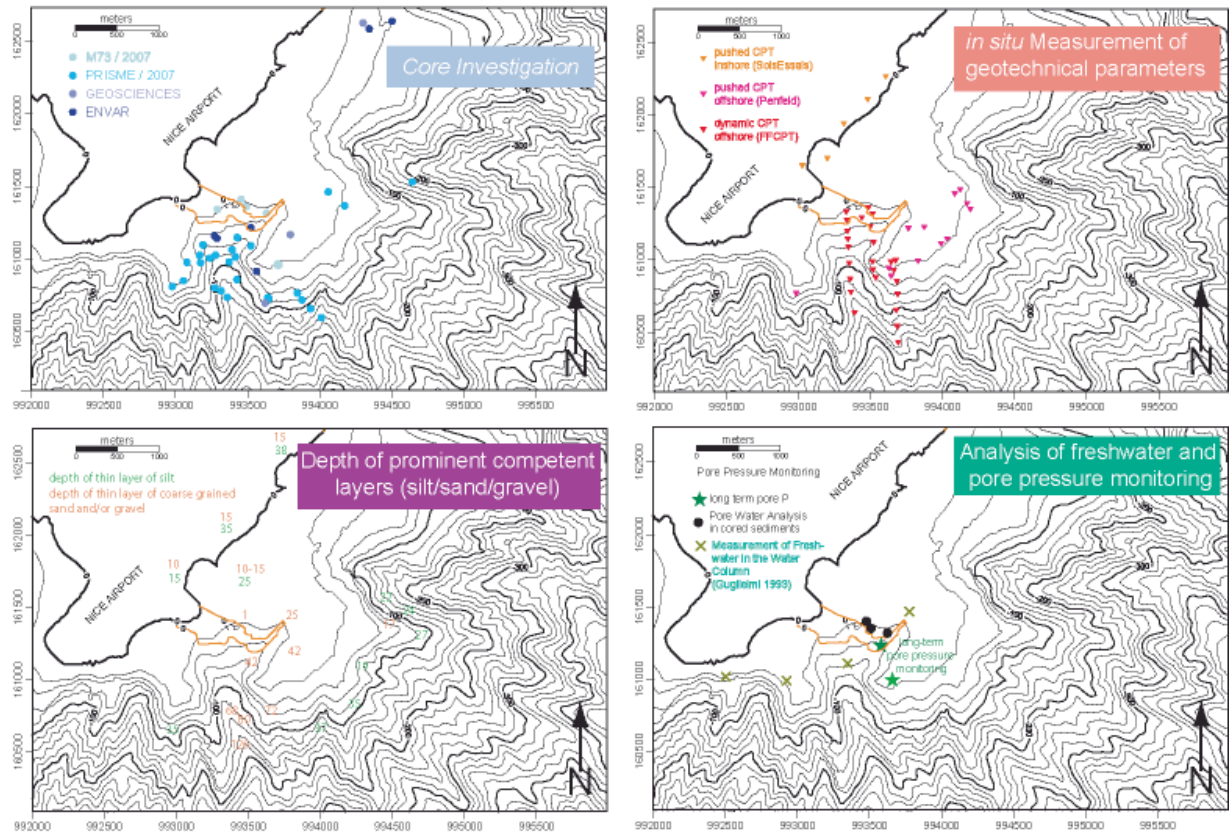




**Fig. 7 continued.**

In order to overcome limited penetration by gravity coring, pushed CPT profiling gathered *in situ* information on the strength of the sediments down to a penetration depth of 28m (Sultan et al., 2008). Those tests were carried out during PRISME cruise with R/V *L'Atalante* (fall 2007) using the Penfeld penetrometer (Meunier et al., 2004). The experiments focused on the stable western part of the Nice Slope. Based on 35 gravity cores (Fig. 8a) and 37 CPT profiles (12 pushed / 25 free fall) (Fig. 8b), which can also be used to define the profiled sediments lithologically by soil types (e.g. Ramsey, 2002), significant sandy/silty layers were correlated successfully with commercial onshore CPT tests by SolsEssaies that were carried out shortly after the 1979 catastrophe. The coarser grained thin layers (cm scale) are deposited in the upper part of the slope in ~20mbsf and ~40mbsf (Fig. 8c). The *in situ* information also attests that (i) prominent sand/gravel layers are found in the Quaternary succession (Fig. 8c), (ii) developing shear zones in the Holocene foreset series,

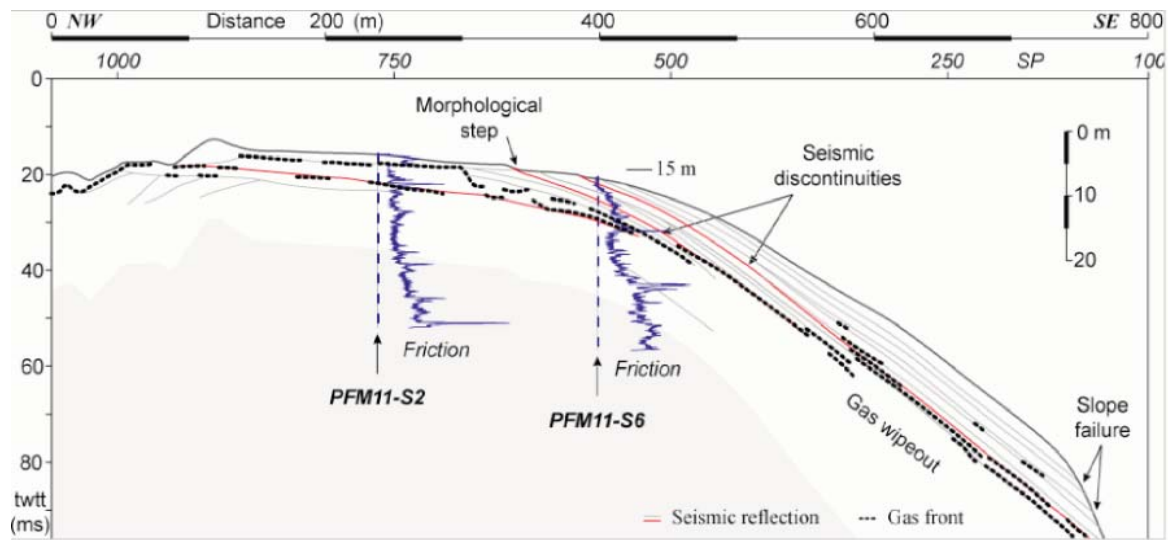
as evidenced by low cone resistance and decreasing p-wave velocity when running the sonic CPT mode (see Fig. 9; Sultan et al., in press), and (iii) a sharp increase in cone resistance for 2 of the onshore tests that reached up to 60 m subbottom depth (Fig. 8c). This latter discontinuity is found in ca. 35-40 m depth, which corresponds to about the extrapolated top level of the Pliocene package (unit a; see above).



**Fig. 8:** Compilation of data collected in the NAIL area during several previous expeditions, showing locations of a) gravity cores, b) *in situ* measurements of sedimentary strength and pore pressure with different CPT devices, c) depth information of prominent silt, sand and gravel layers from coring and CPT testing, and d) locations of freshwater occurrence in the sediments or in the overlying water body (the latter from Guglielmi & Priour 1997).

Based on a finite element model relying on geotechnical and sedimentological data, Dan et al. 2007 postulated a combination of trigger mechanisms including (i) the creeping of the sensitive clay layer, (ii) the point load of the construction and, (iii) the circulation of fresh water in the permeable sandy layers. Furthermore, their calculation attested the metastable state of the Nice Slope before and after the construction work. The “sensitive layer” hypothesis is supported by the good correlation between the maximum thickness of the sliding mass (max. 38 m) and the depth of the sensitive clay. Furthermore, the progressive failure scenario according to the creeping process agrees well with the observations mentioned in the official report (cracks, settlements, failures, collapses) following

landfilling operations (Seed et al., 1988). Due to the presence of these sensitive, mechanically weak clay layers, failure of the Nice Slope could have occurred regardless of the additional load posed upon the slope by the construction (Savoye et al., 2005; Dan et al., 2007). These zones exhibit a significant loss of strength between 3 and 9 mbsf during CPT profiling in the non-failed area (Sultan et al., in press). Following Leroueil et al. (2001) these zones can be defined as shear zones often associated with progressive failure (Thakur et al., 2006).



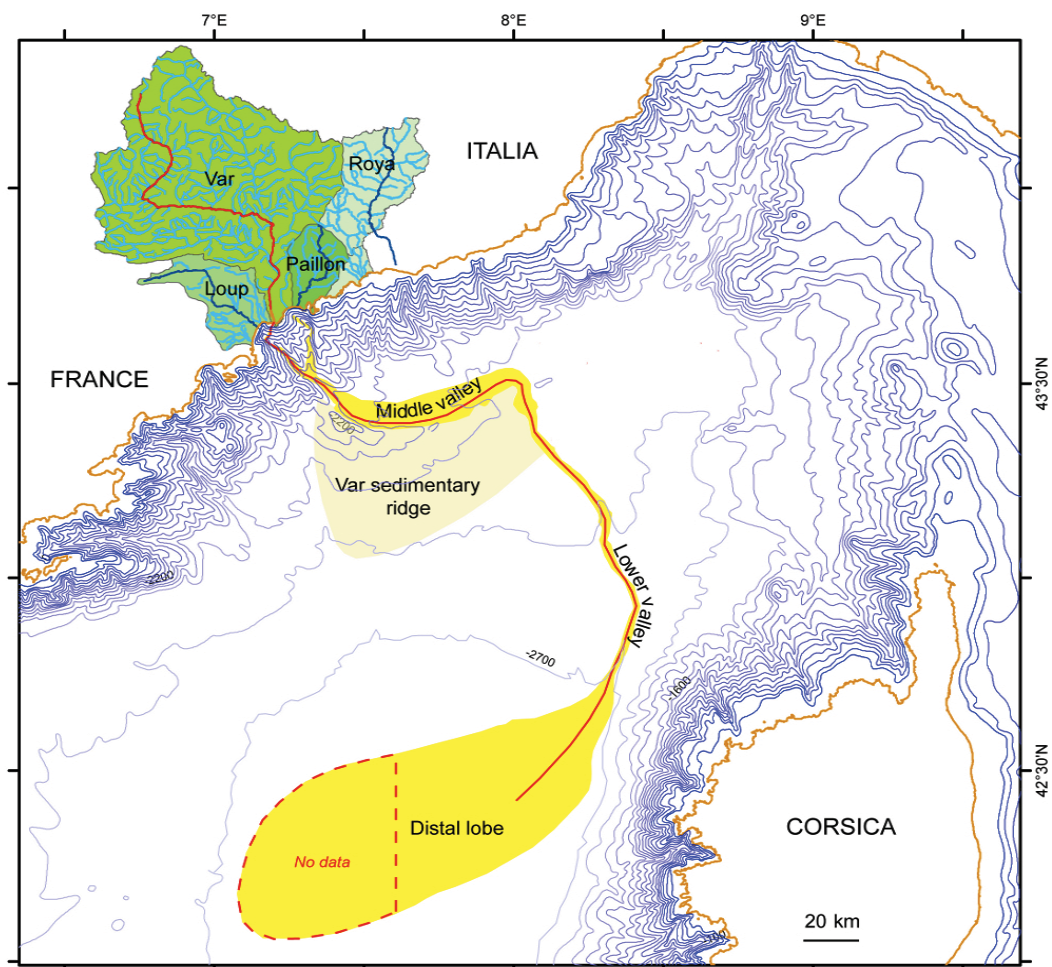
**Fig. 9:** Results from two Penfeld CPT deployments in the area immediately east of the NAIL scar. Data show low p-wave velocities (not shown here) and low frictional resistance in the slope apron where clay minerals are abundant and minor amounts of gas are also suspected (from Sultan et al., in press).

Another crucial factor that episodically saps the stability of the Nice Slope is the hydrological regime in this area. For instance, the 1979 landslide occurred after a period of exceptionally heavy rainfall and river discharge (see above). Submarine freshwater sources are known to occur along the Ligurian coast (see Gugliemi, 1993; Guglielmi & Prieur, 1997; see above), which can affect the stability of the slope by lowering the effective strength of clays. Geochemical analyses on pore water extracted from coarse-grained, permeable layers in gravity cores attest the occurrence of fresh water in several locations within the NAIL scar (see Fig. 8d, and Kopf et al., 2009). Furthermore, a long-term piezometer installed in the NAIL scar recorded an increase in pore pressure linked to the amount of precipitation. Mid-term CPTU deployments in the same area have equally attested ambient overpressures up to 8 kPa, which in the location of deployment is very close to the overburden stress (Kopf et al., 2008).



### *Sedimentary processes in the Var canyon*

Apart from landslide-related processes, the fate of material being mobilised in the shallow part of the Nice slope, the Var delta, or areas further upstream is of increasing interest. In general, canyon-turbidite systems collect, by a series of single, energetic and catastrophic events, a significant amount of the continental erosion products. Much of the material that accumulates at the shelf break or on the upper continental slope is in an instable situation and likely to move down the slope. Such movements impact on the slope and the deep-sea environments, determine the depositional architecture and evolution of deep-sea sedimentary systems. One of the distinctive feature of these turbiditic systems is the concentration and channelling of the terrigenous bed load from the mouth of large rivers (or the edges of platforms) to the abyssal plain. Processes involved in sediment transfers appear to be very efficient for particle grain size segregation and are a way to create huge sand accumulations in the deep-sea, providing in that way high quality reservoirs of high interest for the oil industry as it is moving deep offshore. These processes are also a major source of geohazards and damage for infrastructures lying on the sea floor and on coastal areas.



**Fig. 10:** The Var canyon-turbidite system from source to sink.



The sedimentary system of the Var is placed on an unusual passive margin, presenting a very narrow continental slope (2 to 3 km) and a steep continental slope that was reshaped during the Messinian crisis. The PlioQuaternary Var turbidite system has been supplied by 3 main canyons: the Var, the Paillon and Roya (Fig. 10). The canyons are active in both lowstand and highstand periods, with the preserved canyon activity during the present highstand period being a major research focus. The Var watershed is supposed to be the main sediment source of its fan (2830 km<sup>2</sup>, highly mountainous). The Var river connects with the Var canyon head. The turbiditic activity in the canyon is hence controlled by the seasonal cycle of the river.

The mean flow of the Var river, at its mouth, is estimated to be around 53 m<sup>3</sup>.s<sup>-1</sup>. Nevertheless the river regime is characterised by sudden floods surpassing 10 folds the mean runoff. The sediment discharge related to the Var river is not well estimated. Present days estimation indicates a total annual sediment discharge of 1,63.10<sup>6</sup> tons/yr; extreme values being twice this estimation. There is significant evidence that during floods hyperpycnal flows occur at the head of the Var canyon. This regular and controlled activity is the main reason the Var turbiditic system may be considered as a natural laboratory for the study of turbidity currents.

Along the slope, the Var canyon presents a regular U shape during 25 km long. Its width increases from 300 m at the head to 1 km at its transition to the upper valley. Its depth presents a longitudinal variation as well. From 130 m depth at the head its incision reach 370 m further down the slope. The increase of the canyon transverse section correlates to the decreasing of its mean slope from 16 % to 3,3 %. Several terraces bordering the canyon present fine sediment deposits whereas the canyon is characterized by gravels and coarse sand. After its canyon, the Var system develops a long valley, 155 km long from canyon's confluence to the distal lobe at the base of the Corsican marge. The Upper Valley is 5 km long. Its width is comprised between 1,7 to 4,8 km and its slope varies from 3,3% to 3% at 2000 m water depth. The Middle Valley presents a long eastward turn of 50 km to 2500 m water depth where it turns again southwards. Its very wide channel (15 to 5 km) is bordered by a high and continuous right-hand levee, called the Var Sedimentary Ridge, above which turbiditic events regularly overspill. The left-hand levee is very low and discontinuous. At the end of the Middle Valley the slope has decreased to 0,4%. The 100 km long Lower Valley is characterized by a long, straight and shallow (20 to 30 m deep) by-pass channel and discontinuous flat levees. Its slope decreases to a very low value of 0,2% by 2700 m water depth at the location of the distal halocene lobe of 80 km long and 40 km wide.

The simplified morphology of the Var system and its present days activity constitutes an optimum to study and model turbidity currents. The direct connection to the Var river, the Canyon and the associated terraces, the overspilling ridge and the extent of its lower valley present singular features to constrain and be approached by numerical modelling.

#### **4. Scientific rationale and State-of-the-art**

(A. Kopf, P. Henry, S. Stegmann, J. Blandin, R. Silva Jacinto)

##### ***Overview***

The stability of marine sediment at ocean margins is a function of the intrinsic strength of the material and forces counteracting this strength (e.g. Hampton & Lee, 1996). When broken down to the particle scale, the strength is controlled by the friction coefficient for the individual mineral particles at a given confining stress, minus the pore pressure that is compensating for some of the external stress. This relationship, known as the effective stress (Terzaghi, 1946), is a crucial aspect in slope stability since pore pressures may equal the overburden stress, exceed lithostatic values, and hence cause liquefaction (in coarse-grained sediment) or softening (in fine-grained material) by destroying the particle network (e.g. Maltman, 1994; Moore et al., 1995). Both non-destructive soft sediment deformation (creeping, slumping, liquefaction), as well as brittle failure (faulting, hydrofracture), are important processes in mass wasting along continental slopes.

The inherent mechanisms and factors governing slope stability and submarine landslides are known because of extensive research carried out by academia and industry (e.g. Hampton et al., 1996; Locat 2001; Locat & Lee, 2002; Mienert, 2004; Lee, 2009), however, the temporal and spatial variability of landslide processes remain poorly understood. In general, submarine landslides occur in areas of weakness, often posed by the presence of weak mineral phases such as clay minerals, or by excess fluid that enhances pore pressure. Spatially, slides are a global phenomenon occurring in fjords, river deltas and fan-canyon systems, open continental slopes and volcanic flanks (e.g. Huehnerbach & Masson 2004). Temporally, they are influenced by the sedimentology of depocenters as well as variations in seafloor pressure and temperature, seismicity and volcanic activity, or groundwater flow conditions (Lee, 2009). Although the abovementioned processes are broadly understood, the exact trigger mechanisms of only a few given submarine landslides are known with certainty (Mienert et al. 2003; Sultan et al. 2004). For the majority of slides, multiple triggers are usually considered, with pore pressure being the favourite, but ineluctably unsatisfactory explanation because of an uncompromising lack of evidence (see below).

Submarine landslides range greatly in their size, from small, frequently occurring failures in active environments such as coastal zones and canyons, to failures that involve hundreds of km<sup>3</sup> of sediment but occur much more infrequently. In either case, they represent a major geohazard for offshore infrastructure (platforms, pipelines, cables and submarine

installations; e.g. Vaunat & Leroueil, 2002; Longva et al., 2003; Sultan et al., 2004) and, if tsunamigenic, to coastal structures and populations, both locally and in the far-field (Tappin et al., 2001). Slope failure is generally controlled by long-term governing factors and short-term triggers (Leroueil et al., 2001; Locat 2001; Sultan et al., 2004). The first include topographic effects such as slope gradient, the geodynamic evolution of the margin (sedimentary or tectonic loading, unroofing, erosion, etc.) or other effects (glacial loading/unloading, marine transgression/regression, etc.; Lee, 2009). The second group of trigger mechanisms acts at a much shorter time-scale and usually causes a significant change in stress state. Among the processes most crucial to slope stability are (i) seismic loading (i.e. earthquakes), (ii) storm wave loading, (iii) rapid sedimentation (in deltas, through mass wasting, etc.), (iv) gas hydrate dissociation, (v) deep-seated fluid generation, upward-migration and seepage, (vi) oversteepening, (vii) cyclic loading by tides, (viii) gas charging, and (ix) groundwater charging (see Locat and Lee, 2002 for details on many of those points). Despite the variety of processes in this list, one overarching aspect is the transient change in pore pressure that is the primary or indirect result of all of them. One of the key goals in landslide research is hence to establish the relationship between the pre-conditioning factors governing the area and the short-term triggers causing the slope to fail.

There are regions on Earth where wide stretches of ocean margins provide evidence for mass flows at many scales and a wide range of water depths (e.g. Maslin et al., 2004; Lee, 2009). Within Europe, the Mediterranean Sea represents such a region. Mass wasting has been reported from many of the large estuaries and delta systems in both the Eastern and Western Mediterranean (e.g. Ebro (e.g. Urgeles et al., 2006), Rhone, Var (e.g. Dan et al., 2007), and Nile fans, to name just a few), the seismogenic Algerian (e.g. Dan et al., 2009) or Ligurian margin (e.g. Klaucke & Cochonat, 1999), the Mediterranean Ridge and Cretan margin (e.g. Chronis et al., 2000), the Florence Rise, Anaximander mountains, Cyprean and Hellenic Arcs, or slopes of islands forming the Aegean volcanic arc. With approximately 46000 km of coastline, 160 Million along it (plus an additional 135 Million tourists each year, i.e., 30% of the global tourism), landslides pose a considerable risk. The French Riviera, northern Ligurian basin, seems particularly vulnerable because it is one of the areas with the highest population density (e.g. Marseille, Toulon, Cannes, Nice, Monte Carlo) and clearly with the largest economical vulnerability (i.e. insured capital). From these cities, Nice is the 5<sup>th</sup> largest city in France and the 2<sup>nd</sup> busiest international airport in France with a potential of 13 million passengers each year (Anthony, 2007).

When returning to tectonically active, hazard-prone zones like the Ligurian Margin, the key issue remains whether brittle failure in a formation or slip on an existing fault is triggered by fluid pressure transients, or solely by the mineralogy of the fault gouge (see competing hypotheses by e.g., Byerlee, 1978, 1990 vs. Rice, 1992). A considerable amount of work has been done in recent years to solve this problem (Logan & Rauenzahn, 1987; Saffer et al., 2001; Kopf & Brown, 2003), attesting that the pore pressure may be of similar importance as the friction coefficient of the gouge material itself. As a consequence, one of the central research goals into the behaviour and evolution of sediment failure is to separate the effects of intrinsic frictional properties and fluid pressure variations. For research expedition P386, the main aim is to clearly distinguish between those effects by

- **Cone Penetrating Testing (CPT)** where pore pressure and sediment strength are obtained,
- Measuring mid-term fluid pressure background and transients related to seismic events (in collaboration with IFREMER Brest, France, using mid- to long-term piezoprobes), and
- Doing selected laboratory tests on sediment gravity cores to measure the mechanical response to static and dynamic loads.

### ***In situ geotechnical testing***

Cone Penetration Tests are a widely used method for *in situ* sediment characterisation in onshore and offshore settings, both in science and industry (e.g., Lunne et al., 1997). With the autonomous, modular free-fall probes (hereafter as FF-CPT) developed in Bremen, a straightforward cost- and time-effective way was found to measure sediment resistance and pore pressure response to insertion into soft sediments. Measurements are carried out pogo-style, and after retrieval of the data disk, pore pressure evolution and sediment stiffness (measured as frictional resistance of the tip and a mantle sleeve; see Fig. 11a) as well as temperature are immediately available. In addition to the direct observations, other parameters can be rapidly estimated from the CPT data.

The maximum insertion pressure produced at the probe tip can be used to estimate the undrained shear strength of the sediment ( $C_u$ ). For typical deep sea sediments, Esrig et al. (1977) suggest the relation:  $C_u = U_{\text{imax}}/6$ , where  $U_{\text{imax}}$  is the maximum insertion pressure. The decay of excess pore pressure produced by the insertion is governed by the consolidation process around the probe and can be modeled as radial consolidation. Bennett et al. (1985) predict the coefficient of horizontal consolidation ( $C_h$ ) from the time taken for

50% of  $U_{\text{imax}}$  to dissipate, and  $C_h$  can then be used to determine the permeability  $k$ . In places where coring and Penfeld deployments are too time-consuming, pogo-style CPT measurements will not only provide first-hand *in situ* results, but with secondary parameters to estimate slope stability and hazard potential. In order to make use of the above *in situ* data in hazard mitigation, longer-term observations become a necessity. Temporal records of pore pressure changes have been demonstrated to correlate with regional tectonic stresses and seismic activity in a number of places (e.g. the Juan de Fuca Ridge; Becker & Davis, 2003; see also next chapter). For this reason, the previously used piezometer v1 as well as a refined design, the piezometer v2 (Fig. 11b), were to be deployed during cruise P386 for time series recordings of pore pressure and temperature in the Nice Airport slide scar and adjacent slope. This joint work by MARUM Bremen and IFREMER Brest represents the continuation of two successful cruises beforehand in the same area: R/V *Meteor* cruise LIMA-LAMO in July/August 2007 (Kopf et al., 2008) and R/V *L'Atalante* cruise PRISME in Oct./Nov. 2007 (Sultan et al., 2008).



**Fig. 11:** (a) MARUM CPT lance; (b) IFREMER piezometer v2; (c) MARUM dynamic triaxial apparatus; (d) MARUM ring shear apparatus.

### ***Long-term pore pressure monitoring***

Pore pressure is known not only for its prevalent role in faulting and other geodynamic processes (e.g. Rice, 1992), but also as a powerful proxy for strain (see Bredehoeft, 1967; Davis et al., 2004). So far, the routine procedure in ODP/IODP has been the deployment of tapered downhole probes (e.g. the DVTPP) during drilling, which have been used in a wide range of geological settings at shallow-moderate depths to obtain measurements of *in situ* pore pressure (e.g. Moore et al., 2001; Morris et al., 2003; Flemings et al., 2008). However, the interpretation of the probe measurements is often problematic, because of limited time



available for the induced pressure spike caused by probe insertion to dissipate. Another key element in ODP/IODP are pore pressure measurements in CORK long-term observatories (Circulation Obviation Retrofit Kit; cf. Davis & Becker [2001]) juxtaposing a cased borehole, which is hydraulically separated from the overlying water body. In the past, direct measurements of pore pressure have provided powerful constraints on regional scale flow models; for example, two CORK measurements at the Barbados margin (Foucher et al., 1997; Becker et al., 1997) within a few km of the trench provide tight bounds on the permeability of matrix and fault rocks in the outer wedge (Bekins & Screaton, 2007). In subduction zones, ambient pore pressure information (Davis et al., 2006) has been correlated with that inferred from laboratory consolidation tests on core samples collected during drilling (e.g. Karig, 1993; Morgan & Ask, 2004), and porosities obtained from shipboard index properties (e.g. Screaton et al., 2002) and inferred from seismic velocity (e.g. Cochrane et al., 1996; Hayward et al., 2003).

Using pore pressure signals as a proxy for seismic strain has been neatly demonstrated at the Juan de Fuca Ridge flank as well as the Nankai Trough accretionary complex (Davis et al., 2001; 2006). In the first case, a M 4.6 earthquake on the western flank of the Juan de Fuca Ridge caused a discrete pore pressure spike in three adjacent boreholes. The signal reached <0.2 kPa above background value some 70 km away from the epicenter, but up to 3.2 kPa excess pore pressure in 10-20 km distance at Site 1025 (for details, see Davis et al., 2001). Similarly, a series of low-frequency earthquakes were recorded in a CORKed hole (Site 808) in 2003, causing a 140 kPa pressure anomaly in some formations within the >900 m of instrumented hole through the frontal accretionary complex (Davis et al., 2006). Even seafloor seismometers and fluxmeters have been successfully used to suggest a relationship between seepage and seismic events in the vicinity (i.e., in the Costa Rica forearc, Brown et al., 2005). Along a similar line of methodology, IFREMER piezometers have been successfully recording pore pressure variations related to changes in charged aquifers in the Nice Airport Landslide scar for periods exceeding one year, with the excess signals reaching 15 kPa (Sultan et al., 2008).

### ***Geotechnical laboratory experiments***

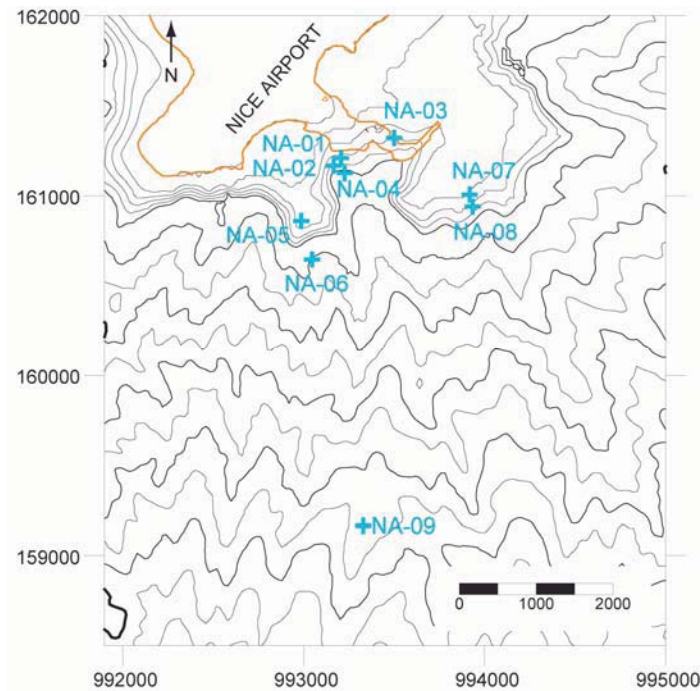
A growing body of geotechnical laboratory work attests that frictional stability may be more important than the absolute shear strength of a material in controlling failure and sliding/faulting (see review by Scholz, 1998). Frictional stability is a function of the change in friction coefficient ( $\mu$ ) at a given effective stress, which is primarily rate dependent.

While high-porosity rocks show velocity strengthening (i.e.  $\mu$  increases with increasing shear rate, e.g. during slip), low-porosity rocks weaken. In general, EQs are believed to nucleate in unstable materials, so that the replacement of clays in "weak" shear zones by precipitation (carbonate, zeolites, quartz) or mineral transformation processes would result in either unstable stick slip or conditionally stable behaviour (Moore & Saffer, 2001). Similarly, mechanically weak constituents such as sensitive clay minerals are believed to provide the failure plane for landslides and other hazardous mass wasting processes.

To ground-truth both our *in situ* data (see previous two paragraphs) and the geophysical information of the seafloor and shallow subbottom, designated soil mechanical laboratory experiments are part of the overall study P386 (see Ch. 6, *Methods* below). These include standard soil mechanical procedures to obtain the sediments index properties (wet and dry density, porosity), grain size distribution, liquid and plastic limits, and permeability and shear strength at various confining stresses and rates. Simple tests are conducted on board (vane shear apparatus, falling cone penetrometer) while more sophisticated ones will be carried out shore-based (e.g. dynamic triaxial tests [Fig. 11c] or ring shear tests [Fig. 11d]). Especially the latter suite of parameters provides a profound measure on slope stability on the seafloor, on how stable a given sediment may deform under certain conditions (namely at depth), and whether permeability allows for the build-up of significant pore pressures.

In addition, a number of locations from an earlier as well as a recently proposed IODP drilling expedition were proposed to be visited during P386 (Fig. 12). The main objective of this endeavour is to collect data for ground-truthing of some of the hypothesis put forward in the proposal (i.e. mechanical stability, pore water chemistry).





**Fig. 12:** Bathymetric chart of the NAIL area including the nine proposed locations for IODP mission-specific drilling (proposal 748-full; Stegmann et al., 2009).

### *Technological refinements for long-term measurements*

Among the various types of sub-sea observatories, non-cabled infrastructures are worth considering given the following features that make them attractive in numerous scientific areas and situations:

- Their price is approximately 1 to 2 orders of magnitude less than cabled infrastructures, making them affordable to multidisciplinary teams of relatively modest size.
- They can be successively implemented at different sites within their lifetime, each time allowing the acquisition of long time series, without being necessarily left in place for more than 20 years.

They also represent a very useful way of investigating a site before making the decision of whether or not a heavier (and generally more pricy) cabled infrastructure is worth developing and deploying. However, the application field of non-cabled infrastructures is limited by the modest amount of data they can transmit. ADCPs, seismometers, echosounders, still and video cameras are among the sensors that are not impossible but still difficult to implement on non cabled observatories, when near real time communication of data is required.

Within the last ten years in Europe, several research institutions have implemented acoustic modems for observatory applications, often in close relationship with their manufacturer,

but the results were sometimes disappointing in terms of achieved data rates and reliability. From those separate experiences, it is difficult to point out which manufacturer/model is the most suitable for long term observatories. In other respects, recent progresses in digital signal processing can make hope that data rates of several thousands of bits per second are achievable for vertical links on a routine base. Those data rates are displayed by most manufacturers, but it is impossible to discriminate actual performances from commercial arguments without a series of in-depth tests.

The objective of the deployment during cruise P386 was to evaluate and select the most appropriate acoustic modems on the world market for fixed, long term observatory applications. This task was broken down into three steps:

- 2007: Paper selection of 5 modems on the world market, the primary selection criterion being the quantity of energy necessary to transmit one bit at a given distance.
- 2008: Short term transmission tests aboard R/V *L'Europe* (Commodac cruise), between a sea-bed station (MAP2) at 2200 mbsl (meters below sea level) and the ship. Among the five manufacturers selected at step 1, only three were fully ready for the integration deadline before the cruise.
- 2009-2010: Long term tests of the models ranked 1 and 2 at step 2, between the MAP2 seabed station at 2200 mwd and a surface buoy (Borel). The deployment of MAP2 and Borel was scheduled for the P386 cruise, and recovery is planned for early 2010 with R/V *L'Europe* (see below).

The testing principles are described in more detail in the Methods section of this report (Chapter 6.1).

### ***Long-term data on sediment dynamics***

Direct observation of turbidity currents were seldom obtained, and time series data are even less common. The Var system is probably the only system world-wide where regular observations (appx. every 2 years) have been made in order to observe, quantify and characterise turbidity events. The observations have been carried out by the means of moorings where different devices are installed. Data obtained with “classical” moorings concern turbidity (not calibrated), pressure, temperature, punctual current meters and sediment traps. This type of moorings have shown to be efficient to observe turbidity currents but not efficient enough to quantify and characterize them. At the same time, this moorings are intrusive and hence subject to the action of the turbidity currents. Entrainment

by currents may displace the moorings or at least affect their stability and the accuracy of the measurements obtained.

The main purpose of the ongoing study is to test and improve new tools for the direct observation and quantification of turbiditic events along the Var canyon. For this purpose, the “classical” IFREMER moorings were improved by the integration of an ADCP current meter able to record the vertical structure of the currents up to several tens of meters and hence its values near the canyon bed where the current magnitude is supposed to be the highest. Other systems include mounted 75 kHz ADCP current meters 300 m above the canyon's talweg to shed light on the vertical structure and hence the thickness of the turbiditic events.

The various instruments deployed along the pathway of the Var canyon is described in some detail in Chapter 6.2 (see below).

## 5. Logistical approach

(A. Kopf)

Given the number and size of instruments to be deployed during expedition *Poseidon* P386, we split the shiptime into two stretches.

Leg A was mostly dedicated to the long-term deployments in the Var Canyon area and the mooring and corresponding sealevel buoy further SE (see Ch. 6.1 and 6.2 below). Given that deck operations involving to move/lift/deploy heavy gear are restricted to daylight hours, we operated the CPT lance, Rn counter as well as the lightweight ROV during the remainder of the time. Given that the majority of the instruments got deployed during the first couple of days (e.g. Borel buoy, MAP2 station, Anitra, Ibsen and Peer Gynt instruments including a number of anchor weights), Leg A spanned only from June 20-26, 2009 before returning to the mid-cruise port call. For most of the time, we operated R/V *Poseidon* very close to Nice shore (Fig. 13).



**Fig. 13:** R/V *Poseidon* in front of the Promenade des Anglais, Nice.

For Leg B, we then loaded two piezometer probes of  $>6$  m length as well as a seafloor unit (Seamonice) for communication with one piezometer. The second leg went from June 26 – July 6, 2009. It was mostly dedicated to gravity coring, CPT and piezometer deployments, and Rn measurements. Since the deployment of the piezometer v1 plus Seamonice unit

required a scuba diver, we arranged for a second vessel aside of R/V *Poseidon* to optimise operations.

Three research scuba divers joined expedition P386 for the period June 27-30. They were based onshore and came out to the NAIL study area with the rented platform *Poseidon III* during the day (Fig. 14). During that period, *Poseidon III* also hosted the Rn counter and a scientist accompanying the measurements. Vice versa, the divers were picked up by the dinghy of R/V *Poseidon* regularly for scientific discussion and handing over rhizon samples taken from the shallowmost sub-seafloor.



**Fig. 14:** Diving vessel *Poseidon III* operating in front of NiceAirport.

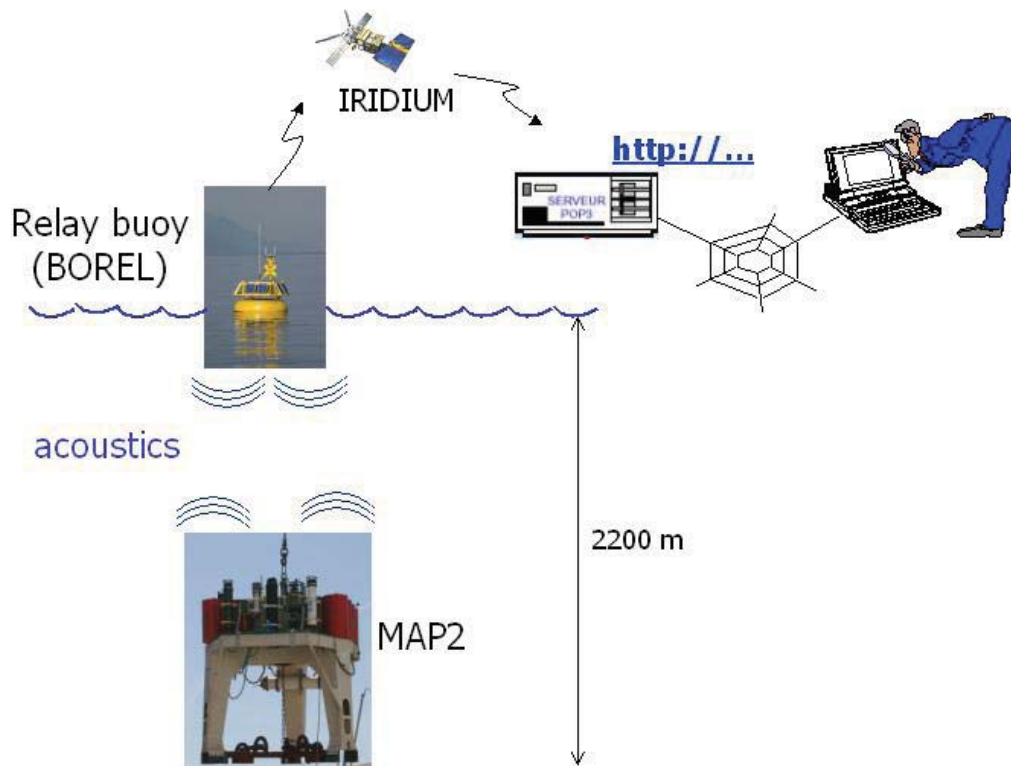
## 6. Methods

### 6.1. Long term tests of acoustic modems for subsea observatories

(J. Blandin, J.-P. Brulport, P. Crassous, G. Gruyader, J. Legrand, P. Pichavant)

The two manufacturers selected for these tests are Evologics GmbH (Berlin) and Sercel UAD (Brest). The modems under test are mounted between the top of a seabed station (MAP2), deployed at a water depth of 2200 m, and the keel of a surface buoy (Borel) moored within acoustic range of MAP2 (see schematic layout in Fig. 15). On MAP2, an electronic unit (Costof) sequences periodic emissions of data files of various sizes, alternatively through each modem under test. The energy quantity consumed on MAP2 for each transmission is measured and transmitted to the buoy. The buoy sends the result of the transmission (number of errors if any, consumed energy) to shore via the Iridium satellite system. The functioning parameters of both the surface and seabottom modems can be modified at any moment from shore if necessary. The buoy periodically performs local measurements (atmospheric pressure, wind speed, X, Y inclination) that are logged on shore and can be correlated with the acoustic data transmission results.

The scheduled duration of these tests is seven months.



**Fig. 15:** Sketch showing the long term testing principle using the Borel buoy.



## 6.2. Sediment traps, ADCP and current meters

(R. Jacinto Silva, J. Legrand, P. Pichavant, J. Blandin, G. Gruyader)

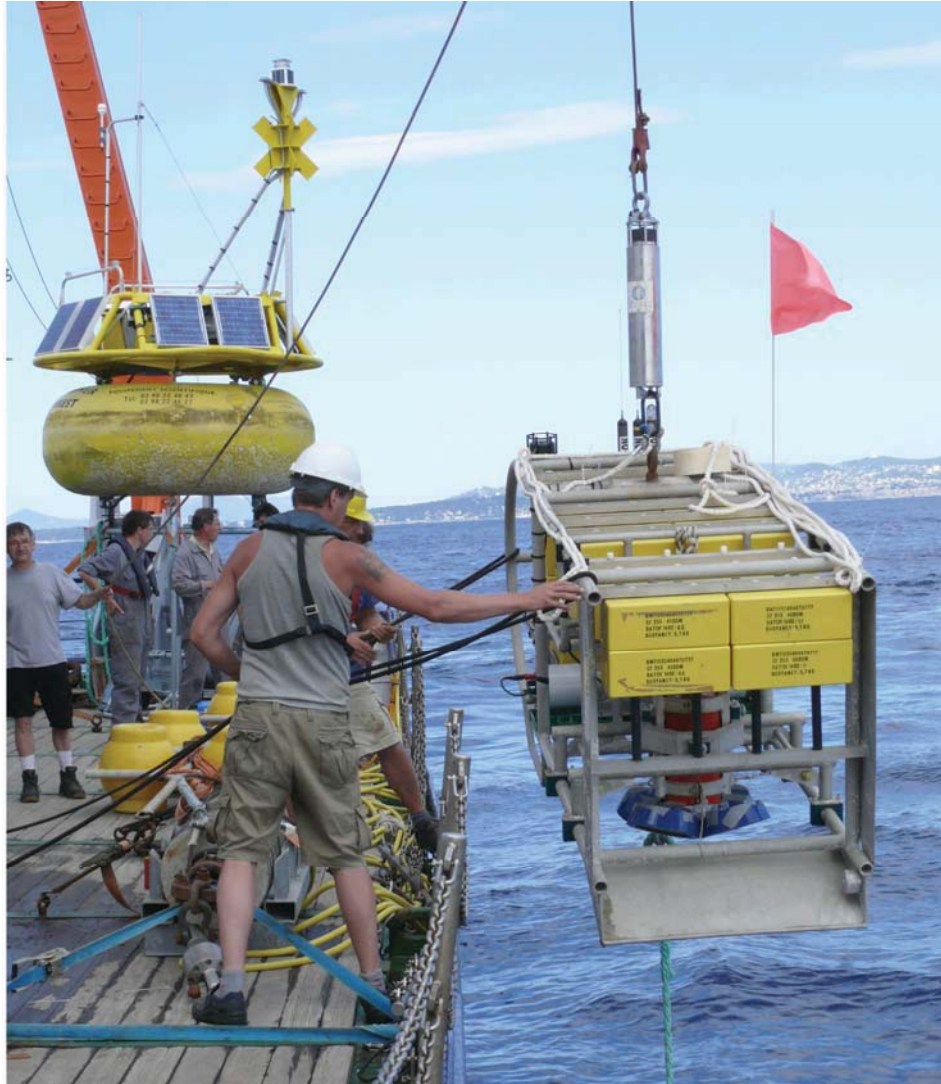
The main purpose of the on-going study is to test and improve new tools for the direct observation and quantification of turbiditic events along the Var canyon. For this purpose, the “classical” moorings (termed “Peer Gynt”; see Fig. 16) were improved by the integration of an ADCP current meter able to record the vertical structure of the currents and hence its values near the canyon bed where the current magnitude is supposed to be the highest. This reference current meter is placed 25 m above the talweg and should provide directional information of the currents.



**Fig. 16:** Photograph of part of the Peer Gynt mooring prior to deployment.

Complementary to Peer Gynt, a new non-intrusive mooring system has been deployed for test purposes. The “Aniitra” system (Anchorage of Non-Intrusive Instruments to Track and Record under-water Avalanches; Fig. 17) is a buoyant structure mounted with a 75 kHz ADCP current meter may stay at a vertical position (300 m above the canyon's thalweg) higher than the expected current events. The Aniitra system should provide the vertical structure and hence the current thickness of the turbiditic events, a crucial information to

quantify the events and constrain any numerical modelling of these events. It hence improves the resolution of the vertical structure of the current, but it is unable to give directional information. It is hence to be deployed in conjunction with Peer Gynt.



**Fig. 17:** Photograph of the Aniitra system during deployment.

In order to obtain a Lagrangian observation of the currents together with a longitudinal capability of the currents to entrain and transport, an Inflow Buoy for Sediment Entrainment (Ibsen; Fig. 18) has been developed. Its fairly negative buoyancy becomes positive in presence of a denser fluid, as it is supposed to be the case in sediment-laden flows. The Ibsen buoy records its vertical position by the means of a pressure gauge. Assuming its displacement follows the canyon axis, any vertical position (water depth) is supposed to be associated with a single position along the canyon. The quantification of its displacement through time provides an estimation of the Ibsen velocity.





**Fig. 18:** Photograph of the Ibsen mooring prior to deployment.

Sediment traps (Fig. 19) are installed in the “classical” moorings at VV and VA. A rotational reservoir replaces one of the 24 bottles every 7 days. This means that sediment traps are a very low frequency device providing only a qualitative information on particles vertical fluxes. By themselves they are not very accurate, but they provide only information available about particles in the suspension. When correlated to current velocity and Var river runoff, particle fluxes are objectively the effective signature of the turbid nature of the measured currents.



**Fig. 19:** Photograph of a sediment trap (upper centre) used during expedition P386.

### **6.3. Shallow water methodology**

#### **6.3.1. Echosounder**

(A. Kopf, S. Stegmann)

During cruise P386, all research activities could be based on earlier quality bathymetric charts recorded with multibeam systems from KONGSBERG MARITIME (formerly SIMRAD) during R/V *Meteor* cruise M73/1 (Kopf et al., 2008) as well as data acquired by our colleagues from IFREMER beforehand. The only area not mapped prior to cruise P386 was the portion immediately south of Nice airport, because larger vessels have too much draught to navigate safely that close to shore.

With R/V *Poseidon*, we were able to utilise the Pilot echosounder by Krupp-Atlas-Elektronik, which is designed for extremely shallow water depths ( $< 50$  m), ideally even for 20 m and below. The x, y data from this system were logged every second. As a consequence of the time-consuming station work, in particular during deployments of the piezometers, longer CPT tests, Rn counting, and ROV dives, we tried to gather a comprehensive data set north of the existing bathymetric chart.

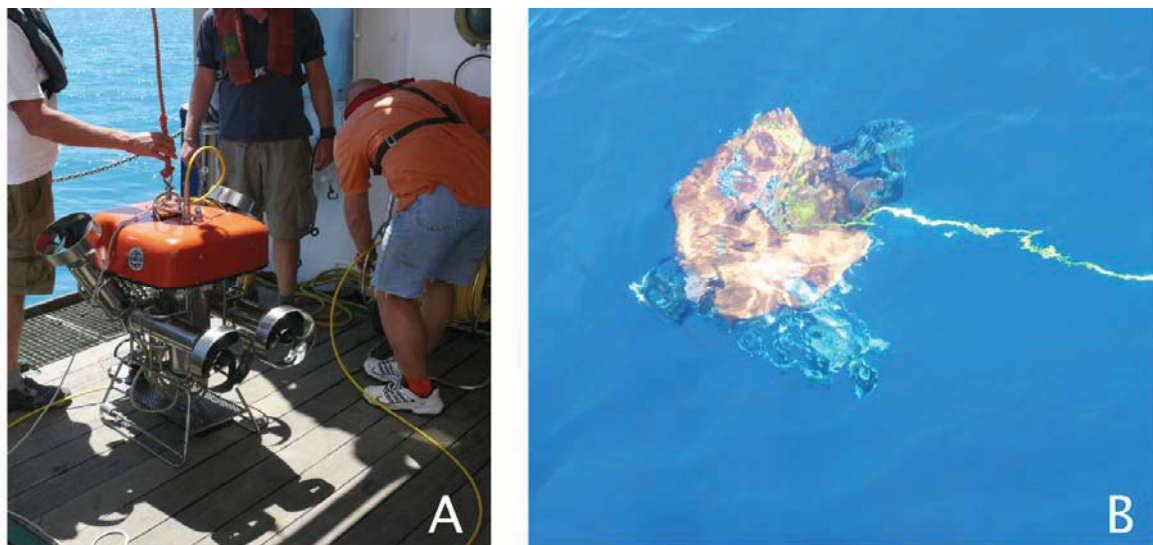
#### **6.3.2. Underwater video surveys (ROV, scuba dives)**

(A. Kopf, T. Pichler, R. Price, M. Seydel)

##### ***Remotely Operated Vehicle SPY***

The remotely-operated vehicle (ROV) “Spy” is a shallow-water device operable down to 250 m water depth (Fig. 20). Its depth range is largely limited by the total length of the cable, which is supplied on a separate winch; for the Nice Airport area, however, this does not pose a problem given water depths  $< 100$  m. The ROV is powered by either 230 DC or 350 DC and is controlled by a console unit with VHS TV screen and a keyboard for the operations. The ROV is equipped with two underwater cameras. One is looking towards the ground while the other one is looking forward. For operation at night or in areas with poor visibility, it is equipped with a pair of headlights. Two turbines at the back control forward/backward movement, while another pair of subvertically mounted turbines control submersion or ascent (Fig. 20). Its total weight of 60 kg (in air) has to be balanced depending on water density and payload. During cruise P386, it was largely used for

surveying the seafloor to find morphological anomalies or evidence for seepage (using the cameras).



**Fig. 20:** ROV “Spy” for surveying the sea bottom for locations of fluid seepage; (a) on deck, (b) in the water.

For part of P386 Leg B, research scuba divers joined the P386 science party to do video surveying, deploy *in situ* temperature probes (see Ch. 6.3.3. below) and take fluid samples out of the shallow sub-seafloor.

### 6.3.3. *In situ* temperature measurements

(A. Kopf, T. Pichler)

On cruise P386 the *in situ* temperature gradients were measured with miniaturised autonomous temperature data loggers (MTL, Fig. 21). For technical specifications and detailed information, refer to Pfender & Villinger (2002).

Parameters of autonomous temperature data loggers:

Instruments serial no.:	sediment and water temp. logger: 18543-65C, -67C, -68C, -70C, -75C, -77C, -78C, -79C
Sample rate:	1 min
Spacing:	1 m, 2 m, 3m, etc. below the weight set; One water temperature sensor at weight set with sensor tip looking up.

Measurements (seafloor penetration) were planned to be carried in two different ways:

(i) Stick MTL into shallow subseafloor (10-30 cm), performed by the scuba divers. The probes are marked with flags along a line and remain fully sediment-covered in the sub-



seafloor for a period of several days before they get recovered. For P386, the planned MTL arrays were within the hydrologically most active portions of the Nice slope.

(ii) Mount MTL to gravity core barrel and get gradient at 1m – spacing as well as reference temperature in the water column. The probe remains in the seafloor sediment for several minutes to allow for some dissipation of artificial frictional heat from inserting the gravity corer.



**Fig. 21:** Miniature temperature logger (MTL) and its housing with supporting fin along the steel barrel of e.g. the gravity corer (top) and deployed in the shallow sediment by a scuba diver (bottom).

#### 6.3.4. *In situ* CPT testing

(S. Stegmann, A. Kopf, A. Förster)

On R/V *Poseidon* cruise P386 , we used the lightweight MARUM free-fall CPTu probe (see Fig. 22a, and Stegmann et al., 2006). Cone Penetration Testing (CPT) is an effective method for *in situ* measurements of these geotechnical parameters with one instrument (Lunne et al., 1997), namely sedimentary strength (tip resistance, sleeve friction), pore pressure, tilt and acceleration. For these measurements, the CPT system relies on 15 cm<sup>2</sup> standard industry piezo-cone (Fig. 22b) with the sensors at the tip and a pressure housing containing a microprocessor at the top. In addition, deceleration and tilt are monitored for vertical profiling of the penetrated sediment column. The lightweight (40-170 kg), shallow water (100-200 m depth) lance works completely autonomously with a volatile memory and battery package. It has exchangeable CPT probes at its tip to accommodate for the various geological settings it is used in.

##### *Instrument*

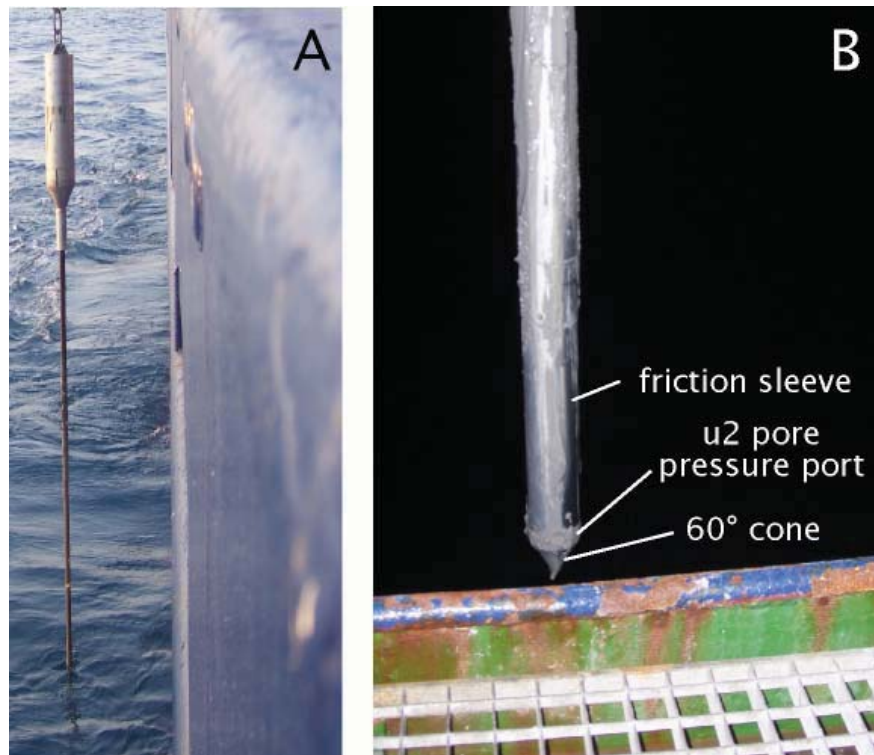
The lightweight free-fall CPT (FF-CPT) instrument for shallow marine use consists of an industrial 15 cm<sup>2</sup> piezocone and a water-proof housing containing a microprocessor, volatile memory, battery, and accelerometer (Fig. 22; see Stegmann et al., 2006 for details). Strain gauges inside the probe measure the cone resistance and sleeve friction by subtraction. A single pore pressure port ( $u_2$ ) is equipped with an absolute 10 MPa (CPT probe 1) and 20 MPa (CPT probe 2) pressure sensor. An inclinometer is used installed to monitor the penetration angle at  $\pm 20^\circ$  relative to vertical. Four different accelerometers with different ranges ( $\pm 1.7g$ ,  $\pm 5g$ ,  $\pm 18g$ ,  $\pm 100g$ ) provide information about the descent velocities and deceleration behaviour of the instrument upon penetration. These data allow the researcher to calculate velocity penetration depth during multiple deployments by 1<sup>st</sup> and 2<sup>nd</sup> integration. The aluminium pressure housing tolerates 2 MPa confining pressure (ca. 200 m water depth) and hosts the power supply and microprocessor. Frequency of data acquisition is variable and depends on the data logger used (see next paragraph). Binary data are temporarily stored on a Micro Flash Card and then downloaded to a PC. The two non-volatile battery packs available provide performance times of about six and twelve hours, respectively. The length of the lance may be varied from 0.5 m to a max. 6.5 m depending on what type of sediment is anticipated. The extension is accomplished by adding 1m-long metal rods and internal extension data/power cables within them. The weight of the instrument thus

ranges from ca. 45 kg to max. 110 kg. If deep penetration is desired, modular weight pieces (15 kg each) can be mounted to the pressure housing at the top of the instrument, then reaching a max. 170 kg. The instrument is deployed pogo-style and remains in the seafloor for about 20 minutes for individual measurements.

### *Modes of deployment*

The FF-CPT instrument was used with two different types of CPT-probes, two different data logging units, and in two types of deployments (profiling vs. pore pressure dissipation). During cruise P386, the probe was generally deployed in 3.5 m long mode with 4 weight sets (i.e. 60 kg) attached.

As for the CPT probe, two systems supplied by GEOMIL (Alphen, NL) were used. The first, more sensitive unit is only designed for 100 m water depth (i.e. 1 MPa absolute pore pressure transducer, 25 MPa cone resistance strain gauge, 0.25 MPa sleeve friction strain gauge). The less sensitive 200 m tip comprises a 2 MPa absolute pore pressure transducer and 100 MPa (cone resistance) and 1 MPa (sleeve friction) strain gauges.



**Fig. 22:** Shallow-water FF-CPTu instrument (left) and detail of the CPT probe (right).

Two different types of microprocessor data recording units were used. The older model contains a TigerBasics microcontroller which logs the data at 40 Hz. It was usually utilised for tests aiming at the shape of the pore pressure dissipation curves ( $\gg$  30 mins. deployment

time). In contrast, a recently developed 1000 Hz AVISARO microcontroller was utilised during deployments, which largely aimed at the vertical profiling of the sedimentary succession. This usually takes less than 1-2 secs. and at the high sampling rate, provides the user with data of a vertical resolution  $< 1$  cm thickness. The controllers are directly linked to the two fundamentally different modes of deployment. The first (type A) aims at a high-resolution vertical record of crucial *in situ* sediment physical properties. The probe is veered at 1.2 – 1.5 m/s winch speed and then dynamically decelerated until its terminal depth of several meters sub-seafloor. The instrument is recovered immediately after the probe came to a complete halt. The second approach (type B) is initially similar, however, aims at the recording of the pore pressure evolution once the instrument is stuck in the sediment. Pore pressure dissipation is usually recorded for 30 mins. (assuming the ship can be held at the location for that long), occasionally even for 60 mins. Given that R/V *Poseidon* does not have a dynamic positioning system, the majority of the deployments were either type A or B, but avoided dissipation periods exceeding 30 mins.

#### **6.3.5. Piezometer deployments**

(P. Pelleau, R. Approuial, S. Stegmann, A. Kopf)

Owing to the interesting hydro-geological processes in the study area, the *in situ* monitoring of pore pressure and temperature are a major focus of the P386 research. In addition to the deployment of MTLs (Ch. 6.3.3.) and CPT profiling (Ch. 6.3.4.), those key physical properties were measured in different depth levels in the sub-seafloor sediment using piezometer probes developed by IFREMER. The IFREMER piezometer is a free-fall device composed of a lance and an upper body consisting of the power supply, data storage unit and a package of recoverable weights.

The IFREMER piezometer is a modular free-fall device composed of a lance and an upper recoverable part with pieces of weights, power supply and data acquisition (Sultan et al. 2007). It is already existing in a second generation instrument Piezo v2, which has been improved in a number of places compared to the earlier v1 version. The overall design is schematically shown in Figure 23.



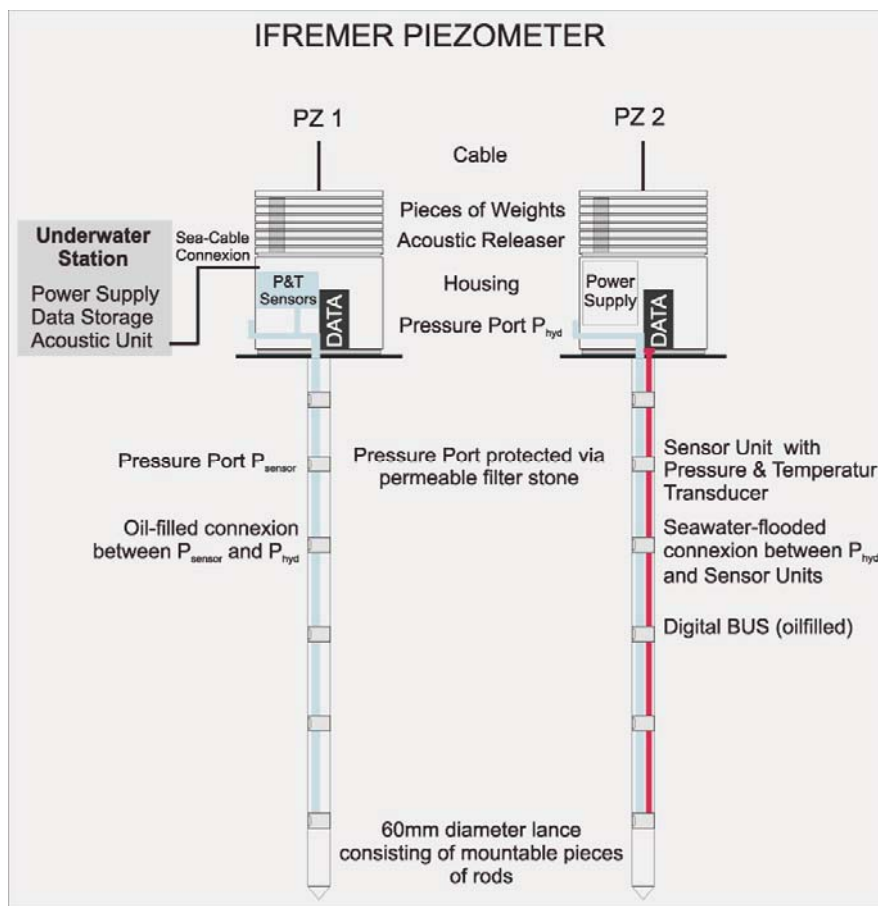


Fig. 23: Piezometer v1 (left) and piezometer v2 (right) used during R/V *Poseidon* cruise P386.

Depending on the requirements for the installation of the piezometer in a given location, the instrument can be set up in different configurations. The 60 mm-diameter lance consists of single rods (0.75m or 1.50m) intersected by sensor packages. The spacing and length of rods between the “piezomodules” define the depth levels where pore P and T are measured. The maximum total length of the lance is limited to 10 m for stability reasons. Each module contains a sensor package comprising a KELLER pore pressure transducer and a standard temperature sensor. Pore pressure is measured differentially with a resolution of  $\pm 0.2$  kPa by coupling the pore pressure at the of each sediment level with the open seawater (hydrostatic reference) by a tubing. The sampling rate can be set up individually before each measurement, with the maximum rate being 1 Hz.

In the first generation (Piezo v1) the pressure transducer of each port is installed at the top of the instrument where the hydrostatic reference port is situated, while the lower port is connected via tubing along the lance (Fig. 23, left). The disadvantage is the compliance of the tubing in which gas may be trapped during deployment. The advancement in the second generation instrument (Piezo v2) is the direct contact of the pressure

transducer with both the formation and the hydrostatic reference because the transducer has one port as close to the formation as physically possible, whereas the second port points towards the inside of the probe through which open flow of seawater over the complete length is achieved (Fig. 23, right). Saturation with seawater of both systems is accomplished prior to each deployment by dipping the instrument for 20 minutes over its complete length into the water at moderate depth above the seafloor. For the final stage of the deployment, the instrument is lowered with the winch to the seafloor and the lance penetrates the sediment using its own mass.

The piezometer can be used for short-term (hours to days) as well as long-term (weeks to months) installations. For short-term measurements, the instrument is usually deployed on different locations without recovery on deck of the vessel in “yo-yo-style” (e.g. Sultan et al. 2008). For long-term monitoring, the piezometer can be connected to an underwater-station providing continuous power and additional data storage capacity. An acoustic communication module of the underwater-station allows the transfer of the data without recovering the piezometer. During cruise P386, we had one piezometer v1 funded by IFREMER) and one piezometer v2 (funded by MARUM) available for long-term deployment. Regarding the setup of the two instruments, mode of deployment (yo-yo vs. long-term), sampling rates and locations, see Ch. 7.3.5 below.

#### **6.3.6. Gravity coring and sediment description**

(A. Förster, T. Fleischmann, K., Weber, S. Stegmann, A. Kopf)

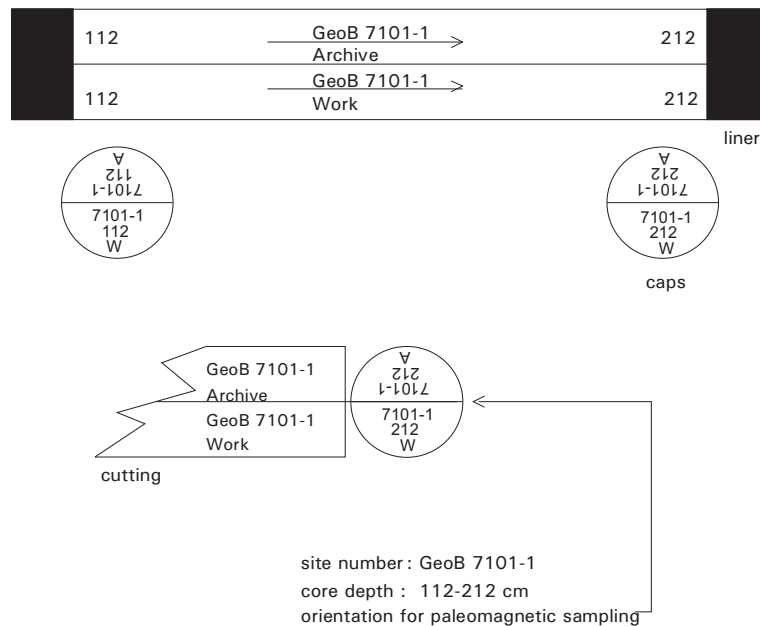
In order to recover sediment cores, two sampling systems were used during P386: (i) a gravity corer with tube lengths of 3 to 6 m and a weight of approximately 2 tons (Fig. 24a), and (ii) a light-weight “bobcorer” of only 150 cm length and smaller diameter for use in very shallow water (Fig. 24b). Before using the coring tools, the plastic liners (placed inside the steel tubes in case of the gravity corer, but representing the outer cylinder in case of the bobcorer) have been marked lengthwise with a straight line in order to retain the orientation of the core for potential paleomagnetic analyses.



**Fig. 24:** Gravity corer (a) and Bobcorer (b) on board R/V *Poseidon*.

Once on board, the sediment cores were cut into sections of 1 m length, closed with caps on both ends and labelled according to a standard scheme (Fig. 25). By definition, the half core with the marked line was stored as archive half (after having passed the Multi-Sensor Core Logger – see Ch. 6.3.6.3.), while description, sampling, etc. were carried out on the remaining half. For the detailed procedures each working half core underwent, see below.

Inscription:

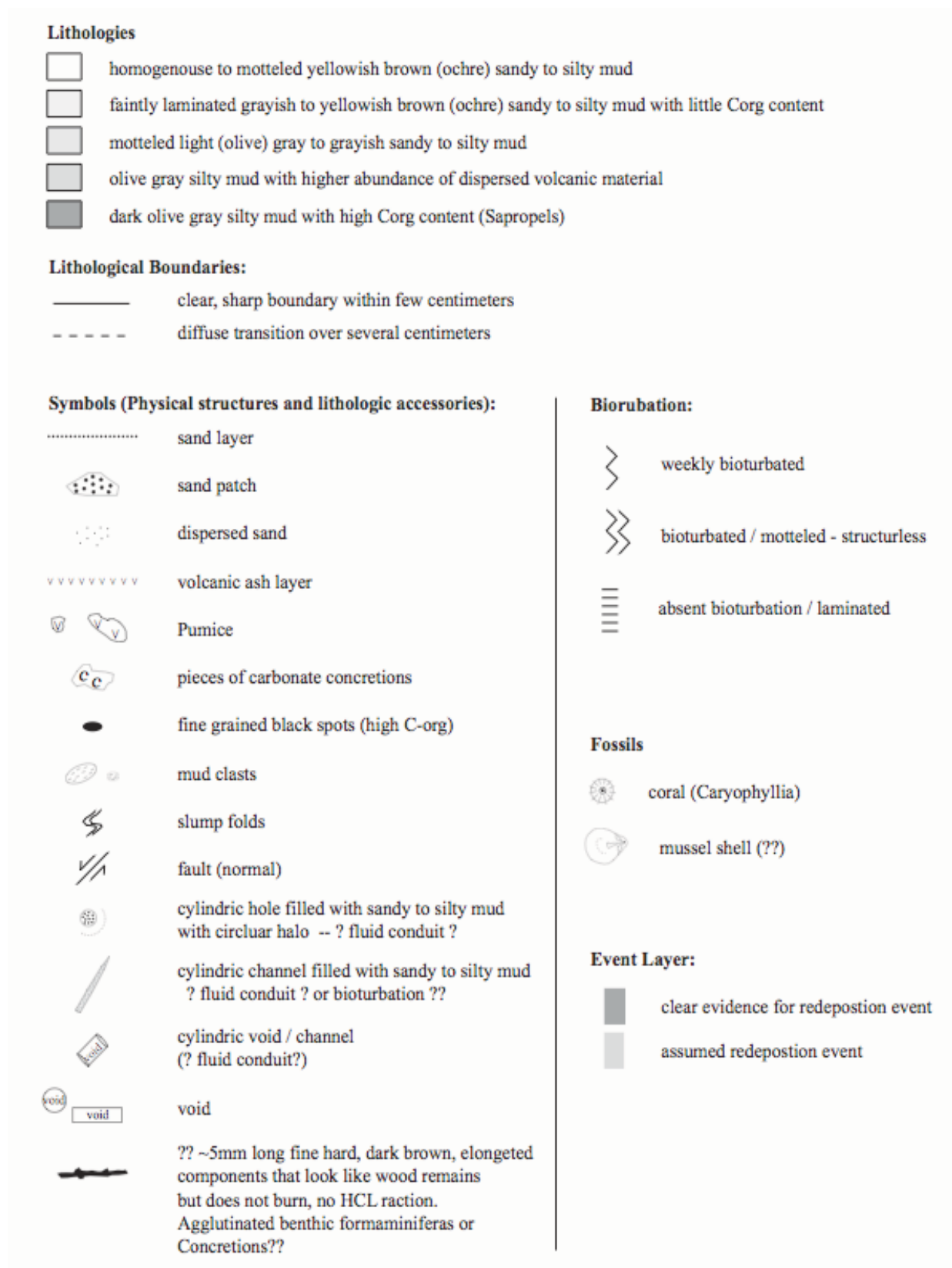


**Fig. 25:** Scheme of the inscription of gravity core segments used during P386 .

### *Sediment description*

Split gravity cores were photographed and described from a largely sedimentological standpoint. Grain size and composition of sediments were determined mainly visually using a simple hand-lens, HCl-testing and analyzing smear slides of dominant lithologies under a cross-polarizing microscope in accordance with Rothwell (1989). The size of grains was assessed based on Wentworth's (1922) classification. The colour of the material was determined visually on board using Munsell's colour chart nomenclature, and also has been studied spectrophotometrically after the cruise on the Multi-Sensor Core Logger (MSCL; see Appendix 10.3). For each core, a composite one-page core log sheet was compiled. It shows core photographs next to a graphical core log and gives information on redeposition-/event layers (i.e., sand layers, volcanic ash layers or clear evidence for mass movement deposits, such as mud clasts in muddy or sandy matrix, tilted beds and repetition of strata), bioturbation and the assigned lithological units in three different columns. The core log is combined with results from the fall cone penetration test (see below). A wide variety of features, such as sediment lithology, primary sedimentary structures, bioturbation, soft-sediment deformation, and coring disturbance is indicated by patterns and symbols in the graphic logs. A key to the full set of patterns and symbols used on the barrel sheets is shown in Figure 26. The symbols are schematic, but they are placed as close as possible to their proper stratigraphic position. All core descriptions are provided in Appendix 10.2 (see below).





**Fig. 26:** Key of symbols for barrel sheets of gravity core description.

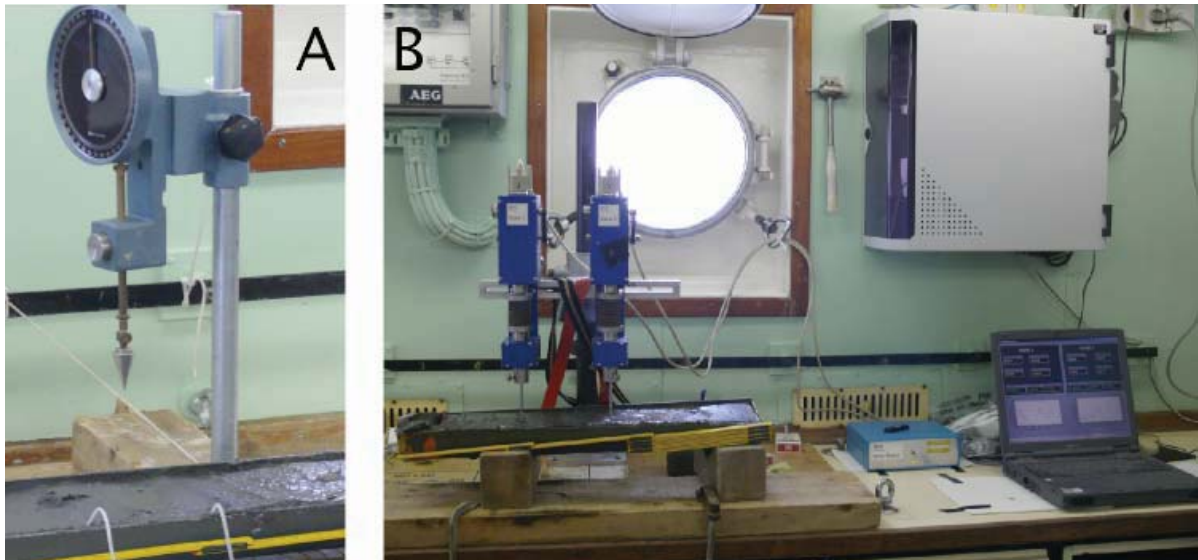
### 6.3.7. Physical properties

(A. Förster, T. Fleischmann, S. Stegmann, K. Weber)

During cruise P386, shipboard physical properties measurements were restricted to falling cone penetration tests and vane shear tests on the working half of the core. Since no container with a Multi-Sensor Core Logger (MSCL) could be placed on board RV *Poseidon*, these measurements on the undisturbed archive half of the cores were carried out immediately after the cruise at MARUM Bremen. A description of the instrument is given below (Ch. 6.3.7.3.).

#### 6.3.7.1. Cone penetrometer

The geotechnical properties along the sediment cores were determined according to British Standards Institutions (BS1377, 1975). A Wykeham-Farrance cone penetrometer WF 21600 (Fig. 27a) was used for a first-order estimate of the sediment's stiffness. For the measurement, the metal cone was brought to a point exactly on the split core face. A manual displacement transducer was then used to measure the distance prior to and after release of the cone (i.e. penetration after free fall of the cone). Precision is 0.1 mm of displacement. The distances measured can then be translated into sediment strength (see Hansbo, 1957).



**Fig. 27.** (a) Falling cone penetrometer and (b) PC-interfaced IFREMER double-vane shear device used on the split core surface.

A falling cone penetrometer with a defined weight (80.51 g) and geometry (30° cone) was used by Hansbo (1957) during a detailed study of the relationship between the cone penetration and soil strength. The undrained shear strength  $s_u$  can be calculated from the

variables mass and tip angle of the falling cone, gravity  $g$ , penetration depth  $d$  and the cone factor  $k$  via the “cone factor”. Wood (1985) calculated from fall-cone and miniature vane tests average values of cone factors (in our case  $k=0,85$  for a  $30^\circ$  cone). The undrained shear strength can then be calculated using the equation  $s_u = (k \cdot m \cdot g) / d^2$ .

Shore-based laboratory testing will include ring shear experiments as well as dynamic triaxial shear tests to obtain residual strength and rate-dependent frictional properties as well as the liquefaction potential of the materials recovered.

#### **6.3.7.2. Vane shear testing**

In addition to the Cone Penetrometer a double vane shear apparatus by GSC ATLANTIC was used for more information about sediment stiffness and residual shear strength (Fig. 27b). The distance between the two vanes is 15 cm. For the measurements, four-bladed vanes ( $L = 12.5$  mm,  $h = 6.25$  mm,  $d = 12.5$  mm) were inserted into the split undisturbed core faces and rotated at a constant rate of  $90^\circ/\text{min}$ . Data are logged via an interface module (GSC ATLANTIC) using the Testpoint software package.

A spring transmits the rotation at the vane. The torque required shearing the sediment along the vertical and horizontal edges of the vane. The undrained shear strength,  $s_u$  depends on the torque  $T$ , the vane constant  $K$ , the maximum torque angle at failure  $\sigma$  and the spring constant  $B$  that relates the deflection angle to the torque (Blum, 1997). The vane constant,  $K$  is a function of the vane size and geometry and was used during the measurements with  $K = \pi \cdot d^2 \cdot (h/2) + \pi \cdot (d^2/6)$  for full dipping vanes. The undrained shear strength can then be calculated using the equation  $s_u = T/K$ . Shore-based laboratory testing will include ring shear tests to obtain residual strength and rate-dependent frictional properties of the materials recovered.

#### **6.3.7.3. Multi-sensor core logger**

The GEOTEK MSCL device at MARUM Bremen combines three sensors on an automated track (see schematic diagram in Fig. 28). The P-wave velocity, gamma ray attenuation (bulk density), and the magnetic susceptibility were recorded, and from this data the fractional porosity and impedance were calculated. RGB images were also produced with a full color digital line scan imaging system. Magnetic susceptibility, bulk density, and line scan photography were generally measured on all cores.

### Magnetic Susceptibility

Magnetic susceptibility was measured with a Bartington point sensor MS2 using an 80-mm internal diameter sensor loop (88-mm coil diameter) operating at a frequency of 565 Hz and an alternating field of 80 A/m (0.1 mT). The sensitivity range was set to the low sensitivity setting (1.0 Hz). The sample period and interval were set to 2 s and 4 cm, respectively, unless noted otherwise. The mean raw value of the measurements was calculated and stored automatically. The quality of these results degrades in XCB and RCB cores, where the core may be undersized and/or disturbed. Nevertheless, general downhole trends are useful for stratigraphic correlations. The MS2 meter measures relative susceptibilities, which have not been corrected for the differences between core and coil diameters.

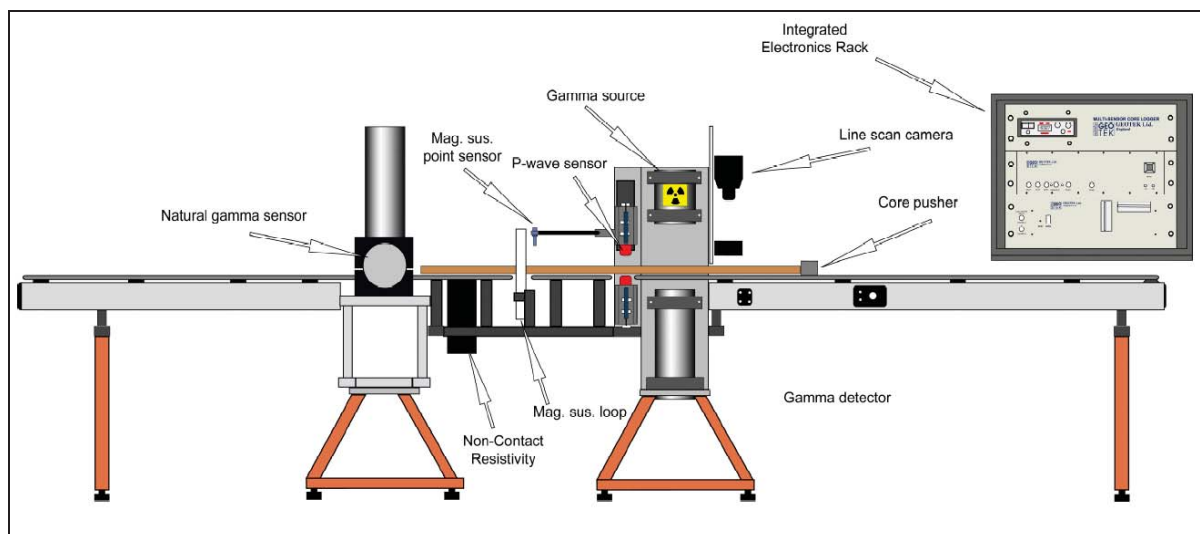
### Gamma-Ray Attenuation

Bulk density was estimated for split core sections as they passed through the GRA bulk densiometer using sampling periods and intervals of 2 s and 4 cm, respectively, unless noted otherwise. A thin gamma beam from a Caesium-137 source with energies around 0.662 MeV is passed through the core and the relative intensity of this beam can be used to measure the gamma density. These photons are scattered by electrons in the core and lose some of their energy. To determine the gamma density the number of unscattered electrons is measured by counting photons with the same principle energy as the photon source. The gamma density of an aluminum billet of stepped thickness is used to obtain calibration equations to convert gamma density into actual density values.

### P-Wave Velocity

The P-wave velocity is measured at 4-cm intervals and 2-s periods using two PWL transducers. The PWL measured P-wave velocity across the unsplit core sections. In order to determine the P-wave velocity, the PWL transmits 500-kHz P-wave pulses through the core at a frequency of 1 kHz. The transmitting and receiving transducers are aligned perpendicular to the core axis while a pair of displacement transducers monitors the separation between the P-wave transducers. Variations in the outer diameter of the liner do not degrade the accuracy of the velocities, but the unconsolidated sediment or rock core must completely fill the liner for the PWL to provide accurate results. During this measurement good acoustic coupling between the core liner and transducer is achieved by adding water to the contact points.





**Fig. 28:** Schematic of the Geotek Multi Sensor Core Logger (MSCL).

### 6.3.8. Pore water chemistry

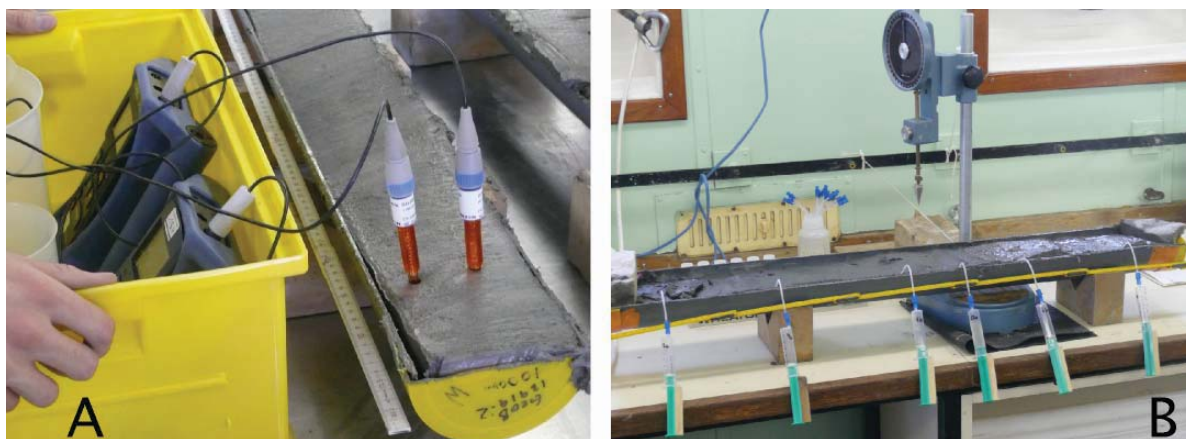
(T. Pichler, S. Pape, S. Hammerschmidt, R. Price, M. Seydel)

#### *Pore water sampling*

All gravity cores were taken by plastic liners and cut into 1 m segments on deck. To prevent a warming of the sediments on board, the sediment cores were immediately transferred into the cooling room after recovery and maintained at a temperature of about 4°C. The wet sediment was exposed by means of cutting a small ‘window’ in the plastic liner at an interval of 25 cm. Eh and pH were measured directly in the sediment using punch-in electrodes before the pore water was extracted (Fig. 29a). From most of the cut segments of the cores 5 ml syringe samples of wet sediment were taken for methane analysis. The pore water was then extracted by means of rhizons (pore size 0.1 µm) (see Fig. 29b). The gravity cores were each processed in this way within a few hours after recovery. Depending on the porosity of the sediments, the amount of pore water recovered ranged between 4 and 20 ml. Solid phase samples of the majority of cores were taken for total digestions, sequential extractions and mineralogical analyses at 25 cm intervals, kept in gas-tight glass- and heavy plastic bottles under an argon atmosphere and stored at 4°C.

Pore water analyses of the following parameters were carried out during this cruise: Eh, pH, ammonium, alkalinity, iron ( $\text{Fe}^{2+}$ ). Salinity was also measured using a conductivitymeter for selected cores where fluid freshening was suspected. Eh and pH, as mentioned earlier, were determined with punch-in electrodes before pore water was extracted. Ammonium was measured using a conductivity method. Alkalinity was calculated

from a volumetric analysis by titration of either 0.5 or 1 ml of the pore water samples with 0.01 M HCl, respectively. For the analyses of dissolved iron ( $\text{Fe}^{2+}$ ), subsamples of 1 ml were taken from pore water extracted by rhizons, immediately complexed with 50  $\mu\text{l}$  of “Ferrospectral” and determined photometrically. Salinity was measured using a conductivity probe placed directly into the pore water samples.



**Fig. 29:** (a) pH measurement and (b) rhizon pore water extraction in split working half of the gravity core.

For further analyses at the University of Bremen aliquots of the remaining pore water samples were diluted 1:10 and acidified with ultra pure  $\text{HNO}_3$  for determination of cations (Ca, Mg, Sr, K, Ba, S, Mn, Si, B, Li) by ICP-OES. Additionally, 0.6 mL of a ZnAc solution was added to a 1.5 mL subsamples of the pore to fix hydrogen sulfide as ZnS for later analysis. Finally, all remaining pore water was stored at 4 °C for additional analyses at the University of Bremen. A complete overview of sampling procedures and analytical techniques used on board and in the laboratories at the University of Bremen is available on <http://www.geochemie.uni-bremen.de/>.

To test for direct venting of submarine groundwater into the shallow water portion of the study site pore waters were collected every 10 m along the transect prepared with MTLs (see Ch. 6.3.3. above). These were collected into 60 mL syringes by inserting the syringes approximately 5 cm into the sediment and slowly pulling the plunger. The entrainment of fine particles could not be avoided, nevertheless, these were filtered out once the syringes were passed to the geochemists onboard R/V *Poseidon* for further analyses. After filtration, these samples passed the same analytical routines as those extracted from the gravity cores.

### **6.3.9. *In situ* Radon measurements**

(A. Mayer, P. Henry)

#### ***Overview***

Radon-222 is a radioactive noble gas produced by decay of radium-226. The half-life of radon is 3.8 days, which implies that this gas is never “far” from its source (radium). Several studies have shown that groundwater often presents high radon activity. This is due to the presence of radium at the surface of the aquifer solids. Groundwater may reach in some cases an activity of millions of Bq/m<sup>3</sup>. By contrast, due to atmosphere degassing and decay (or more correctly the distance from the radon source), radon activity in seawater is very low (10-14 Bq/m<sup>3</sup>). Seawater affected by seepage of groundwater might thus be detected because of the large contrast in radon concentrations. In addition, steady state radon inventory in water column implies that radon natural decay is sustained by radon production, thus radon concentrations might be readily translated into water fluxes.

Radon concentrations measured at different depths along a vertical profile off the Nice airport might be used to detect local seepage of groundwater, and estimate involved seepage flux once knowing radon activities in a) groundwater and b) offshore seawater.

#### ***Methods***

The available (up-to date ) radon measurement methods developed by Adriano Mayer (CEREGE) allows precise measurement of radon activity *in situ*, without the need for collection a sample. Two alpha spectrometers, gas-exchange cell, water stripping system might be installed in a water resistant wooden box (1.2 x 0.6 x 0.8 m, about 40 kg; Fig. 30a), allowing continuous measurement of radon, with 30 minutes count integration for each acquisition. Once launched, the apparatus does not require presence of personnel, and may be used on a small (3-4m long) rubber craft (Fig. 30b). Typically, the measurement in one spot - one depth requires: 5 minutes for installation, 30 minutes for purge of previous measurement (might be done earlier), 1h 30 minutes acquisition (for six values, having 2 spectrometers). More precise values are obtained with longer acquisition time.

During acquisition, a 12V immersion pump (turbine) with attached flexible pipe produces a continuous water flow of about 1.5-3 litre/minute from the desired depth to the gas exchanger in the wooden box. The seawater is discharged to the sea after radon degassing (no sample is retained). In addition to the Rn counts, conductivity measurements are carried out in the water cylinder surrounding one of the filters oof the pump. This way the

researcher can tell immediately whether fresh, brackish or saline water is entering the system, and can hence relate this information to the Rn counts. The latter are estimated at real time by an acoustic signal. The precise protocol of the Rn counts is measured by two. The sampling depth is attained maintaining the flexible pipe and 12V cable in vertical position, tied to a rope with a weight attached to its lower end. During cruise P386, both concrete weights as well as a metal weight (both appx. 10-15 kg) were used to keep the hose close to the seafloor. A buoyant device was tied to the nozzle of the hose to ensure that the open end of the hose is not dipped into the sediment-water interface (Fig. 30c).

### *Application*

Rn measurements were usually not carried out as a stand-alone measurement, but complemented other deployments at the same station (CPT, gravity core). Depending on the time spent for the measurements, radon concentrations could be measured on station from the deck or dinghy (see previous paragraph and Fig. 30), or continuously near the sea surface while the dinghy or the ship is slowly sailing (max. 3-5 knots). In the latter case, a horizontal transect of radon concentrations of the near surface seawater is obtained, which would nicely supplement the vertical Rn profiles (see above). If the radon background concentration in the local seawater, far from the radon source, as well as the concentration of radon in the groundwater are known, under given assumptions a groundwater seepage rate may be calculated. The strategy for the Nice slope was (a) to collect sufficient data near the sealevel as well as in the deeper water to determine a “background Rn concentration” for the ocean water in the Nice landslide vicinity, (b) to carry out measurements in the estuary of the river Var to determine the “input Rn concentration”, and (c) to measure Rn concentrations very close to the seafloor in locations where (gas) flares were seen in 3.5 kHz seismic profiles (based on Sultan et al., 2008) or in locations where previous workers found evidence for freshening of the seawater (Guglielmi & Prieur, 1997; Kopf et al., 2008, 2009).



**Fig. 30:** (a) Setup of the Rn counters, pumps, filters and conductivity meter in the wooden box on the deck of R/V Poseidon; (b) Rn setup on the dinghy; (c) buoyancy device attached to lower end of hose. See text.

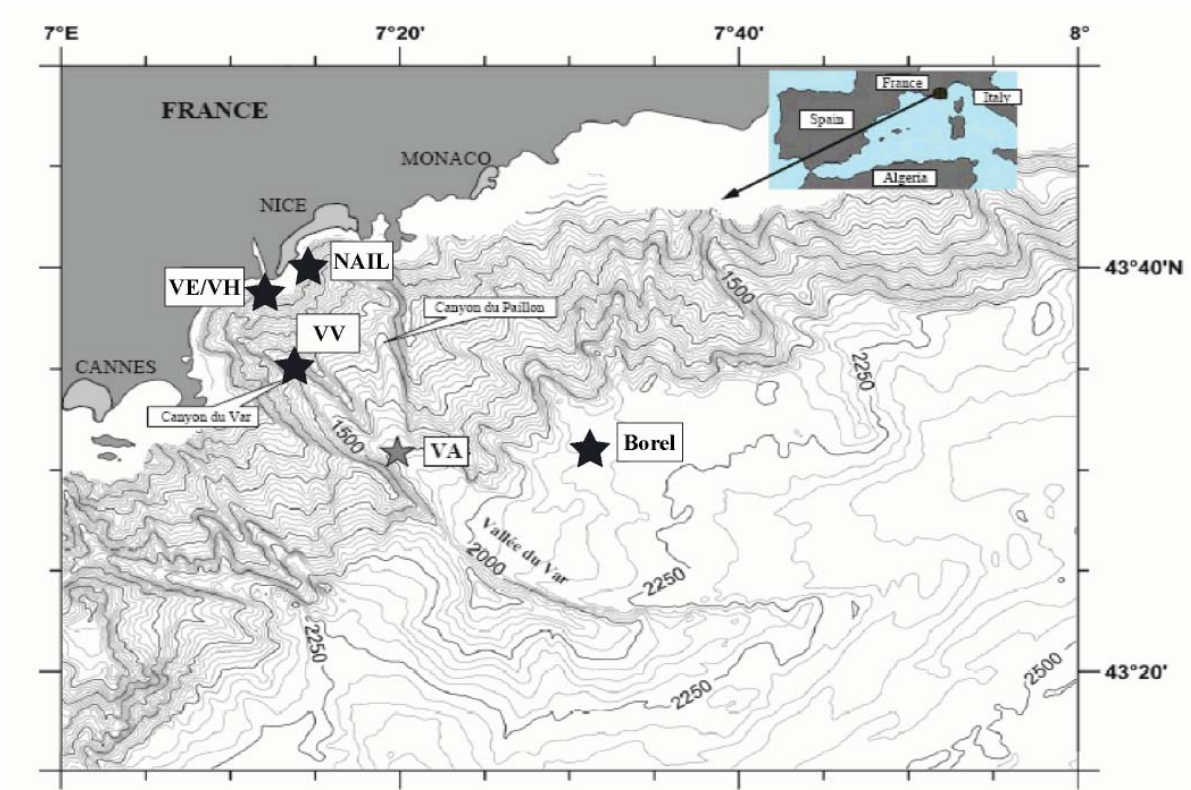


Figure 30 shows the two types of deployment strategies used on P386. The first approach has the Rn measuring unit on deck of R/V *Poseidon*, close to the railing. The hose with the nozzle is lowered either to a few meters sub-sealevel depth (to determine the background water body Rn concentration) or lowered to the seafloor where a buoyancy device hinders sucking of sediment suspension into the pump, filters and Rn counter (Fig. 30a). Although this is the least laborious setup, the disadvantage is the fact R/V *Poseidon* usually does not remain on station for very long periods of time (only 20 mins. for gravity coring, and appx. 40 mins. for a CPTu test). Hence, the Rn measurements from deck served mostly the collection of background data (see Type “a” above). Only in spots where mid-term pore pressure dissipation tests were planned with the CPTu instrument (see Ch. 6.3.4. above), the hose was lowered all the way to the seafloor to get signals at fresh water sites. For longer term Rn counts, the unit was either placed onto the dinghy (Fig. 30b) or onto the diving platform *Poseidon III* (see Fig. 14). Both small watercrafts aimed for fresh water locations only, so that measurements of up to >2 hrs. got achieved.

## 7. Preliminary Results

The preliminary results from cruise P386 can be divided into three major topics:

(i) Technological developments regarding acoustic data communication for seafloor observatories, (ii) deployments for sedimentological research in the Var Canyon turbiditic system, and (iii) the wealth of geological, geotechnical and geochemical measurements and long-term deployments in the Nice Airport slide area. Figure 31 provides a map where the three objectives were carried out. In the following, results from each of them are documented in consecutive chapters.

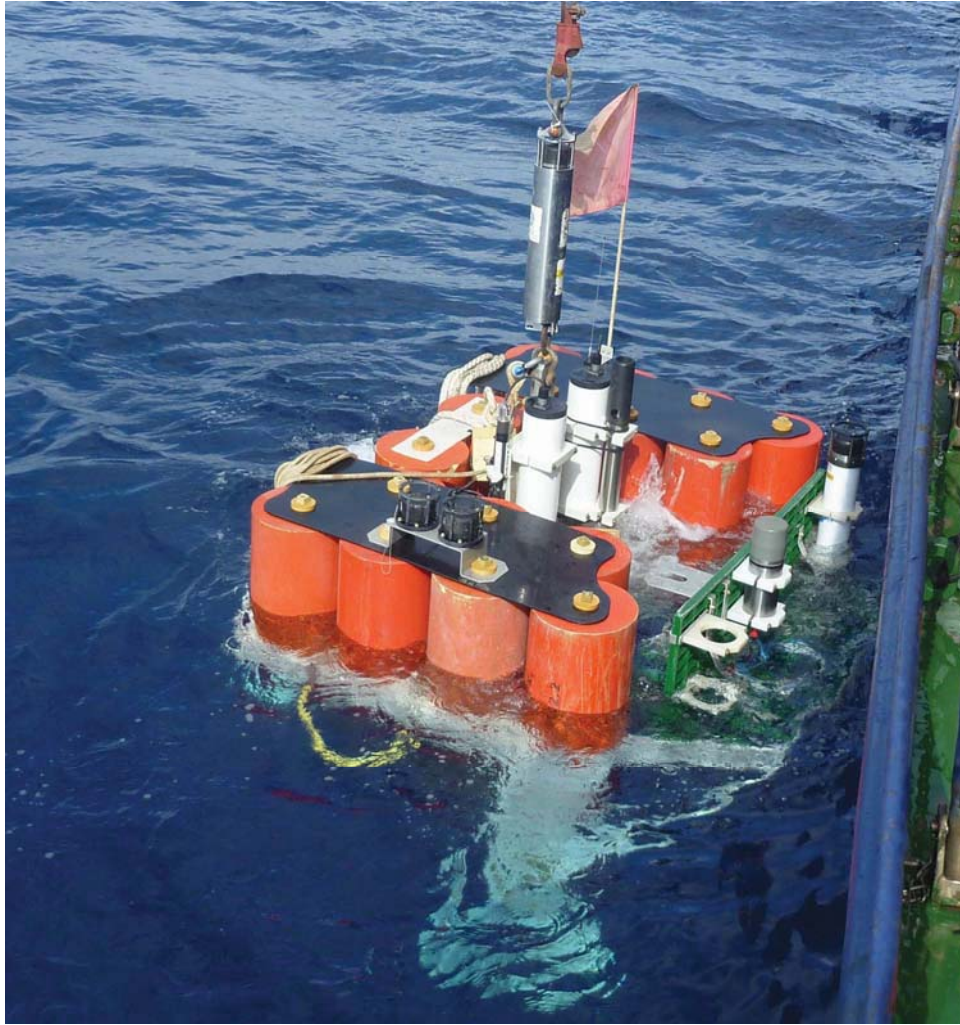


**Fig. 31:** The study areas (black stars) visited during cruise P386. The main focus was on the Nice Airport Slide (NAIL), mooring deployments in the Var Canyon talweg (VE, VH, VV) and on long-term acoustic communication tests using the Borel buoy (Borel). VA is a point of a former deployment unrelated to P386.

### 7.1. Long term tests of acoustic modems for subsea observatories

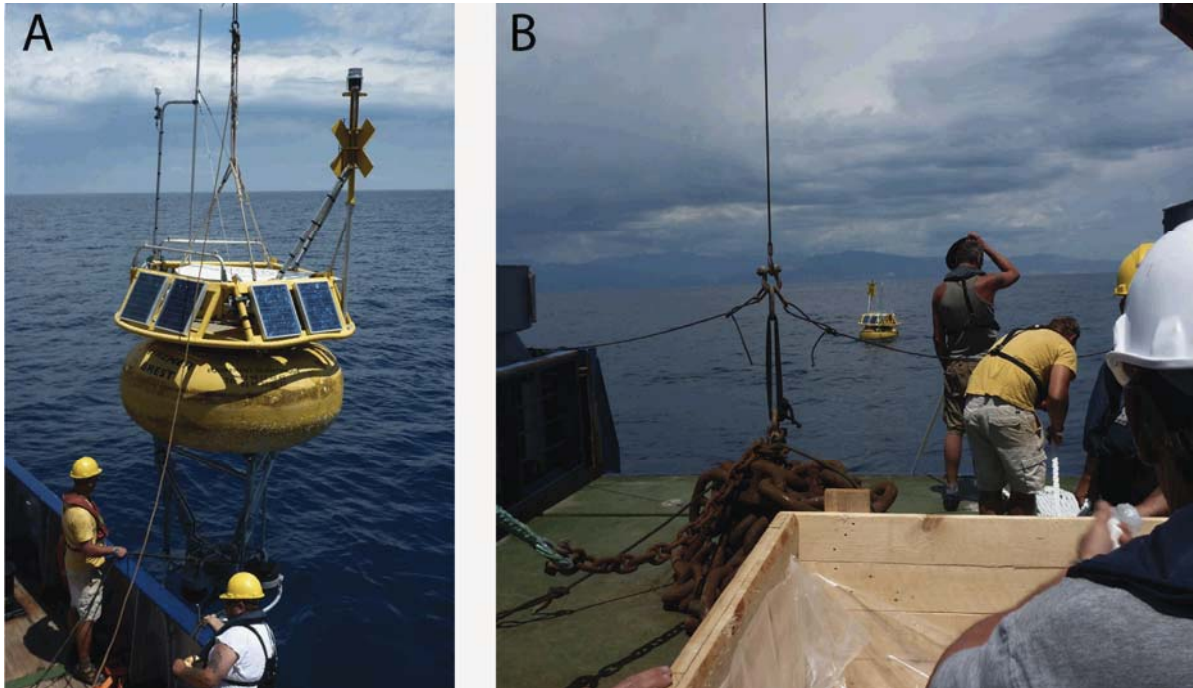
(J. Blandin, J.-P. Brulport, P. Crassous, G. Gruyader, J. Legrand, P. Pichavant)

The MAP2 station (Fig. 32) containing the acoustic communication hardware was deployed on June 22, 2009. It was attached to a deep-sea cable with an acoustic release, then lowered from the ship to 2080 m below sea level, and was finally released and traveled the last 100 m to the seabed in free fall.



**Fig. 32:** The station MAP2 has been moved overboard, ready to be lowered.

The Borel buoy was deployed on June 22, 2009 by first bringing it out overboard at a point 4000 m below wind of the target point for the deployment. Afterwards, the 2400 m of line were paid out as the ship proceeded slowly towards the target point (see Fig. 33B). When all the line was paid out, R/V *Poseidon* continued its route until 650 m beyond the target point, where the 1900 kg of ballast were released overboard.



**Fig. 33:** The Borel buoy over the port side of R/V *Poseidon* (A) and when being released during paying out the mooring line (B). Note also ballast chain waiting to be deployed.

The link between MAP2, the Borel buoy and shore was established immediately after deployment of the buoy. During leg A of expedition P386, the modems from one manufacturer performed successful data transmissions every two hours, as scheduled. The top modem of the other manufacturer showed difficulties in receiving the messages transmitted from the bottom, even with a low data rate and high transmission power. The situation was described to the manufacturer who proposed to send a replacement electronic board to be installed in the waterproof container of the buoy transducer. This operation required good weather and the ability to lift the buoy back to the side on deck-level in order to retrieve the transducer from the buoy. This was achieved during leg B where a replacement board brought by the second science party was mounted successfully. However, tests during the second half of leg B failed to attest successful data communication between the second MAP2 modem, the buoy and the shore.

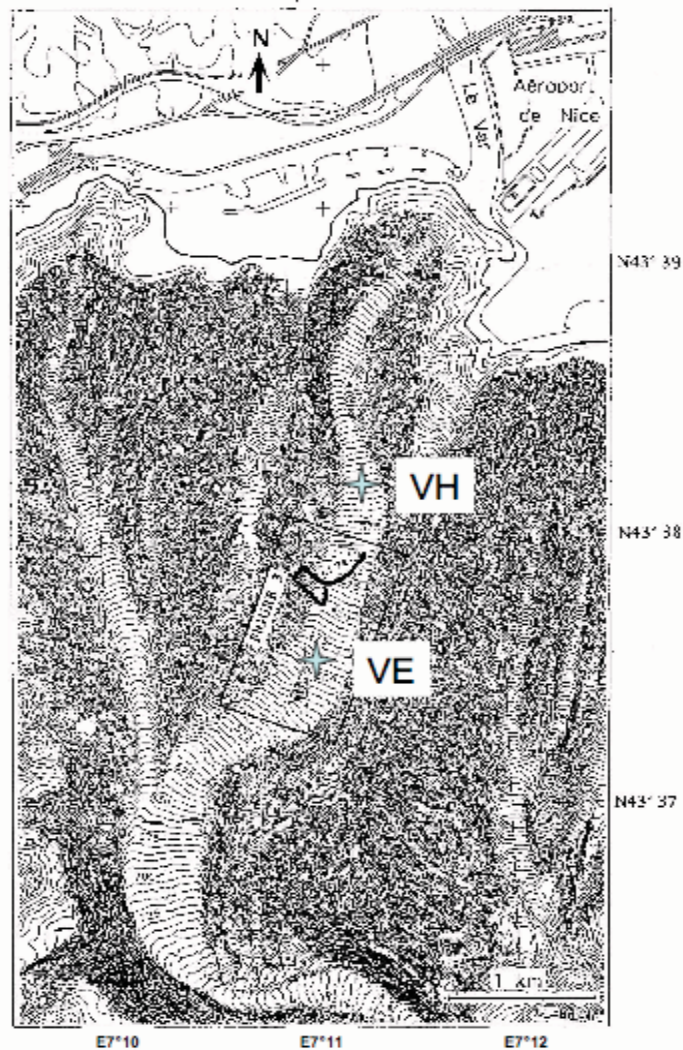
The Borel buoy and MAP2 station are scheduled to be recovered in January 2010 from R/V *L'Europe*, together with the Var Canyon observation devices (see next chapter).



## 7.2. Sediment traps, ADCP and current meters in the Var Canyon

(R. Jacinto Silva, J. Legrand, P. Pichavant, J. Blandin, G. Gruyader)

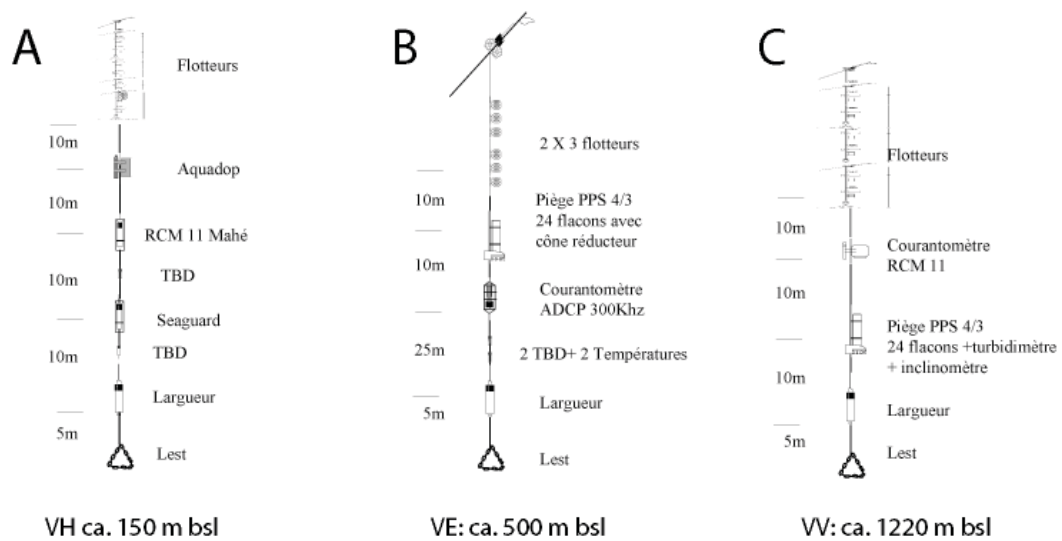
Current meters are placed at three locations along the Var canyon: VE, VH and VV (see Fig. 31). Moorings VH and VE were deployed to provide detailed information for the upper Var Canyon (see detailed map in Fig. 34). At location VH (Fig. 35a), three punctual current meters are installed at 15m, 25m and 35m above the canyon's talweg in order to provide the current structure at the head of the canyon. The mooring placed at VE (Fig. 35b) has a 300kHz ADCP 30 m above the talweg in order to provide a continuity to VH monitoring.



**Fig. 34:** Detailed bathymetric chart of the upper submarine Var Canyon with the locations of moorings VH and VE. See text.

The station VV is the place for a “classical” mooring with a control current meter placed 25 m above the talweg (Fig 35c). This current meters should provide a directional information of the currents. At the same location, the Anitra mooring is deployed with its 75kHz ADCP current meter.





**Fig. 35:** Schematic diagrams of the moorings installed during cruise P386. Mooring VV contains the Anitra unit (see Fig. 17). See Figs. 31 and 34 for locations of deployments.

### 7.3. Nice Airport landslide

#### 7.3.1. Echosounder

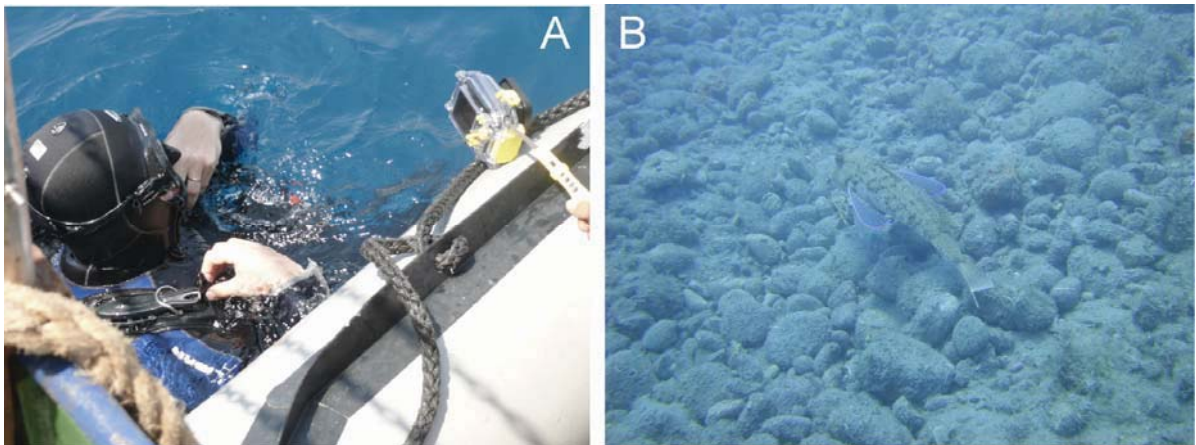
(S. Stegmann, A. Kopf)

No multibeam swathmapping system was mounted on R/V *Poseidon* during cruise P386, and no geophysicists were part of the scientific crew. As a result, we were only able to record the echosounder depth and position at intervals of 1 minute using the shipboard DATAVIS system. These XYZ-coordinates are filtered regionally and serve to slightly extend the existing bathymetric charts by IFREMER and MARUM towards the shore. This was possible because R/V *Poseidon* has lower draft (4.5 m) than R/V *Meteor* (Kopf et al., 2008) or R/V *L'Atalante* (Sultan et al., 2008) when surveying the area two years earlier. Post-cruise, the P386 XYZ data were pooled with similar XYZ coordinates from the French “Haligüre” cruise acquiring Chirp profiles on a dinghy in late August 2009 (P. Henry, pers. comm., 2009). The combined data set is currently processed and will be available in the near future.

### 7.3.2. Underwater video surveys (ROV, scuba dives)

(A. Kopf, T. Pichler)

Underwater photo and video documentation was severely hindered by large amounts of suspended matter in the water column, mostly caused by a period of gusty winds and rainy thunderstorms in June 2009. As a result, scuba diving operations served mostly to deploy temperature loggers (see next section) and take pictures to document their sites of deployment (see example in Fig. 21). There is also a set of photographs using a digital camera in a transparent pressure housing (Fig. 36a). The scuba diving surveys confirm some of the ROV footage of largely fine-grained drape with variable amounts of pebbles representing the dominant seafloor lithology in the landslide scar as well as along the steeper portion of the headwall. Above the escarpment produced by the 1979 failure, an area with a shallower slope gradient, the amount of pebbles increases significantly and in places appears almost like a “cobblestone pavement”. Sizes range from cm- to dm- diameter (Fig. 36b).



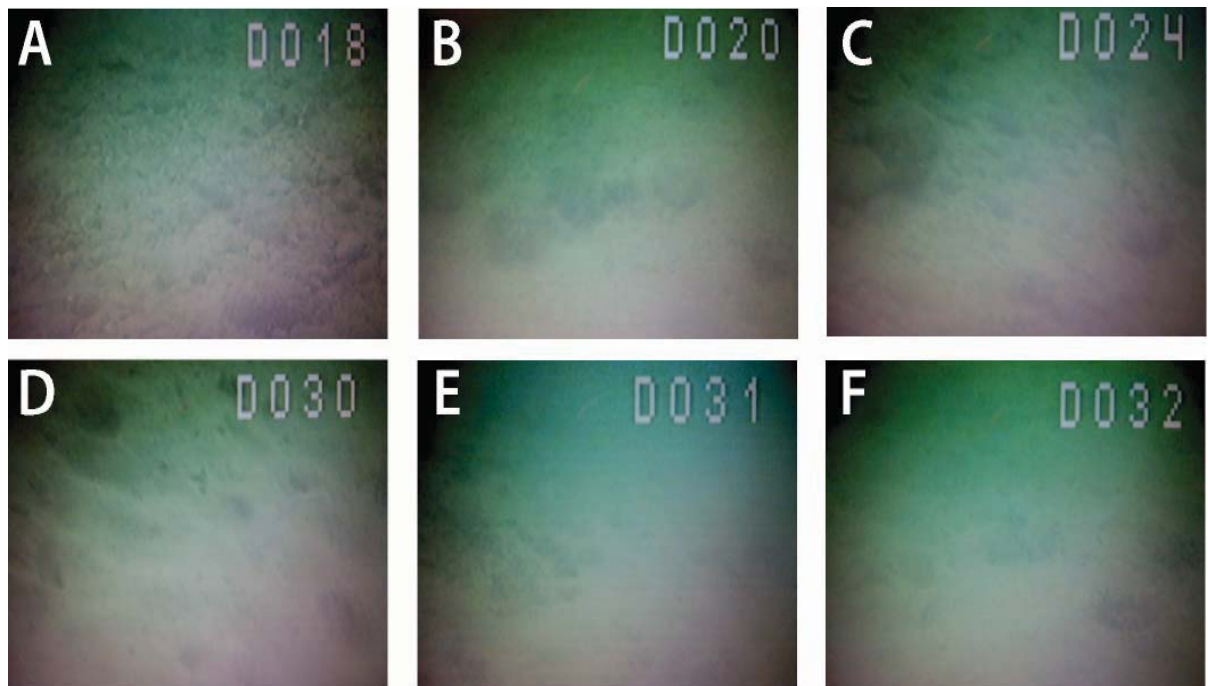
**Fig. 36:** (a) Scuba diver with camera preparing for dive during P386 operations; (b) pebbly seafloor above the headwall of the 1979 landslide. See fish (appx. 25 cm length) for scale.

Only one long successful dive could be carried out using ROV *Spy* before, as a consequence of bad weather and some mishap in navigation of the vehicle, the device was hit by the propeller of R/V *Poseidon* and could not be repaired on board. This dive, however, was a successful transect starting from some place above the headwall of the NAIL landslide scar resulting from the October 1979 event.

Given the cloudy seawater condition, daylight is limited and headlights were used additionally; hence, some of the still photographs shown here are of limited quality. What is apparent when studying the videos is the fairly flat topography just above the headwall. The seafloor seems to be paved with pebbles of small diameter ( $<5$  – ca. 10 cm across) with no or very little loose sediment in between. No clouds of dispersed material are experienced

when landing the ROV on the seabed (Fig. 37a). Vegetation is limited to the hummocky surface, and no larger seagrass or algae are observed despite operating in the photic zone (15-19 mbsl). When crossing the gently curved headwall while diving down, a drape of soft, loose deposits with occasional pebbles (now larger in size; Fig. 37b) are observed. Both the somewhat steeper gradient and the amount of clasts relative to sediment-covered seafloor continues to depths around 27 mbsl (see Fig. 37c as an example). At around 28 mbsl and below, the seafloor becomes less inclined and unconsolidated sediment prevails. The surface of the sediment shows depressions of small (<5 cm across) to medium size (10±5 cm across) which may represent fluid escape structures. Otherwise, the seafloor is smooth and populated by sparse vegetation (see Fig. 37d-f).

Owing to an increase in wind and swell and the close proximity to the airport of Nice, we had to recover the ROV unexpectedly at this point. Because of the lack of exact positioning of R/V *Poseidon* relative to the vehicle, the ascent of the ROV resulted in a collision with the propeller of the vessel. No other dives were possible during expedition P386 because of the structural damage to the vehicle.



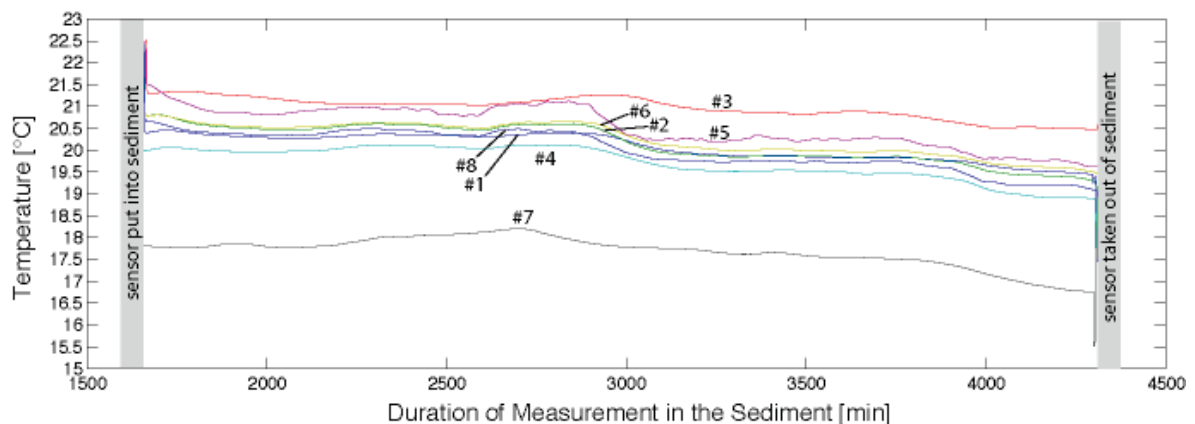
**Fig. 37:** Panel of ROV still photographs showing typical features from the headwall of the 1979 slide to its central scar in >30 m water depth. Numbers in upper right corner indicate depth in mbsl. (a) Flat area near headwall with a “pavement” of small pebbles (5-10 cm diameter); (b) Larger pebbles (15-20 cm) scattered on soft sediment; (c) inclined slope with pebbles of various size in headwall scar; (d) “pockmark”-like depressions (2-5 cm diameter) in soft, gently dipping sediment at base of headwall; (e) soft sediment with some algae and plant debris; (f) some vegetation and larger (5-10 cm diameter) depressions in the loose sediment (dewatering or degassing structures?). See text.

### 7.3.3. *In situ* temperature measurements

(A. Kopf, T. Pichler)

In order to test for venting of submarine groundwater discharge (SGD) in a very shallow area close to shore where operation of the R/V *Poseidon* (Fig. 13) is limited, a survey by research divers was carried out from June 26 to 29, 2009 using the vessel *Poseidon III* (Fig. 14). The objective was to deploy temperature probes (this section), to collect pore waters (see Ch. 7.3.8) and to visually survey the seafloor for venting of SGD (see previous Ch. 7.3.2). The purpose of deploying temperature loggers was to test if there would be a measurable change in pore water temperature across several tide cycles. If there had been a measurable change in temperature this would be interpreted as a result of changing the rate of venting as a result of the tide.

The transect was established in approximately east to west direction (110°) across a location where during previous M73/1 operations (Kopf et al., 2008) fresh water was encountered in sediment cores (Kopf et al., 2009). The transect was appx. 120 m long and the whole distance was roped and stakes were driven into the sediment every 10 m. Temperature loggers were then deployed at transect positions 0, 20, 30, 40, 50, 60, 70, and 120 m (see example in Fig. 21). The corresponding water depths were 15.5, 18.5, 19.9, 21.1, 20.5, 19.9, 22, and 29.5 mbsl. The end point of the transect was marked by a buoy, whose location was N43.64703 and E7.21861 (see map in Fig. 39).



**Fig. 38:** Temperature data from MTL deployment over almost 48 hrs. along a WNW-ESE transect from above the 1979 landslide headwall to a site close to the long-term piezometer station “Seamonice” (Fig. 39). Note that the westernmost sensor showed by far the lowest T signal, which is interpreted to represent SGD.

The temperature loggers went into the sediment from SE to NW in the following order: 7, 4, 1, 2, 8, 6, 5, and 3. Data of the deployment period, which spanned almost 48 hrs., are presented in Figure 38. It can be seen that a fairly consistent trend between temperature and



water depth is recognised. MTL #7 (29.5 mbsl) shows a significantly lower temperature (appx. 2.2°C) than the suite of other sensors, which scatter between 19 and 21°C (all deployed in the headwall of the NAIL scar). MTL #3 exhibits higher values (20.5-21.5°C), which is attributed to its shallowmost position (15.5 mbsl) above the scar of the 1979 landslide. The measurements indicate indirectly that groundwater seepage is unlikely to occur during the time of the deployment, because the MTLs show a consistent depth-dependent temperature trend. In the shallowmost subseafloor deposits near the headwall of the 1979 landslide scar (MTL #7), temperature is similar to ambient seawater (22-23°C) whereas in the landslide scar in appx. 30 mbsl, it is significantly colder (17-18°C). A SGD signal, which would be lower than ambient seawater during summer, can not unambiguously ruled out for the deeper part of the diving transect (which in fact ends close to the Seamonice station where fresh water is evident; see Ch. 7.3.8 below). However, rhizon sampling from the subseafloor locations equipped with MTLs does not support a groundwater influence (see Ch. 7.3.8 below).

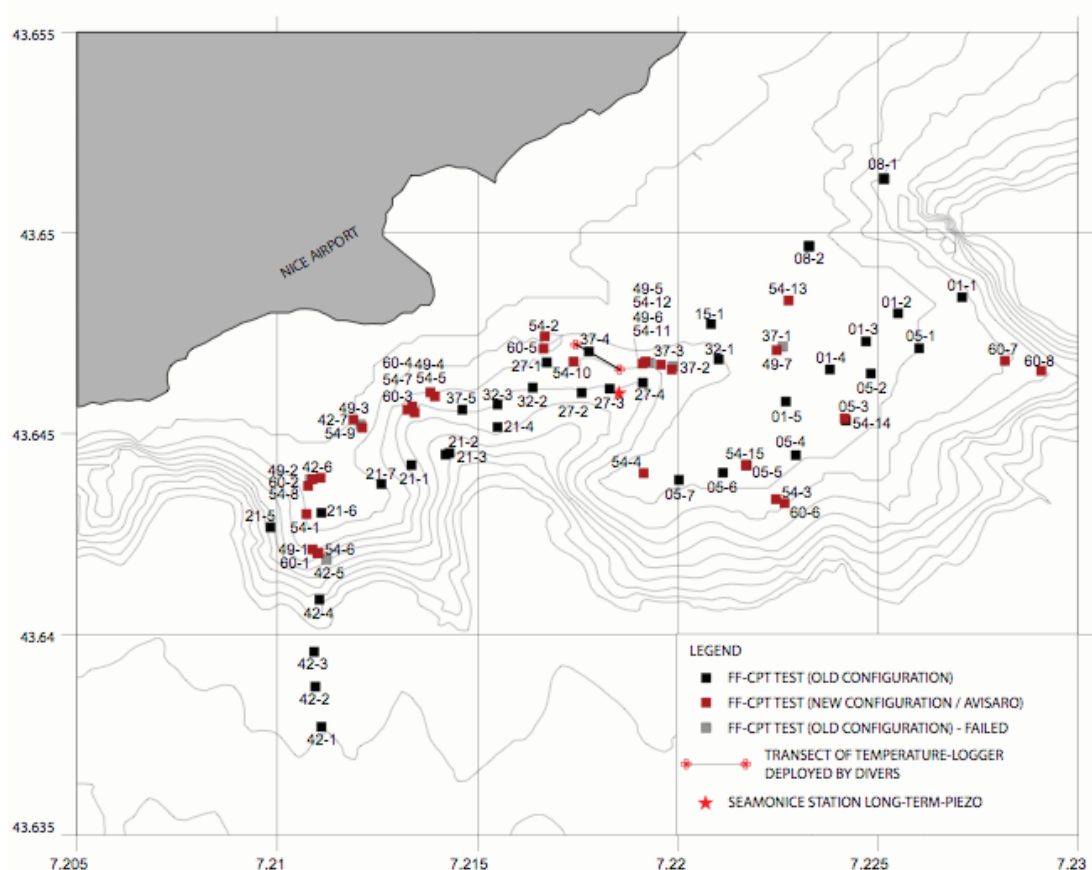
#### **7.3.4. *In situ* CPT testing**

(S. Stegmann, A. Kopf, A. Förster)

A total of 74 FF-CPT drops were conducted over the complete study area (Fig. 39) in water depths between 12 m and 200 m maximum (Table 1). Penetration depth ranged between 1 m and 4 m below the seafloor.

CPT deployments addressed following strategy:

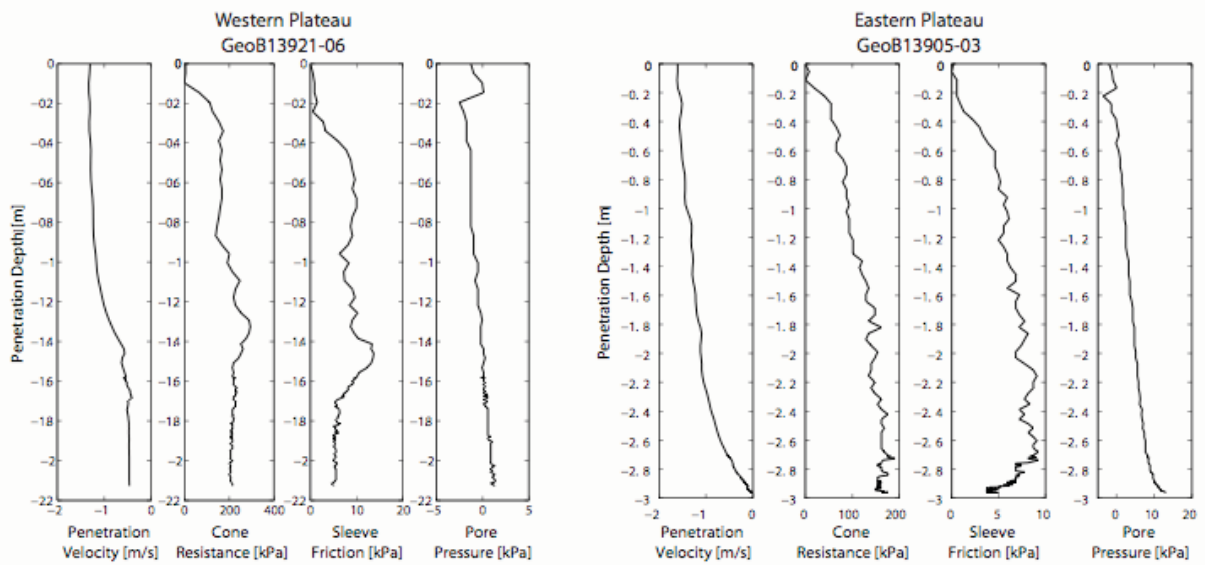
- Completion of the already existing FF-CPT data set of the M73 cruise (Kopf et al., 2008)
- Investigation of the spatial distribution of coarse-grained layers in the level of 40mbsl and its pore pressure regime
- *In situ* characterisation of sediments running down the western slope
- Comparison between freefall CPT test and CPT profiles pushed with constant velocity (Penfeld CPT, refer to report of PRISME cruise 2007: Sultan et al., 2008)



**Fig. 39:** Map showing the locations of the various FF-CPTu deployments carried out during cruise P386. Some “landmarks” are also shown: “Seamonice” site (star in centre of map), buoy and transect for scuba diving (grey bar).

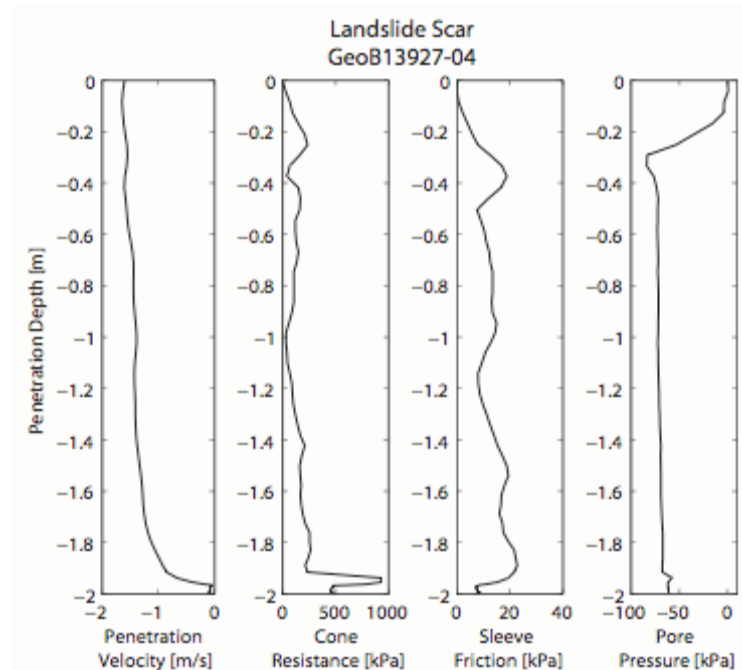
Owing to the huge number of the FF-CPTu profiles and limited space in the cruise report, only three profiles are illustrated here. They serve to represent the characteristic mechanical differences between the sediments on the plateaus (GeoB13921-06 [Western Plateau]; GeoB13905-03 [Eastern Plateau]) and in the landslide scar (GeoB13927-04).

The sediments on the plateau are characterised by low cone resistance  $q_t$  and pore pressure, which is rising after the penetration up to 100 kPa (Fig. 40). Dissipation is never reached in these profiles. Due to the soft und homogeneous composition of the sediments penetration is much higher than in the landslide scar. Maximum penetration depth is 3.70 (estimated, e.g. GeoB13914, -15). For some profiles on the plateau penetration depth is lower, maybe due to the occurrence of coarser-grained layers, which have been detected before with the Penfeld Penetrometer in these deposits (Sultan et al., 2008).



**Fig. 40:** CPTu records from stations GeoB13921 (W) and -05 (E).  
See text and map in Fig. 39 for location.

CPTu profiling carried out in the landslide scar delivered penetration depths ranging between 0.9 mbsf and 2.7 mbsf. When running deployments along the 40 mbsl isopach, the coarse-grained, gravel-bearing layer was hit nearly in all CPTu profiles and often terminated the penetration. Cone resistance increased here to up to 1MPa, as illustrated in Figure 41. In contrast to the profiles on both plateaus, pore pressure shows a dilatant behaviour with a sudden drop to negative values.



**Fig. 41:** CPTu record from station GeoB13927. See text and map in Fig. 39 for location.

GeoB 139-	LAT	LON	Date	WD [m]	PTR [m] estimated	PTR [m] calculated	Dissipation [min]
01-1	43,64845	7,22623	21.06.13	18,20	3,50	3,50	30
01-2	43,64812	7,22572	21.06.13	17,10	3,50	3,20	30
01-3	43,64727	7,22467	21.06.13	16,40	1,50	2,00	30
01-4	43,64662	7,22375	21.06.13	14,80	1,00	1,40	30
01-5	43,64585	7,22278	21.06.13	14,60	3,50	1,60	30
05-1	43,6471	7,22582	22.06.13	20,10	3,50	2,60	30
05-2	43,64653	7,22483	22.06.13	17,20	2,80	3,00	30
05-3	43,64617	7,22508	22.06.13	21,00		2,90	30
05-4	43,6448	7,22307	22.06.13	19,60	>1,5	1,80	30
05-5	43,64418	7,22177	22.06.13	18,20	3,50	2,20	30
05-6	43,64407	7,22115	22.06.13	17,80	3,50	2,20	30
05-7	43,64385	7,22003	22.06.13	15,80	3,50	4,00	30
08-1	43,6515	7,2252	23.06.13	51,00	1,50	1,40	30
08-2	43,6497	7,2232	23.06.13	13,50	2,00	2,20	30
15-1	43,6478	7,2209	25.06.13	13,30			
21-1	43,6442	7,2133	28.06.13	61,00	1,50	1,60	30
21-2	43,6445	7,2142	28.06.13	62,00	1,70	1,80	30
21-3	43,6445	7,2143	28.06.13	64,00	2,00	1,60	30
21-4	43,6451	7,2156	28.06.13	49,20	2,30	1,50	30
21-5	43,6427	7,2101	28.06.13	16,00	2,00	1,30	30
21-6	43,6431	7,2110	28.06.13	13,80	2,00	2,10	30
21-7	43,6438	7,2126	28.06.13	17,00	1,50	1,80	30
27-1	43,6467	7,2173	29.06.13	37,50	2,00	2,30	30
27-2	43,6461	7,2174	29.06.13	44,00	2,70	2,10	30
27-3	43,6461	7,2184	29.06.13	32,50	2,20	2,30	30
27-4	43,6463	7,2192	29.06.13	20,30	1,70	2,00	30
27-5	43,6467	7,2202	29.06.13	16,80	failed	failed	30
32-1	43,6467	7,2210	30.06.13	16,10	1,70	1,30	30
32-2	43,6461	7,2164	30.06.13	39,90	1,50	1,00	30
32-3	43,6458	7,2156	30.06.13	40,80	1,30	1,30	30
37-1	43,6472	7,2225	01.07.13	12,20			
37-2	43,6468	7,2201	01.07.13	18,00			
37-3	43,6468	7,2193	01.07.13	25,90			
37-4	43,6469	7,2176	01.07.13	31,10	2,00	1,00	30
37-5	43,6456	7,2147	01.07.13	41,10		1,90	30
42-1	43,6377	7,2111	02.07.13	17,60	2,20	1,40	30
42-2	43,6387	7,2110	02.07.13	14,70	3,60	3,60	30
42-3	43,6397	7,2109	02.07.13	116,00		2,00	30
42-4	43,6396	7,2109	02.07.13	112,00	1,10	0,90	30
42-5	43,6419	7,2111	02.07.13	62,00			
42-6	43,6438	7,2106	02.07.13	14,00			
42-7	43,6452	7,2120	02.07.13	22,00			
49-1	43,6421	7,2110	03.07.13	62,00	1,00	not processed	30
49-2	43,6439	7,2109	03.07.13	13,40		not processed	30
49-3	43,6454	7,2119	03.07.13	14,50	2,00	not processed	30
49-4	43,6457	7,2134	03.07.13	40,90	1,50	not processed	30
49-5	43,6468	7,2192	03.07.13	?	2,00	not processed	30
49-6	43,6466	7,2198	03.07.13	?	0,90	not processed	30
49-7	43,6471	7,2225	03.07.13	?	1,40	not processed	30
54-1	43,6429	7,2107	04.07.13	13,80	2,00	not processed	30
54-2	43,6474	7,2167	04.07.13	22,00		not processed	30
54-3	43,6433	7,2226	04.07.13	39,70	3,50	not processed	30
54-4	43,6439	7,2196	04.07.13	14,70	2,50	not processed	30
54-5	43,6461	7,2138	04.07.13	31,60	1,00	not processed	30
54-6	43,6421	7,2111	04.07.13	72,00	1,25	not processed	30
54-7	43,6456	7,2133	04.07.13	42,60	1,90	not processed	30
54-8	43,6437	7,2108	04.07.13	13,30	2,20	not processed	30
54-9	43,6451	7,2122	04.07.13	42,60	0,50	not processed	30
54-10	43,6468	7,2173	04.07.13	?	1,00	not processed	30
54-11	43,6468	7,2191	04.07.13	?	1,20	not processed	30
54-12	43,6467	7,2196	04.07.13	?	1,60	not processed	30
54-13	43,6484	7,2228	04.07.13	?	0,00	not processed	30
54-13	43,6486	7,2230	04.07.13	?	0,00	not processed	30
54-13	43,6487	7,2230	04.07.13	?	0,00	not processed	30
54-14	43,6454	7,2242	04.07.13	?	3,70	not processed	30
54-15	43,6442	7,2217	04.07.13	?	3,70	not processed	30
60-1	43,6421	7,2109	05.07.13	57,00	1,50	not processed	30
60-2	43,6438	7,2111	05.07.13	13,50	1,50	not processed	30
60-3	43,6459	7,2141	05.07.13	33,20	1,80	not processed	30
60-4	43,6456	7,2134	05.07.13	50,00	2,00	not processed	30
60-5	43,6474	7,2167	05.07.13	24,20	0,00	not processed	30
60-5 (repeat)	43,6471	7,2167	05.07.13	28,50	1,50	not processed	30
60-6	43,6432	7,2227	05.07.13	43,70		not processed	30
60-7	43,6468	7,2281	05.07.13	35,50	3,00	not processed	30
60-8	43,6466	7,2291	05.07.13	45,10	3,50	not processed	30

Table 1: List of CPTu deployments.



### 7.3.5. Piezometer deployments

(P. Pelleau, R. Approuial, S. Stegmann, A. Kopf)

#### 7.3.5.1. Operations

Three different types of deployments were carried out with the two piezometer instruments during cruise P386. The position of the tests and some details regarding the configuration of the probes and deployment procedures are summarised in Table 2.

##### *1. Longterm-installation at the SEAMONICE station using a Piezo v1*

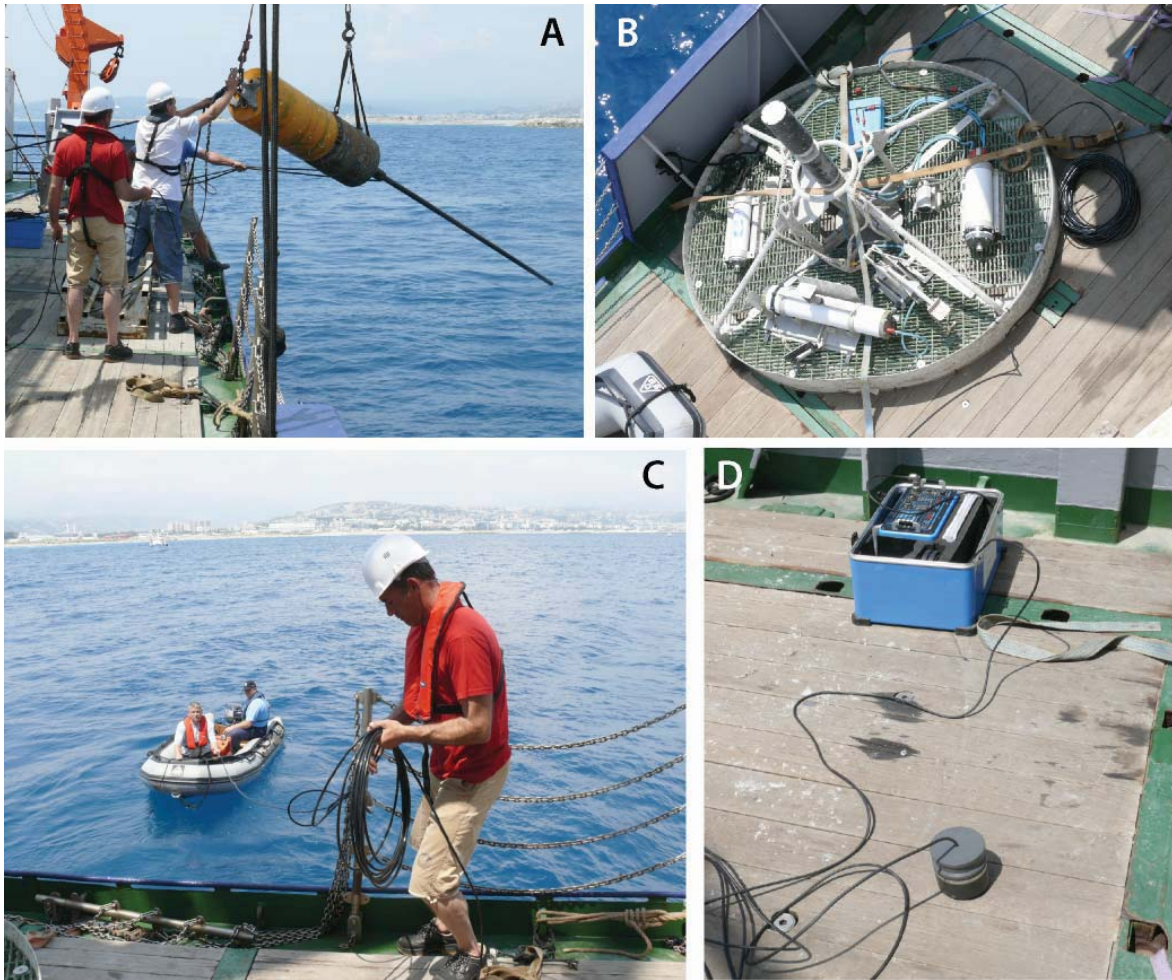
The longterm installation at Seamonice provided a continuation of longterm monitoring, which started with a Piezo v1 in November 2006. This instrument was recovered in spring 2009 as one of the connectors was broken and data download by scuba divers became impossible. After maintenance and repair the piezometer was re-deployed during Leg B of cruise P386. The capacity of the power supply is calculated for several years. The connection of the piezometer with the underwater station Seamonice allows an acoustic data transfer without recovery of the piezo.

The deployment at this position took place in several steps (see also Figure 42):

- a) At first the piezometer v1 was deployed at the same position as in the earlier installation (see Fig. 42a, and Sultan et al., 2008). It was lowered to a few meters below sealevel for saturation of the pore pressure lines, and then deployed at full winch speed (1.3-1.5 m/s).
- b) For the release of the piezometer, scuba diving activity was necessary because the acoustic release unit was not designed for weights exceeding 1 ton. As a result, a research diver released the shackle of the instrument (June 29, 2009 at noon).
- c) Once the diver had left, the underwater station (Fig. 42b) was lowered to the seafloor within a distance of 10 meters to the piezometer v1. During this operation the cable, which is used for the connection between the piezometer to the underwater station, was paid out simultaneously. It was crucial to hold both the cable from the deployed piezo v1, but also that of the Seamonice underwater station tight to ensure that Seamonice does not get placed onto the loose cable and possibly damage it. This operation was done using the dinghy with a technician handling the two ends of the cable (Fig. 42c).
- d) After the seafloor unit was acoustically released from the winch cable in appx. 5 m above the seafloor, it settled into its final position for long-term acquisition. The

technician then released the remaining loose cable to the seafloor and the dinghy was recovered.

For more details regarding the positions and configuration of the instrument, refer to Table 2. A simple acoustic communication test (Fig. 42d) between the ship and the Seamonice Piezo v1 was performed immediately after deployment to ensure that the long-term set up is working. This test was successful. In addition, the scuba diver who detached the shackle from the instrument attested by visual inspection and an underwater photograph that the instrument went into the ground vertically to subvertically. The first data set is anticipated to be downloaded by research divers during a cruise in early 2010 (on R/V *L'Europe* led by IFREMER).



**Fig. 42:** The “Seamonice” long-term deployment of piezometer v1: (a) Piezo v1 lowered over the side; (b) the seafloor unit for data acquisition, power supply and communication on deck prior to deployment; (c) dinghy operations to control cable handling during deployment; (d) pinger for acoustic communication test between instrument and ship.

## 2. *Short-term deployments using a Piezo v2*

The piezometer v2 (Fig. 43) was deployed on three different positions for periods of 24 hours each (yoyo-mode). Configuration of the lance for the piezo is given in Table 2. Water depth ranged between appx. 10 and 50m. For the duration of the measurement the instrument was decoupled of the wire of the vessel and “moored” with a buoy for recovery. The data were downloaded on board after each test.



**Fig. 43:** The piezometer v2 ready for deployment offshore Nice airport.

Deployment GeoB13933 took place on June 30, 2009 from 6.00 a.m. onwards. The instrument was first lowered above the planned position of deployment on the non-failed portion of the slope west of the NAIL 1979 scar. After 20 mins. on the wire in 10 mbsl for saturation of the pore pressure tubing, the device was veered at a rate of 1 m/s until it penetrated the sediment. It was then detached from the winch cable, and a surface buoy was mounted for the 24hr-dissipation test (Fig. 44). The position corresponds to that of a gravity core (station GeoB13946; see below and station list in Appendix 10.1).

On July 1<sup>st</sup>, 2009 GeoB13933 was ended by recovering the instrument (appx. 6.00 a.m.) and downloading the data on deck. After about an hour, while R/V Poseidon had drifted to the next position at the northern rim of the 1979 NAIL scar, the piezometer was deployed again for 24 hrs. following the above procedure (station GeoB13938). The position corresponds to that of gravity core GeoB13953 (see below and station list in Appendix 10.1).



The piezometer was again recovered on July 2<sup>nd</sup>, 2009 (6.00 a.m.), followed by successful data download on deck. It was noted that penetration was highly efficient since fine-grained sediment was found both on top of the base plate as well as various places on the weight set overlying the base plate (see Fig. 23 above). The instrument was redeployed at station GeoB13945 in the eastern, non-failed slope in the position where a gravity core was taken earlier (GeoB13919; see “Lithostratigraphy” section below and Appendix 10.1). A day later, the piezometer was recovered with a slight bent as a consequence of having pulled it out of the seafloor at an angle. Data were recovered successfully and the instrument was thereafter prepared for the long-term deployment (see next paragraph).



**Fig. 44:** Surface buoy of piezometer v2 after deployment offshore Nice airport.

Station GeoB-	Latitude	Longitude	Date	Test		WD [m]	Duration [h]	Sensors	Sampling Rate [s]	Weight in air [t]
13931	43.6457	7.2178	29.06.2009	Piezo v1	long-term	40,3	still installed	P1 (0.50m), P2 (1.50m), P3 (2.25m), P4 (3.00m), P5 (3.75m)	300	1,1
13933	43.6426	7.2110	30.06.2009	Piezo v2	yoyo	14,4	24	P1 (4.75m), P2 (0.80m), P3 (2.40m), P4 (1.60m), P5 (3.20m)	1	1,2
13938	43.6414	7.2123	01.07.2009	Piezo v2	yoyo	13,2	23	P1 (0.80m), P2 (1.60m), P3 (2.40m), P4 (3.20m), P5 (4.75m)	1	1,2
13945	43.6471	7.2166	02.07.2009	Piezo v2	yoyo	34,0	23	P1 (0.80m), P2 (1.60m), P3 (2.40m), P4 (3.20m), P5 (4.75m)	1	1,2
13959	43.6440	7.2194	04.07.2009	Piezo v2	long-term	15,2	still installed	P1 (0.80m), P2 (1.60m), P3 (2.40m), P4 (3.20m), P5 (4.75m), P6 (5.50m)	300	0,25

**Table 2:** Information regarding the deployment and configuration of the various piezometer tests.

### 3. Longterm-installation using a Piezo v2

After the yoyo-tests the piezometer v2 was deployed for a longterm-test at station GeoB13959. This location has been chosen to be identical to an earlier deployment by IFREMER during the *PRISME* cruise (Sultan et al., 2008). The capacity of the power supply

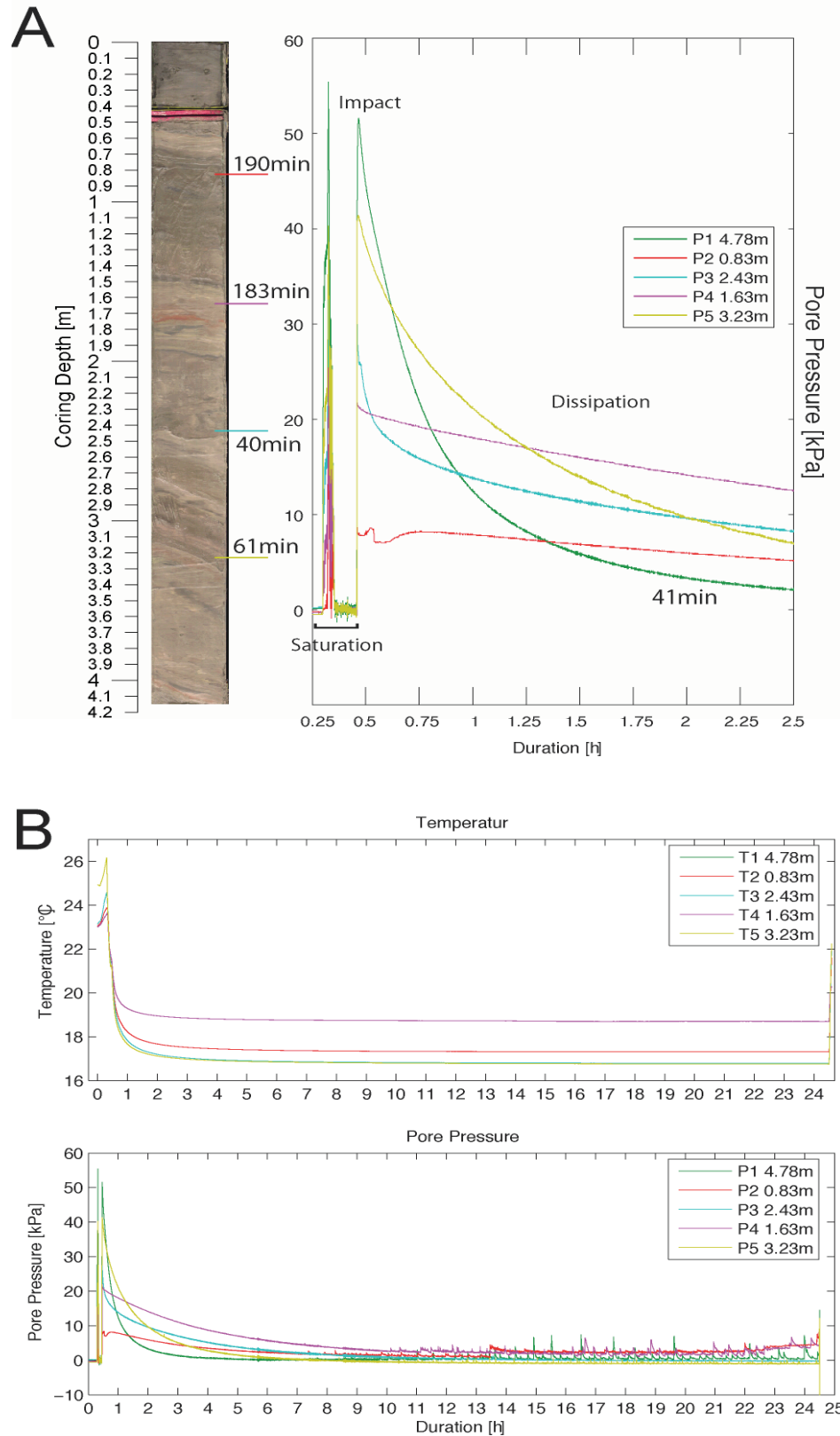


was calculated for 2 years and sampling was set to a period of 5 minutes. Sampling was synchronised with the Seamonice piezometer v1 to get a comprehensive data set from the pair of instruments in the stable (v2) and failed (v1 plus Seamonice) portion of the Nice slope. In contrast to the piezo v1, the new instrument cannot be visited by scuba divers for data download, but has to be recovered.

On July 4<sup>th</sup>, 2009, the piezometer v2 was prepared for the long-term monitoring task tentatively set up for 24 months. Preparation included the replacement of the bent section of the instrument, its elongation by another 75 cm-long segment plus one piezomodule, and attachment of a small buoyant device for it to be recognised by research divers for future recovery. After the obligatory saturation of the pore pressure tubing in the water column (9:30 a.m.), the device was deployed at 1 m/s winch speed. The weight set was then released acoustically and got recovered back on deck at 9:44 a.m. During the upcoming cruise led by IFREMER in early 2010 (on R/V *L'Europe*), divers will inspect the piezo v2 when downloading data from the v1 instrument.

#### **7.3.5.2. Preliminary results**

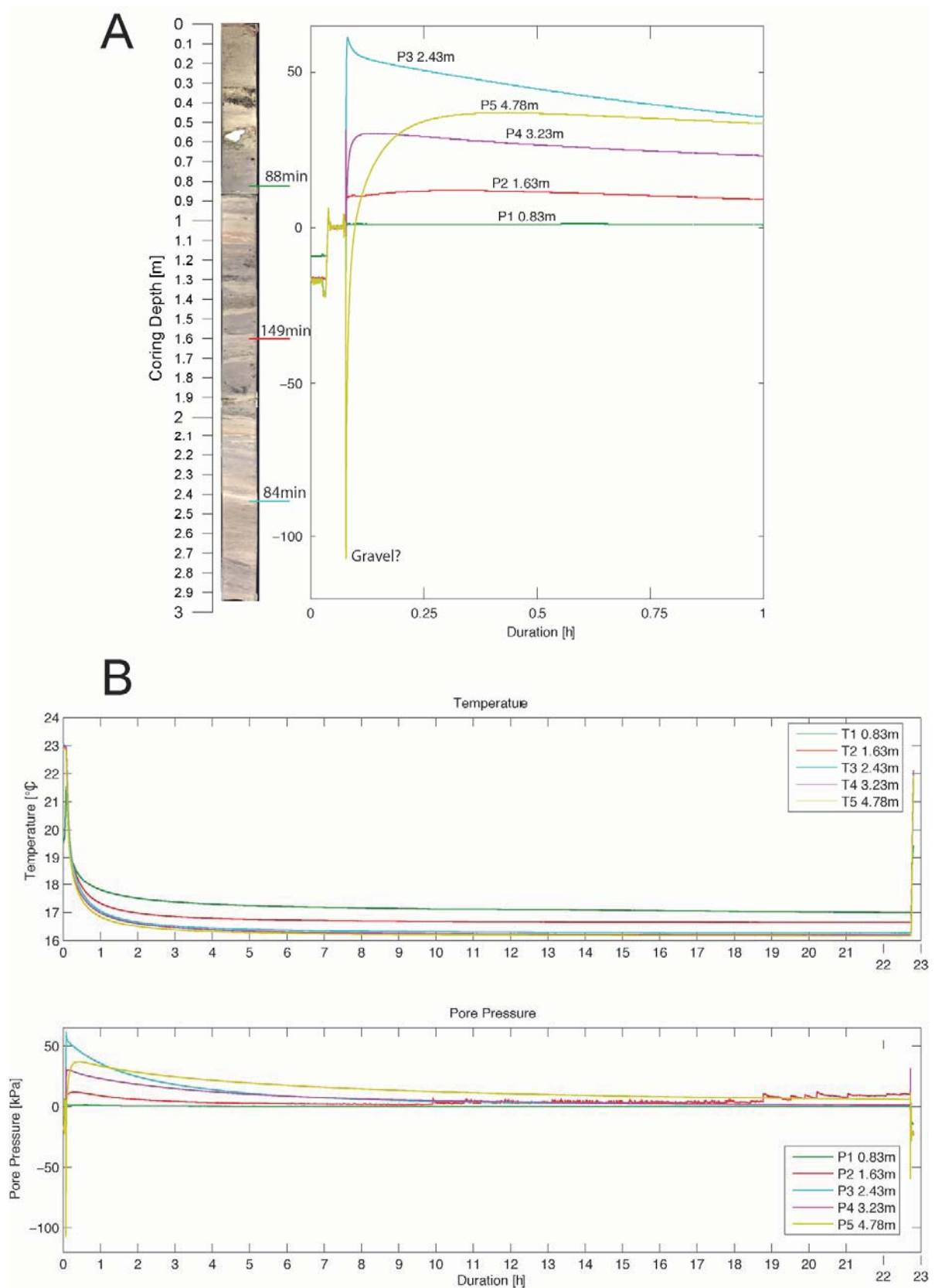
The first “yo-yo” style piezometer deployment targeted the non-failed portion of the Nice slope west of the NAIL scar. The measurement at five levels recorded the artificial pore pressure spike during impact followed by 24hr-dissipation curves (GeoB13933; Fig. 45). In the same position, core GeoB13946 recovered sediment down to 4.15 mbsf. The data illustrate that depending on the lithology encountered at each depth level, both the magnitude of the initial pressure spike as well as the  $t_{50}$  values from pore pressure dissipation (see Davies et al., 1991) vary significantly. In the shallow portion where clay-rich deposits dominate (level P2, P4; Fig. 45a), the decay of the initial pore pressure value is slow and half of the peak is reached only after 183-190 mins. In contrast, the somewhat siltier portion of the slope (below 2 mbsf) allowed fluid to be displaced during the insertion of the piezometer, and equally faster decay of the pore pressure pulse. As a consequence,  $t_{50}$  values range between 40 and 61 mins. (Fig. 45a) and decrease along shallower gradients. All pore pressure ports reach a “quasi-steady state” with a plateau after 8 and 11 hrs. after deployment and generally remain at this level for the remainder of the measurement period. At the deeper levels, those “background values” are very close to hydrostatic pressure at the respective depth (P1, P3, P5) whereas the shallower, less permeable deposits at level P2 and P4 show pore pressures of 2-4 kPa in excess of  $P_{hyd}$  (Fig. 45b).



**Fig. 45:** Data from piezometer v2 deployment GeoB13933 offshore Nice airport. (a) Data during insertion and  $t_{50}$  values derived from them. The locations of the individual piezo modules at depth is plotted on a gravity core photograph at the same site. (b) Long term behaviour of T and pore P at this station. See text.

There are two rather interesting phenomena observed in the second half of the 24hr. deployment. First, all pressure ports become increasingly noisy after appx. 7 hrs. and remain this way throughout. There does not seem to be a difference in noise level between the more permeable layers compared to the upper clayey levels. The spikes, sometimes a few kPa in magnitude, are not necessarily synchronous, so they can hardly be explained by tidal variations (the latter being rather small in the Baye des Anges anyway). At this level, we can only speculate about gas migration as a possible candidate to explain these patterns. The second interesting phenomenon was observed only in the slightly overpressured ports P2 and P4. After appx. 22.5 hrs in the deployment, the pore P level started to gently rise to levels of 5-7 kPa excess pore pressure (Fig. 45b). During the same period, the more permeable layers did not transmit any pressure change to the instrument. It is unclear if this late increase is approaching the “true ambient” background pressures, or whether external forcing in the shallowmost succession has to be held responsible.

For the second “yo-yo” deployment of the v2 instrument, the northern headwall area of the NAIL scar was chosen. The piezometer test (GeoB13938) is complemented by a gravity core taken in the same location (GeoB13953; see map in Fig. 48 below). Data from the piezotest are shown in Fig 46. Given that the core recovered was somewhat short of 3 m length, the lowermost piezomodules (P4, P5) are unconstrained regarding the lithology they were inserted into. The plot of the results vs. 24 hrs. of deployment reveals two distinct pore pressure responses. Ports P1-3 show the anticipated strong increase in pore pressure upon penetration of the instrument, which is followed by an exponential decay towards a background value. Calculated  $t_{50}$  values range between 40 and 61 mins. (Fig. 46a). In contrast, ports P4 and P5 show a less dramatic increase during insertion of the piezometer, which becomes less and less strong and tapers off towards maximum 10-30 mins., not seconds. After having reached the maximum value, pore pressure slowly decreases with time, eventually approaching ambient values. The majority of the pore pressure ports (namely P1, P3, P4) reach hydrostatic pressure over the course of the experiment. Transducer P2 at 1.63 mbsf also approaches hydrostatic levels, however, but after 10 hrs. within the test the signal becomes noisy and shows a subtle increase in pore pressure (Fig. 46b). This saw tooth pattern, which was also observed in deployment GeoB13933 (see above; Fig. 45b), becomes more accentuated after appx. 19 hrs.; the increase in noise is accompanied by an overall increase in pore pressure to values of  $10 \pm 2$  kPa in excess of  $P_{hyd}$  (Fig. 46b). An exception to the overall behaviour is the deepest transducer P5 (Fig. 46b).



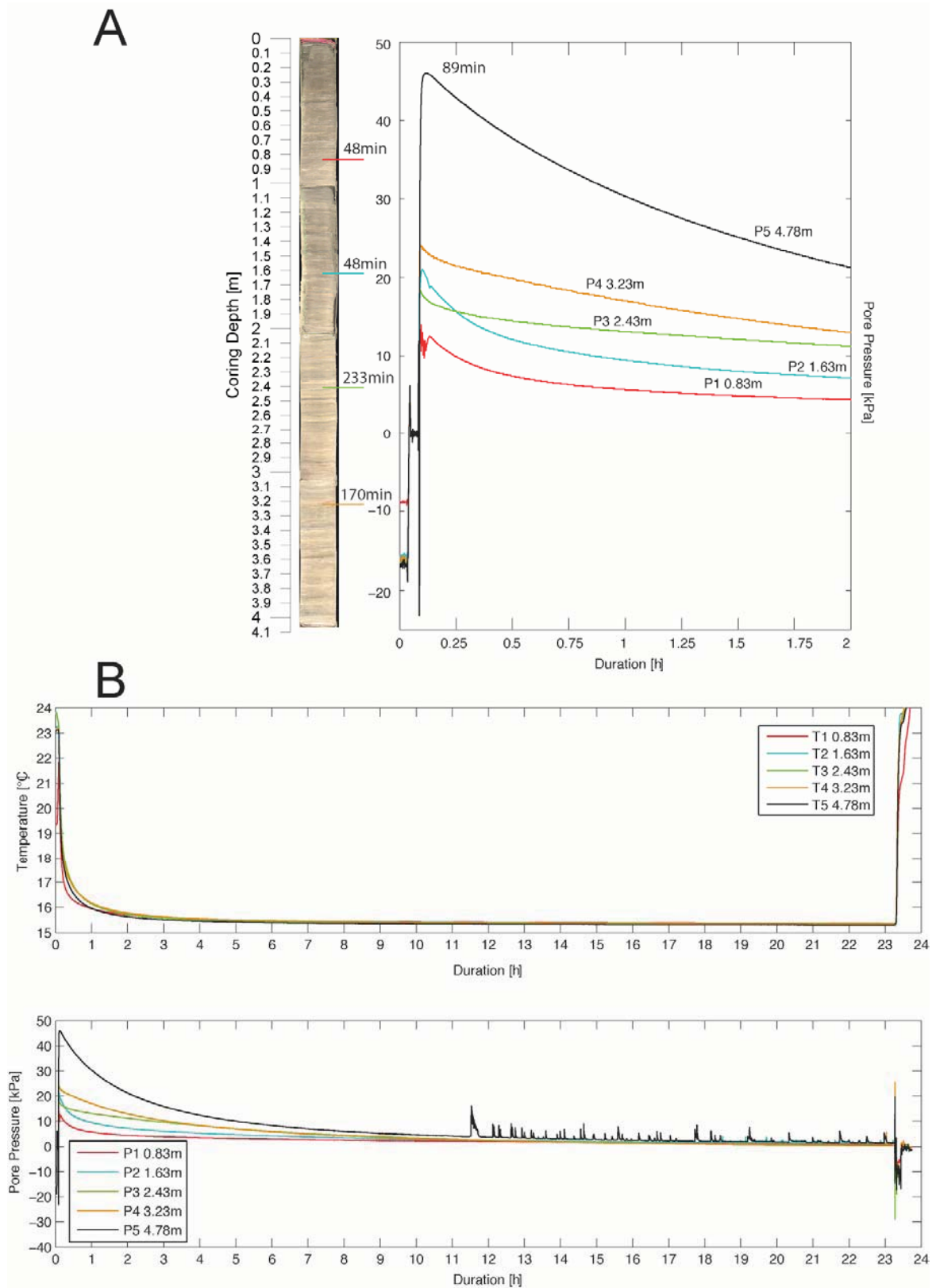
**Fig. 46:** Data from piezometer v2 deployment GeoB13938 offshore Nice airport. (a) Data during insertion and  $t_{50}$  values derived from them. The locations of the individual piezo modules at depth is plotted on a gravity core photograph at the same site. (b) Long term behaviour of T and pore P at this station. See text.



After having reached the maximum value, pore pressure levels off towards an excess pore pressure value of 6 kPa. Given that the gravity corer did not penetrate that far, it is unclear what lithology is related to the subtle overpressures. A careful comparison to quasi-static Penfeld CPT tests (Sultan et al., 2008) is required as part of the post-cruise research. In summary, core GeoB13953 was the most diverse of all gravity cores recovered during cruise P386 (see detailed description in section 7.3.6 on “Lithostratigraphy” below), so that it is not surprising that the pore pressure response is also found rather variable.

The third v2 deployment was positioned on the slope east of the NAIL scar. It mirrors the position of an earlier piezometer test in 2007 (PZ21-2; see Sultan et al., 2008) and is complemented by gravity core GeoB13919 (see 7.3.6 and Appendix 10.3). The piezometer test was also a pilot study for the long-term deployment of the v2 instrument, which was performed in exactly the same position later during the cruise (see station GeoB13959 in section 7.3.5.1 above; also refer to station list in Appendix 10.1).

Similar to test GeoB13933 at its western counterpart, all 5 piezomodule tests GeoB13945 east of NAIL show the typical strong increase in pore pressure during insertion of the probe. This spike is followed by a moderately strong (P3, P4) to strong (P1, P2, P5) decay (Fig. 47a), which results in  $t_{50}$  values of less than an hour (48 mins. for the upper, silt-dominated portion) and between 89 and 233 mins. for the clay-dominated section below 2 mbsf (see Fig. 47a, and Appendix 10.3). When regarding the entire period of the deployment, both T and pore P show a rapid exponential decrease towards ambient values. For the temperature, this is 15.5°C whereas the pore pressure is very close to hydrostatic values (maybe a little higher for P5 at the deepest level). Interestingly, this transducer also shows the noisiest record from approx. 11.5 hrs. into the deployment onwards, showing spikes that exceed the background decay curve by 5-12 kPa in places. Like for the variations depicted in the earlier deployments, it is not easy to explain those fluctuations. Despite the fact that free gas is inferred from geophysical data and observations on cores (see Sultan et al., 2008, in press, and section 7.3.6 below), it is impossible to assess with certainty that gas migration or expansion can be held responsible for pressures which in places are close to lithostatic values. Post cruise experimental work on the corresponding cores as well as the long-term data records from the two piezometers deployed for months to years will hopefully help explain some of these preliminary observations.



**Fig. 47:** Data from piezometer v2 deployment GeoB13945 offshore Nice airport. (a) Data during insertion and  $t_{50}$  values derived from them. The locations of the individual piezo modules at depth is plotted on a gravity core photograph at the same site. (b) Long term behaviour of T and pore P at this station. See text.

### 7.3.6. Gravity coring and sediment description

(A. Förster, T. Fleischmann, K., Weber, S. Stegmann, A. Kopf)

During cruise P386, we took 23 gravity cores as well as a pair of “bobcores”, the majority of which were recovered in the NAIL area. Gravity cores GeoB13910, -11, -12, -13 and -14 complemented earlier coring in the deeper (>1500 mbsl) research on the so-called “Western slide complex” adjacent to the Var Canyon (see M73/1 cruise report by Kopf et al., 2008, and Förster et al., 2009). The cores were left closed for shore-based geotechnical testing. For exact location of these cores, please refer to the station list in Appendix 10.1 below. An initial sedimentological description from post-cruise work is given in Appendix 10.2.

The two “bobcores” served as a proof-of-concept with the recently developed lightweight coring system. The recovery was found low (<50 cm) despite repeated use of the falling weight and the predominantly fine-grained material. Given that gravity cores were taken nearby, the two bobcores were also left unsplit and got archived. For exact location, please refer to the station list in Appendix 10.1 below.

The lithological description focuses entirely on the NAIL slide scar and adjacent slope. The wealth of cores is shown in map view in Figure 48. Broadly speaking, they can be separated into three groups: (i) cores in the headwall and scar area of the 1979 event; (ii) cores in the non-failed slope E, N and W of the NAIL scar, and (iii) cores recovered in somewhat deeper water where the slope has also been stable to date. All these cores were taken in water depths less than 100 mbsl except for core GeoB13918; for exact depths refer to station list in Appendix 10.1 below. The grouping of the cores is as follows:

Group I: Cores GeoB13925, -29, -30, -34, -39, -40, -53, -63 and -64.

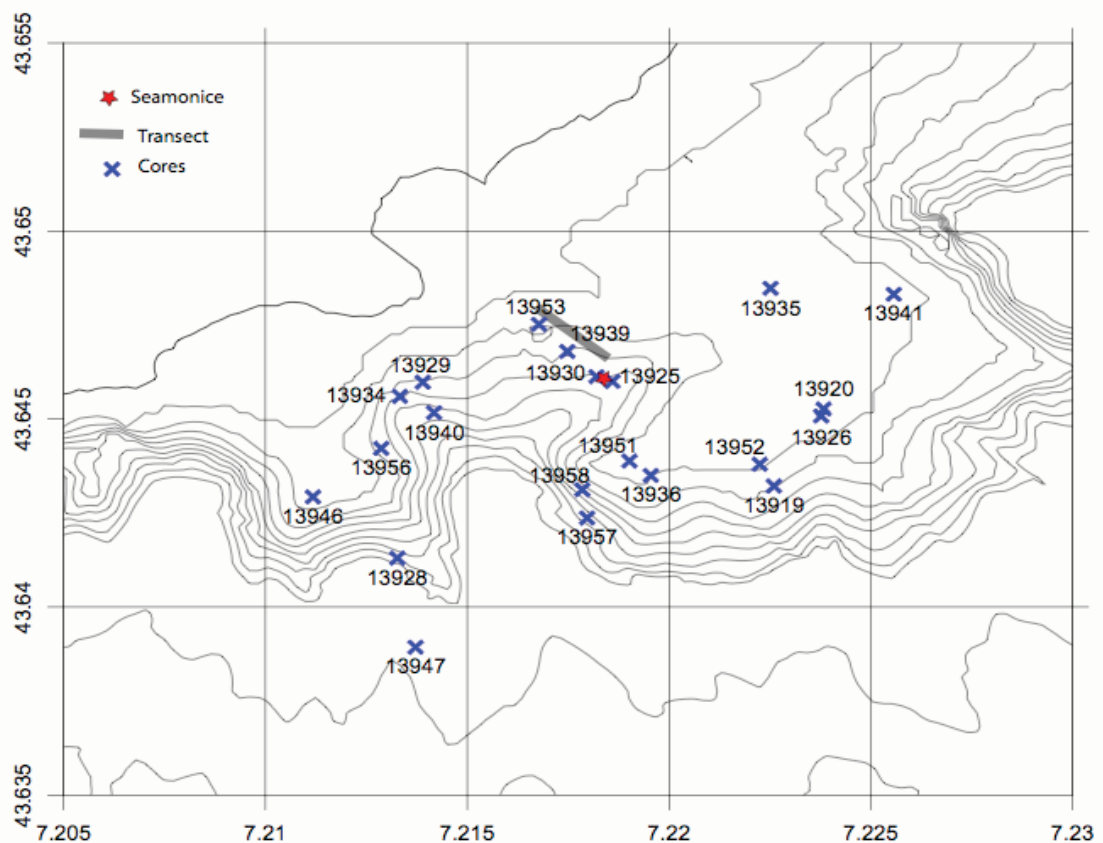
Group II: Cores GeoB13928, -46 (both W' of NAIL), and cores -19, -20, -26, -35, -36, -41, -42, -51, and -52 (E' of NAIL).

Group III: Core GeoB13947 (W' of NAIL), and cores -56, -57, -58 and -64 (E' of NAIL). In addition, cores GeoB13918 and -48 were taken south in and adjacent to a block of sediment which presumably slid to its present position in October 1979.

Note that the cores which are underlined above were not opened during cruise P386 so that core description does not exist.

Regardless of the geographical distinction into several groups, a group of gravity cores is also to be separated because they represent the shallowmost portion of nine locations where IODP drill sites have been proposed (IODP proposal 748-full by Stegmann et al., 2009).

These cores are GeoB13928 (NA-01), -29 (NA-02), -39 (NA-03), -40 (NA-04), -46 (NA-05), -47 (NA-06), -52 (NA-07), -19 (NA-08) and -18 (NA-09). Most of the NAIL cores plot in the vicinity of Nice airport, however, GeoB13918 (i.e. NA-08) lies some 2-3 km south of the 1979 scar in appx. 150 m water depth (see Fig. 12; and also Stegmann et al. [2009] and station list in Appendix 10.1).



**Fig. 48:** Map of the Nice airport region showing the locations of the majority of the gravity cores taken during P386. Note that cores GeoB13918 into a slid block of the 1979 event and -48 (a little north of -18) are located south of the map. The grey bar marks the scuba diving transect and the red star represents the “Seamonice” long-term piezometer.

When regarding the sediment recovered in the different areas, there is a clear separation between the groups. They are described one by one summarizing the main caharcteristic sedimentological and structural features. Detailed lithological columns with descriptions, grain size classification, and some physical properties are given in Appendix 10.2 below. Scanned images of the entire core s well as results from MSCL logging of the cores (split as well as unsplit ones) is found in the “Physical Properties” section below (Ch. 7.3.7) as well as on the DVD in the back sleeve of this volume (Appendix 10.3, only available electronically).



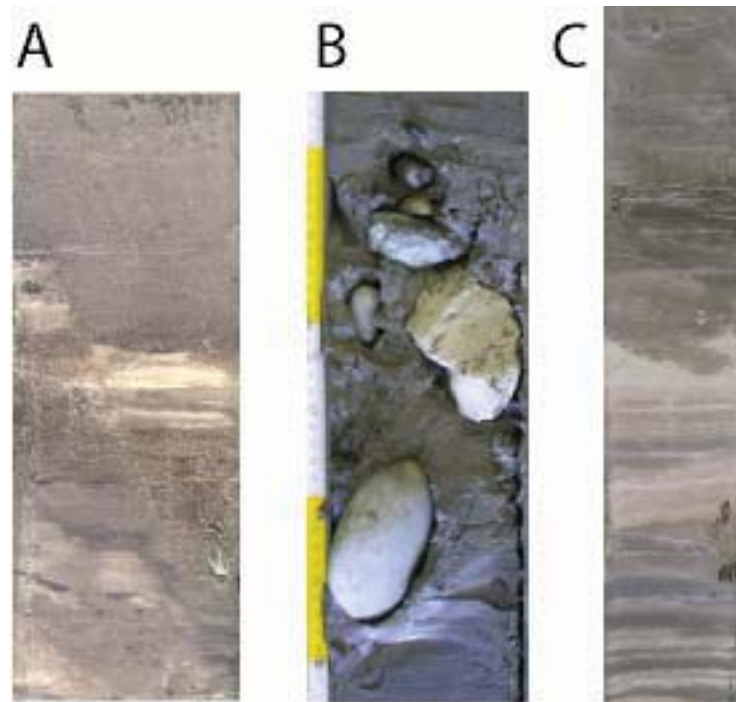
### *Group I cores in the 1979 landslide scar*

The headwall area and steeply inclined scar of the 1979 failure were among the main goals of coring and sampling during cruise P386. As a result, nine gravity cores targeted this zone in water depths between approximately 20 and 40 mbsl (Fig. 48). Core recovery was highly variable because fine-grained, soft sediments are interbedded with gravel layers.

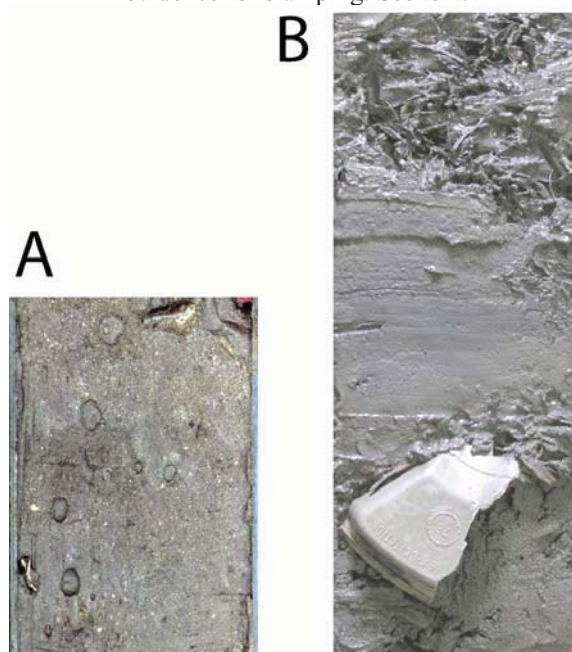
The major lithologies in the cores recovered were clays with variable amounts of silt. These sediments occasionally show darker, organic-rich layers (mm to a few cm) or lenses, but are usually medium to light grey to yellowish. Shell fragments, bioturbation, wood pieces or sand patches are also observed. Some of the clay-rich intervals show distinct fractures and conduits which were interpreted as evidence for fluid escape (see core GeoB13940 below 250 cm bsl; refer also to lithological descriptions, Appendix 10.3). Apart from core GeoB13940, each of the headwall cores also showed at least one layer of gravel (e.g. Fig. 49b). The size of the generally well-rounded pebbles varied from 1-10 cm across, embedded in a yellowish, sandy and silty matrix. Examples from cores GeoB13929, -30, and -34 are given in Fig. 49a-c and show the disturbed nature of some of the layers. The suite of observations include normal faulting, slumping, erosive contacts between layers, and entrainment of silt/sand into finer areas. For the full set of observations, refer to litholog diagrams in Appendix 10.2.

A extraordinary core was recovered at station GeoB13953 in the northern headwall (Fig. 48). It was taken right at the northern rim of the NAIL headwall in 19.7 m water depth. In the upper portion (0-140 cm bsf), it comprises predominantly yellowish to beige sand with pebbles and shell fragments, rarely interbedded with dark grey silt. The interval between 30 and 60 cm shows rapidly buried seagrass in large quantities (Fig. 50a) and further contains a several cm long plastic fragment, including the threaded opening of what appears to be a food container. The date of manufacturing of this artifact, 09/1976, is embossed into the fragment (Fig. 50b). We tentatively interpret this deposit as directly related to the 1979 catastrophic event, either as a landslide deposit burying seagrass or as a tsunami deposit in very shallow water. The plastic container may have served as a fisherman's buoy at the time, or was simply rubbish floating around. Below this rather unusual layer, silty and sandy layers are interbedded with finer-grained silt. In various places, thin, red clay bands and layers are observed. Clay lenses are also found and may represent remobilized material

associated with the landslide. Below 170 cm bsf, the sediment comprises almost pure clay (for details, see Appendix 10.2).



**Fig. 49:** Cores from the headwall area of the Nice airport slide. (a) GeoB13929, 147-162 cm with clearly developed normal fault in clay-silt interbeds; (b) GeoB13930, 47-78cm showing coarse gravel deposits in a yellowish to beige clay matrix; and (c) GeoB13934, 103-155 cm with tilted, sometimes erosive contacts and evidence for slumping. See text.

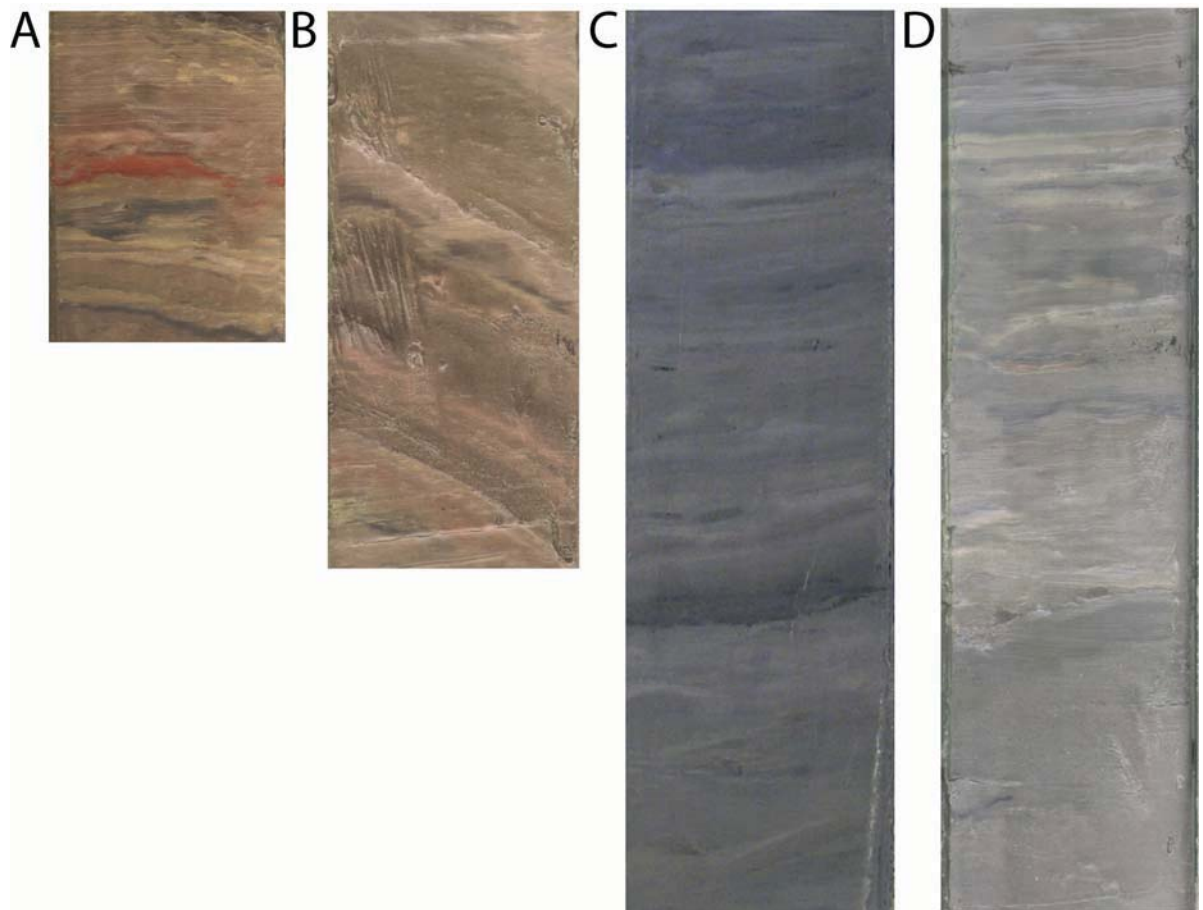


**Fig. 50:** CoreGeoB13953 from the headwall area of the Nice airport slide. (a) coarse-grained sand with pebbles (8-20 cm bsf); (b) Inferred „tsunami“ or „syn-depositional landslide“ deposit with the plastic bottle fragment with date (32-62 cm bsf).

*Group II cores at the non-failed slope adjacent to the 1979 landslide scar*

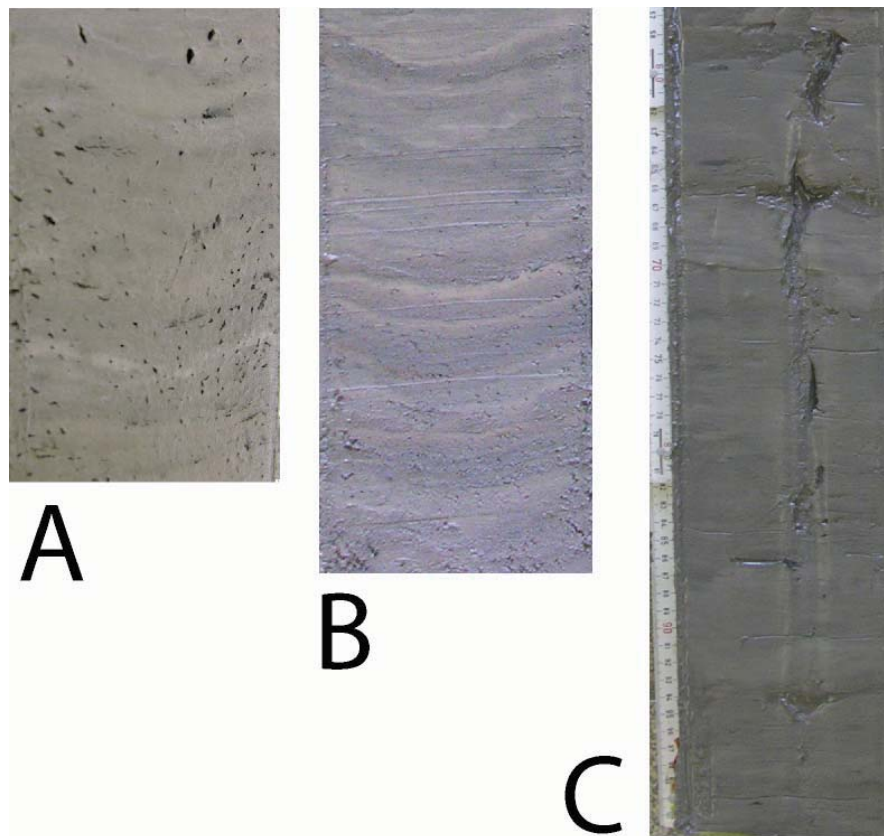
A total of eleven gravity cores were taken in the non-failed slope east (9) and west (2) of the 1979 NAIL scar (Fig. 48). Core recovery was generally good because of the poorly to normally consolidated sediments. The sediments comprise fine-grained (clay, silt) deposits of poor to normal consolidation. In several cores, underconsolidation and evidence for the presence of gas is observed. This is manifested by gas pockets and fluid escape structures as well as gas expansion cracks in the sediment (see Fig. 51).

The cores taken in the non-failed portion of the slope are rarely west of the slide scar (GeoB13928, -46), mostly because the “plateau there is rather narrow (Fig. 48). The majority was taken east of NAIL, namely cores GeoB13919, -20, -26, -35, -36, -41, -42, -51, and -52. Since one of the key goals of the expedition is to characterize some geotechnical properties, half of the cores in question were left unsplit and were shipped back to MARUM, Univ. Bremen. MSCL data of the unsplit cores are available in Appendix 10.3 (only on CD in back pocket).



**Fig. 51:** Cores from the slope adjacent to the Nice airport slide, often showing homogeneous, undeformed clayey sediments with occasional silt bands. Examples given are from intervals (a) GeoB13946, 36–49 cm, (b) GeoB13946, 69–89 cm, (c) GeoB13919, 328–365 cm, and (d) GeoB13952, 157–179cm. For location of cores, see Fig. 48.

The majority of the cores taken on the shallow-dipping slope east and west of the NAIL scar are characterized by homogeneous clay of brownish to ellowish and grayish colours. Colour banding and interbedding with silt is also common (e.g. Fig. 51). Rarely, irregular sedimentation patterns such as tilted surfaces or clay clasts and lenses are found. Given the extremely fine-grained matrix of the dominant lithology, permeability is low (Weber & Kopf, unpubl. data) and fluids are confined in these sediments at in situ conditions. Once the core is recovered and opened, fluids such as microbial methane expand and cause porous (mousse-like) textures and small (1-4 mm diameter) gas pockets in the otherwise undisturbed matrix (Fig. 52a, b). Aqueous fluid also migrated through the fine-grained sediment, causing entrainment of some matrix material during the ascent. Evidence for dewatering and fluidisation is found as near-vertical channels and conduits (e.g. Fig. 52c).



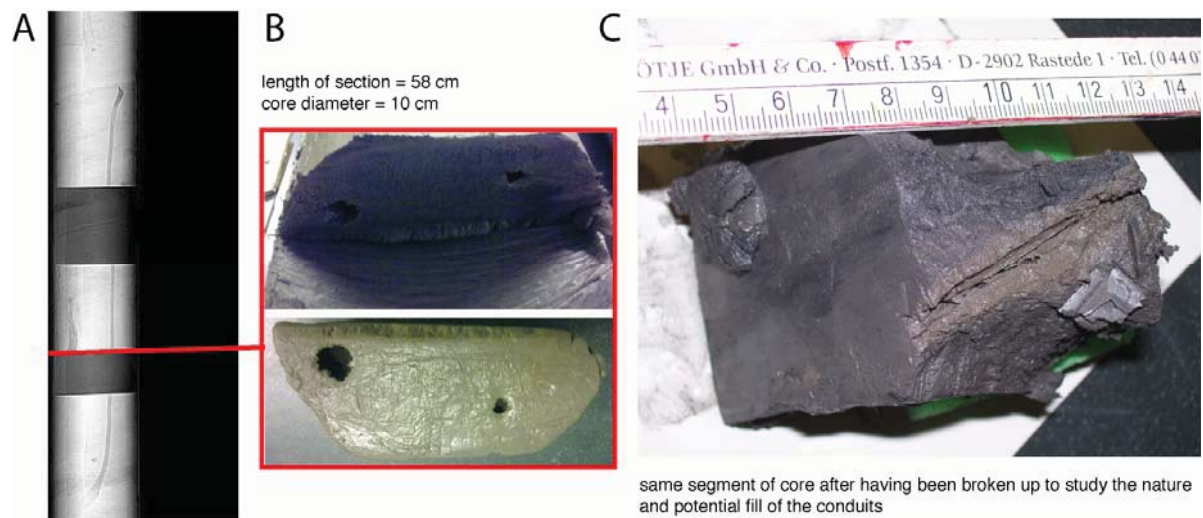
**Fig. 52:** Cores from the slope adjacent to the Nice airport slide, dominated by clayey sediments with abundant evidence for aqueous and gaseous fluids. Examples given are from intervals (a) disruption from gas expansion (b). Examples given are (a) GeoB13928, 286-300cm, (b) GeoB13946, 372-394 cm, (c) GeoB13926, 141-177 cm. For location of cores, see Fig. 48.

#### *Group III cores at the somewhat deeper slope*

This group can be divided into two subgroups. The first subgroup comprises cores GeoB13947, -56, -57, -58 and -62. It shows fairly homogeneous, fine-grained sediments which got recovered in cores of 4.59 to 5.39 m total length. These cores have mostly been



taken for post-cruise geotechnical studies on slope stability under different conditions. They were not opened except for a few sections of cores GeoB13957 and -58. Most interestingly, section GeoB13957-3 has several conduits of 5 mm to 12 mm diameter and several tens of cm in length (Fig. 53a, b). They are subvertical and intersect a clayey interval which is under- and overlain by silty, more permeable units. One of the conduits connects the two silt layers and may have been a result of fluidisation and release of overpressure by causing a predecessor to hydraulic failure (see Mörz et al., 2007).



**Fig. 53:** Core GeoB13957: (a) X-ray scan of a temporarily opened whole core cut layer-parallel in order to show the diameter of the fluid conduits (b); one segment was further broken up (c). See text.

In contrast, the second subgroup contains two cores located in significantly deeper water some 2-3 km south of the 1979 scar where the mass flow migrated downslope towards the Var Canyon. One of these cores, GeoB13918, equals the proposed drill site NA-09 into a portion of partly stratified sediment which is inferred a slid block. Three meters of silty clay with darker layers, fine- to medium sand interbeds and lenses, and occasional shell fragments were recovered. In the shallowmost portion, the clay layers are water-rich and free of internal structures. Deeper in the predominantly homogeneous core, areas rich in organic matter and irregular contacts occur (Fig. 54). Lenses of clay or silt are abundant between 100-200 cm bsl, however, it is impossible to decide whether they represent rip-up clasts. At the base of the core (290-300 cm bsl) is a gravel layer in which the gravity corer lost its momentum and did not penetrate further. The pebbles are well rounded, composed of quartzite and claystone/siltstone, and measure a few cm in diameter. Although the presence of these pebbly layers is generally associated with landsliding in the Nice area (see Group I above where each core has at least one pebbly layer, often the area where fresh water is measured (see “Geochemistry” section below), it is not clear at this stage whether the

material is unambiguously part of a remobilized block formerly located in the upper slope. The second of these cores, GeoB13948, is located somewhat upslope at the northern border of the inferred slid block. From seismic reflection data, the location may have “Upper Pliocene” substratum (*sensu* Savoye et al., 1993) cropping out at the seafloor. Since this stratum is an assumed potential failure horizon, we tried to sample it for geotechnical testing. However, the core has not been split and described yet.



**Fig. 54:** (a) Photograph of GeoB13918, interval 110-155 cm bsl, showing light to dark grey, clayey and silty deposits with irregular surfaces and erosive contacts. Top of core is left. See text.

### 7.3.7. Physical properties

(A. Förster, T. Fleischmann, S. Stegmann, K. Weber, A. Kopf)

Key physical properties for the landslide study offshore Nice Airport were measured on the fresh, split core (namely shear strength) and also shore based in a non-destructive manner (density, porosity, magnetic susceptibility and p-wave velocity using the MSCL). A number of other properties was further determined on discrete samples for specific projects and is not reported here. Instead, the following two subchapters focus on the shear strength and MSCL data. All shear strength data from fall cone experiments and vane shear tests can be found in Appendix 10.2; all MSCL data are given electronically in Appendix 10.3 (CD-ROM only).

#### ***Shear strength***

As for the core description, the shear strength data are presented as regional groups of cores. Group I in the headwall scar of NAIL often shows a gradual increase in strength, with values <10 kPa in the upper meter and then higher values (appx. 10-25 kPa for vane shear, and somewhat higher values for fall cone tests) below. Although layers rich in pebbles were avoided, maximum strength results may reach values >200 kPa (e.g. GeoB13925). We interpret these data as exceptions, possibly because a shell fragment or indurated clast was hit during the measurement. Silty and sandy horizons often show twice the strength as their

finer-grained counterparts. Areas with unusual deposits or other anomalies (e.g. the seagrass in GeoB13853) were avoided for strength measurement. Group II in the stable portion of the slope generally shows lower strength, because the majority of the cores recovered mainly clayey muds. Even long (i.e. >4 m) cores rarely exceed strengths of 10 kPa. All cores show a subtle increase in strength with depth, neatly mirroring incipient settling and compaction. Even fall cone data, which tend to accentuate shear strength trends because of the dynamic mode of measurement, plot below 10 kPa except for individual measurements (see GeoB13919 and -46, lower part) or core GeoB13926, where silt is more abundant. Group III cores remained largely unsplit, so that only GeoB13918 delivers shear strength data at this stage. Despite the fact that the main lithology is clay, the majority of the vane shear data ranges >10 kPa and the fall cone data largely plotting between 10 and 35 kPa. We tentatively interpret this observation as a result of the core being taken at position NA-09 (NAIL IODP drilling proposal by Stegmann et al., 2009). This site represents a block of slid material and, as a consequence, may have been modified during emplacement so that more indurated material is now in the shallow subsurface.

### ***MSCL***

From the suite of MSCL data, only density (and, derived from that, fractional porosity) plus some susceptibility information will be regarded. For all other data, refer to CD-ROM in back pocket (Appendix 10.3).

Group I cores in the NAIL headwall show average densities ranging from appx. 1.8 g/cm<sup>3</sup> (GeoB13925, -53) to 2.05 g/cm<sup>3</sup> (GeoB13934). In core GeoB13939, very soft mud (1.7 g/cm<sup>3</sup>) overlies significantly denser sediment (2.15 g/cm<sup>3</sup>). We interpret these variations as evidence for unroofing during the 1979 event, i.e. in places where densities are high the soft overburden got remobilized and transported downslope. Fractional porosity mirrors these trend in opposite direction, and magnetic susceptibility values often are high in sections where density is low owing to clay mineral-rich mud.

In Group II cores on the non-failed slope E and W of NAIL, many cores show low bulk density values of  $1.75 \pm 0.05$  g/cm<sup>3</sup>. Examples include cores GeoB13926, -28, -41, -51 and -52. Other cores show somewhat higher densities and porosities of appx. 45-50% (GeoB13920, -46). Core GeoB13919 shows exceptionally high densities (and resulting porosities of appx. 40%), which is in contradiction with the observations from core description and shear strength measurement (see above and Appendix 10.2). It appears that these soft (shear strength < 10 kPa) silty clays contain high contents of dark, fibrous organic

matter, which may be responsible for the higher density. Magnetic susceptibility and p-wave velocity do not show any unusual excursion in this core, so that post-cruise study on discrete samples may be required to confirm the density values of  $2.1 \text{ g/cm}^3$  on average.

Cores of Group III taken downslope of the landslide scar show consistent physical properties. Since the majority of these cores remained unopened, MSCL data are the only information about the material recovered at this point. In general, density shows a gradual increase with depth, starting at ca.  $1.7 \text{ g/cm}^3$  at the seafloor and gently increasing to up to  $1.9 \text{ g/cm}^3$  at the terminal depth of the core. Some cores appear extremely rich in fluid in the shallow sub-seafloor, starting with densities of  $1.5 \text{ g/cm}^3$  and porosities of ca. 70%. Magnetic susceptibility is generally below 10, however, there are two exceptions where values are fairly high: Cores GeoB13947 (0.6 – 3.3. mbsf) and -57 (0.7 – 2.2. mbsf). Since the latter core was opened and examined because of its fluid channels (see above and Figs. 53, 54b).

For a more comprehensive overview, see Appendices 10.2 and 10.3 below.

### **7.3.8. Pore water geochemistry**

(T. Pichler, S. Pape, S. Hammerschmidt, R. Price, M. Seydel)

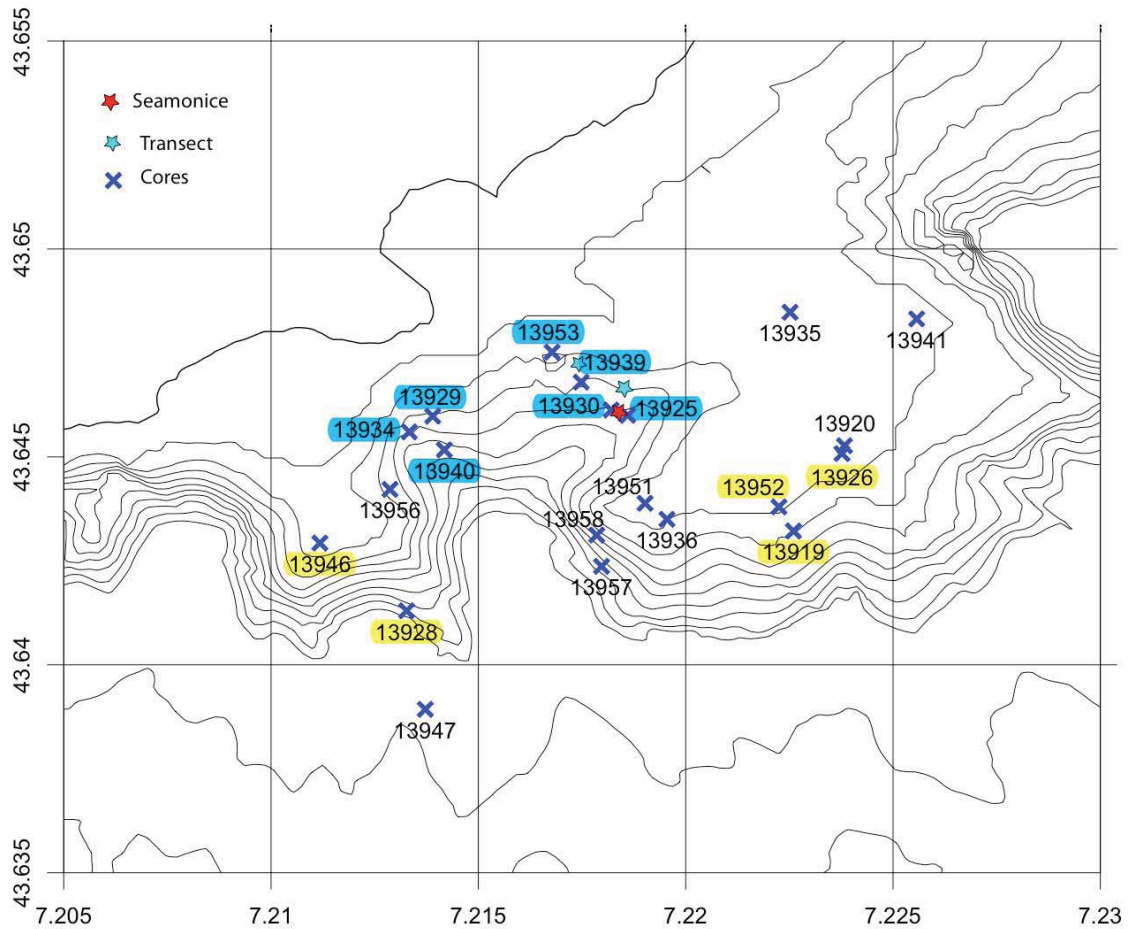
This chapter is split in two. The first (larger) section will tackle the pore water geochemistry of GeoB cores, while the second half will introduce the results from pore waters extracted from the shallowmost subseafloor using syringes.

In total 225 pore water samples were collected from 13 gravity cores and analysed for physical and chemical parameters. A detailed listing of these parameters is given in Tables X1 and X2. Salinity ranged from that of fresh to seawater, i.e.,  $<100 \text{ mg/L}$  to  $35\,000 \text{ mg/L}$ . Seven sediment cores (13925, -29, -30, -34, -39, -40, -53) showed a clear impact of freshwater, while cores 13919, -26, -28, -46, and 13952 had the pore water composition which indicated only seawater. Those cores where a fresh water component was observed were generally located in the center of our study site (Fig. 55). Fresh water, although present in the cores, did not seem to exit the sediments in the form of submarine groundwater discharge (SGD). All the pore water profiles changed to more or less seawater composition within the top 50 to 100 cm (Fig. 56). This was also confirmed by the pore waters, which were collected by scuba (see below). In general, the pore water profiles can be divided

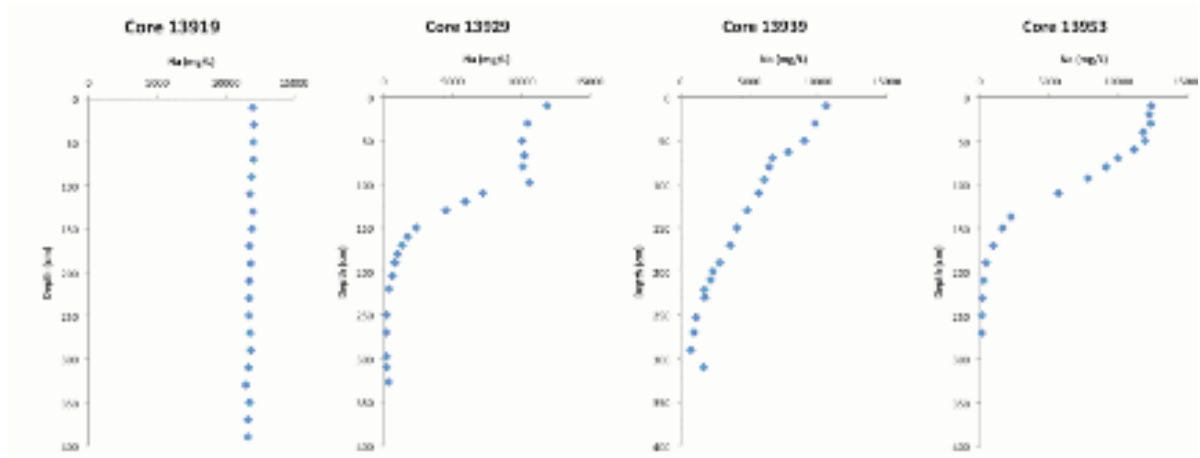


following Schlüter et al. (2004):

- profiles which did not show any fresh water impact (linear profiles of Cl and Na);
- profiles where fresh water is present at depth and where curvature of the Cl and Na data series indicates that some advective transport was present;
- profiles where fresh water is present at depth and where the linearity of the Cl and Na data series indicates that diffusive transport was present.

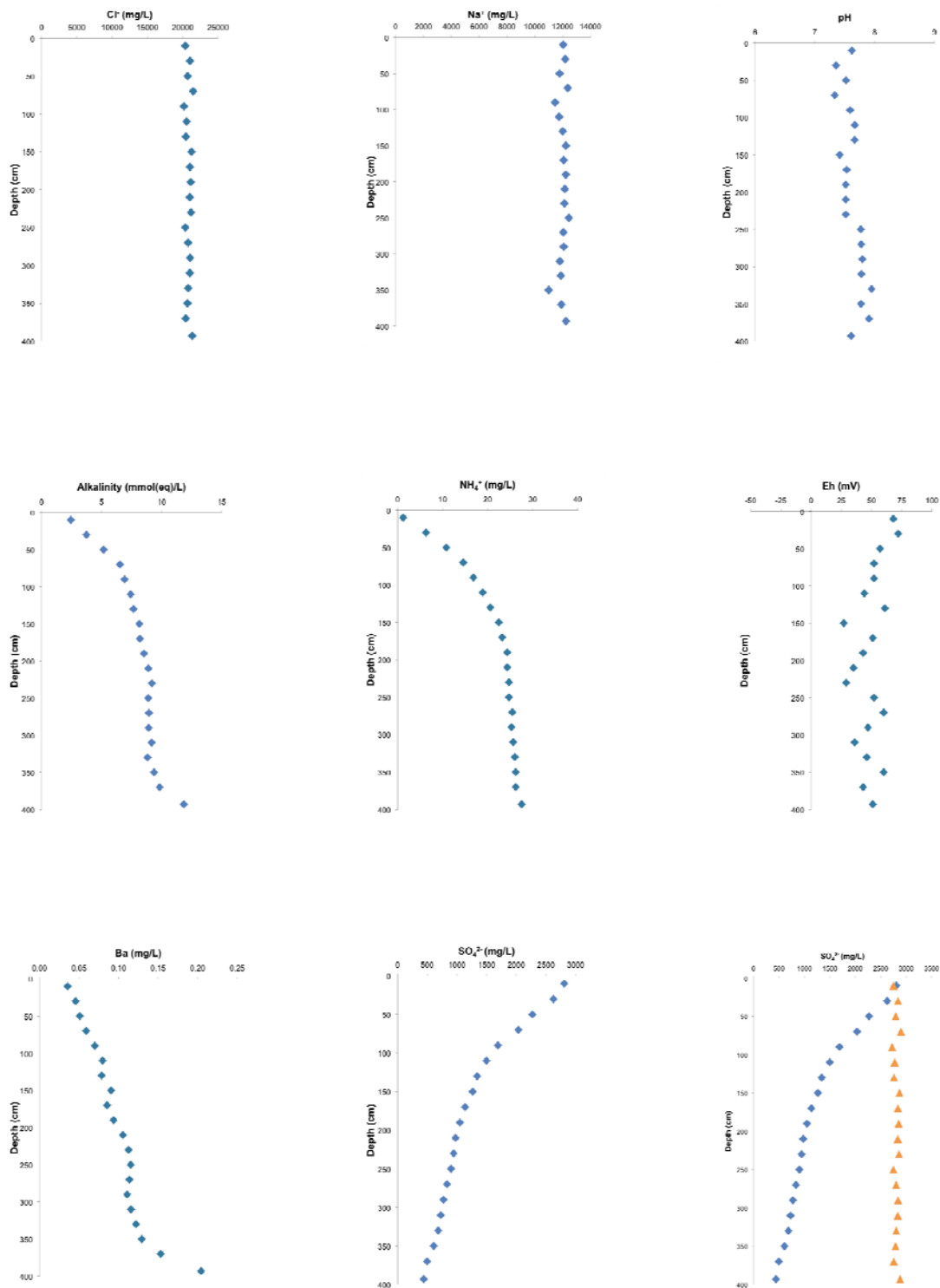


**Fig. 55:** Location of those gravity cores where pore water profiles were collected. Site numbers highlighted in “yellow” indicate pore water profiles with seawater salinities and linear Cl and Na data series. Site numbers highlighted in “blue” indicate pore water profiles, which contained a fresh water component.

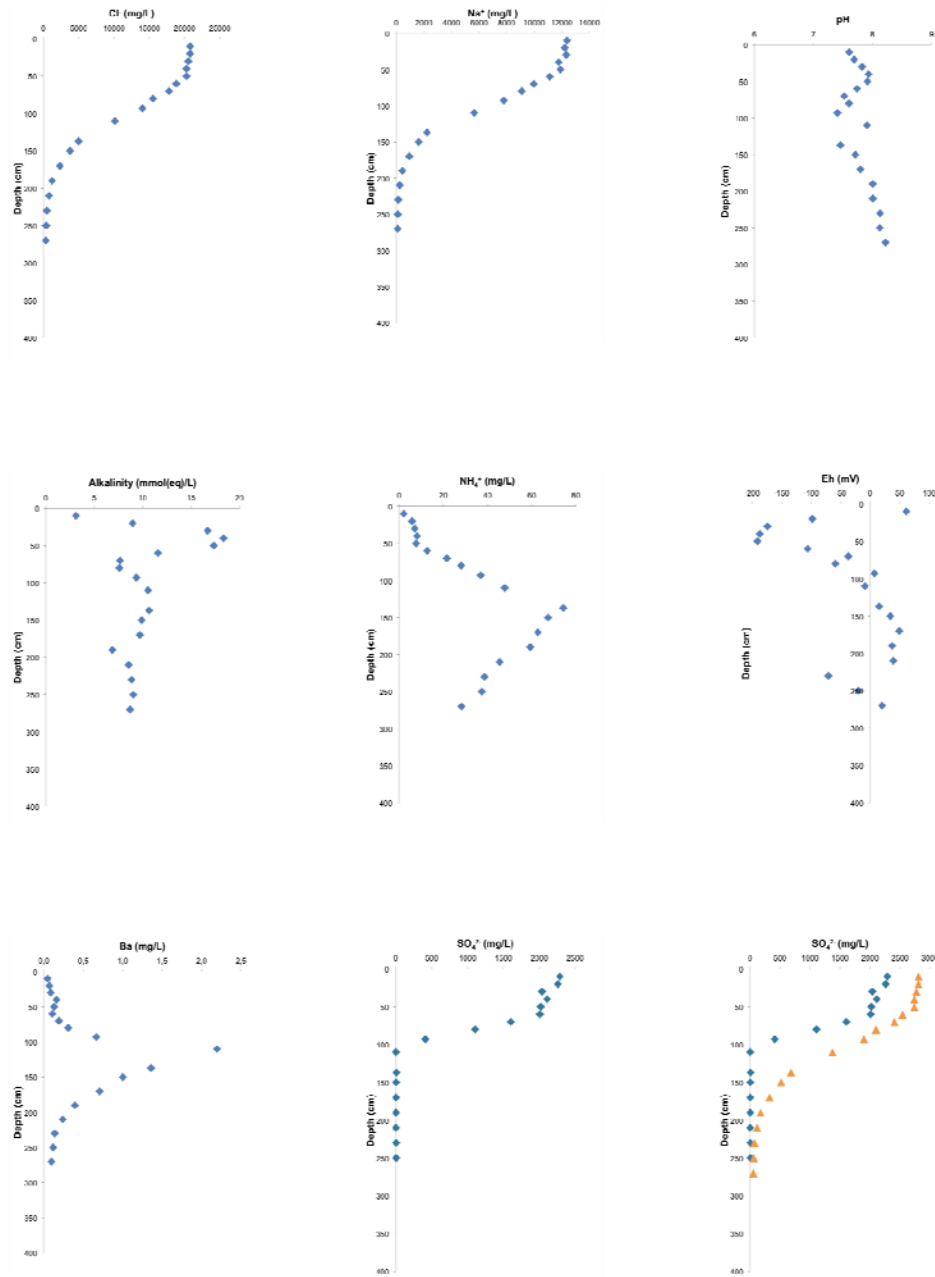


**Fig. 56:** Pore water profiles of sodium (Na) concentration in mg/L for cores 13919, -29, -39, and -53.

The pore water profiles 13952, 13953 and 13939 were examined closer, because they are examples for (a) a seawater water dominated profile, (b) a profile with advective transport and (c) a profile with diffusive transport, respectively. These profiles are presented in Figures 57, 58 and 59.



**Fig. 57:** Pore water profiles for Cl, Na, pH, Alk, NH<sub>4</sub>, Eh, Ba, SO<sub>4</sub> and SO<sub>4</sub> calculated for gravity core 13952. The yellow triangles in the profile in lower right corner represent SO<sub>4</sub> values, which were calculated based on the Cl/SO<sub>4</sub> ratio in seawater.

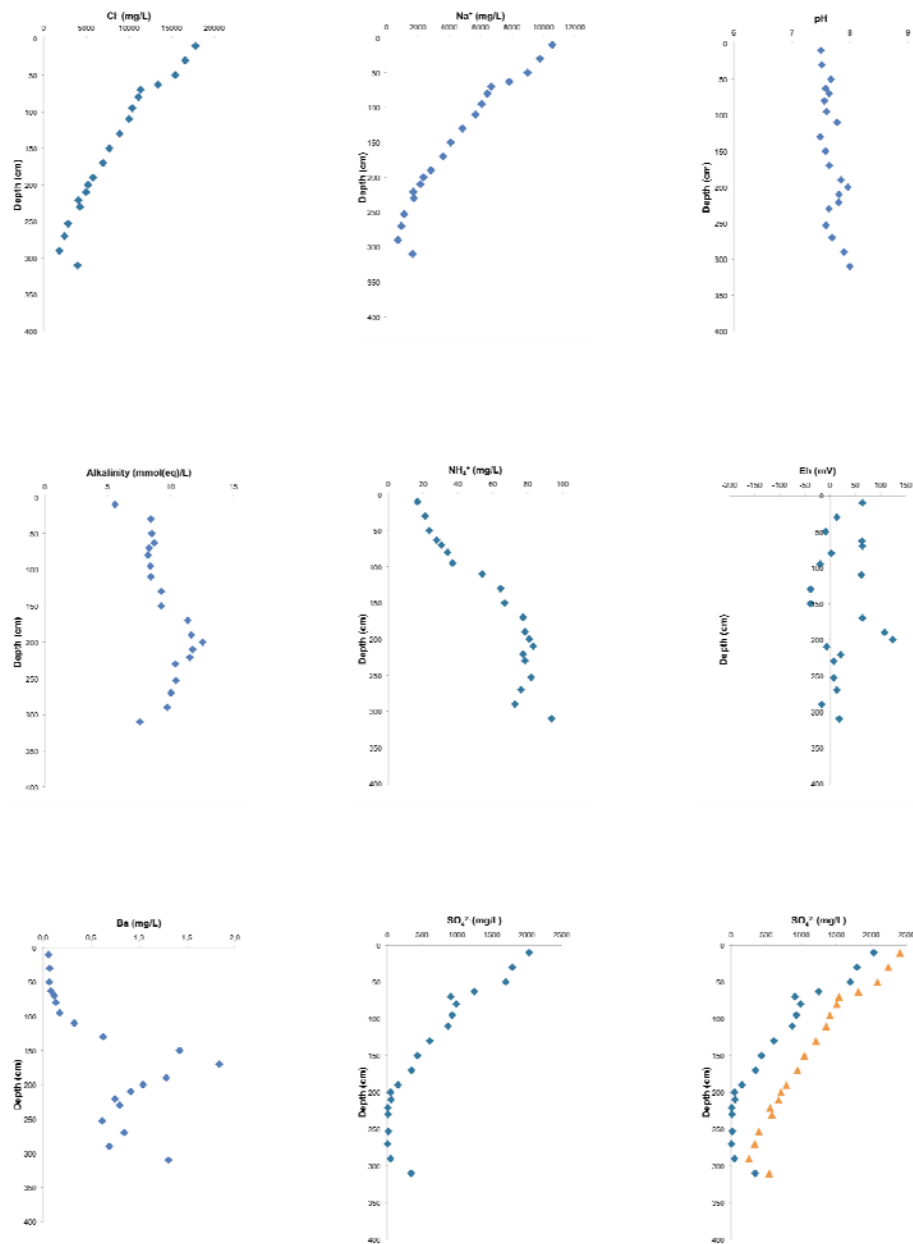


**Fig. 58:** Pore water profiles for Cl, Na, pH, Alk, NH<sub>4</sub>, Eh, Ba, SO<sub>4</sub> and SO<sub>4</sub> calculated for gravity core 13953. The yellow triangles in the profile in lower right corner represent SO<sub>4</sub> values which were calculated based on the Cl/SO<sub>4</sub> ratio.

Pore water profile 13952 was chosen as a representative of a profile dominated exclusively by seawater. Here, all Cl and Na values show no variation with depth and values were around 20,000 mg/L for Cl and 12,000 mg/L for Na, which are representative of Mediterranean seawater. pH values showed a little variation generally ranging between 7.4 and 7.6. These values are slightly lower than expected for seawater. Alkalinity and ammonia increase with depth to several times seawater values. Eh shows some variation, which is likely to two the uncertainty of the measurement, however, values are always positive. Barium increases with depth from the seawater value to about 0.2 mg/L. Sulfate declines



from almost 3000 mg/L (a value expected for seawater) to about 500 mg/L since Cl and Na do not show this decrease in concentration it is expected that sulfate does not behave inert. The likely explanation for the decrease in sulfate is microbial reduction to sulfide (e.g., Schulz et al., 1994; Winfrey et al., 1981). The amount of sulfide production can be estimated based on the Cl concentrations. Assuming that the Cl/SO<sub>4</sub> ratio in seawater is constant, the concentration of sulfate can be calculated using the measured Cl value. The comparison between the measured and calculated sulfate profiles can be seen in Fig. 57. Sulfate reduction increases constantly with depth.



**Fig. 59:** Pore water profiles for Cl, Na, pH, Alk, NH<sub>4</sub>, Eh, Ba, SO<sub>4</sub> and SO<sub>4</sub> calculated for gravity core 13953. The yellow triangles in the profile in lower right corner represent SO<sub>4</sub> values which were calculated based on the Cl/SO<sub>4</sub> ratio.

Pore water profile 13953 was chosen as an example of advective transport as indicated by the curvature of the Cl and Na profiles. Both start at sea water concentration and remained stable to about 50 cm sediment depth, after which they decreased to concentrations expected for groundwater in the area (Guglielmi & Mudry, 1996; Guglielmi & Prieur, 1997). pH increases to about 8 in the top 50 cm then declines again to about 7.4, followed by an increase to 8. The pH value of 8 at 110 cm should be evaluated as an outlier – potentially due to an unreliable measurement. Alkalinity shows a similar profile to pH with the exception of the outlier at 110 cm, however here variations are more pronounced. A sharp increase in the top 50 cm is followed by a sharp decrease over the next 40 cm. Ammonia increases to a depth of about 150 cm from seawater values to 80 mg/L and then decreases towards the bottom of the profile to about 20 mg/L. Eh values are extremely negative in the top 50 cm where the seawater seems to be the dominating pore water source. This contrasts the Eh profile seen in core 13952, which was chosen to be the seawater example. Barium shows a very similar profile to that observed in core 13939 (see below), except that the highest barium value is already reached at about 120 cm sediment depth. The reactive layer in which Ba is released from the sediment to the pore water coincides with a sharp decline in sulfate. Thus the barite solubility is the likely control for its concentration in the pore water. Sulfate remains more or less stable in the top 50 cm of the rich there is a sharp decline over the next 50 cm down to a sediment depth of 100 cm, a depth at which its concentration is close to that expected for groundwater in southern France (Guglielmi & Mudry, 1996; Guglielmi & Prieur, 1997). This however is not likely explained by the presence of groundwater, but rather by microbial sulfate reduction. Based on the same assumption as for core 13952 a sulfate profile was calculated (Fig. 58). In the calculated profile groundwater concentrations are only reached at a depth of 210 cm. Interestingly is the decline in concentration much less dramatic than in the measured profile, indicating the presence of a pronounced reaction zone.

Pore water profile 13939, which is representative of diffusive transport (Fig. 59), shows more or less a linear decline in Cl and Na concentrations with depth. PH remains relatively stable at around 7.5 to 7.8 and only at the depths of 200 and 300 cm values approach those anticipated for seawater. Alkalinity and ammonia increase to a depth of about 200 to 220 cm after which they remain more or less constant. Barium values start at approximately seawater concentration and increase sharply to about 2 mg/L at a depth of 180 cm after

which the concentration decreases sharply but never falls below 0.6 mg/L. The sulfate concentration show the same linear decline, which was observed for Cl and Na, however, again sulfate values were slightly lower than expected (exclusively explained by mixing seawater and groundwater). The calculated profile shows much less variation and the decrease between 50 and 300 cm is more or less linear – exemplifying diffusion as the important process (Schlüter et al., 2004). Detailed results are also reported in Tables 3 and 4 (available on CD-ROM in back pocket).

#### *Sediment geochemistry*

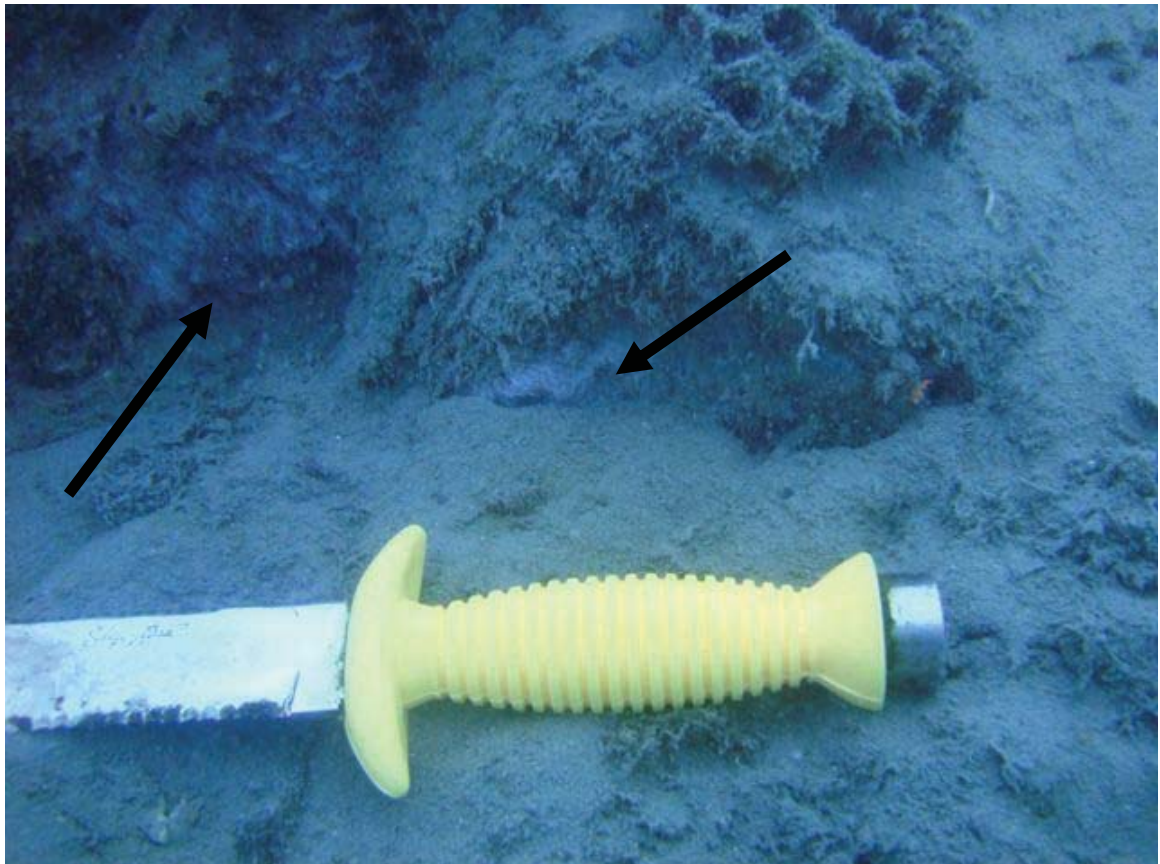
The results for those cores, which were selected for chemical analyses by total digestions and ICP-OES are presented in Table 5 (available on CD-ROM in back pocket). Despite the large variation in pore water profiles and the presence of fresh water only little variation was observed in the chemical composition of the sediments. Most values varied within their analytical uncertainty. Particularly surprising was that Ba values did not vary, considering the large increases of Ba in the pore water fraction of core 13953 of up to 200-times seawater concentration. Despite the proximity to shore and, thus, the airport and industrial areas in the western part of Nice, the metals Cr, Cu, Ni, V and Zn were not elevated. Values corresponded to those expected for “normal” marine sediments (Li, 2000).

A second set of pore waters was recovered using rhizons (i.e. 50 ml syringes) stuck into the shallow subseafloor by scuba divers. The water samples were taken along the same transect along which *in situ* temperature measurements were carried out (see Ch. 7.3.3 above). Compared to the T loggers, pore water samples were extracted at transect positions 0, 10 (2), 20 (2), 25, 27, 30 (2), 35, 40 (2), 50, 60, 70, 80 (2), 90, 100, 110 and 120 m ([2] in parantheses means that a second sample was taken during a second dive). The corresponding water depths range between 15.5 mbsl at the NW’ end of the transect and 29.5 mbsl at its SE’ termination near the buoy (see Fig. 39, black bar). Pore water samples were taken along the transect every 10 m from a depth of approximately 5 - 10 cm. The purpose was to investigate if submarine groundwater discharge (SGD) was present in the area where most of the sediments, which were collected gravity coring showed a fresh component in their pore water. Results are presented in Table 6 (available on CD-ROM in back pocket) and none of the 13 samples indicates SGD – all measured concentrations were within their analytical uncertainty those expected for seawater.

### *Visual observations by SCUBA*

In addition visual observations were made by SCUBA, which would indicate SGD, such as sediment discolorations, shimmering water, temperature anomalies and discrete vent orifices. No such features were observed. The only indication that there might be SGD was the discovery of minor microbial mats (Fig. 60), which may have developed due to a redox or nutrient gradient (e.g. Bussmann et al., 1999). Nevertheless, a pore water sample did not show any fresh water. As a consequence, we deduce that groundwater that may reach the deeper subseafloor successions owing to their increased permeability is not discharged into the ocean.

There is two obvious explanations for this observation. First, the hydraulic gradient may not be high enough to allow outflow into the overlying water body at a given depth. Second, the scuba divers may have missed the outcrops of the rather thin (usually <20 cm thick) beds of gravel which are charged with fresh water from the Var estuary and adjacent aquifer. Only long-term observations at multiple levels below the seafloor can shed unambiguous light on this open question.



**Fig. 60:** Development of small microbial mats at the boundary between seawater and sediment (see arrows).

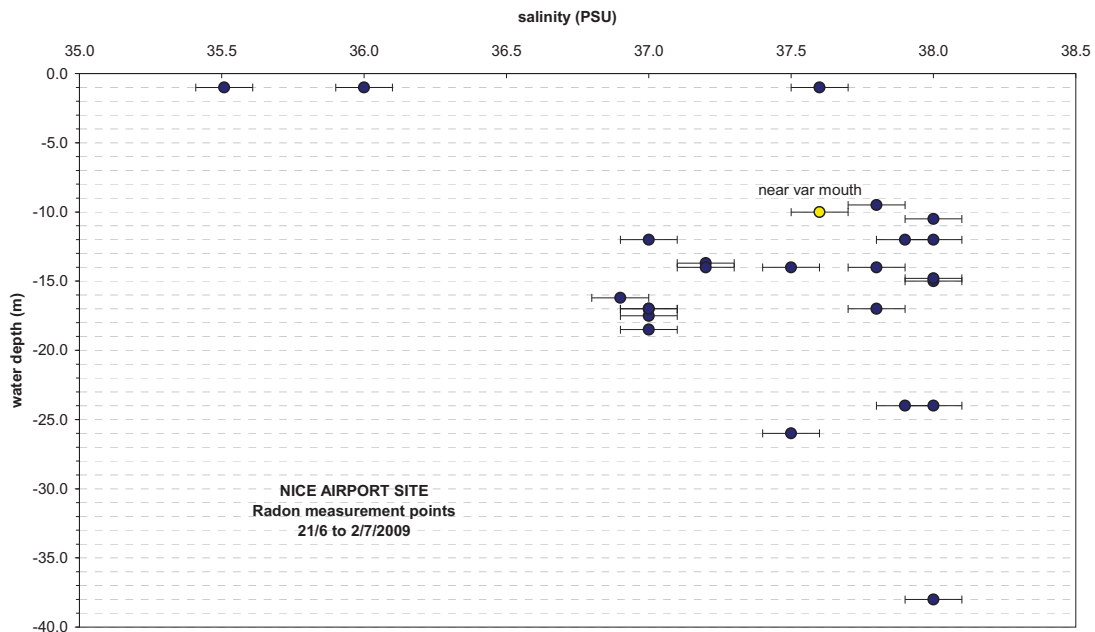


### 7.3.9. *In situ* Radon measurements

(A. Mayer, P. Henry)

Table 7 reports the results of the measurements. Figure 61 reports the vertical distribution of salinity in all radon measurement stations. It is evident from the figure that surface water contains a significant fraction of freshwater that, at the time of the measurement sessions, was almost certainly derived from the Var river, particularly during falling tides. In the limits of the salinity measurements precision, no significant input of freshwater from the seafloor is detected. Variations of salinity are interpreted as due to variable proportion of Var river water.

Radon concentrations are shown in Figure 62. The level of radon activity is quite low (just above the limit of detection of the method, i.e. ca. 1.5 Bq/m<sup>3</sup>) for most of the radon stations. Slightly higher activities are observed in zones of shallower water depth in the northern sector, but no localised radon input point is detected in this area, nor the gas flares.



**Fig. 61:** Vertical distribution of salinity.

Figure 63 illustrates the vertical distribution of radon in seawater. Radon activity is low, but higher than the activity supported by <sup>226</sup>Ra dissolved in seawater (blue vertical line) (Schmidt & Reiss, 1996). This is true in particular for the deepest station (-37 m), with salinity 38.0 psu, which yielded radon activity clearly higher than <sup>226</sup>Ra supported activity. The slight excess of radon indicates that a slight contribution from pore or submarine ground water (GW) occurs in the water column. The figure also shows that for a given depth, north-

western measurements stations yielded slightly higher radon activities in respect to central and southern stations, suggesting that part of the radon ‘excess’ arises from eastward spreading of the Var river water (out of scale in the Fig. 63). Var river water, measured at the mouth, has a radon activity of 173 Bq/m<sup>3</sup>. Degassing and ageing of this water contribution reduce the radon net additions to seawater (arrows in Fig. 63).

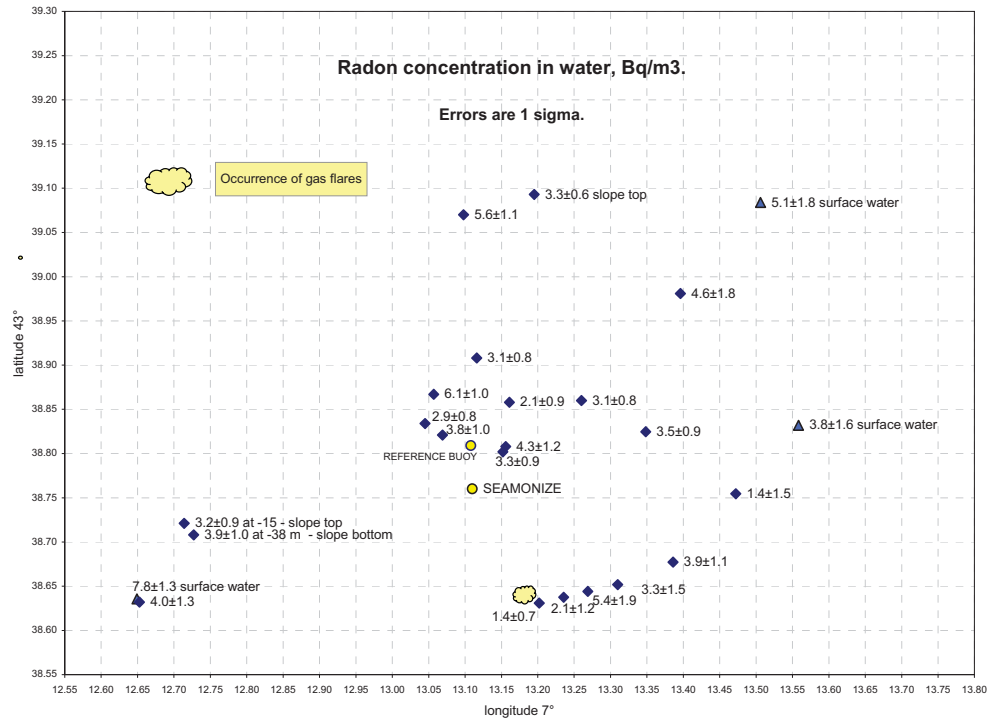


Fig. 62: Radon activity in the investigated area.

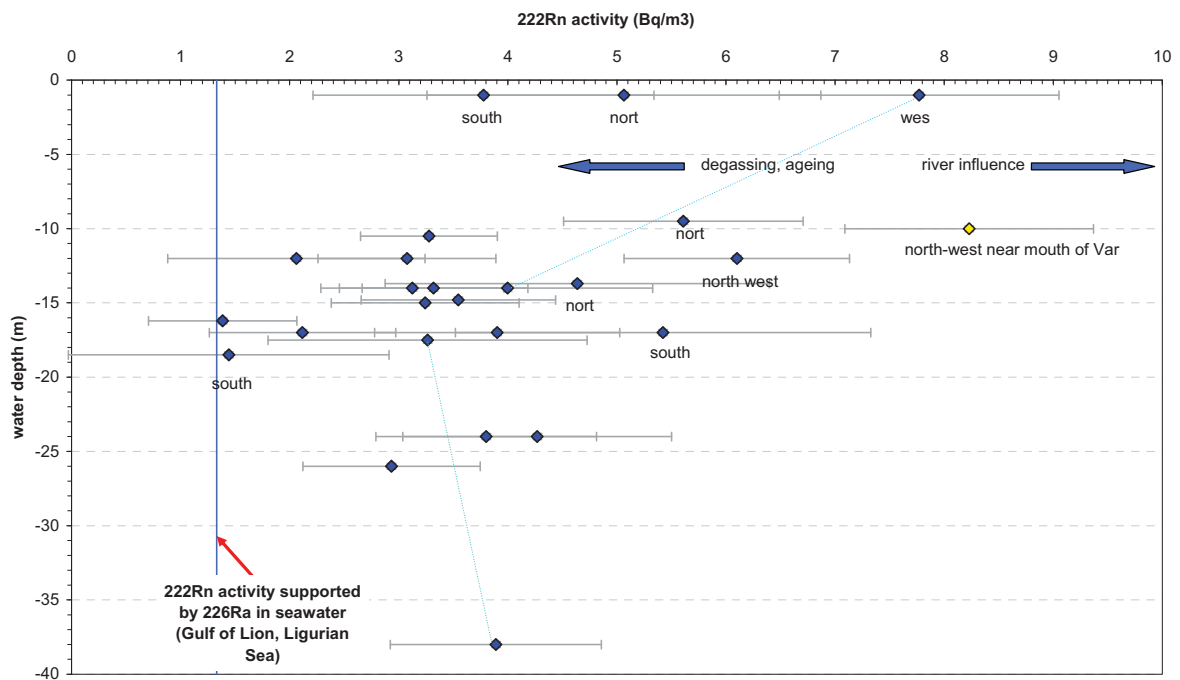
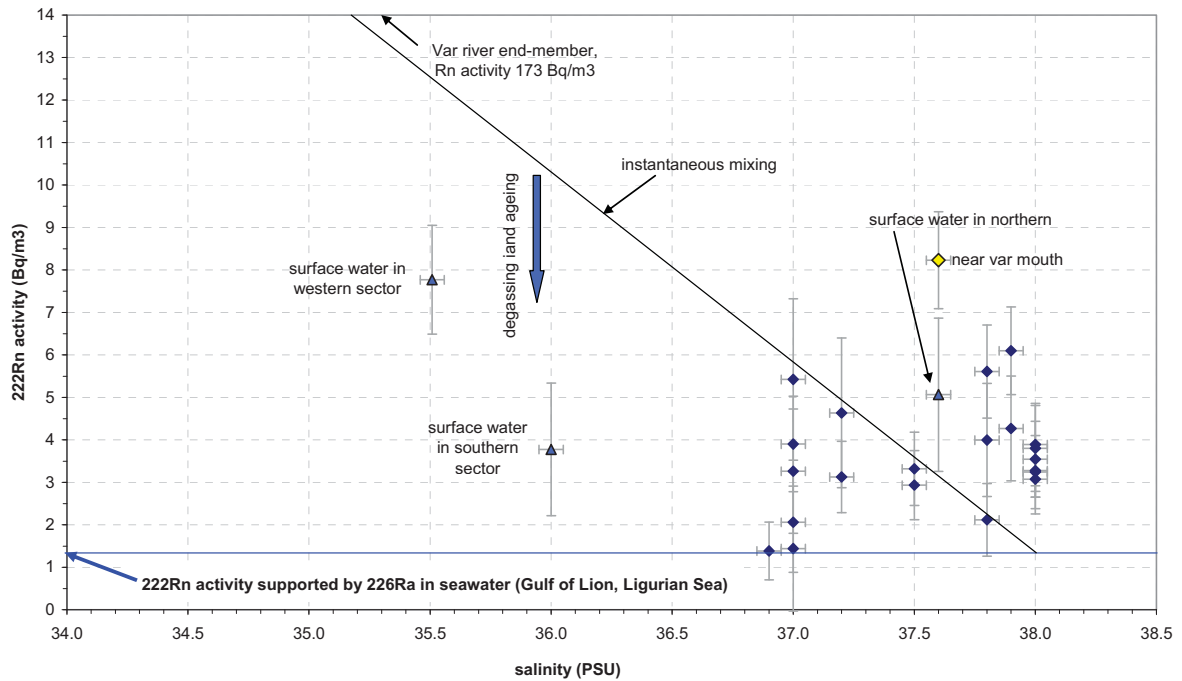


Fig. 63: vertical distribution of radon in seawater. North, south, west, indicates the location of the station sectors in respect to the main canyon (encroachment). Solid line indicates measurements made at different depth in the same stations.

Figure 64 illustrates the relationships between salinity and radon activity. About half of the measurement stations plots above the instantaneous mixing line between the sea water end-member and the Var river end-member. This line represents the maximum activity that can be achieved in seawater by mixing with the river water, since the mixing is considered instantaneous and degassing is neglected. Samples plotting above this line cannot be explained by simple radon addition and salinity sink due to mixing with Var river water, even considering the incertitude on the measurements. The results suggest that a small contribution of radon from groundwater of normal (or close to normal) salinity exists in the area. Alternatively, some radon may be input from re-suspended particles and diffusive exchange through the seafloor.



**Fig. 64:** Radon activity versus salinity.

### ***Discharge rates***

An estimate of the maximum discharge rate of the groundwater can be done using the measured radon activities and assumed radon activity of groundwater. Dissolved  $^{226}\text{Ra}$  in the Ligurian Sea accounts for about 1.33 Bq/m<sup>3</sup> (Schmidt and Reiss, 1996). Taking an average water depth in the investigated area of 20m and an average radon activity of 4 Bq/m<sup>3</sup>, the excess inventory in the water column in respect to the dissolved  $^{226}\text{Ra}$  is 53 Bq/m<sup>2</sup>. For this inventory, the lost of radon by radioactive decay and atmospheric escape is estimated to be around 20 Bq/m<sup>2</sup>/day. To maintain in steady state the radon inventory, radon inputs from groundwater should occur. The necessary water flux could be calculated if radon activity in

groundwater would be known. Assuming an activity of groundwater of 3.5 kBq/m<sup>3</sup>, a common value measured in the Adriatic Sea and at the submarine spring of Port Miou near Marseille, the resulting water flux is ca. 5 litres / m<sup>2</sup> seafloor / day, which correspond to a seepage rate of 5 mm /day. This result is of the same order as the discharge rate inferred by Guglielmi and Prieur (1997), although the latter neglected the contribution of Var river water and the contribution of recycled seawater. Large incertitude exists, of course, in this calculations due to unverifiable assumptions made above.

radon station 139xx-x	lat 43° minutes	long 7° minutes	Depth m	Salinity	radon activity in water Bq/m <sup>3</sup> abs error 1S	
06-01	38.832	13.558	-1	36.0	3.8	1.6
06-01 and drifting to next	38.755	13.472	-18.5	37.0	1.4	1.5
06-02	38.677	13.386	-17	37.0	3.9	1.1
06-03	38.652	13.310	-17.5	37.0	3.3	1.5
06-04	38.644	13.269	-17	37.0	5.4	1.9
drifting between stations	38.638	13.235	-12	37.0	2.1	1.2
06-05	38.631	13.202	-16.2	36.9	1.4	0.7
09-01	39.084	13.506	-1	37.6	5.1	1.8
09-02	38.981	13.396	-13.7	37.2	4.6	1.8
16-01	38.860	13.260	-14	37.2	3.1	0.8
16-02	38.802	13.152	-14	37.5	3.3	0.9
22-1	38.858	13.161	-17	37.8	2.1	0.9
22-2 core42	38.834	13.045	-26	37.5	2.9	0.8
22-3	38.867	13.057	-12	37.9	6.1	1.0
22-4	38.821	13.069	-24	38.0	3.8	1.0
22-5	38.908	13.116	-12	38.0	3.1	0.8
43-1	39.070	13.098	-9.5	37.8	5.6	1.1
43-2	39.093	13.195	-10.5	38.0	3.3	0.6
44	38.636	12.649	-1	35.5	7.8	1.3
50-1	38.632	12.653	-14	37.8	4.0	1.3
50-2	38.721	12.714	-15	38.0	3.2	0.9
50-3	38.808	13.156	-24	37.9	4.3	1.2
50-4	38.825	13.348	-14.8	38.0	3.5	0.9
55	38.708	12.727	-38	38.0	3.9	1.0
61-1	39.256	12.006	-0.6	0.0	172.6	6.7
61-2	38.701	11.603	-10	37.6	8.2	1.1

**Table 7:** Results from radon measurements.

### ***Perspective for the continuation of the research***

In order to refine the calculation made above, radon activity should be measured in groundwater extracted from nearest piezometers. In addition, sediment water equilibration experiment should be performed to determine radon activity in pore water and radon diffusion rate from the sediments. A more detailed model of vertical diffusion in the water column and atmospheric escape should also be carried out to improve the estimate of the rate of radon inventory lost.



## 8. References

- Anthony, E.J., 2007. Problems of hazard perception on the steep urbanised Var coastal floodplain and delta, French Riviera. *Méditerranée* 108: 91-97.
- Anthony, E.J., Julian, M., 1997. The 1979 Var Delta Landslide on the French Riviera: A Retrospective Analysis. *Journal of Coastal Research* 13/1: 27-35.
- Ask, M.V.S., Camerlenghi, A., Kopf, A., Morgan, J.K. and participants of the 2008 ESF Magellan workshop “Ocean Drilling for Seismic Hazard in European Geosystems, 2008. Scientific Ocean Drilling to Assess Submarine Geohazards along European Margins *EOS, Trans. AGU* (Suppl.), 1pp.
- Assier-Rzadkiewicz, S., Heinrich, P., Sabatier, P.C., Savoye, B., and Bourillet, J.F., 2000. Numerical Modelling of a Landslide-generated Tsunami: The 1979 Nice Event. *Pure Appl. Geophys.* 157: 1707–1727.
- Becker, K., Fisher, A.T., Davis, E.E., 1997. The CORK experiment in hole 949C: Long-term observations of pressure and temperature in the Barbados accretionary prism. In: T.H. Shipley et al., *Proc. ODP, Sci. Results*, 156: 247-252.
- Becker, K., Davis, E.E., 2003. New evidence for age variation and scale effects of permeabilities of young oceanic crust from borehole thermal and pressure measurements. *Earth Planet. Sci. Letts.* 210: 499-508.
- Bekins, B.A., Screatton, E.J., 2007. Pore Pressure and Fluid Flow in the Northern Barbados Accretionary Complex: A Synthesis. In: *The Seismogenic Zone of Subduction Thrust Faults*, edited by T. Dixon et al., Columbia University Press: 148-170
- Bennett, R.H., L. Huon, P.J. Valent, J. Lipkin, M.I. Esrig, 1985. In situ undrained shear strengths and permeabilities derived from piezometer measurements. In: R.C. Chaney & K.R. Demars (eds), *Strength Testing of Marine Sediments: Laboratory and In Situ Measurements, American Society for Testing and Materials*: 88-100.
- Bredehoeft, J.D., 1967. Response of well-aquifer systems to Earth tides, *J. Geophys. Res.* 72: 3075-3087.
- Brown, K.M., et al., 2005, Correlated transient fluid pulsing and seismic tremor in the Costa Rica subduction zone. *Earth Planet. Sci. Lett.* 238: 189-203.
- British Standards Institutions, BS 1377, 1975. Methods of testing soils for civil engineering purposes. London: BSI: 174pp.
- Bussmann, I., Dando, P.R., Niven, S.J., Suess, E., 1999, Groundwater seepage in the marine environment: role for mass flux and bacterial activity. *Marine Ecology-Progress Series* 178: 169-177.
- Byerlee, J. D., 1978. Friction of rocks. *Pure Appl. Geophys.* 116: 615-625

- Byerlee, J. D., 1990. Friction, overpressure and fault normal compression. *Geophys. Res. Lett.* 17: 2109-2112
- Camerlenghi and co-proponent, 2008. MEDSLIDES Geohazard from submarine landslides, IODP proposal 715-full, 25 pp.
- Chronis, G., Lykousis, V., Anagnostou, C., Karageorgis, A., Stavrakakis, S., Poulus, S., 2000. Sedimentological processes in the southern margin of the Cretan Sea (NE Mediterranean). *Progress in Oceanography* 46, 143-162.
- Clauzon, G., Suc, J.P., Aguilier, J.P., Ambert, P., Cappetta, H., Cravatte, J., Mischeaux, J., Roiron, J.L., Savoye, B., Vernet, J.L., 1990. Pliocene geodynamic and climate evolutions in the French Mediterranean region. *Paleontol. Evol. Mem. Espec.* 2, 132-186.
- Clayton, C.R.I., Hababa, M.B., Simons, N.E., 1985. Dynamic penetration resistance and the prediction of the compressibility of a fine-grained sand a laboratory study. *Geotechnique* 35/1: 19-31
- Cochonat P., Bourillet J.F., Savoye B., Dodd L., 1993. Geotechnical characteristics and instability of submarine slope sediments, the Nice slope (N-W Mediterranean Sea). *Mar Georesour Geotech*, 11: 131-151.
- Cochrane, G., J.C. Moore, H.J. Lee, 1996, Sediment pore-fluid overpressuring and its effect on deformation at the toe of the Cascadia accretionary prism from seismic velocities, in *Subduction top to bottom*, edited by G. Bebout, et al., Geophysical Monograph 96, American Geophysical Union: Washington, DC, United States, 57-64.
- Dan, G., 2007. Processus gravitaires et evaluation de la stabilite des pentes: Approches geoloigues et geotechnique. PhD thesis, Univ. Bretagne occidentale, Brest, 364pp.
- Dan, G., Sultan, N., Savoye, B., 2007. The 1979 Nice harbour catastrophe revisited: Trigger mechanism inferred from geotechnical measurements and numerical modelling. *Mar. Geology* 245: 40-64.
- Dan, G., N. Sultan, A. Cattaneo, J. Déverchère, K. Yelles, 2009. Mass-Transport Deposits on the Algerian Margin (Algiers Area): Morphology, Lithology and Sedimentary Processes Mosher, DC., Shipp, C., Moscardelli, L., Chaytor, J., Baxter, C., Lee, H., and Urgeles, R. (eds.), Submarine Mass movements and their consequences IV. *Advances in Natural and Technological Hazards Series*, Springer: 527-540.
- Davis, E.E., Becker, K., 2001. Using ODP boreholes for studying subseafloor hydrogeology: Results from the first decade of CORK observations, *Geosci. Can.* 28: 171-178.
- Davis, E.E., et al., 2001. An episode of seafloor spreading and associated plate deformation inferred from crustal fluid pressure transients. *J. Geophys Res.* 106, 21953-21963.
- Davis, E.E., et al., 2004. Hydrological response to a seafloor spreading episode on the Juan de Fuca ridge, *Nature* 430: 335-338.

- Davis, E.E., et al., 2006. A discrete episode of seismic and aseismic deformation of the Nankai Trough subduction zone accretionary prism and incoming Philippine Sea plate. *Earth Planet. Sci. Lett.*, 242: 73-84.
- De La Tullaye, M., 1989. Un aéroport gagné sur la mer: Nice-Côte d'Azur. *Revue XYZ*, 38: 43-45.
- Dubar, M., Antony, E.J., 1995. Holocene Environmental Change and River-Mouth Sedimentation in the Baie des Anges, French Riviera. *Quaternary Research* 43: 329-343
- Esrig, M.I., R.C. Kirby, R.G. Bea, 1977. Initial development of a general effective stress method for the prediction of axial capacity for driven piles in clay. *Proc. 9th Offshore Technology Conference*: 495-501
- Flemings, P.B., Long, H., Dugan, B., Germaine, J., John, C.M., Behrmann, J.H., Sawyer, D., IODP Expedition 308 Scientists, 2008. Pore pressure document high overpressure near the seafloor where multiple landslides have occurred on the continental slope, offshore Louisiana, Gulf of Mexico. *Earth Planet. Sci. Letts.*, 269: 309-325.
- Förster, A., Spiess, V., Kopf, A., Dennielou, B., 2009. Mass wasting dynamics at the deeper slope of the Ligurian Margin (Southern France). In: Mosher, DC., Shipp, C., Moscardelli, L., Chaytor, J., Baxter, C., Lee, H., and Urgeles, R. (eds.), Submarine Mass movements and their consequences IV. *Advances in Natural and Technological Hazards Series*, Springer: 67-78.
- Foucher, J.-P., Henry, P., Harmegnies, F., 1997. Long-term observations of pressure and temperature in hole 948D, Barbados accretionary prism. In: Shipley, T.H. et al. (eds.), *Proc. ODP, Sci. Results*, 156: 239-245.
- Genesseeux, M., Mauffret, A., Pautot, G., 1980. Les glissements sousmarins de la pente continentale niçoise et la rupture des câbles en mer Ligure (Méditerranée occidentale). *C.R. Acad. Sc. Paris* 290.
- Guglielmi, Y., 1993. Hydrogéologie des aquifères Plio-Quaternaires de la Basse Vallée du Var. Thèse d'Etat, Académie d'Aix-Marseille : 170 pp.
- Guglielmi, Y., Mudry, J., 1996. Estimation of Spatial and Temporal Variability of Recharge Fluxes to an Alluvial Aquifer in a Fore Land Area by Water Chemistry and Isotopes. *Ground Water* 34, 6, 1017-1023.
- Guglielmi, Y., Prieur, L., 1997. Locating and Estimating submarine freshwater discharge from an interstitial confined coastal aquifer by measurements at sea: example from the lower Var Valley, France. *Journal of Hydrology* 190, 111-122.
- Hampton, M.A., Lee, H.J., 1996. Submarine Landslides. *Rev. Geophys.* 34, 1, 33-59.
- Hampton, M.A., Lee, H.J., Locat J., 1996. Submarine landslides. *Rev. Geophys.* 3, 33-59.
- Hansbo, S., 1957. A new approach to the determination of the shear strength of clay by the fall-cone test. Royal Swedish Geotechnical Institute Proc., 14, Stockholm.

- Hayward N., G.K. Westbrook, S. Peacock, 2003, Seismic velocity, anisotropy, and fluid pressure in the Barbados accretionary wedge from an offset vertical seismic profile with seabed sources, *J. Geophys. Res.*, 108, doi:10.1029/2001JB001638.
- Henry, P., Person, R., Paull, C.K., Savoye, B., Romanowicz, B., Charvis, P., Kopf, A., 2005. Installation of borehole observatories on the Ligurian Margin. IODP-proposal 685-full, 25 pp.
- Hugot, A., 2000. Modélisation des écoulements gravitaires catastrophiques par une approche objet dynamique: érosion-transport-dépôt. Thèse, Université Paris 6, pp. 410.
- Huehnerbach, V., Masson, D.G., 2004. Landslides in the North Atlantic and its adjacent seas: an analysis of their morphology, setting and behaviour. *Marine Geology*, 213, 343-362.
- Klaucke, I., Cochonat, P. 1999. Analysis of past seafloor failures on the continental slope off Nice (SE France). *Geo-Marine Letters*, 19, 245-253.
- Klaucke, I., Savoye, B. Cochonat, 2000. Patterns and processes of sediment dispersal on the continental slope off Nice, SE France. *Marine Geology*, Vol. 162, pp. 405-422.
- Kopf, A., Brown, K.M., 2003. The stress state of the Nankai and Barbados subduction thrusts. *Mar. Geol.* 202: 193-210
- Kopf, A., Alves, T., Heesemann, B., Kaul., N.E., Kock, I., Krastel, S., Reichelt, M., Schäfer, R., Stegmann, S., Strasser, M., Thölen, M., 2006. REPORT AND PRELIMINARY RESULTS OF POSEIDON CRUISE P336: CRESTS - Cretan Sea Tectonics and Sedimentation. *Berichte aus dem Fachbereich Geowissenschaften der Univ. Bremen*, No. 253: 140pp.
- Kopf, A., Stegmann, S., Krastel, S., Förster, A., Strasser, M., Irving, M., 2007. Marine deep-water Free-fall CPT measurements for landslide characterisation off Crete, Greece (Eastern Mediterranean Sea) --- PART 2: Initial data from the western Cretan Sea. In: Lykousis, V., Sakellariou, D., Locat, J. (eds.), *Submarine Mass movements and their consequences. Advances in Natural and Technological Hazards Series*, Springer: 199-208.
- Kopf, A., Alexandrakis, E.C.C., Blees, J., Bogus, K., Dennielou, B., Förster, A., Girault, F.E., Haarmann, T., Hanff, H., Hentscher, M., Kaul., N.E., Klar, S., Krastel, S., Lange, M., Meier, M.-A., Metzen, J.F., Spiess, V., Stegmann, S., Strozyk, F., Volen Krumova, T., 2008. REPORT AND PRELIMINARY RESULTS OF METEOR CRUISE M73/1: LIMA-LAMO. *Berichte aus dem Fachbereich Geowissenschaften der Univ. Bremen*, No. 264: 169pp.
- Kopf, A., Kasten, S., Blees, J., 2009. Geochemical evidence for groundwater-charging of slope sediments: The Nice airport 1979 landslide and tsunami revisited. In: Mosher, DC., Shipp, C., Moscardelli, L., Chaytor, J., Baxter, C., Lee, H., and Urgeles, R. (eds.), *Submarine Mass movements and their consequences IV. Advances in Natural and Technological Hazards Series*, Springer: 203-214.
- Kopf, A., 2009. The Deep-Sea and Sub-Seafloor Frontier initiative – a key to link EC research and international scientific ocean drilling. *Proc. EGU Conference*, April 2009 Vienna, 1pp.



- Lee, H.J., 2009. Timing of occurrence of large submarine landslides on the Atlantic Ocean margin. *Marine Geology*, in press.
- Leroueil, S., 2001. Natural slopes and cuts: movement and failure mechanisms. *Geotechnique*, 51,3, 197-243.
- Li, Y.-H., 2000. A compendium of geochemistry: from solar nebula to the human brain: Princeton, Princeton University Press, 476 pp.
- Locat J., 2001. Instabilities along ocean margins: a geomorphological and geotechnical perspective. *Mar. Petr. Geology*, 18: 503-512
- Locat J., Lee H.J., 2002. Submarine landslides: advances and challenges. *Can. Geotech. J.*, 39: 193-212.
- Logan, J. M., Rauenzahn, K. A., 1987. Frictional dependence of gouge mixtures of quartz and montmorillonite on velocity, composition and fabric. *Tectonophysics*, 144: 87-108.
- Lunne, T., Robertson P.K., Powell, J.J.M., 1997. Cone Penetration Testing in Geotechnical Practice, Blackie Academic & Professional London: pp. 312
- Lykousis, V., Sakellariou, D., Locat, J. (Eds.), 2008. Submarine Mass Movements and Their Consequences. *Adv. Nat. Techn. Hazard Res.*, Springer, 424pp.
- Maltman, A. (Ed.), 1994. The Geological Deformation of Sediments. Chapman & Hall, London, 363pp.
- Maslin, M., Owen, M., Day, S., Long, D., 2004. Linking continental-slope failures and climate change: testing the clathrate gun hypothesis. *Geology* 32, 1, 53–56.
- Meunier, J., Sultan, N., Jegou, P., Harmegnies, F., 2004. First Tests of Penfeld : a New Seabed Penetrometer. *Proc. 14th (2004) International Offshore and Polar Engineering Conference* Toulon, France, May 23-28, 2004, 338-245.
- Mienert, J., Berndt, C., Laberg, J.S. & Vorren, T.O., 2003: Slope Instability of Continental Margins. In: *Ocean Margin Systems*, eds. *Wefer et al.*, Springer Verlag, New York, p. 179-193.
- Mienert, J. (ed), 2004. COSTA—continental slope stability: major aims and topics. *Marine Geology*, 217, 1-7.
- Migeon S., Mulder T., Savoye B., Sage F., 2006. The Var turbidite system (Ligurian Sea, northwestern Mediterranean) – morphology, sediment supply, construction of turbidite levee and sediment waves: implications for hydrocarbon reservoirs. *Geo-Mar Letts*, 26: 361-371.
- MIP, 1981. Mission d'Inspection Pluridisciplinaire sur le sinistre de Nice du 16 Octobre 1979, Rapport final. Unpublished report.
- Mörz, T., Karlik, E.A., Kreiter, S., Kopf, A., 2007. An experimental setup for fluid venting in unconsolidated sediments: new insights to fluid mechanics and structures *Sedimentary Geology*, 186: 251-267.
- Moore, G.F., A. Taira, A. Klaus, et al., 2001. New insights into deformation and fluid flow processes in the Nankai Trough accretionary prism: Results of Ocean Drilling Program Leg 190, *Geochem.*,

- Geophys., Geosyst.*, 2, 10.129/2001GC000166.
- Moore, C.J. & science party, 1995. Abnormal fluid pressures and fault-zone dilation in the Barbados accretionary prism: Evidence from logging while drilling. *Geology*, 23/7, 605-608.
- Moore, J.C., Saffer, D., 2001. Updip limit of the seismogenic zone beneath the accretionary prism of southwest Japan: An effect of diagenetic to low-grade metamorphic processes and increasing effective stress. *Geology*, 29: 183-186
- Morgan, J.K., M.V.S. Ask, 2004. Consolidation state and strength of underthrust sediment and evolution of the décollement at the Nankai accretionary margin: Results of uniaxial reconsolidation experiments, *Jour. Geophys. Res.* 109, B03102, doi:10.1029/2002JB002335.
- Morris, J.D., Villinger, H.W., Klaus, A., et al., 2003. *Proc. ODP, Init. Repts.*, 205. Available at: [http://www-odp.tamu.edu/publications/205\\_IR/205ir.htm](http://www-odp.tamu.edu/publications/205_IR/205ir.htm).
- Mosher, DC., Shipp, C., Moscardelli, L., Chaytor, J., Baxter, C., Lee, H., and Urgeles, R. (eds.), 2009. Submarine Mass movements and their consequences IV. *Advances in Natural and Technological Hazards Series*, Springer: 786 pp.
- Mulder, T., Savoye, B., Syvitski, J.P.M., 1997. Numerical modelling of a mid-sized gravity flow: the 1979 Nice turbidity current (dynamics, processes, sediment budget and seafloor impact). *Sedimentology*, 44: 305–326.
- Mulder, T., Savoye, B., Piper, D.J.W., Syvitski, J.P.M., 1998. The Var submarine sedimentary system: understanding Holocene sediment delivery processes and their importance to the geological record. In: Stocker, M.S., Evans, D., Cramp, A., Geological processes on continental margins: sedimentation, mass wasting and stability. *Geol. Soc. London, Spec. Publ.*, 129: 146-166.
- Pautot, G., 1981. Cadre morphologique de la Baie des Angers. Mode`le d'instabilité de pente continentale. *Oceanol. Acta* 4, 203–212.
- Pfender, M., H. Villinger, 2002. Miniaturized data logger for deep-sea sediment temperature measurements, *Mar. Geol.*, 186: 557-570.
- Ramsey, N., 2002. A calibrated model for the interpretation of cone penetration tests (CPTs) in North Sea quaternary soils. *Proc. Offshore Site Investigation and Geotechnics: Diversity and Sustainability*, London, UK, pp. 341–356.
- Rice, J.R., 1992. Fault stress states, pore pressure distributions, and the weakness of the San Andreas Fault. In: Evans, B. & Wong, T.-F., Fault mechanics and transport properties of rocks. London (Acad. Press): 475-503.
- Rothwell, R.G., 1989. Identification of Minerals and Mineraloids in Marine Sediments, London/New York (Elsevier).
- Sage, L., 1976. La sédimentation à l'embouchure d'un fleuve côtier méditerranéen. Le Var. Thèse, Université de Nice, 243 pp.

- Saffer, D.M., Frye, K.M., Marone, C., Mair, K., 2001. Laboratory results indicating complex and potentially unstable frictional behavior of smectite clay. *Geophys. Res. Letts.*, 28: 2297-2300
- Savoye, B., Piper, D.J.W., Droz, L., 1993. Plio-Pleistocene evolution of the Var deep-sea fan off the French Riviera. *Mar. Petr. Geol.*, 10, 550-571.
- Savoye, B., Rohais, S., Lopez, S., Dan, G., 2005. Revisiting the 1979 submarine avalanche offshore Nice (French Riviera): impacts on the seafloor, flow reconstruction and modelling. *Proc. ICG Conf. on Submarine Mass Wasting*, NGF, v. 2, p.74.
- Schlüter, M., Sauter, E.J., Andersen, C.E., Dahlggaard, H., Dando, P.R., 2004, Spatial distribution and budget for submarine groundwater discharge in Eckernförde Bay (Western Baltic Sea). *Limnology and Oceanography* 49: 157-167.
- Schmidt, L., Reiss, S. 1996. Radium as internal tracer of Mediterranean Outflow Water. *J. Geoph. Res.* 101, 3589-3596
- Scholz, C.H., 1998. Earthquakes and friction laws. *Nature*, 391: 37-42.
- Schulz, H.D., Dahmke, A., Schinzel, U., Wallmann, K., Zabel, M., 1994, Early diagenetic processes, fluxes, and reaction-rates in sediments of the South Atlantic: *Geochimica et Cosmochimica Acta* 58: 2041-2060.
- Screaton, E.J., D.M. Saffer, P. Henry, S. Hunze, and Leg 190 Shipboard Scientific Party, 2002. Porosity loss within underthrust sediments of the Nankai accretionary complex: Implications for overpressures, *Geology*, 30, p. 19-22.
- Seed, H. B., Seed, R. B., Schlosser, F., Blondeau, F., Juran, I. 1988. The Landslide at the port of Nice on October 16, 1979, Earthquake Engineering Research Center, report No. UCB/EERC-88/10.
- Solheim, A. (ed), 2006. Special issue of Norwegian Geol. J., Proc. IGCP511 conference, Oslo, 2005.
- Stegmann, S., Villinger, H, Kopf, A., 2006. Design of a modular, marine free-fall cone penetrometer. *Sea Technology*, v. 02/2006, 27-33
- Stegmann, S., Strasser, M., Anselmetti, F., Kopf, A., 2007. Geotechnical in situ characterization of landslide deposits: The role of pore pressure transients versus frictional strength. *Geophys. Res. Lett.*, 34, doi: 10.1029/2006GL029122.
- Stegmann, S., and co-proponents. Multi-methodological testing of landslide trigger mechanisms at the Ligurian slope (W' Mediterranean): the Nice Airport Landslide NAIL. IODP proposal 748-full. 25 pp.
- Strasser, M., and co-proponents, 2008. Nankai Trough Submarine Landslides, IODP 738-APL, 5pp.
- Sultan, N., Cochonat, P., Bourillet, J.F., and Cayocca, F., 2001. Evaluation of the Risk of Marine Slope Instability: A Pseudo-3D Approach for Application to Large Areas. *Marine Georesources and Geotechnology*, 19, 107-133.
- Sultan, N., Cochonat, P., Canals, M., Cattaneo, A., Dennielou, B., Haflidason, H., Laberg, J. S., Long, D., Mienert, J., Trincardi, F., 2004. Triggering mechanisms of slope instability processes

- and sediment failures on continental margins: a geotechnical approach: *Marine Geology*, 213: 291-321
- Sultan, N., Gaufin, M., Berne, S., Canals, M., Urgeles, R., Lafuerza, S., 2007. Analysis of slope failures in submarine canyon heads: An example from the Gulf of Lions. *Journal Geophysical Research*, 112, 29pp. (10.1029/2005JF000408)
- Sultan, N., and shipboard party, 2008. Prisme Cruise (R/V Atalante Toulon - Toulon; 2007): Reports and Preliminary Results. *IFREMER Internal Report*, Ref: IFR CB/GM/LES/08-11, 180pp.
- Sultan, N., Savoye, B., Jouet, G., Leynaud, D., Cocchonot, P., Stegmann, S., Kopf, A., in press. Investigation of a possible submarine landslide at the Var delta front. *Can. Geotechnical Journal*.
- Thakur, V., Grimstad, G., Nordal, S., 2006. Instability in Soft Sensitive Clays, ECI Conference on Geohazards, 43,
- Tappin, D.D., Watts, P., McMurtry, G.M., Lafoy, Y., Matsumoto, T., 2001. The Sissano, Papua New Guinea tsunami of July 1998 – offshore evidence on the source mechanism. *Marine Geology*, 175, 1-23.
- Terzaghi, K., 1946. *Theoretical Soil Mechanics*. John Wiley & Sons, Inc., New York, pp. 510.
- Urgeles, R., Leynaud, D., Lastras, G., Canals, M., Mienert, J., 2006. Back-analysis and failure mechanisms of a large submarine slide on the Ebro continental slope, NW Mediterranean, *Marine Geology*, 226: 185-206.
- Wentworth, C.K., 1922. A scale of grade and class terms of clastic sediments. *J. Geol.*, 30: 377-392.
- Winfrey, M.R., Marty, D.G., Bianchi, A.J.M., Ward, D.M., 1981. Vertical distribution of sulfate reduction, methane production and bacteria in marine sediments. *Geomicrobiology Journal* 2: 341-362.
- Wood, D.M., 1985. Cone penetrometer and liquid limit. *Geotechnique*, 32 (2): 152-157.

## 9. Acknowledgements

We thank Master Michael Schneider and his officers on the bridge for his willingness to approach shallow portions of the study area, his cooperation, and outstanding support during complex operations oftentimes stretching the limits of what is possible this close to shore. Special thanks go also to Frank Schrage and the entire crew of R/V *Poseidon* for their friendly support and efficient technical assistance with the various devices used, the large-scale equipment handled, and frequent use of the dinghy.

Our colleagues at IFREMER, namely Jean-Xavier Castrec and Nabil Sultan are acknowledged for their helpful discussion and negotiations with discussion of scientific targets during earlier meetings. Jean-Xavier Castrec is thanked for providing crucial hints regarding the local authorities and airport security for receiving a research permission.

Max-Planck-Institution for Marine Microbiology, and Volker Meyer in particular, is thanked for having provided the SPY shallow-water ROV and many hours of technical advice and wisdom.

Partners at MARUM Bremen (Goetz Ruhland, Volker Diekamp) as well as at IfM-GEOMAR (Thomas Müller) have also provided crucial help with expedition planning, logistical decisions, and post-cruise demobilisation. Additionally, Klaus Bohn is thanked for his repeated professional logistical assistance.

Thanks go also to the German Science Foundation (DFG) for providing the funds to realise the *NAIL* cruise within the frame of MARUM research area SD5.



## **10. Appendices**

### **10.1 Station list**

### **10.2 Lithologs and shear strength data**

### **10.3 MSCL data logs and core photographs (electronic version only)**

## **10.1 Station list**

CRUISE	YEAR	HOUR	GEOB 139-	DEVICE	ACTION	LAT	LONG	DEPTH	TEMP. WATER	WINCH	WIRE LENGTH	REMARKS
POS-386	2009	06 20 18	18 31	Piezometer cast (CPT)	@ Station	43.64845	7 22623	18.6	24.2			
POS-386	2009	06 20 18	24 03	Piezometer cast (CPT)	Station started	43.64843	7 22608	18.1	24.2			
POS-386	2009	06 20 18	24 31	Piezometer cast (CPT)	to water	43.64843	7 22612	18.0	24.2			
POS-386	2009	06 20 18	33 04	Piezometer cast (CPT)	at bottom	43.64842	7 22610	18.1	24.2	W2	25	Piezometer remains 30 min in bottom
POS-386	2009	06 20 19	01 51	Piezometer cast (CPT)	heave started	43.64840	7 22587	17.7	23.9	W2	25	
POS-386	2009	06 20 19	07 02	Piezometer cast (CPT)	at surface	43.64818	7 22567	17.1	24.0	W2	25	
POS-386	2009	06 20 19	08 29	Piezometer cast (CPT)	to water	43.64812	7 22572	17.7	23.9	W2	25	
POS-386	2009	06 20 19	12 38	Piezometer cast (CPT)	at bottom	43.64820	7 22568	17.1	23.9	W2	25	
POS-386	2009	06 20 19	45 17	Piezometer cast (CPT)	at surface	43.64805	7 22530	16.1	23.8	W2	25	
POS-386	2009	06 20 20	02 31	Piezometer cast (CPT)	to water	43.64727	7 22467	16.4	23.9	W2		
POS-386	2009	06 20 20	05 12	Piezometer cast (CPT)	at bottom	43.64725	7 22455	16.1	24.0	W2	21	heave with 0.3 m/s
POS-386	2009	06 20 20	34 58	Piezometer cast (CPT)	heave started	43.64727	7 22457	15.9	24.1	W2	22	
POS-386	2009	06 20 20	36 36	Piezometer cast (CPT)	at surface	43.64723	7 22458	16.7	24.1	W2		
POS-386	2009	06 20 20	44 04	Piezometer cast (CPT)	to water	43.64682	7 22375	14.8	24.1	W2		
POS-386	2009	06 20 20	47 42	Piezometer cast (CPT)	at bottom	43.64655	7 22368	14.6	24.2	W2	20	
POS-386	2009	06 20 21	16 09	Piezometer cast (CPT)	heave started	43.64658	7 22372	14.7	24.2	W2	20	
POS-386	2009	06 20 21	18 47	Piezometer cast (CPT)	at surface	43.64642	7 22377	14.8	24.2	W2	20	
POS-386	2009	06 20 21	30 39	Piezometer cast (CPT)	to water	43.64585	7 22278	14.5	24.2	W2	20	
POS-386	2009	06 20 21	32 20	Piezometer cast (CPT)	at bottom	43.64585	7 22272	14.7	24.2	W2	19	
POS-386	2009	06 20 21	59 19	Piezometer cast (CPT)	heave started	43.64585	7 22255	14.1	24.3	W2	19	
POS-386	2009	06 20 21	59 42	Piezometer cast (CPT)	heave started	43.64585	7 22253	14.0	24.3	W2	19	
POS-386	2009	06 20 22	02 38	Piezometer cast (CPT)	at surface	43.64565	7 22283	14.9	24.2	W2	19	
POS-386	2009	06 20 22	07 59	Piezometer cast (CPT)	on deck	43.64567	7 22305	15.2	24.1	W2	19	
POS-386	2009	06 20 22	08 28	Piezometer cast (CPT)	Station completed	43.64568	7 22312	15.3	24.1	W2	19	
POS-386	2009	06 21 07	43 50	Mooring ANITRA	Station arrived	43.57508	7 23822	1279.0	22.8	W3		
POS-386	2009	06 21 07	46 25	Mooring ANITRA	Mooring at water	43.57508	7 23818	1279.0	22.8	W3		
POS-386	2009	06 21 07	59 19	Mooring ANITRA	Anittra to water	43.57508	7 23820	1279.0	22.9	W3		
POS-386	2009	06 21 08	00 34	Mooring ANITRA	Anittra dived	43.57510	7 23828	1280.0	22.9	W3	20	
POS-386	2009	06 21 08	34 51	Mooring ANITRA	Mooring at bottom	43.57508	7 23825	1280.0	22.9	W3	1045	Hydrophone to water
POS-386	2009	06 21 08	35 47	Mooring ANITRA	released, heave started	43.57507	7 23825	1280.0	22.9	W3	1045	Hydrophone on deck
POS-386	2009	06 21 08	48 04	Mooring ANITRA	upper releaser at surface	43.57532	7 23858	1280.0	22.9	W3		
POS-386	2009	06 21 08	49 36	Mooring ANITRA	upper releaser on deck	43.57537	7 23865	1279.0	22.9	W3		station completed
POS-386	2009	06 21 08	53 03	Ibsen Mooring	to water	43.57542	7 23853	1279.0	22.9	W2		station started
POS-386	2009	06 21 09	29 49	Ibsen Mooring	at bottom	43.57542	7 23838	1278.0	22.9	W2	1270	Hydrophone to water
POS-386	2009	06 21 09	30 54	Ibsen Mooring	released, heave started	43.57537	7 23843	1279.0	22.9	W2	1270	Hydrophone on deck
POS-386	2009	06 21 09	43 28	Ibsen Mooring	releaser on deck	43.57568	7 23910	1281.0	22.8	W2		station completed
POS-386	2009	06 21 11	05 54	Mooring Peer Gynt	start slack out	43.57513	7 23782	1279.0	22.8	W2		station started
POS-386	2009	06 21 11	10 28	Mooring Peer Gynt	anchor to water	43.57465	7 23870	1285.0	22.8	W2		
POS-386	2009	06 21 11	12 28	Mooring Peer Gynt	station completed	43.57398	7 24140	1296.0	22.8	W2		
POS-386	2009	06 21 11	52 43	Peer Gynt Mooring	Head Buoy to water	43.62472	7 18250	508.0	23.7			Station arrived
POS-386	2009	06 21 11	58 58	Peer Gynt Mooring	anchor weight to water	43.62360	7 18345	515.0	23.6			
POS-386	2009	06 21 11	59 25	Peer Gynt Mooring	Head buoy dived	43.62332	7 18343	518.0	23.6			station completed
POS-386	2009	06 21 12	14 00	Ibsen Mooring	station arrived	43.62465	7 18410	500.0	23.7	W2		
POS-386	2009	06 21 12	14 37	Ibsen Mooring	to water	43.62467	7 18417	501.0	23.7	W2		Benthos + Releaser t/water
POS-386	2009	06 21 12	34 51	Ibsen Mooring	at bottom	43.62450	7 18352	505.0	23.6	W2	490	Hydrophone t/water - Benthos released
POS-386	2009	06 21 12	35 10	Ibsen Mooring	heave started	43.62450	7 18350	506.0	23.6	W2	490	Hydrophone t/water - Benthos released
POS-386	2009	06 21 12	35 36	Ibsen Mooring	heave started	43.62448	7 18350	508.0	23.6	W2	490	Hydrophone @ deck
POS-386	2009	06 21 12	42 12	Ibsen Mooring	on deck	43.62472	7 18335	504.0	23.8	W2		Release on deck
POS-386	2009	06 21 12	43 19	Ibsen Mooring	Station completed	43.62465	7 18340	503.0	23.8	W2		
POS-386	2009	06 21 13	33 47	Ibsen / Peer Gynt (VH) Mooring	Station arrived	43.64673	7 18633	131.0	23.2			
POS-386	2009	06 21 13	34 22	Ibsen / Peer Gynt (VH) Mooring	to water	43.64670	7 18630	137.0	23.2			Top buoy t/water
POS-386	2009	06 21 13	35 35	Ibsen / Peer Gynt (VH) Mooring	to water	43.64660	7 18617	128.0	23.3			Trap + ADCP t/water



POS-386	2009	06	22	11	55	37		Borel Mooring	start stacking line	43.58110	7.61063	1798.0	20.8				
POS-386	2009	06	22	12	14	19		Borel Mooring	1st 600 m slacked out	43.57292	7.60407	2012.0	21.1				
POS-386	2009	06	22	16	51	50	08-1	Piezometer (CPT)	to water	43.65147	7.22520	57.0	23.0			station arrived	
POS-386	2009	06	22	17	07	42		Piezometer (CPT)	at bottom	43.65133	7.22512	51.0	23.0	W2	83	Boko 77 m	
POS-386	2009	06	22	17	32	56		Piezometer (CPT)	heave started	43.65143	7.22513	49.6	23.0	W2	83		
POS-386	2009	06	22	17	39	29		Piezometer (CPT)	on deck	43.65147	7.22518	54.0	23.0	W2		Station completed	
POS-386	2009	06	22	17	53	33	08-2	Piezometer (CPT)	to water	43.64967	7.22327	13.1	23.0	W2		Station started	
POS-386	2009	06	22	17	56	29		Piezometer (CPT)	at bottom	43.64965	7.22327	13.6	23.0	W2	24	Boko 24 m	
POS-386	2009	06	22	18	16			Piezometer (CPT)	heave started	43.64970	7.22320	13.3	23.1	W2			
POS-386	2009	06	22	18	25	32		Piezometer (CPT)	on deck	43.64973	7.22317	13.1	23.1	W2			
POS-386	2009	06	22	18	57	26		Piezometer (CPT)	on deck	43.64155	7.22738	48.2	23.0	W2		Station work ceased	
POS-386							09	Rn stations from deck									
POS-386	2009	06	23	06	07	18	10	Gravity Corer	Station started	43.52902	7.35573	1552.0	20.5	W3			
POS-386	2009	06	23	06	08	20		Gravity Corer	to water	43.52903	7.35578	1533.0	20.5	W3			
POS-386	2009	06	23	08	41	27		Gravity Corer	at bottom	43.52925	7.35603	1528.0	20.7	W3	1730	Boko 1722 m	
POS-386	2009	06	23	06	41	42		Gravity Corer	heave started	43.52925	7.35602	1529.0	20.7	W3	1730		
POS-386	2009	06	23	07	09	18		Gravity Corer	at surface	43.52925	7.35570	1540.0	20.7	W3			
POS-386	2009	06	23	07	10	32		Gravity Corer	on deck	43.52933	7.35585	1529.0	20.7	W3		station completed	
POS-386	2009	06	23	07	55	20	11	Gravity Corer	station started	43.53502	7.35182	1417.0	21.0	W3			
POS-386	2009	06	23	07	55	31		Gravity Corer	to water	43.53503	7.35180	1417.0	21.0	W3			
POS-386	2009	06	23	08	22	18		Gravity Corer	at bottom	43.53497	7.35168	1418.0	21.0	W3	1590	Boko 1580m	
POS-386	2009	06	23	08	22	41		Gravity Corer	heave started	43.53500	7.35167	1418.0	21.0	W3	1590	Boko 1580m	
POS-386	2009	06	23	08	48	58		Gravity Corer	on deck	43.53503	7.35205	1424.0	21.1	W3			
POS-386	2009	06	23	08	49	41		Gravity Corer	station completed	43.53498	7.35212	1423.0	21.1	W3			
POS-386	2009	06	23	10	16	15	12	ROV	Station arrived	43.64635	7.21858	33.8	23.1	W2			
POS-386	2009	06	23	10	32	00		ROV	Station started	43.64638	7.21877	29.3	23.0	W2			
POS-386	2009	06	23	10	34	40		ROV	to water	43.64620	7.21872	30.0	23.0	W2			
POS-386	2009	06	23	10	36	46		ROV	on deck	43.64625	7.21902	28.0	23.0	W2			
POS-386	2009	06	23	11	19	14		ROV	to water	43.64648	7.21842	33.7	22.8	W5a		ROV scrap	
POS-386	2009	06	23	12	28	53		ROV	Station suspended	43.64192	7.22935	159.0	23.4	W5a		Hydrophone to water	
POS-386	2009	06	23	14	55	02		MAP 2	Station arrived	43.54572	7.57897		21.0				
POS-386	2009	06	23	14	56	02		MAP 2	start drifting	43.54577	7.57922		21.0				
POS-386	2009	06	23	15	50	46		MAP 2	drifting ended	43.55032	7.58140		21.0			hydrophone on deck	
POS-386	2009	06	23	16	00	01		MAP 2	hydrophone to water	43.54705	7.57570		21.0				
POS-386	2009	06	23	16	05	01		MAP 2	hydrophone on deck	43.54740	7.57683		21.0				
POS-386	2009	06	23	17	00	39		MAP 2	station finished	43.54753	7.57972		20.9				
POS-386	2009	06	24	04	06	25	13	Gravity corer	station arrived	43.51085	7.35648	1766.0	21.0	W3			
POS-386	2009	06	24	04	07	25		Gravity corer	to water	43.51082	7.35647	1766.0	21.0	W3			
POS-386	2009	06	24	04	38	11		Gravity corer	at bottom	43.51085	7.35637	1768.0	21.1	W3	1907	Boko 1897 m	
POS-386	2009	06	24	04	38	47		Gravity corer	heave started	43.51085	7.35640	1768.0	21.1	W3	1907		
POS-386	2009	06	24	05	09	28		Gravity corer	on deck	43.51142	7.35643	1763.0	21.1	W3		station completed	
POS-386	2009	06	24	05	48	03	14	Gravity corer	station started	43.52252	7.35312	1630.0	21.2	W3			
POS-386	2009	06	24	05	49	02		Gravity corer	to water	43.52247	7.35322	1631.0	21.2	W3			
POS-386	2009	06	24	06	18	11		Gravity corer	at bottom	43.52250	7.35333	1650.0	21.1	W3	1794	Boko 1784m	
POS-386	2009	06	24	06	18	19		Gravity corer	heave started	43.52250	7.35332	1650.0	21.1	W3	1794	Boko 1784m	
POS-386	2009	06	24	06	48	00		Gravity corer	on deck	43.52262	7.35338	1647.0	21.1	W3			
POS-386	2009	06	24	08	11	31	15-1	CPT	Station started	43.64778	7.22087	13.3	22.4	W2			
POS-386	2009	06	24	08	12	42		CPT	to water	43.64778	7.22097	13.1	22.4	W2			
POS-386	2009	06	24	08	21	43		CPT	at bottom	43.64772	7.22082	15.2	22.5	W2	20		
POS-386	2009	06	24	09	21	47		CPT	heave started	43.64772	7.22088	14.3	22.8	W2	20		
POS-386	2009	06	24	09	22	10		CPT	at surface	43.64775	7.22087	14.1	22.8	W2	20		
POS-386	2009	06	24	09	23	23		CPT	on deck	43.64782	7.22095	12.9	22.8	W2	20		
POS-386	2009	06	24	09	38	49		CPT	Station started	43.64672	7.21918	26.6	22.9	W2			
POS-386	2009	06	24	09	38	56		CPT	to water	43.64672	7.21918	26.6	22.9	W2			
POS-386	2009	06	24	09	45	02		CPT	on deck	43.64682	7.21918	25.9	22.9	W2		Station ceased	





POS-386	2009	06	27	14	19	06		CPT plium		heave started	43.64513	7.21527	55.0	23.4		72		Boko 52m
POS-386	2009	06	27	14	22	09		CPT plium		at surface	43.64512	7.21552	51.0	23.3	W2			
POS-386	2009	06	27	14	26	11		CPT plium		on deck	43.64500	7.21597	62.0	23.3	W2			
POS-386	2009	06	27	14	54	00	21-5	CPT plium		station arrived	43.64268	7.21010	15.4	23.6	W2			
POS-386	2009	06	27	14	56	07		CPT plium		to water	43.64272	7.21000	15.2	23.5	W2	5		
POS-386	2009	06	27	15	01	31		CPT plium		at bottom	43.64265	7.21022	15.5	23.5	W2	19		Boko 16m
POS-386	2009	06	27	15	31	20		CPT plium		heave started	43.64283	7.21037	15.1	23.4	W2	38		
POS-386	2009	06	27	15	34	58		CPT plium		on deck	43.64297	7.20988	15.3	23.3	W2			
POS-386	2009	06	27	15	51	12		CPT plium		on deck	43.64275	7.20998	15.4	23.2	W2			station completed
POS-386	2009	06	27	16	04	02	21-6	CPT plium		to water	43.64310	7.21097	14.0	23.4	W2			station arrived
POS-386	2009	06	27	16	07	03		CPT plium		at bottom	43.64303	7.21110	14.1	23.5	W2	19		Boko 16m
POS-386	2009	06	27	16	38	01		CPT plium		heave started	43.64302	7.21105	14.9	23.3	W2	26		Boko 16m
POS-386	2009	06	27	16	39	36		CPT plium		at surface	43.64303	7.21100	14.6	23.2	W2			
POS-386	2009	06	27	16	59	10	21-7	CPT plium		to water	43.64375	7.21258	25.4	23.5	W2	5		
POS-386	2009	06	27	17	00	46		CPT plium		at bottom	43.64377	7.21247	21.6	23.4	W2	22		Boko 17m
POS-386	2009	06	27	17	31	40		CPT plium		heave started	43.64363	7.21265	36.7	23.5	W2	52		Boko 17m
POS-386	2009	06	27	17	35	23		CPT plium		at surface	43.64373	7.21278	34.5	23.4	W2			
POS-386	2009	06	27	17	39	56		CPT plium		on deck	43.64380	7.21260	30.8	23.4	W2			station completed
POS-386							22-1	Rn stations from Poseidon 3										
POS-386	2009	06	27	18	51	00	23-1	Bobcore		station arrived	43.64285	7.21043	15.1	23.2				
POS-386	2009	06	27	18	51	35		Bobcore		to water	43.64288	7.21040	15.0	23.2				
POS-386	2009	06	27	18	53	28		Bobcore		to water	43.64287	7.21027	17.4	23.2	W2	20		Boko 15
POS-386	2009	06	27	18	54	39		Bobcore		at surface	43.64283	7.21027	18.8	23.3	W2	20		Boko 15
POS-386	2009	06	27	18	54	49		Bobcore		on deck	43.64285	7.21028	16.6	23.3	W2	20		Boko 15
POS-386	2009	06	27	18	56	27		Bobcore		station completed	43.64290	7.21035	15.6	23.2	W2	20		Boko 15
POS-386	2009	06	27	19	04	12	23-2	Bobcore		station arrived	43.64323	7.21092	14.4	22.8	W2			
POS-386	2009	06	27	19	11	07		Bobcore		to water	43.64312	7.21083	14.4	22.8	W2			
POS-386	2009	06	27	19	13	44		Bobcore		at bottom	43.64322	7.21075	14.4	22.8	W2	22		Boko 16m
POS-386	2009	06	27	19	13	59		Bobcore		heave started	43.64320	7.21077	14.3	22.8	W2	22		Boko 16m
POS-386	2009	06	27	19	16	32		Bobcore		on deck	43.64333	7.21090	14.4	22.7	W2	22		Boko 16m
POS-386	2009	06	27	19	18	14		Bobcore		station completed	43.64325	7.21058	14.4	22.6	W2			
POS-386	2009	06	28	06	14	52	24-1	Bobcore	anchor deployment for scuba divers	station arrived	43.64668	7.21867	25.3	22.3	W3			
POS-386	2009	06	28	06	15	02		Bobcore	anchor deployment for scuba divers	anchorweight to water	43.64668	7.21865	25.4	22.4	W3			
POS-386	2009	06	28	06	18	13		Bobcore	anchor deployment for scuba divers	on deck	43.64675	7.21867	23.4	22.3	W3			interrupted, anchoring to short
POS-386	2009	06	28	06	24	56		Bobcore	anchor deployment for scuba divers	to water	43.64695	7.21862	16.6	22.3	W3			
POS-386	2009	06	28	06	27	36		Bobcore	anchor deployment for scuba divers	station completed	43.64608	7.21807	34.2	22.3	W3			
POS-386	2009	06	28	06	39	55	25	GC		station arrived	43.64603	7.21863	29.3	22.3	W3			
POS-386	2009	06	28	06	41	02		GC		to water	43.64600	7.21860	29.4	22.3	W3			
POS-386	2009	06	28	06	42	43		GC		at bottom	43.64600	7.21853	30.1	22.3	W3	42	34	
POS-386	2009	06	28	06	50	12		GC		on deck	43.64607	7.21855	30.6	22.3	W3			Banana
POS-386	2009	06	28	07	31	30		GC		station completed	43.63362	7.20772	358.0	22.5	W3			Banana
POS-386	2009	06	28	07	55	05	26	GC		station arrived	43.64482	7.22222	16.2	22.6	W3			
POS-386	2009	06	28	08	16	37		GC		to water	43.64507	7.22380	20.5	22.5	W3			
POS-386	2009	06	28	08	18	48		GC		at bottom	43.64507	7.22368	19.8	22.5	W3	25		Boko 17m
POS-386	2009	06	28	08	18	53		GC		heave started	43.64507	7.22367	19.8	22.5	W3	25		Boko 17m
POS-386	2009	06	28	08	24	29		GC		on deck	43.64508	7.22380	20.6	22.5	W3			
POS-386	2009	06	28	08	24	57		GC		station completed	43.64508	7.22387	20.8	22.5	W3			
POS-386	2009	06	28	08	53	01	27-1	CPT plium		station arrived	43.64667	7.21725	32.5	22.4	W2			
POS-386	2009	06	28	09	03	34		CPT plium		to water	43.64668	7.21737	34.4	22.3	W2			
POS-386	2009	06	28	09	16	14		CPT plium		at bottom	43.64675	7.21728	34.4	22.4	W2	41		Boko 36
POS-386	2009	06	28	09	52	50		CPT plium		on deck	43.64658	7.21727	32.7	22.4	W2			
POS-386	2009	06	28	09	53	35		CPT plium		Station completed	43.64657	7.21730	34.1	22.4	W2			
POS-386	2009	06	28	10	02	08	27-2	CPT plium		Station arrived	43.64612	7.21738	41.6	22.4	W2			
POS-386	2009	06	28	10	02	52		CPT plium		to water	43.64615	7.21735	42.2	22.3	W2			
POS-386	2009	06	28	10	17	07		CPT plium		at bottom	43.64600	7.21757	44.5	22.5	W2	52		Boko 48m

POS-386	2009	06	28	10	47	41		CPT plium		heave started		43.64590	7.21750	47.1	22.5	W2	52	Boko 48m
POS-386	2009	06	28	10	49	20		CPT plium		at surface		43.64597	7.21752	45.9	22.5	W2	58	
POS-386	2009	06	28	10	59	49	27-3	CPT plium		to water		43.64608	7.21838	30.2	22.6	W2	5	
POS-386	2009	06	28	11	03	58		CPT plium		at bottom		43.64608	7.21827	32.1	22.6	W2	39	Boko 35m
POS-386	2009	06	28	11	34	26		CPT plium		heave started		43.64598	7.21837	30.7	22.7	W2	49	Boko 35m
POS-386	2009	06	28	11	36	24		CPT plium		at surface		43.64605	7.21828	31.7	22.7	W2		
POS-386	2009	06	28	12	01	33	27-4	CPT plium		to water		43.64627	7.21915	20.2	22.7	W2		
POS-386	2009	06	28	12	06	07		CPT plium		at bottom		43.64627	7.21920	18.5	22.7	W2	31	Boko 26
POS-386	2009	06	28	12	34	28		CPT plium		heave started		43.64630	7.21933	18.6	22.6	W2	32	
POS-386	2009	06	28	12	35	47		CPT plium		at surface		43.64628	7.21945	17.8	22.6	W2		
POS-386	2009	06	28	12	36	18		CPT plium		on deck		43.64628	7.21943	17.8	22.6	W2		
POS-386	2009	06	28	12	41	38		CPT plium		station ceased		43.64620	7.21968	17.6	22.6	W2		
POS-386	2009	06	28	13	37	17		CPT plium		station cont.		43.64665	7.22015	16.7	22.8	W2		
POS-386	2009	06	28	13	37	26	27-5	CPT plium		to water		43.64665	7.22015	16.8	22.8	W2	5	
POS-386	2009	06	28	13	58	54		CPT plium		at bottom		43.64662	7.22005	16.6	22.7	W2	23	Boko 16m
POS-386	2009	06	28	14	33	38		CPT plium		heave started		43.64657	7.22017	16.7	23.2	W2	42	Boko 16m
POS-386	2009	06	28	14	36	58		CPT plium		at surface		43.64672	7.22000	16.7	23.3	W2		
POS-386	2009	06	28	14	38	20		CPT plium		station completed		43.64680	7.21987	17.0	23.3	W2		CPT broken
POS-386							22-2		Rn stations from Poseidon 3									
POS-386	2009	06	29	05	58	32	28	GC		station arrived		43.64133	7.21372	100.0	22.1	W3		
POS-386	2009	06	29	06	04	11		GC		to water		43.64132	7.21327	82.0	22.2	W3		
POS-386	2009	06	29	06	06	42		GC		at bottom		43.64133	7.21332	79.0	22.2	W3	84	Boko 76 m
POS-386	2009	06	29	06	06	55		GC		heave started		43.64133	7.21332	83.0	22.2	W3	84	
POS-386	2009	06	29	06	10	18		GC		on deck		43.64128	7.21318	90.0	22.2	W3		
POS-386	2009	06	29	06	10	54		GC		station completed		43.64128	7.21318	90.0	22.2	W3		
POS-386	2009	06	29	06	57	09	29	GC		station arrived		43.64597	7.21402	29.8	22.2	W3		
POS-386	2009	06	29	06	58	51		GC		to water		43.64600	7.21385	29.0	22.3	W3		
POS-386	2009	06	29	07	00	18		GC		at bottom		43.64607	7.21383	28.8	22.3	W3	34	Boko 26m
POS-386	2009	06	29	07	00	39		GC		heave started		43.64607	7.21385	28.9	22.3	W3		Boko 26m
POS-386	2009	06	29	07	03	18		GC		on deck		43.64610	7.21387	29.3	22.3	W3		
POS-386	2009	06	29	07	03	38		GC		station completed		43.64610	7.21388	29.9	22.3	W3		
POS-386	2009	06	29	07	31	08	30	GC		station arrived		43.64603	7.21825	40.8	22.4	W3		
POS-386	2009	06	29	07	32	36		GC		to water		43.64605	7.21825	40.4	22.4	W3		
POS-386	2009	06	29	07	34	25		GC		at bottom		43.64610	7.21822	41.0	22.4	W3	42	Boko 34m
POS-386	2009	06	29	07	39	07		GC		on deck		43.64608	7.21822	41.1	22.3	W3		Barana
POS-386	2009	06	29	10	52	56	31	Seamontice		station arrived		43.64565	7.21782	40.3	22.8	W3		
POS-386	2009	06	29	11	33	48		Seamontice		to water		43.64603	7.21798	35.3	22.8	W3		
POS-386	2009	06	29	11	36	20		Seamontice		at surface		43.64605	7.21830	31.5	22.8	W3		
POS-386	2009	06	29	11	37	27		Seamontice		at depth		43.64605	7.21825	31.4	22.8	W3	20	
POS-386	2009	06	29	11	47	52		Seamontice		at surface		43.64593	7.21835	30.2	22.9	W3	20	
POS-386	2009	06	29	11	48	09		Seamontice		at depth		43.64595	7.21838	29.8	22.9	W3	20	
POS-386	2009	06	29	11	58	31		Seamontice		heave started		43.64600	7.21873	22.6	23.0	W3	20	
POS-386	2009	06	29	11	58	45		Seamontice		at depth		43.64603	7.21868	23.0	22.9	W3	15	
POS-386	2009	06	29	12	02	54		Seamontice		slack started		43.64600	7.21837	30.6	22.9	W3	15	
POS-386	2009	06	29	12	03	56		Seamontice		at bottom		43.64602	7.21837	30.9	22.9	W3	45	Boko 39
POS-386	2009	06	29	12	09	28		Seamontice		heave started		43.64600	7.21833	32.5	22.9	W3	45	Boko 39
POS-386	2009	06	29	12	20	14		Seamontice		to water		43.64597	7.21893	20.8	23.0	W3		
POS-386	2009	06	29	12	20	59		Seamontice		at depth		43.64602	7.21893	22.8	23.0	W3	18	
POS-386	2009	06	29	12	21	41		Seamontice		at bottom		43.64608	7.21892	21.7	23.0	W3		
POS-386	2009	06	29	12	22	42		Seamontice		at bottom		43.64612	7.21867	25.6	23.0	W3		WD max 22m
POS-386	2009	06	29	12	27	54		Seamontice		Station completed		43.64610	7.21850	28.8	22.9	W3		
POS-386	2009	06	29	14	29	01	32-1	CPT		station arrived		43.64670	7.22100	14.9	23.3	W2		stations 376 cont.
POS-386	2009	06	29	14	42	53		CPT		to water		43.64687	7.22102	15.6	23.3	W2		stations 376 cont.
POS-386	2009	06	29	14	55	10		CPT		in water		43.64682	7.22098	15.7	23.4	W2		Hydrophone l/water
POS-386	2009	06	29	14	57	49		CPT		at bottom		43.64685	7.22100	16.0	23.4	W2	19	Hydrophone l/water - Boko 15m

POS-386	2009	06	29	15	25	38		CPT		at bottom		43.64688	7/22087	16.4	23.3	W2	25		Hydrophone on deck
POS-386	2009	06	29	15	32	18		CPT		heave started		43.64688	7/22093	16.3	23.3	W2	25		
POS-386	2009	06	29	15	33	19		CPT		at surface		43.64680	7/22088	16.4	23.3	W2			
POS-386	2009	06	29	16	00	39	32-2	CPT		to water		43.64613	7/21638	41.0	23.2	W2			
POS-386	2009	06	29	16	00	39		CPT		slack started		43.64622	7/21633	39.2	23.1	W2			
POS-386	2009	06	29	16	07	00		CPT		at bottom		43.64620	7/21630	39.9	23.1	W2	41		Boko 35m
POS-386	2009	06	29	16	39	10		CPT		heave started		43.64622	7/21618	40.3	23.0	W2	45		
POS-386	2009	06	29	16	41	52		CPT		at surface		43.64638	7/21638	36.1	23.0	W2	45		
POS-386	2009	06	29	16	57	13	32-3	CPT		to water		43.64675	7/21558	41.2	23.0	W2			
POS-386	2009	06	29	17	01	31		CPT		slack started		43.64573	7/21552	40.9	23.0	W2			
POS-386	2009	06	29	17	02	36		CPT		at bottom		43.64572	7/21545	40.8	23.0	W2	50		Boko 44m
POS-386	2009	06	29	17	33	05		CPT		heave started		43.64573	7/21542	39.4	23.2	W2	50		Boko 44m
POS-386	2009	06	29	17	34	41		CPT		at surface		43.64578	7/21548	40.0	23.2	W2			
POS-386	2009	06	29	17	37	26		CPT		on deck		43.64565	7/21565	41.6	23.2	W2			
POS-386	2009	06	29	17	37	51		CPT		station completed		43.64587	7/21567	41.5	23.2	W2			
POS-386						22-3													
POS-386						22-4													
POS-386						22-4													
POS-386	2009	06	30	06	00	10	33	Piezometer		station arrived		43.64258	7/21102	15.7	22.4	W3			
POS-386	2009	06	30	06	15	46		Piezometer		to water		43.64298	7/21093	14.4	22.5	W3			
POS-386	2009	06	30	06	25	36		Piezometer		at bottom		43.64298	7/21095	14.2	22.6	W4			Boko
POS-386	2009	06	30	06	29	32		Piezometer		Benthos to water		43.64318	7/21047	15.0	22.6				
POS-386	2009	06	30	06	30	12		Piezometer		station completed		43.64313	7/21018	19.3	22.6				
POS-386	2009	06	30	07	09	19	34	Piezometer		station arrived		43.64560	7/21323	37.2	22.8	W3			
POS-386	2009	06	30	07	13	23		Gravity corer		at bottom		43.64562	7/21315	37.4	22.8	W3	48		Boko 40m
POS-386	2009	06	30	07	16	21		Gravity corer		on deck		43.64557	7/21328	34.8	22.8	W3			
POS-386	2009	06	30	07	16	41		Gravity corer		station completed		43.64555	7/21333	34.5	22.8	W3			
POS-386	2009	06	30	07	41	21	35	Gravity corer		station arrived		43.64857	7/22593	17.7	22.9	W3			
POS-386	2009	06	30	07	43	27		Gravity corer		to water		43.64843	7/22550	16.4	22.9	W3			
POS-386	2009	06	30	07	45	07		Gravity corer		at bottom		43.64833	7/22523	16.6	23.0	W3	23		Boko 15 m
POS-386	2009	06	30	07	45	17		Gravity corer		heave started		43.64835	7/22522	16.5	22.9	W3	23		
POS-386	2009	06	30	07	48	03		Gravity corer		at surface		43.64865	7/22522	17.0	22.9	W3			
POS-386	2009	06	30	07	49	05		Gravity corer		on deck		43.64868	7/22522	17.0	22.9	W3			
POS-386	2009	06	30	07	50	02		Gravity Corer		station completed		43.64877	7/22540	16.9	22.9	W3			
POS-386	2009	06	30	08	40	22	36	Gravity Corer		station arrived		43.64345	7/21950	20.5	22.7	W3			
POS-386	2009	06	30	08	40	29		Gravity Corer		to water		43.64343	7/21948	20.5	22.7	W3			
POS-386	2009	06	30	08	42	04		Gravity Corer		at bottom		43.64338	7/21945	20.4	22.7	W3	37		Boko 29 m
POS-386	2009	06	30	08	42	37		Gravity Corer		heave started		43.64342	7/21947	20.4	22.7	W3	37		
POS-386	2009	06	30	08	44	58		Gravity Corer		at surface		43.64343	7/21925	18.8	22.7	W3			
POS-386	2009	06	30	08	45	26		Gravity Corer		on deck		43.64338	7/21913	18.8	22.7	W3			
POS-386	2009	06	30	08	45	47		Gravity Corer		station completed		43.64338	7/21905	18.8	22.7	W3			
POS-386	2009	06	30	10	02	56	37-1	CPT plium		station arrived		43.64715	7/22252	12.3	23.5	W2			
POS-386	2009	06	30	10	26	19		CPT plium		to water		43.64717	7/22263	12.1	22.6	W2			
POS-386	2009	06	30	10	36	40		CPT plium		slack started		43.64715	7/22253	12.1	22.7	W2			
POS-386	2009	06	30	10	38	09		CPT plium		at bottom		43.64715	7/22258	12.1	22.8	W2	17		Boko 12m
POS-386	2009	06	30	11	07	46		CPT plium		heave started		43.64720	7/22248	12.1	23.4	W2	22		Boko 12m
POS-386	2009	06	30	11	08	54		CPT plium		at surface		43.64720	7/22245	12.1	23.5	W2			
POS-386	2009	06	30	11	21	53		CPT plium		at surface		43.64677	7/22017	17.7	23.8	W2			
POS-386	2009	06	30	11	22	22	37-2	CPT plium		to water		43.64682	7/22012	19.1	23.9	W2			
POS-386	2009	06	30	11	31	37		CPT plium		at bottom		43.64672	7/22000	18.6	23.9	W2	21		Boko 18m
POS-386	2009	06	30	12	01	25		CPT plium		heave started		43.64675	7/22000	20.0	24.3	W2	31		Boko 18m
POS-386	2009	06	30	12	02	31		CPT plium		at surface		43.64677	7/22008	19.4	24.3	W2			
POS-386	2009	06	30	12	21	56		CPT plium		at surface		43.64685	7/21927	26.4	24.2	W2			
POS-386	2009	06	30	12	22	10	37-3	CPT plium		to water		43.64683	7/21930	26.0	24.1	W2	5		
POS-386	2009	06	30	12	26	58		CPT plium		at bottom		43.64677	7/21930	26.0	24.1	W2	31		Boko 26m
POS-386	2009	06	30	12	46	38		CPT plium		heave started		43.64683	7/21928	26.3	24.5	W2	31		Boko 26m

POS-386	2009	06	30	12	49	03		CPT plium		on deck	43.64697	7.21927	25.8	24.6	W2		
POS-386							22-5	Rn stations from Poseidon 3									
POS-386							24-2	Scuba diving results									
POS-386	2009	06	30	13	17	20	24-3	Anchor for scuba divers		at station	43.64705	7.21853	21.9	24.0	W2		
POS-386	2009	06	30	13	17	55		Anchor for scuba divers		picked up	43.64710	7.21852	23.6	24.0	W2		
POS-386	2009	06	30	13	18	40		Anchor for scuba divers		on deck	43.64718	7.21848	19.9	24.1	W3		
POS-386	2009	06	30	13	39	39		CPT plium		at surface	43.64685	7.21757	32.7	24.6	W2		
POS-386	2009	06	30	13	40	29	37-4	CPT plium		to water	43.64688	7.21760	34.4	24.7	W2	5	
POS-386	2009	06	30	13	51	48		CPT plium		at bottom	43.64698	7.21765	34.1	23.6	W2	35	Boko 31m
POS-386	2009	06	30	14	22	27		CPT plium		heave started	43.64703	7.21780	32.8	22.5	W2	39	Boko 31m
POS-386	2009	06	30	14	24	50		CPT plium		at surface	43.64705	7.21772	31.9	22.5	W2		
POS-386	2009	06	30	14	41	23	37-5	CPT plium		to water	43.64560	7.21748	40.8	22.8	W2		station arrived Boko 41 m
POS-386	2009	06	30	14	51	32		CPT plium		at bottom	43.64560	7.21460	41.1	22.7	W2	46	
POS-386	2009	06	30	15	21	38		CPT plium		heave started	43.64563	7.21465	37.2	22.7	W2	48	
POS-386	2009	06	30	15	23	05		CPT plium		at surface	43.64562	7.21470	41.9	22.7	W2		
POS-386	2009	06	30	15	26	15		CPT plium		on deck	43.64563	7.21478	41.1	22.8	W2		
POS-386	2009	07	01	06	09	18	38	Piezometer		station arrived	43.64142	7.21228	92.0	22.9	W4		
POS-386	2009	07	01	06	20	51		Piezometer		Kopbole an Deck	43.64260	7.21140	21.1	22.9	W4		
POS-386	2009	07	01	06	28	29		Piezometer		at surface	43.64285	7.21135	14.7	23.0	W4		
POS-386	2009	07	01	07	15	14		Piezometer		new position arrived	43.64732	7.21673	19.6	22.9	W4		
POS-386	2009	07	01	07	24	02		Piezometer		to water	43.64752	7.21680	12.9	23.0	W4		
POS-386	2009	07	01	07	26	37		Piezometer		at bottom	43.64742	7.21672	16.1	23.0	W4		Boko 16 m
POS-386	2009	07	01	07	31	13		Piezometer		Benthos to water	43.64717	7.21683	24.3	23.0	W4		
POS-386	2009	07	01	07	33	42		Piezometer		station completed	43.64660	7.21613	26.7	23.0	W4		
POS-386	2009	07	01	07	39	24	39	Gravity Corer		station started	43.64672	7.21750	29.1	22.9	W3		
POS-386	2009	07	01	07	40	27		Gravity Corer		to water	43.64677	7.21757	27.1	23.0	W3		
POS-386	2009	07	01	07	41	41		Gravity Corer		at bottom	43.64672	7.21755	27.7	23.0	W3	38	Boko 30 m
POS-386	2009	07	01	07	41	48		Gravity Corer		heave started	43.64672	7.21753	27.8	23.0	W3	38	Boko 30 m
POS-386	2009	07	01	07	43	00		Gravity Corer		at surface	43.64677	7.21748	28.7	23.0	W3		
POS-386	2009	07	01	07	43	58		Gravity Corer		on deck	43.64678	7.21747	28.5	23.0	W3		
POS-386	2009	07	01	07	46	30	39 (2 Versu	Gravity Corer		station started	43.64678	7.21775	24.1	23.0	W3		2nd trial
POS-386	2009	07	01	07	52	01		Gravity Corer		to water	43.64687	7.21760	25.5	23.1	W3		
POS-386	2009	07	01	07	54	15		Gravity Corer		at bottom	43.64675	7.21743	30.8	23.1	W3	40	Boko 32 m
POS-386	2009	07	01	07	54	19		Gravity Corer		heave started	43.64675	7.21743	30.6	23.1	W3	40	Boko 32 m
POS-386	2009	07	01	07	55	36		Gravity Corer		at surface	43.64675	7.21742	31.9	23.1	W3		
POS-386	2009	07	01	07	56	48		Gravity Corer		on deck	43.64672	7.21737	33.5	23.1	W3		
POS-386	2009	07	01	08	07	04		Gravity Corer		station completed	43.64513	7.21388	49.4	23.0	W3		
POS-386	2009	07	01	08	07	35	40	Gravity Corer		station arrived	43.64513	7.21383	51.0	23.0	W3		
POS-386	2009	07	01	08	23	10		Gravity Corer		to water	43.64522	7.21425	43.7	23.1	W3		
POS-386	2009	07	01	08	25	13		Gravity Corer		at bottom	43.64512	7.21413	44.4	23.1	W3	63	Boko 55 m
POS-386	2009	07	01	08	25	18		Gravity Corer		heave started	43.64513	7.21413	44.7	23.1	W3	63	Boko 55 m
POS-386	2009	07	01	08	27	03		Gravity Corer		at surface	43.64513	7.21400	44.1	23.1	W3		
POS-386	2009	07	01	08	27	57		Gravity Corer		on deck	43.64517	7.21395	42.4	23.1	W3		
POS-386	2009	07	01	08	28	44		Gravity Corer		station completed	43.64518	7.21387	43.0	23.1	W3		
POS-386	2009	07	01	08	50	29	41	Gravity Corer		station arrived	43.64830	7.22557	16.0	23.5	W3		
POS-386	2009	07	01	08	51	26		Gravity Corer		to water	43.64835	7.22562	18.2	23.5	W3		
POS-386	2009	07	01	08	53	34		Gravity Corer		at bottom	43.64835	7.22568	18.3	23.5	W3	22	Boko 14 m
POS-386	2009	07	01	08	53	38		Gravity Corer		heave started	43.64835	7.22568	18.4	23.5	W3	22	Boko 14 m
POS-386	2009	07	01	08	55	02		Gravity Corer		at surface	43.64838	7.22575	18.6	23.5	W3		
POS-386	2009	07	01	08	55	55		Gravity Corer		on deck	43.64835	7.22578	19.0	23.5	W3		
POS-386	2009	07	01	08	56	08		Gravity Corer		station completed	43.64835	7.22580	19.0	23.5	W3		
POS-386	2009	07	01	10	21	46	42-1	CPT cast		station arrived	43.63767	7.21705	178.0	23.5	W2		
POS-386	2009	07	01	10	22	13		CPT cast		to water	43.63767	7.21707	180.0	23.5	W2	5	
POS-386	2009	07	01	10	33	57		CPT cast		at bottom	43.63772	7.21702	174.0	23.6	W2	195	Boko 188m
POS-386	2009	07	01	11	04	18		CPT cast		heave started	43.63768	7.21718	170.0	23.5	W2	203	Boko 188m





POS-386	2009	07	02	07	48	07	47	Gravity corer	station arrived	43.63877	7.21373	133.0	23.2	W3			
POS-386	2009	07	02	07	49	38		Gravity corer	to water	43.63862	7.21363	131.0	23.2	W3			
POS-386	2009	07	02	07	52	49		Gravity corer	at bottom	43.63898	7.21375	123.0	23.2	W3	162	Boko 154 m	
POS-386	2009	07	02	07	52	55		Gravity corer	heave started	43.63898	7.21375	121.0	23.2	W3	162	Boko 154 m	
POS-386	2009	07	02	07	55	56		Gravity corer	at surface	43.63902	7.21390	120.0	23.2	W3			
POS-386	2009	07	02	07	56	50		Gravity corer	on deck	43.63902	7.21390	119.0	23.2	W3			
POS-386	2009	07	02	07	57	43		Gravity corer	station completed	43.63897	7.21387	126.0	23.2	W3			
POS-386	2009	07	02	08	19	50	48	Gravity corer	station arrived	43.63910	7.21360	382.0	23.4	W3			
POS-386	2009	07	02	08	24	37		Gravity corer	to water	43.63902	7.21357	388.0	23.4	W3			
POS-386	2009	07	02	08	31	13		Gravity corer	at bottom	43.62998	7.21363	392.0	23.5	W3	436	Boko 428m	
POS-386	2009	07	02	08	31	31		Gravity corer	heave started	43.63900	7.21363	404.0	23.5	W3	436		
POS-386	2009	07	02	08	39	24		Gravity corer	on deck	43.63902	7.21240	388.0	23.5	W3	436		
POS-386	2009	07	02	08	52	55		Gravity corer	station arrived	43.62978	7.21370	388.0	23.6	W3			
POS-386	2009	07	02	08	59	03		Gravity corer	to water	43.63905	7.21357	383.0	23.7	W3			
POS-386	2009	07	02	09	03	58		Gravity corer	at bottom	43.62998	7.21353	392.0	23.7	W3	445	Boko 437m	
POS-386	2009	07	02	09	04	03		Gravity corer	heave started	43.62997	7.21353	388.0	23.7	W3	445	Boko 437m	
POS-386	2009	07	02	09	11	57		Gravity corer	on deck	43.63023	7.21328	381.0	23.6	W3			
POS-386	2009	07	02	09	12	53		Gravity corer	Station completed	43.63028	7.21323	380.0	23.6	W3			
POS-386	2009	07	02	11	31	19	49-1	CPT cast	Station arrived	43.64205	7.21100	99.0	24.0	W2	5		
POS-386	2009	07	02	11	31	26		CPT cast	to water	43.64203	7.21102	99.0	24.0	W2	5		
POS-386	2009	07	02	11	40	16		CPT cast	slack started	43.64197	7.21102	99.0	24.2	W2	5		
POS-386	2009	07	02	11	41	23		CPT cast	at bottom	43.64207	7.21098	99.0	24.2	W2	67	Boko 62m	
POS-386	2009	07	02	12	17	53		CPT cast	heave started	43.64207	7.21103	55.0	24.1	W2	67	Boko 62m	
POS-386	2009	07	02	12	20	00		CPT cast	at surface	43.64215	7.21105	44.2	24.0	W2			
POS-386	2009	07	02	12	23	50		CPT cast	on deck	43.64233	7.21095	38.1	23.9	W2			
POS-386	2009	07	02	12	49	22	49-2	CPT cast	to water	43.64393	7.21090	13.4	24.0	W2			
POS-386	2009	07	02	13	06	46		CPT cast	slack started	43.64398	7.21088	13.6	23.9	W2	5		
POS-386	2009	07	02	13	07	59		CPT cast	at bottom	43.64403	7.21087	13.3	23.8	W2	23	Boko 18m	
POS-386	2009	07	02	13	41	04		CPT cast	heave started	43.64403	7.21087	13.6	24.0	W2	28	Boko 18m	
POS-386	2009	07	02	13	41	57		CPT cast	at surface	43.64407	7.21092	13.3	24.0	W2			
POS-386	2009	07	02	13	43	12		CPT cast	on deck	43.64412	7.21097	13.3	23.9	W2			
POS-386	2009	07	02	13	56	21	49-3	CPT cast	to water	43.64535	7.21192	15.0	24.2	W2			
POS-386	2009	07	02	13	56	38		CPT cast	slack started	43.64537	7.21193	14.4	24.2	W2	5		
POS-386	2009	07	02	13	58	01		CPT cast	at bottom	43.64537	7.21190	12.9	24.2	W2			
POS-386	2009	07	02	13	58	53		CPT cast	at bottom	43.64538	7.21188	12.7	24.1	W2	29	Boko 25m	
POS-386	2009	07	02	14	30	50		CPT cast	heave started	43.64552	7.21197	18.5	24.3	W2	46	Boko 25m	
POS-386	2009	07	02	14	33	45		CPT cast	at surface	43.64550	7.21217	25.5	24.3	W2			
POS-386	2009	07	02	14	47	47		CPT cast	at surface	43.64567	7.21330	41.3	24.2	W2			
POS-386	2009	07	02	14	49	16	49-4	CPT cast	to water	43.64570	7.21337	42.2	24.2	W2	5		
POS-386	2009	07	02	14	52	23		CPT cast	slack started	43.64573	7.21328	43.7	24.3	W2	5		
POS-386	2009	07	02	14	53	44		CPT cast	at bottom	43.64585	7.21327	35.0	24.2	W2	44	Boko 39m	
POS-386	2009	07	02	15	25	51		CPT cast	heave started	43.64565	7.21340	41.4	24.3	W2	47	Boko 39m	
POS-386	2009	07	02	15	27	01		CPT cast	at surface	43.64570	7.21335	38.9	24.3	W2			
POS-386	2009	07	02	15	55	45		CPT cast	at surface	43.64677	7.21923	24.3	24.3	W2			
POS-386	2009	07	02	15	55	50	49-5	CPT cast	to water	43.64678	7.21923	25.9	24.3	W2	5		
POS-386	2009	07	02	16	01	07		CPT cast	slack started	43.64682	7.21927	25.0	24.3	W2	5		
POS-386	2009	07	02	16	01	59		CPT cast	at bottom	43.64685	7.21925	24.6	24.3	W2	31	Boko 25m	
POS-386	2009	07	02	16	31	39		CPT cast	heave started	43.64678	7.21913	24.8	24.0	W2	35	Boko 25m	
POS-386	2009	07	02	16	35	36		CPT cast	at surface	43.64695	7.21913	26.5	24.0	W2			
POS-386	2009	07	02	16	44	17		CPT cast	at surface	43.64660	7.21975	18.0	24.3	W2			
POS-386	2009	07	02	16	45	09	49-6	CPT cast	to water	43.64660	7.21983	17.8	24.2	W2	5		
POS-386	2009	07	02	16	49	14		CPT cast	slack started	43.64673	7.21987	18.9	24.1	W2	5		
POS-386	2009	07	02	16	50	06		CPT cast	at bottom	43.64672	7.21982	18.1	24.0	W2	24	Boko 19m	
POS-386	2009	07	02	17	23	57		CPT cast	heave started	43.64673	7.21985	19.5	24.0	W2	31	Boko 19m	
POS-386	2009	07	02	17	25	37		CPT cast	at surface	43.64673	7.21975	20.3	24.0	W2			

POS-386	2009	07	02	17	56	36		CPT cast				43.64708	7.22245	12.9	24.0	W2			
POS-386	2009	07	02	17	57	15	49-7	CPT cast	at surface			43.64708	7.22252	13.0	24.0	W2	5		
POS-386	2009	07	02	18	02	47		CPT cast	slack started			43.64723	7.22253	12.8	23.9	W2	5		
POS-386	2009	07	02	18	04	33		CPT cast	at bottom			43.64720	7.22258	13.0	23.8	W2	19	Boko 14m	
POS-386	2009	07	02	18	31	56		CPT cast	heave started			43.64723	7.22255	12.4	24.1	W2	19	Boko 14m	
POS-386	2009	07	02	18	35	38		CPT cast	at surface			43.64728	7.22258	12.3	24.1	W2			
POS-386	2009	07	02	18	39	06		CPT cast	on deck, station completed			43.64630	7.22293	14.6	24.1	W2			
POS-386	2009	07	03	05	58	13	50	Rn measurements from deck											
POS-386	2009	07	03	06	06	43		Piezometer	station arrived			43.64245	7.22138	40.0	23.8	W4			
POS-386	2009	07	03	06	10	10		Piezometer	Top buoy, picked up			43.64305	7.22243	47.8	23.8	W4			
POS-386	2009	07	03	06	10	10		Piezometer	heave started			43.64300	7.22258	53.0	23.7	W4			
POS-386	2009	07	03	06	22	45		Piezometer	on deck			43.64312	7.22258	48.6	23.8	W4			
POS-386	2009	07	03	06	44	06		Piezometer	station completed			43.63668	7.23055	286.0	24.0	W4			
POS-386	2009	07	03	07	05	03	51	GC	station arrived			43.64382	7.21870	15.5	23.8	W3			
POS-386	2009	07	03	07	06	13		GC	to water			43.64383	7.21895	15.9	23.8	W3			
POS-386	2009	07	03	07	09	36		GC	at bottom			43.64402	7.21913	14.9	23.8	W3	20	Boko 12 m	
POS-386	2009	07	03	07	09	50		GC	heave started			43.64402	7.21910	14.8	23.8	W3	20	Boko 12 m	
POS-386	2009	07	03	07	13	17		GC	at surface			43.64395	7.21917	15.8	23.9	W3			
POS-386	2009	07	03	07	14	19		GC	on deck			43.64395	7.21917	15.5	23.9	W3			
POS-386	2009	07	03	07	14	43		GC	station completed			43.64393	7.21917	15.5	23.9	W3			
POS-386	2009	07	03	07	32	18	52	GC	station arrived			43.64385	7.22227	24.8	23.9	W3			
POS-386	2009	07	03	07	51	19		GC	to water			43.64378	7.22235	26.2	23.8	W3			
POS-386	2009	07	03	07	52	36		GC	at bottom			43.64380	7.22225	25.9	23.8	W3	29	Boko 21m	
POS-386	2009	07	03	07	52	39		GC	heave started			43.64380	7.22225	26.0	23.8	W3	29	Boko 21m	
POS-386	2009	07	03	07	54	10		GC	at surface			43.64380	7.22230	25.7	23.8	W3			
POS-386	2009	07	03	07	55	24		GC	on deck			43.64378	7.22223	24.5	23.8	W3			
POS-386	2009	07	03	07	55	44		GC	station completed			43.64385	7.22223	24.2	23.8	W3			
POS-386	2009	07	03	08	23	08	53	GC	station arrived			43.64750	7.21667	18.0	23.9	W3			
POS-386	2009	07	03	08	26	14		GC	to water			43.64752	7.21678	16.7	24.0	W3			
POS-386	2009	07	03	08	27	47		GC	at bottom			43.64750	7.21677	19.7	24.0	W3	22	Boko 14 m	
POS-386	2009	07	03	08	27	51		GC	heave started			43.64750	7.21677	18.3	24.0	W3	22	Boko 14 m	
POS-386	2009	07	03	08	28	57		GC	at surface			43.64752	7.21677	17.6	24.0	W3			
POS-386	2009	07	03	08	29	55		GC	on deck			43.64753	7.21678	16.4	24.0	W3			
POS-386	2009	07	03	08	30	11		GC	station completed			43.64753	7.21677	16.9	24.0	W3			
POS-386	2009	07	03	10	01	52	54-1	Piezometer CPT	station arrived			43.64292	7.21068	14.0	24.0	W2			
POS-386	2009	07	03	10	06	54		Piezometer CPT	to water			43.64302	7.21072	13.9	23.9	W2			
POS-386	2009	07	03	10	08	34		Piezometer CPT	slack started			43.64303	7.21072	13.8	23.9	W2			
POS-386	2009	07	03	10	17	28		Piezometer CPT	slack started			43.64302	7.21063	13.9	23.9	W2	5		
POS-386	2009	07	03	10	18	07		Piezometer CPT	at bottom			43.64307	7.21063	13.7	23.9	W2	20	Boko 16m	
POS-386	2009	07	03	10	25	02		Piezometer CPT	heave started			43.64313	7.21073	13.6	24.0	W2	26	Boko 16m	
POS-386	2009	07	03	10	28	40		Piezometer CPT	at surface			43.64305	7.21067	13.8	24.0	W2	26	Boko 16m	
POS-386	2009	07	03	10	49	20	54-2	Piezometer CPT	to water			43.64743	7.21668	21.8	24.4	W2	5		
POS-386	2009	07	03	10	51	14		Piezometer CPT	slack started			43.64742	7.21670	24.8	24.4	W2	5		
POS-386	2009	07	03	10	51	34		Piezometer CPT	slack stopped			43.64750	7.21662	25.0	24.4	W2	5		
POS-386	2009	07	03	10	51	51		Piezometer CPT	at bottom			43.64747	7.21662	25.2	24.4	W2	26	Boko 22m	
POS-386	2009	07	03	10	52	43		Piezometer CPT	heave started			43.64742	7.21662	26.6	24.4	W2			
POS-386	2009	07	03	10	53	23		Piezometer CPT	at surface			43.64740	7.21658	26.8	24.4	W2			
POS-386	2009	07	03	11	10	27	54-3	Piezometer CPT cast	station started			43.64333	7.22258	45.7	24.4	W2			
POS-386	2009	07	03	11	10	42		Piezometer CPT cast	to water			43.64333	7.22265	44.8	24.4	W2	5		
POS-386	2009	07	03	11	19	02		Piezometer CPT cast	slack started			43.64337	7.22247	39.5	24.2	W2	5		
POS-386	2009	07	03	11	19	44		Piezometer CPT cast	at bottom			43.64337	7.22245	39.2	24.2	W2	40	Boko 36m	
POS-386	2009	07	03	11	21	48		Piezometer CPT cast	heave started			43.64330	7.22238	39.8	24.1	W2	40	Boko 36m	
POS-386	2009	07	03	11	23	20		Piezometer CPT cast	at surface			43.64335	7.22238	38.3	24.1	W2			
POS-386	2009	07	03	11	37	43		Piezometer CPT cast	at surface			43.64388	7.21957	16.5	24.4	W2			
POS-386	2009	07	03	11	38	16	54-4	Piezometer CPT cast	to water			43.64388	7.21957	16.4	24.4	W2	5		

POS-386	2009	07	03	11	47	57		Piezometer CPT cast		slack stopped at bottom	43.64402	7.21915	14.5	24.1	W2	5	
POS-386	2009	07	03	11	48	16		Piezometer CPT cast		heave started	43.64403	7.21915	14.4	24.1	W2	22	Boko 18m
POS-386	2009	07	03	11	53	10		Piezometer CPT cast		at surface	43.64403	7.21918	14.7	24.1	W2	22	
POS-386	2009	07	03	11	54	07		Piezometer CPT cast		Station started, at surface	43.64403	7.21915	14.5	24.1	W2		
POS-386	2009	07	03	12	09	42		Piezometer CPT cast		to water	43.64607	7.21382	29.7	24.6	W2	5	
POS-386	2009	07	03	12	10	31	54-5	Piezometer CPT cast		slack started at bottom	43.64605	7.21380	30.5	24.5	W2	5	
POS-386	2009	07	03	12	12	12		Piezometer CPT cast		heave started	43.64602	7.21378	31.5	24.5	W2	35	Boko 31m
POS-386	2009	07	03	12	13	00		Piezometer CPT cast		at surface	43.64600	7.21382	30.3	24.5	W2	35	Boko 31m
POS-386	2009	07	03	12	14	42		Piezometer CPT cast		Station started, at surface	43.64600	7.21370	32.3	24.5	W2		
POS-386	2009	07	03	12	33	04		Piezometer CPT cast		to water	43.64203	7.21108	68.0	24.6	W2	5	
POS-386	2009	07	03	12	33	29	54-6	Piezometer CPT cast		slack started at bottom	43.64190	7.21110	74.0	24.5	W2	5	Boko 72m
POS-386	2009	07	03	12	37	52		Piezometer CPT cast		heave started at surface	43.64180	7.21107	81.0	24.5	W2	76	Boko 72m
POS-386	2009	07	03	12	38	45		Piezometer CPT cast		Station started, at surface	43.64173	7.21110	88.0	24.4	W2	21	
POS-386	2009	07	03	12	40	44		Piezometer CPT cast		to water	43.64560	7.21322	46.3	24.7	W2	5	
POS-386	2009	07	03	13	01	19		Piezometer CPT cast		slack started at bottom	43.64562	7.21323	42.0	24.7	W2	5	
POS-386	2009	07	03	13	02	10	54-7	Piezometer CPT cast		heave started	43.64568	7.21325	42.6	24.7	W2	43	Boko 38m
POS-386	2009	07	03	13	03	22		Piezometer CPT cast		Station started, at surface	43.64562	7.21325	43.0	24.8	W2	43	Boko 38m
POS-386	2009	07	03	13	04	53		Piezometer CPT cast		to water	43.64367	7.21077	13.2	24.7	W2		
POS-386	2009	07	03	13	19	44		Piezometer CPT cast		slack started at bottom	43.64368	7.21075	13.3	24.7	W2	5	
POS-386	2009	07	03	13	20	09	54-8	Piezometer CPT cast		Station started, at surface	43.64375	7.21083	13.2	24.7	W2	5	
POS-386	2009	07	03	13	22	00		Piezometer CPT cast		heave started	43.64372	7.21073	13.3	24.7	W2	21	Boko 17m
POS-386	2009	07	03	13	23	27		Piezometer CPT cast		to water	43.64370	7.21070	13.3	24.7	W2	21	Boko 17m
POS-386	2009	07	03	13	24	15		Piezometer CPT cast		slack started at bottom	43.64535	7.21215	41.3	24.8	W2	5	
POS-386	2009	07	03	13	36	04	54-9	Piezometer CPT cast		Station started, at surface	43.64538	7.21210	39.1	24.7	W2	39	Boko 35m
POS-386	2009	07	03	13	41	12		Piezometer CPT cast		heave started	43.64532	7.21205	38.6	24.7	W2	40	
POS-386	2009	07	03	13	41	58		Piezometer CPT cast		Station started, at surface	43.64677	7.21733	33.2	24.9	W2		
POS-386	2009	07	03	14	02	30		Piezometer CPT cast		to water	43.64685	7.21748	30.2	24.9	W2	39	Boko 35m
POS-386	2009	07	03	14	10	56		Piezometer CPT cast		heave started at bottom	43.64687	7.21740	34.2	24.8	W2	39	Boko 35m
POS-386	2009	07	03	14	12	07		Piezometer CPT cast		Station started, at surface	43.64672	7.21910	22.9	24.8	W2		
POS-386	2009	07	03	14	23	27	54-11	Piezometer CPT cast		to water	43.64677	7.21907	23.4	24.9	W2	5	
POS-386	2009	07	03	14	26	26		Piezometer CPT cast		slack started at bottom	43.64678	7.21913	23.1	24.8	W2	5	Boko
POS-386	2009	07	03	14	26	57		Piezometer CPT cast		heave started	43.64675	7.21920	22.2	24.8	W2	31	Boko 26m
POS-386	2009	07	03	14	27	54		Piezometer CPT cast		Station started, at surface	43.64670	7.21963	17.0	24.8	W2	31	Boko 26m
POS-386	2009	07	03	14	28	57		Piezometer CPT cast		to water	43.64672	7.21960	17.2	24.8	W2		
POS-386	2009	07	03	14	32	30	54-12	Piezometer CPT cast		slack started at bottom	43.64668	7.21985	16.0	24.8	W2	5	
POS-386	2009	07	03	14	35	00		Piezometer CPT cast		heave started	43.64665	7.21980	15.6	24.8	W2	24	Boko 20m
POS-386	2009	07	03	14	36	20		Piezometer CPT cast		Station started, at surface	43.64670	7.21983	15.7	24.8	W2	24	Boko 20m
POS-386	2009	07	03	14	37	35		Piezometer CPT cast		to water	43.64837	7.22277	6.8	25.0	W2		
POS-386	2009	07	03	14	47	43	54-13	Piezometer CPT cast		heave started at bottom	43.64835	7.22282	6.5	24.8	W2	9	Boko 6m
POS-386	2009	07	03	14	54	28		Piezometer CPT cast		Station started, at surface	43.64832	7.22278	6.8	24.8	W2	9	Boko 6m
POS-386	2009	07	03	15	06	06		Piezometer CPT cast									

POS-386	2009	07	03	15	10	29		Piezometer CPT cast	on deck	43.64855	7.22300	7.2	24.8	W2		
POS-386	2009	07	03	15	10	37		Piezometer CPT cast	on deck	43.64857	7.22300	7.2	24.9	W2	19	
POS-386	2009	07	03	15	10	49	54-13 (Wed)	Piezometer CPT cast	started	43.64858	7.22300	7.2	24.9	W2	19	
POS-386	2009	07	03	15	11	07		Piezometer CPT cast	at bottom	43.64862	7.22300	7.2	24.8	W2	10	Boko 6m
POS-386	2009	07	03	15	11	23		Piezometer CPT cast	at surface	43.64863	7.22300	7.4	24.8	W2		
POS-386	2009	07	03	15	11	31		Piezometer CPT cast	on deck	43.64865	7.22300	7.3	24.8	W2		
POS-386	2009	07	03	15	16	16		Piezometer CPT cast	station arrived	43.64867	7.22298	6.8	24.9	W2		
POS-386	2009	07	03	15	17	21	54-13 (Wed)	Piezometer CPT cast	to water	43.64867	7.22298	6.9	24.9	W2		
POS-386	2009	07	03	15	17	23		Piezometer CPT cast	at bottom	43.64870	7.22298	6.9	24.9	W2	11	Boko 7m
POS-386	2009	07	03	15	17	12		Piezometer CPT cast	on deck	43.64870	7.22298	6.9	24.9	W2		
POS-386	2009	07	03	15	17	25		Piezometer CPT cast	station completed	43.64872	7.22298	6.9	24.9	W2		
POS-386	2009	07	03	15	29	38		Piezometer CPT cast	Station started, at surface	43.64538	7.22413	20.9	25.1	W2		
POS-386	2009	07	03	15	30	19	54-14	Piezometer CPT cast	to water	43.64538	7.22417	21.4	25.1	W2	5	
POS-386	2009	07	03	15	31	21		Piezometer CPT cast	slack started	43.64533	7.22423	21.9	25.0	W2	5	
POS-386	2009	07	03	15	31	35		Piezometer CPT cast	at bottom	43.64535	7.22420	22.0	25.0	W2	25	Boko 21m
POS-386	2009	07	03	15	32	16		Piezometer CPT cast	heave started	43.64533	7.22422	22.1	25.0	W2	25	Boko 21m
POS-386	2009	07	03	15	33	15		Piezometer CPT cast	at surface	43.64530	7.22427	22.6	25.0	W2		
POS-386	2009	07	03	15	51	00		Piezometer CPT cast	Station started, at surface	43.64422	7.22165	18.6	24.9	W2		
POS-386	2009	07	03	15	51	22	54-15	Piezometer CPT cast	to water	43.64422	7.22168	18.7	24.9	W2	5	
POS-386	2009	07	03	15	52	34		Piezometer CPT cast	slack started	43.64425	7.22172	18.8	24.8	W2	5	
POS-386	2009	07	03	15	53	00		Piezometer CPT cast	at bottom	43.64428	7.22163	18.6	24.8	W2	25	Boko 21m
POS-386	2009	07	03	15	53	21		Piezometer CPT cast	heave started	43.64428	7.22165	18.4	24.8	W2	25	Boko 21m
POS-386	2009	07	03	15	54	20		Piezometer CPT cast	at surface	43.64430	7.22160	18.3	24.8	W2		
POS-386	2009	07	03	15	55	37		Piezometer CPT cast	on deck	43.64428	7.22162	18.4	24.8	W2		
POS-386	2009	07	03	15	55	54		Piezometer CPT cast	Station completed	43.64430	7.22163	18.5	24.8	W2		
POS-386						55		Rn stations from deck								
POS-386	2009	07	04	06	02	23	56	Gravity Corer	Station arrived	43.64422	7.21263	33.4	24.2	W3		
POS-386	2009	07	04	06	04	19		Gravity Corer	to water	43.64422	7.21287	38.4	24.2	W3		
POS-386	2009	07	04	06	05	20		Gravity Corer	at bottom	43.64422	7.21288	42.4	24.2	W3	54	Boko 46 m
POS-386	2009	07	04	06	08	24		Gravity Corer	on deck	43.64423	7.21267	34.8	24.1	W3		
POS-386	2009	07	04	06	43	47		Gravity Corer	station arrived	43.64240	7.21807	69.0	24.4	W3		
POS-386	2009	07	04	06	43	52	57	Gravity Corer	to water	43.64240	7.21805	74.0	24.4	W3		
POS-386	2009	07	04	06	45	24		Gravity Corer	at bottom	43.64238	7.21807	71.0	24.4	W3	73	Boko 65 m
POS-386	2009	07	04	06	45	28		Gravity Corer	heave started	43.64240	7.21807	72.0	24.4	W3	73	Boko 65 m
POS-386	2009	07	04	06	47	42		Gravity Corer	at surface	43.64243	7.21802	69.0	24.4	W3		
POS-386	2009	07	04	06	48	32		Gravity Corer	on deck	43.64245	7.21802	68.0	24.4	W3		
POS-386	2009	07	04	07	11	30	58	Gravity Corer	station arrived	43.64313	7.21783	44.2	24.4	W3		
POS-386	2009	07	04	07	12	09		Gravity Corer	to water	43.64312	7.21787	44.3	24.4	W3		
POS-386	2009	07	04	07	13	41		Gravity Corer	at surface	43.64312	7.21780	47.0	24.4	W3	40	Boko 32 m
POS-386	2009	07	04	07	16	06		Gravity Corer	at bottom	43.64320	7.21778	48.8	24.5	W3		
POS-386	2009	07	04	07	16	35		Gravity Corer	on deck	43.64320	7.21777	50.0	24.5	W3		
POS-386	2009	07	04	09	15	10	59	Piezometer	at station	43.64403	7.21937	14.3	24.7	W3		
POS-386	2009	07	04	09	27	39		Piezometer	to water	43.64405	7.21948	14.9	24.6	W3		
POS-386	2009	07	04	09	49	15		Piezometer	at bottom	43.64395	7.21952	15.9	24.9	W3		
POS-386	2009	07	04	09	49	51		Piezometer	on deck	43.64398	7.21957	15.9	24.9	W3		
POS-386	2009	07	04	09	50	38		Piezometer	Station Completed	43.64403	7.21963	15.4	24.9	W3		
POS-386	2009	07	04	10	59	58	60-1	CPT	Station arrived / to water	43.64213	7.21090	69.0	25.0	W2	5	
POS-386	2009	07	04	11	11	01		CPT	slack started	43.64205	7.21088	64.0	24.9	W2	5	
POS-386	2009	07	04	11	11	53		CPT	at bottom	43.64203	7.21092	67.0	24.9	W2	58	Boko 53m
POS-386	2009	07	04	11	43	53		CPT	heave started	43.64198	7.21093	66.0	25.1	W2	60	Boko 53m
POS-386	2009	07	04	11	46	55		CPT	at surface / bulkhead	43.64210	7.21102	56.0	25.1	W2		
POS-386	2009	07	04	11	55	52		CPT	at surface / bulkhead	43.64393	7.21102	13.5	25.0	W2		
POS-386	2009	07	04	12	00	22	60-2	CPT	to water	43.64382	7.21105	13.3	25.0	W2	5	
POS-386	2009	07	04	12	03	30		CPT	slack started	43.64390	7.21108	13.3	25.0	W2	5	
POS-386	2009	07	04	12	03	54		CPT	at bottom	43.64388	7.21108	13.2	25.0	W2	19	Boko 14m




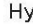

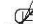


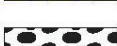




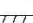

















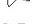







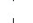











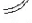
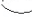
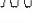
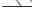
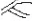





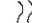
POS-386	2009	07	04	12	28	26		CPT		heave started		43.64375	7.21100	13.5	25.2	W2	40		Boko 14m
POS-386	2009	07	04	12	34	54		CPT		at surface		43.64382	7.21113	13.4	25.3	W2	40		
POS-386	2009	07	04	12	52	28	60-3	CPT		to water		43.64593	7.21407	30.8	25.5	W2	5		
POS-386	2009	07	04	12	59	15		CPT		slack started		43.64593	7.21392	34.9	25.1	W2			
POS-386	2009	07	04	13	00	32		CPT		at bottom		43.64597	7.21398	31.7	25.2	W2	36		Boko 31m
POS-386	2009	07	04	13	30	43		CPT		heave started		43.64593	7.21395	32.3	25.1	W2	39		
POS-386	2009	07	04	13	32	03		CPT		at surface		43.64602	7.21393	31.5	25.1	W2			
POS-386	2009	07	04	13	39	16	60-4	CPT		to water		43.64558	7.21338	49.0	25.3	W2	5		
POS-386	2009	07	04	13	42	23		CPT		slack started		43.64558	7.21338	50.0	25.4	W2	5		
POS-386	2009	07	04	13	43	09		CPT		at bottom		43.64558	7.21340	49.7	25.4	W2	47		Boko 40m
POS-386	2009	07	04	14	11	51		CPT		heave started		43.64560	7.21320	43.1	25.4	W2	50		Boko 40m
POS-386	2009	07	04	14	14	10		CPT		at surface		43.64557	7.21323	49.7	25.4	W2			
POS-386	2009	07	04	14	39	15		CPT		Station arrived / at surface		43.64737	7.21667	24.3	25.5	W2			
POS-386	2009	07	04	14	39	46	60-5	CPT		to water		43.64740	7.21672	24.9	25.4	W2	5		
POS-386	2009	07	04	14	41	26		CPT		slack started		43.64747	7.21665	24.9	25.4	W2	5		
POS-386	2009	07	04	14	42	16		CPT		at bottom		43.64747	7.21665	24.6	25.4	W2	5		on bottom laying
POS-386	2009	07	04	14	42	42		CPT		heave started		43.64748	7.21663	24.0	25.4	W2	5		
POS-386	2009	07	04	14	42	57		CPT		at surface		43.64748	7.21663	25.0	25.4	W2	5		
POS-386	2009	07	04	14	43	36		CPT		at surface		43.64750	7.21665	24.1	25.4	W2	5		
POS-386	2009	07	04	14	44	01		CPT		slack started		43.64753	7.21663	23.8	25.4	W2	5		
POS-386	2009	07	04	14	45	04		CPT		at bottom		43.64755	7.21662	25.0	25.4	W2	22		Boko 18m
POS-386	2009	07	04	14	47	06		CPT		heave started		43.64755	7.21658	22.2	25.3	W2	22		Boko 18m
POS-386	2009	07	04	14	48	05		CPT		at surface		43.64752	7.21655	22.9	25.3	W2			
POS-386	2009	07	04	14	54	45		CPT		Station arrived / at surface		43.64713	7.21663	27.9	25.4	W2			
POS-386	2009	07	04	14	55	14		CPT		to water		43.64712	7.21665	29.1	25.5	W2	5		
POS-386	2009	07	04	14	56	25	60-5 Wieda	CPT		slack started		43.64703	7.21663	28.8	25.5	W2	5		
POS-386	2009	07	04	14	57	05		CPT		at bottom		43.64703	7.21663	28.4	25.5	W2	35		Boko 28m
POS-386	2009	07	04	15	26	40		CPT		heave started		43.64708	7.21652	28.4	25.4	W2	38		Boko 28m
POS-386	2009	07	04	15	36	00		CPT		at surface		43.64708	7.21658	26.2	25.3	W2			
POS-386	2009	07	04	16	08	48	60-6	CPT		Station arrived / at surface		43.64323	7.22265	45.9	25.4	W2			
POS-386	2009	07	04	16	09	33		CPT		to water		43.64327	7.22267	46.0	25.4	W2	5		
POS-386	2009	07	04	16	12	00		CPT		slack started		43.64328	7.22267	39.7	25.4	W2	5		
POS-386	2009	07	04	16	12	47		CPT		at bottom		43.64330	7.22265	40.6	25.4	W2	51		Boko 44m
POS-386	2009	07	04	16	31	39		CPT		heave started		43.64332	7.22255	38.3	25.5	W2	55		Boko 44m
POS-386	2009	07	04	16	33	02		CPT		at surface		43.64335	7.22260	38.9	25.5	W2			
POS-386	2009	07	04	16	54	15	60-7	CPT		Station arrived / at surface		43.64680	7.22812	35.9	25.5	W2			
POS-386	2009	07	04	16	55	00		CPT		to water		43.64680	7.22815	36.3	25.5	W2	5		
POS-386	2009	07	04	16	56	27		CPT		slack started		43.64693	7.22822	34.8	25.5	W2	5		
POS-386	2009	07	04	16	57	10		CPT		at bottom		43.64692	7.22823	35.4	25.4	W2	46		Boko 39m
POS-386	2009	07	04	17	26	27		CPT		heave started		43.64688	7.22813	33.7	25.1	W2	49		Boko 39m
POS-386	2009	07	04	17	30	42		CPT		at surface		43.64697	7.22827	35.3	25.3	W2			
POS-386	2009	07	04	17	40	33		CPT		Station arrived / at surface		43.64655	7.22907	44.9	25.2	W2			
POS-386	2009	07	04	17	41	07	60-8	CPT		to water		43.64657	7.22907	44.8	25.2	W2	5		
POS-386	2009	07	04	17	41	59		CPT		slack started		43.64655	7.22913	45.7	25.2	W2	5		
POS-386	2009	07	04	17	43	01		CPT		at bottom		43.64662	7.22915	45.6	25.2	W2	53		Boko 47m
POS-386	2009	07	04	18	11	08		CPT		heave started		43.64662	7.22912	44.6	25.3	W2	58		Boko 47m
POS-386	2009	07	04	18	12	45		CPT		at surface		43.64663	7.22907	44.3	25.3	W2			
POS-386	2009	07	04	18	18	12		CPT		on deck / station completed		43.64640	7.22908	47.8	25.2	W2			
POS-386							61	Rn in Var mouth with dinghy											
POS-386	2009	07	05	06	09	37	62	GC		station arrived		43.64068	7.21785	99.0	24.5	W3			
POS-386	2009	07	05	06	15	16		GC		to water		43.64087	7.21808	84.0	24.5	W3			
POS-386	2009	07	05	06	15	53		GC		at bottom/heave started		43.64090	7.21807	85.0	24.5	W3	124		Boko 116m
POS-386	2009	07	05	06	19	27		GC		on deck		43.64097	7.21792	84.0	24.5	W3			
POS-386	2009	07	05	06	39	33	63	GC		station arrived		43.64395	7.21565	78.0	24.5	W3			
POS-386	2009	07	05	06	43	58		GC		to water		43.64410	7.21553	74.0	24.5	W3			

POS-386	2009	07	05	06	46	05		GC		at bottom	43.64408	7.21545	75.0	24.5	W3	101	Boko 92m
POS-386	2009	07	05	06	49	38		GC		on deck	43.64413	7.21553	74.0	24.5	W3		
POS-386	2009	07	05	06	49	53		GC		on deck	43.64413	7.21553	73.0	24.5	W3		
POS-386	2009	07	05	07	08	03	64	GC		station arrived	43.64750	7.21678	13.1	24.5	W3		
POS-386	2009	07	05	07	18	52		GC		to water	43.64757	7.21677	13.4	24.5	W3		
POS-386	2009	07	05	07	19	40		GC		at bottom	43.64755	7.21670	15.5	24.5	W3	23	Boko 15 m
POS-386	2009	07	05	07	19	44		GC		heave started	43.64755	7.21670	15.0	24.5	W3	23	Boko 15 m
POS-386	2009	07	05	07	20	59		GC		at surface	43.64747	7.21658	21.2	24.5	W3		
POS-386	2009	07	05	07	22	11		GC		on deck	43.64743	7.21652	20.8	24.5	W3		
POS-386	2009	07	05	07	24	01	64-1	GC		to water	43.64747	7.21650	19.5	24.5	W3		2nd Trial
POS-386	2009	07	05	07	25	20		GC		at bottom	43.64747	7.21663	18.8	24.5	W3	26	Boko 18 m
POS-386	2009	07	05	07	25	26		GC		heave started	43.64747	7.21663	18.7	24.5	W3	26	Boko 18 m
POS-386	2009	07	05	07	26	48		GC		at surface	43.64750	7.21665	16.9	24.5	W3		
POS-386	2009	07	05	07	28	01		GC		on deck	43.64753	7.21662	16.4	24.5	W3		
POS-386	2009	07	05	07	38	11	64-2	GC		to water	43.64750	7.21678	19.2	24.6	W3		3rd trial
POS-386	2009	07	05	07	39	30		GC		at bottom	43.64748	7.21682	19.6	24.6	W3	22	Boko 14 m
POS-386	2009	07	05	07	39	34		GC		heave started	43.64748	7.21682	19.7	24.6	W3	22	Boko 14 m
POS-386	2009	07	05	07	41	21		GC		at surface	43.64745	7.21682	20.3	24.6	W3		
POS-386	2009	07	05	07	42	04		GC		on deck	43.64745	7.21675	20.8	24.6	W3		
POS-386	2009	07	05	07	42	42		GC		station completed	43.64745	7.21672	20.4	24.7	W3		Research works completed

## 10.2 Lithologs and shear strength data

Legend:

	hemipelagic		lamination
	clay		hydrate (dark, reduced organic matter)
	silty-clay and silt		vegetal debris
	silt-sand		lense
	Gravel Pebbles		black dot(s)
	reddish layer		black patch
			shell fragment
			zoophycos
			chondrites
			burrow

<b>Contacts</b>  sharp contact  gradational contact  scoured, sharp contact  scoured contact with graded beds		 bioturbation (moderate)  bioturbation (intense)  Shell (complete)  Shell fragments  Bivalves  Gastropods  Echinoderms  Forams  Corals  Fish debris  Isolated pebble  Ooids  Plant material  Roots  Stromatolites  Nodules and concretions  Echinoids  Crinoids  Solitary coral  Bryozoa	
<b>Intervals</b>  FU Fining upward interval  CU Coarsening upward interval  Normally graded interval  Inversed graded interval			
<b>Bedding</b>  Horizontal laminae  Cross laminae (current and climbing ripples)  Wavy lamination  Wedge-planar laminae-beds  Graded beds (normal)  Graded beds (inverse)  Fingering bedding  Lenticular bedding  Convolute and contorted bedding  Cross stratification  Hummocky/swaley cross stratification  Trough cross stratification  Mudcrack  Loadcast  Water-escape structures  Gas-escape structures			

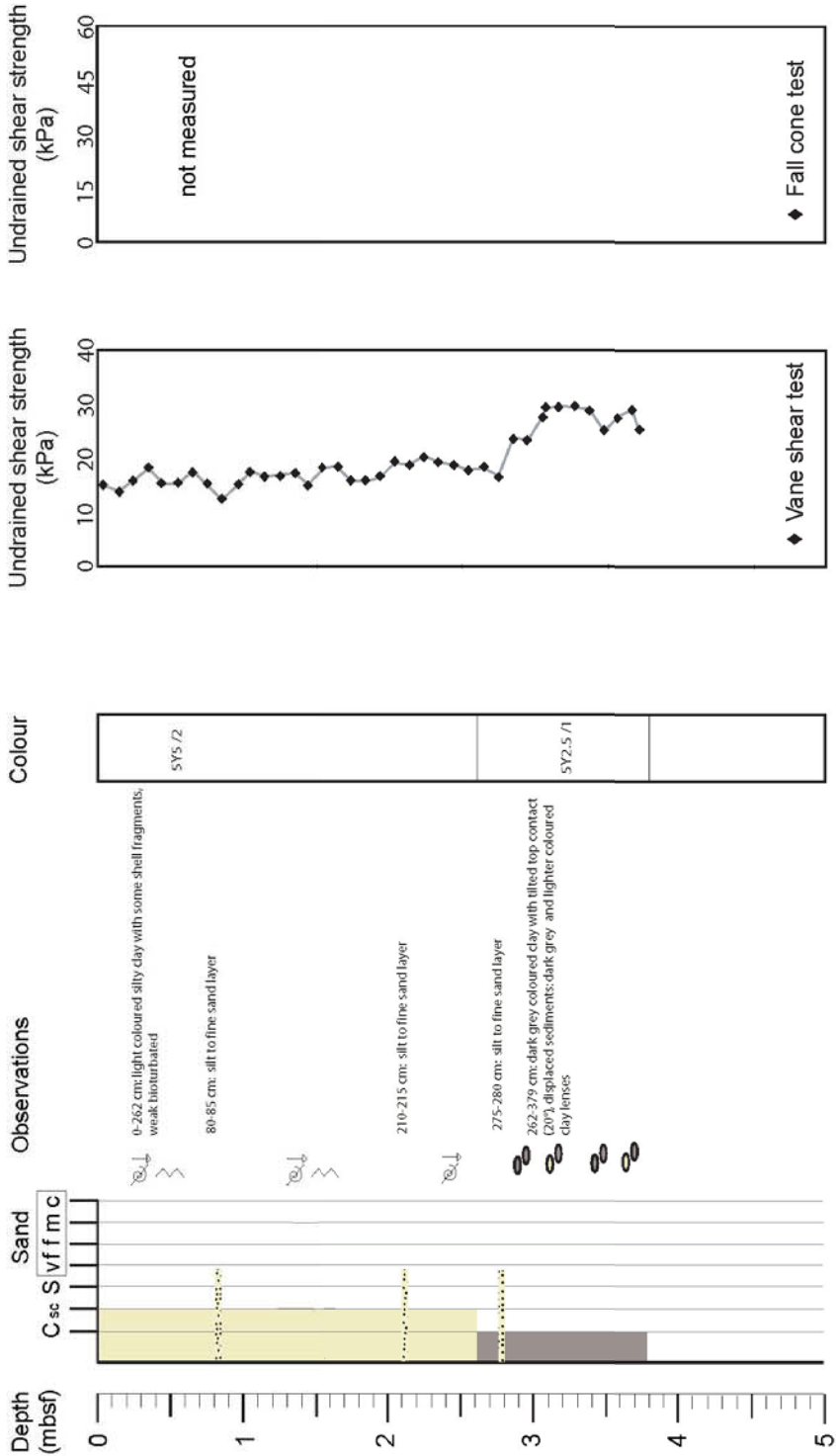
Core log GeoB13910

Study area: deeper slope

Date: 23.06.09  
Station#: GeoB13910  
Time UTC: 06:07

Latitude: 43.52902  
Longitude: 7.35573  
Water depth: 1552.0

Gravity corer length: 6 m  
Core recovery: 3.79 m



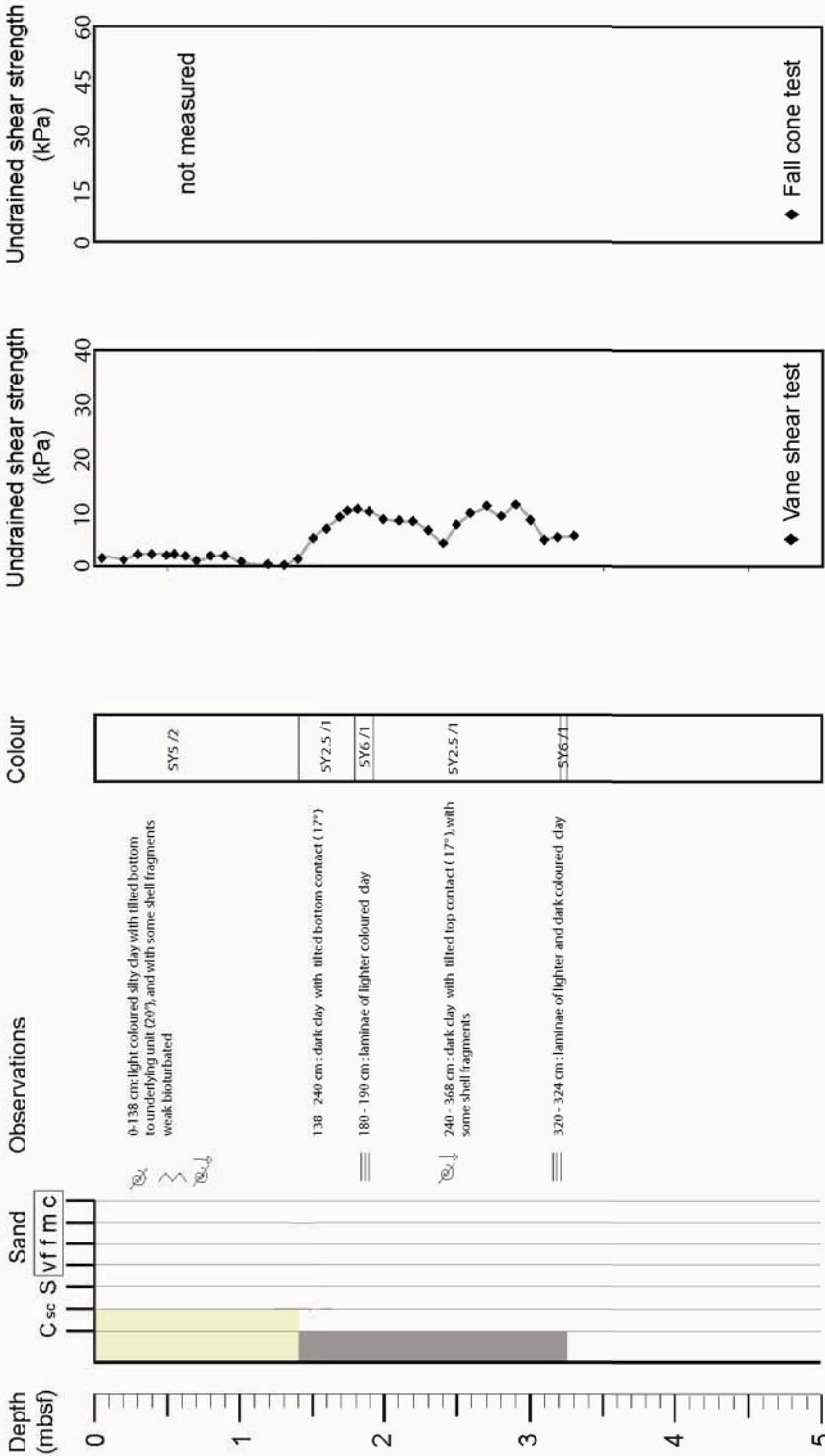
Core log GeoB13911

Date: 23.06.09  
Station#: GeoB13911  
Time UTC: 07:55

Latitude: 43.53502  
Longitude: 7.35182  
Water depth: 1417.0

Study area: deeper slope

Gravity corer length: 6 m  
Core recovery: 3.24 m





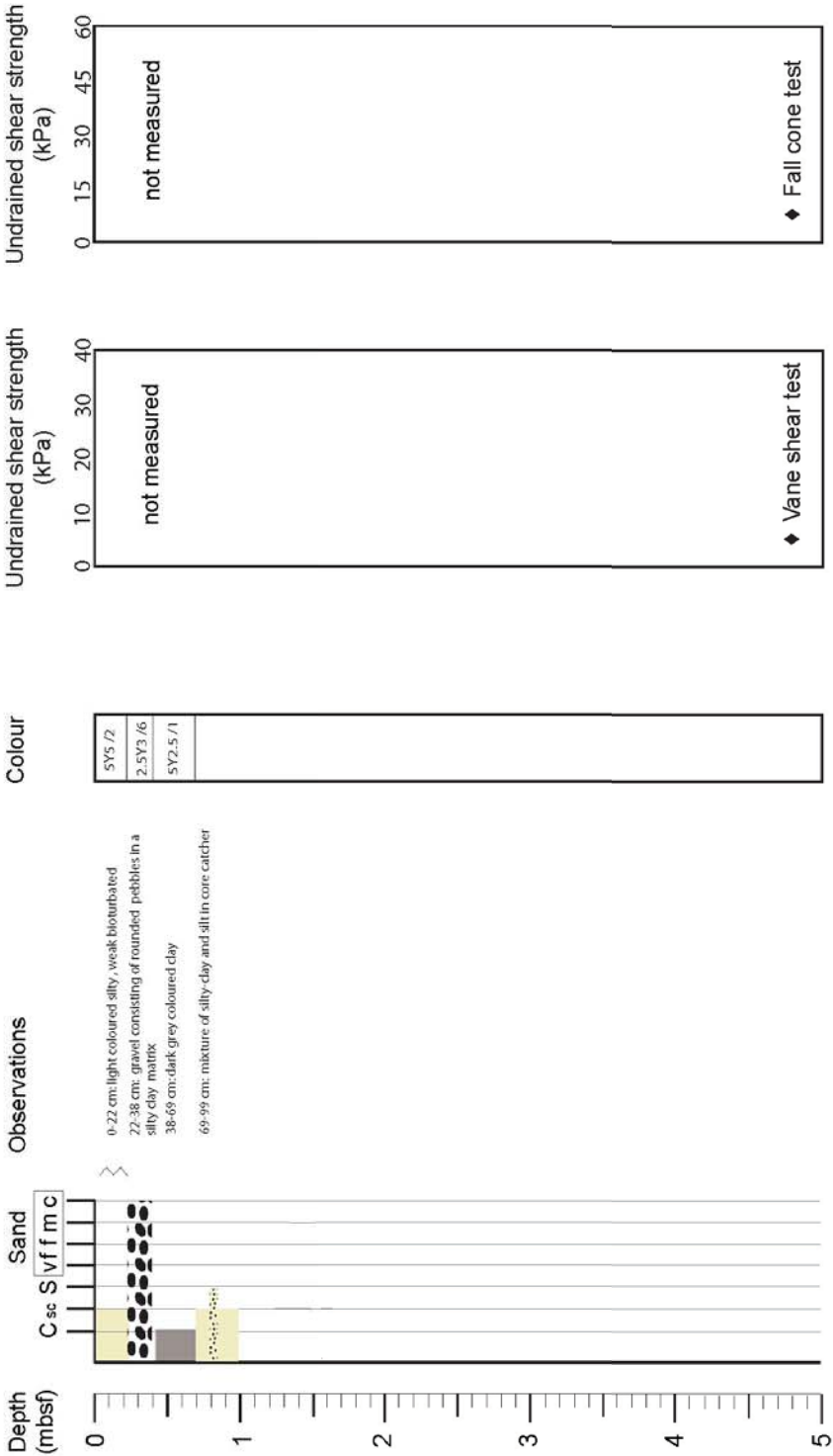
Core log GeoB13913

Date: 24.06.09  
Station#: GeoB13913  
Time UTC: 04:06

Latitude: 43.51085  
Longitude: 7.35648  
Water depth: 1766.0

Study area: deeper slope

Gravity corer length: 6 m  
Core recovery: 1.00 m



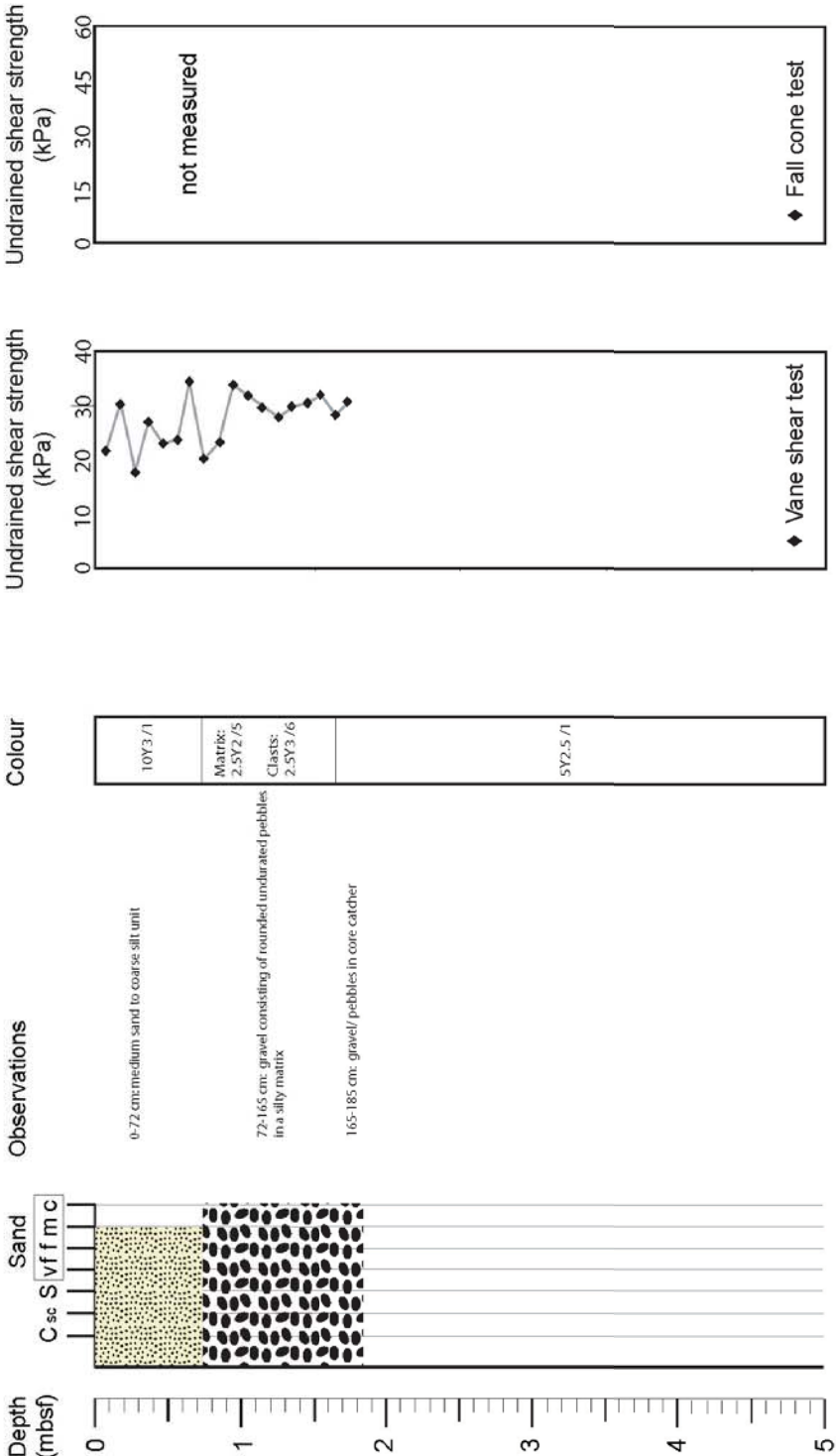
Core log GeoB13914

Study area: deeper slope

Date: 24.06.09  
Station#: GeoB13914  
Time UTC: 05:58

Gravity corer length: 6 m  
Core recovery: 1.85 m

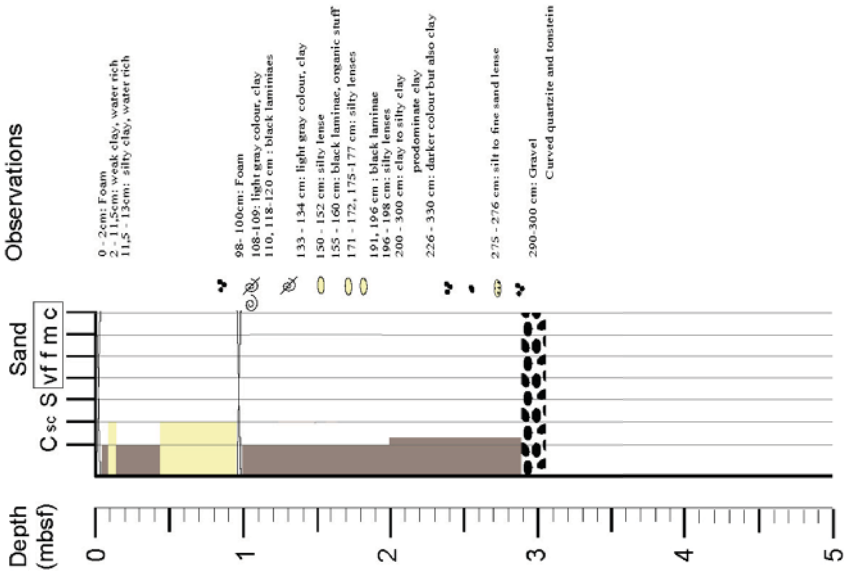
Latitude: 43.52252  
Longitude: 7.35312  
Water depth: 1630.0



Core log GeoB13918

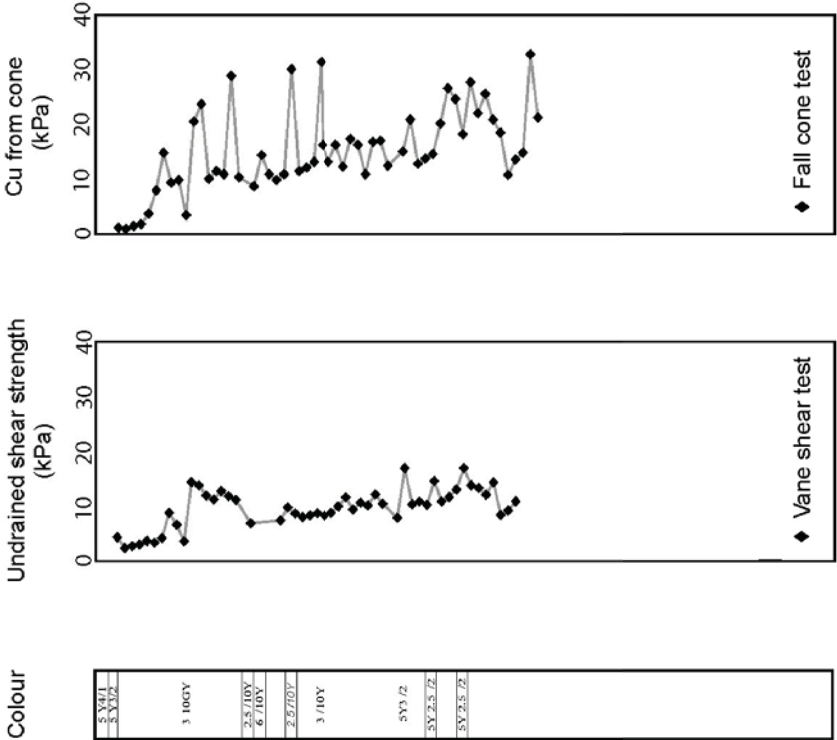
Date: 27.06.09  
Station#: GeoB13918  
Time UTC: 08:33

Latitude: 43.62770  
Longitude: 7.21407  
Water depth: 397 m



Study area: Nice airport

Gravity corer length: 6m  
Core recovery: 3 m



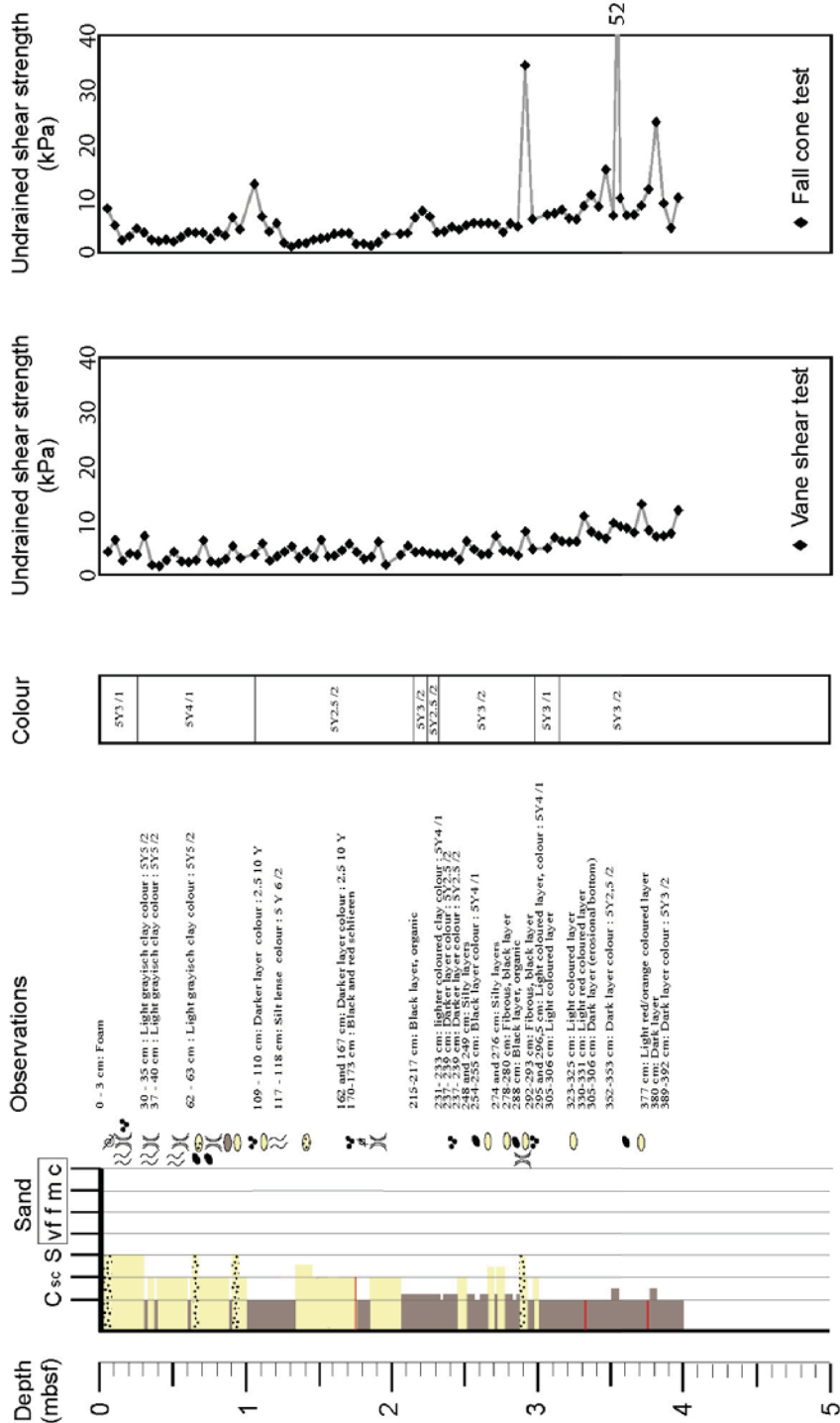
# Core log GeoB13919

# Study area: Nice airport

Date: 27.06.09  
Station#: GeoB13919  
Time UTC: 09:15

Gravity corer length: 6m  
Core recovery: 4 m

Latitude: 43.64317 N  
Longitude: 7.22248 E  
Water depth: 40.8 m



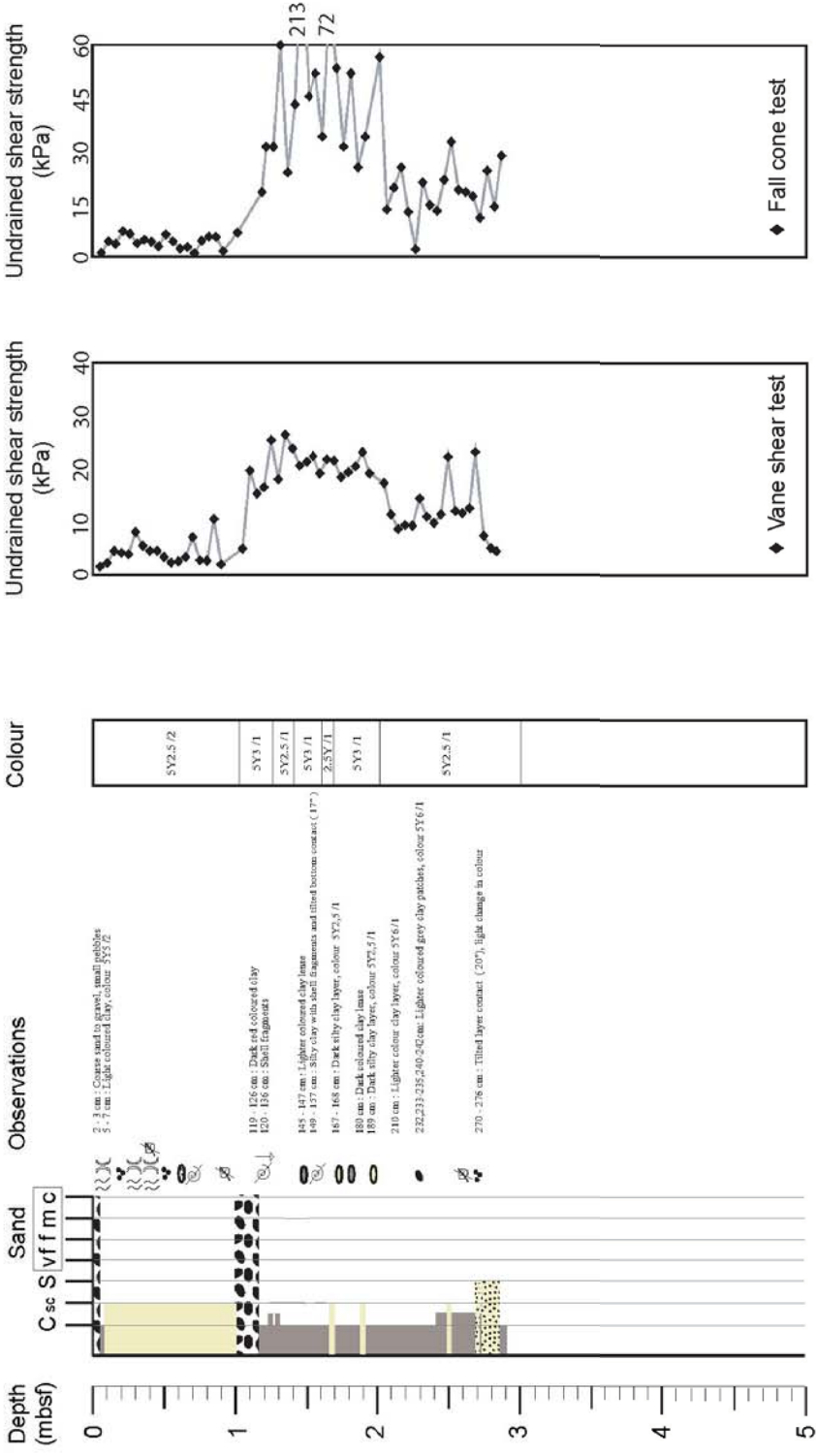
Core log GeoB13925

Date: 28.06.09  
Station#: GeoB13925  
Time UTC: 06:42

Latitude: 43.64600  
Longitude: 7.21853  
Water depth: 30.1

Study area: Nice airport

Gravity corer length: 6 m  
Core recovery: 2.90 m

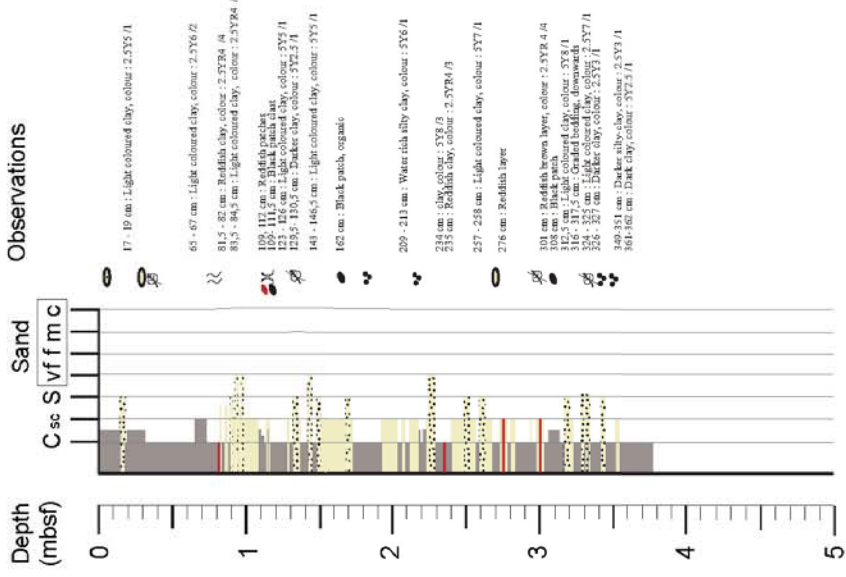




Core log GeoB13926

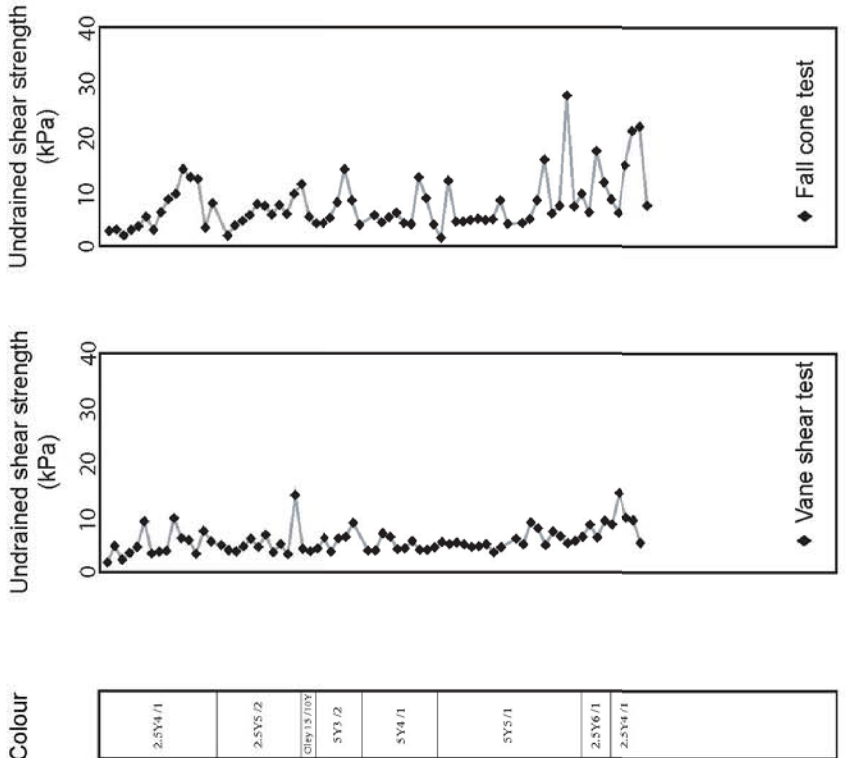
Date: 28.06.09  
Station#: GeoB13926  
Time UTC: 08:18

Latitude: 43.64507  
Longitude: 7.22368  
Water depth: 19.8



Study area: Nice airport

Gravity corer length: 6 m  
Core recovery: 3.77 m



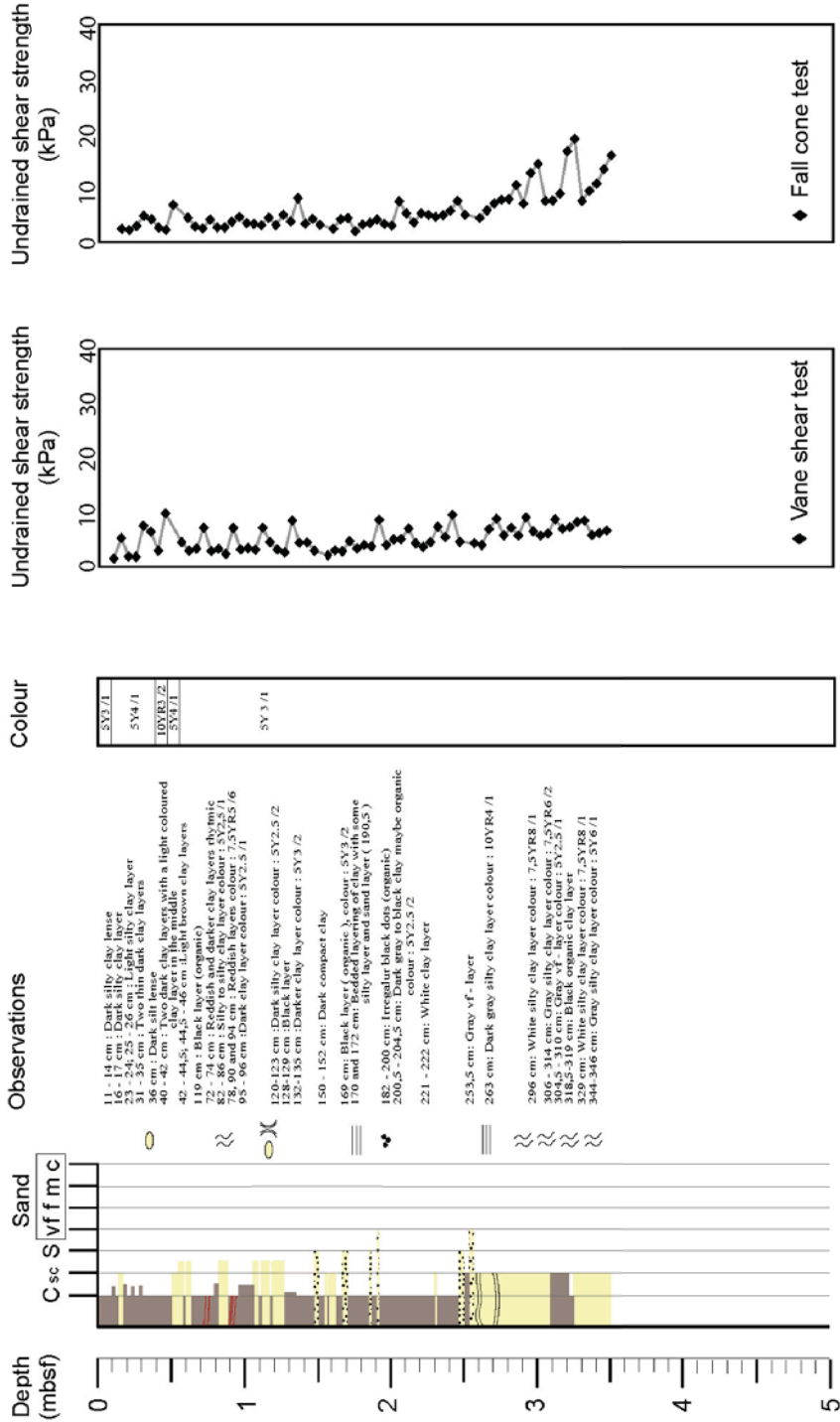
# Core log GeoB13928

Date: 29.06.09  
Station#: GeoB13928  
Time UTC: 06:06

Latitude: 43.64133 N  
Longitude: 7.21332 E  
Water depth: 79.0 m

# Study area: Nice airport

Gravity corer length: 6 m  
Core recovery: 3.51 m



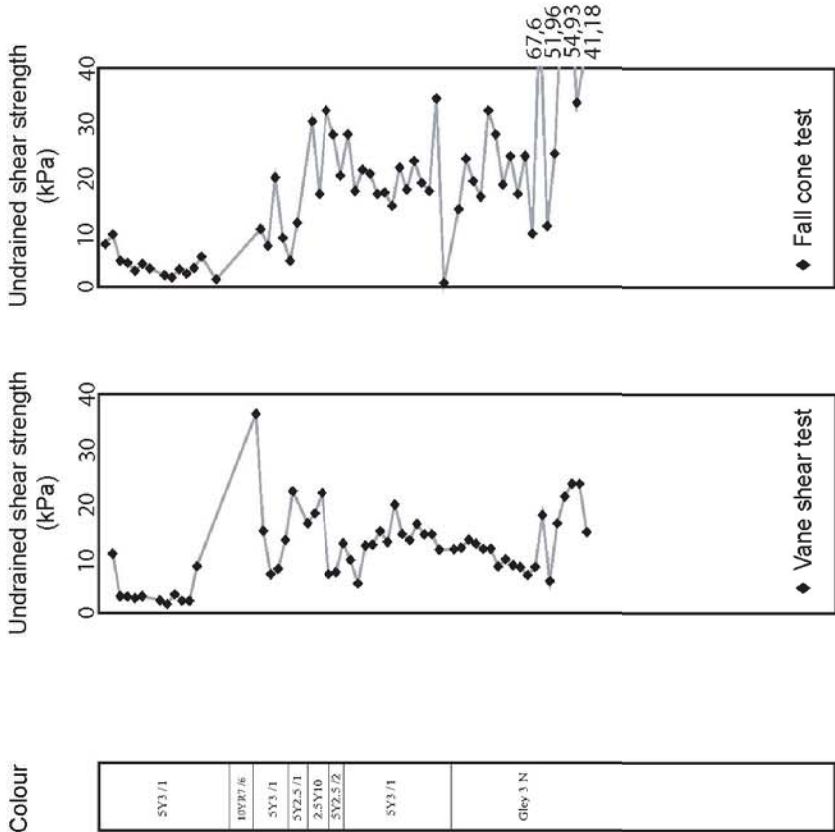
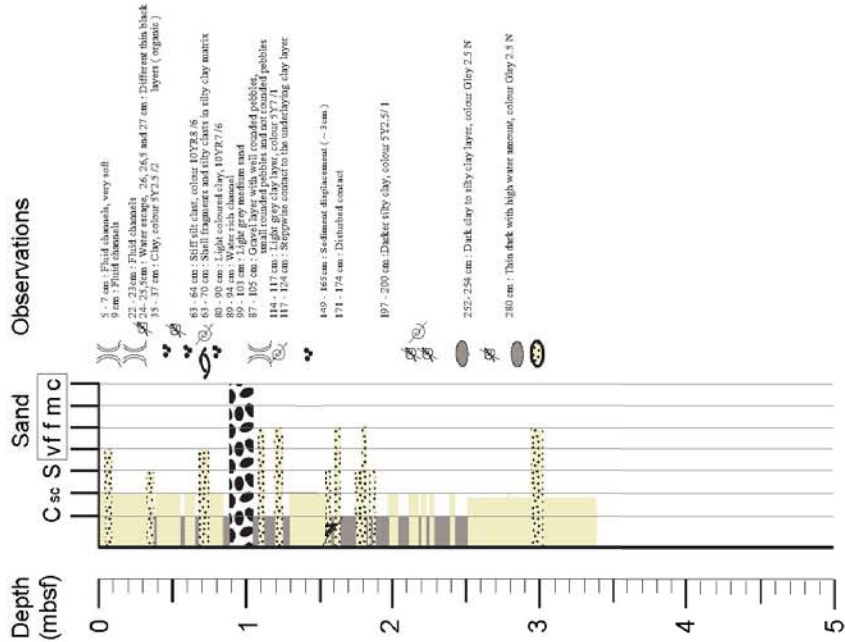
Core log GeoB13929

Date: 29.06.09  
Station#: GeoB13929  
Time UTC: 07:00

Latitude: 43.64607 N  
Longitude: 7.21383 E  
Water depth: 28.8

Study area: Nice airport

Gravity corer length: 6 m  
Core recovery: 3.37 m

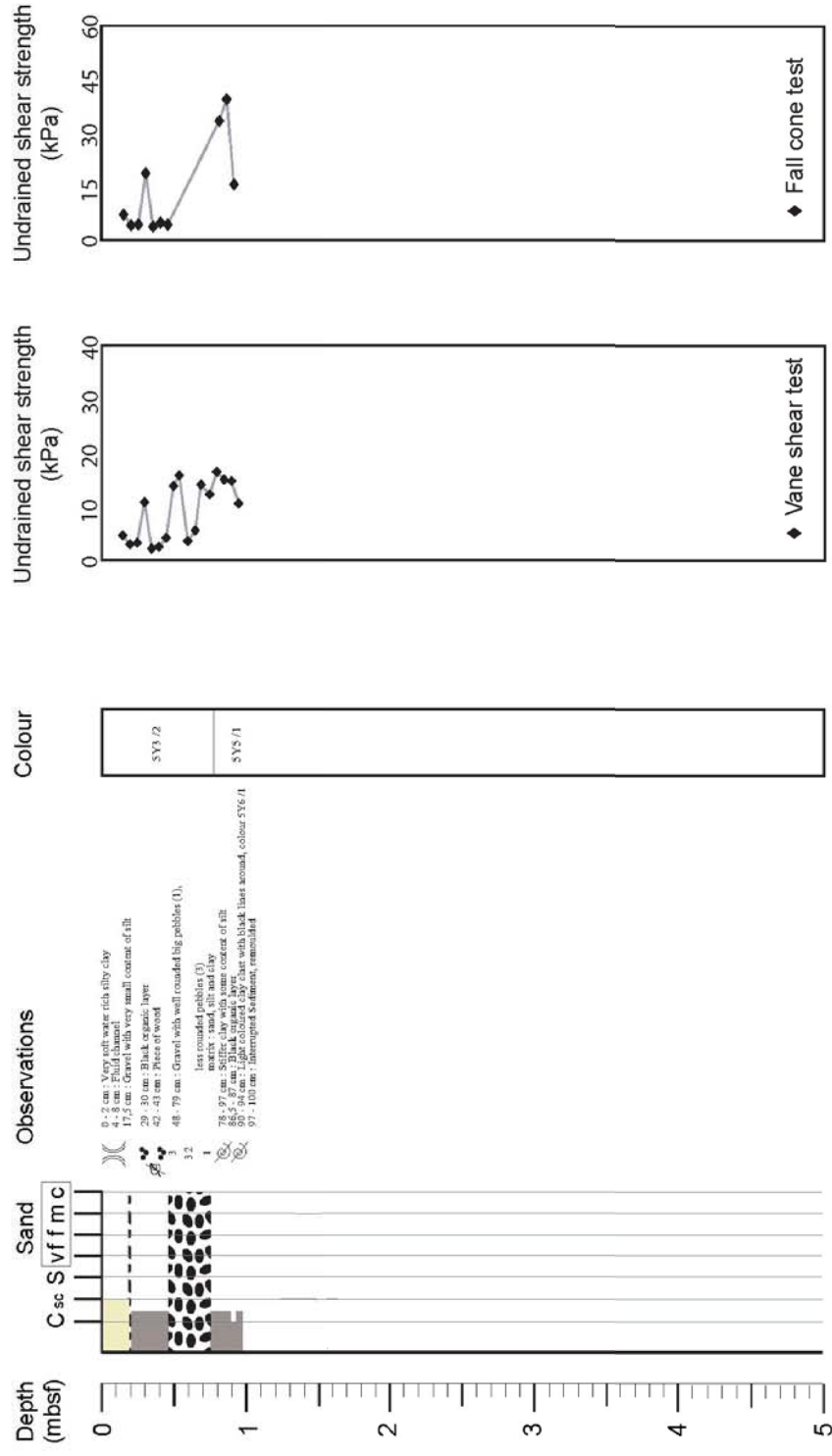


Core log GeoB13930

**Date:** 29.06.09  
**Station#:** GeoB13930  
**Time UTC:** 07:34  
**Latitude:** 43.64610  
**Longitude:** 7.21822  
**Water depth:** 41

**Study area:** Nice airport

Gravity corer length: 6 m  
Core recovery: 1 m

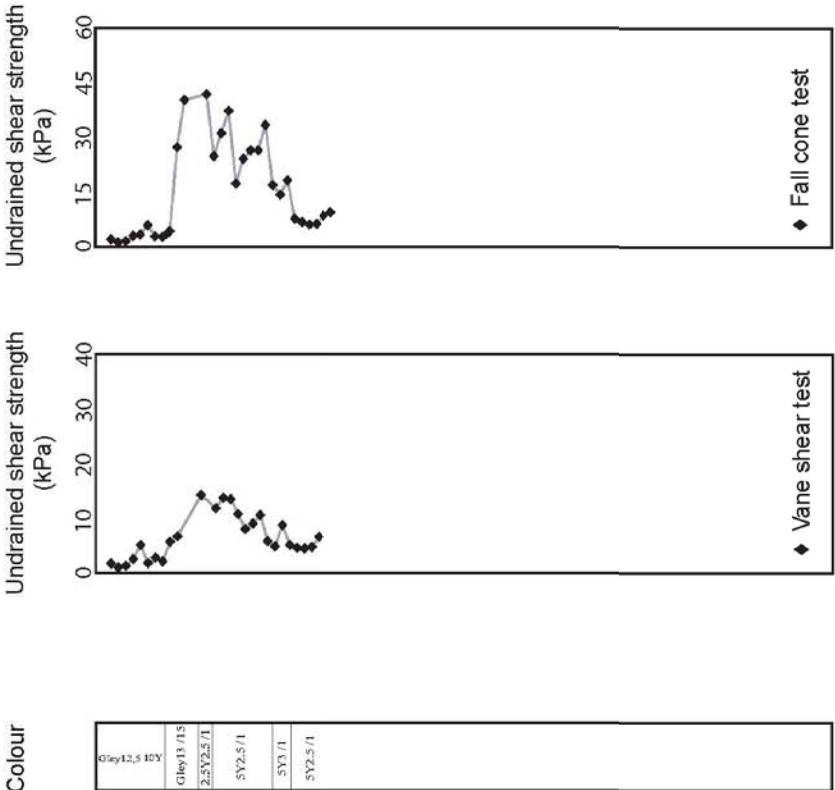
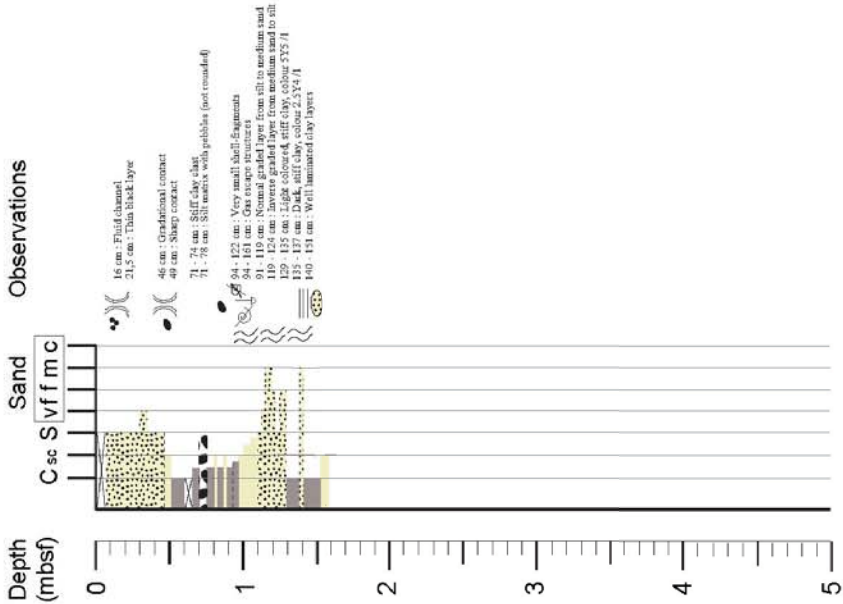


Core log GeoB13934

Date: 30.06.09      Latitude: 43.64562 N  
Station#: GeoB13934      Longitude: 7.21315 E  
Time UTC: 07:13      Water depth: 37.4

Study area: Nice airport

Gravity corer length: 6 m  
Core recovery: 1.61 m





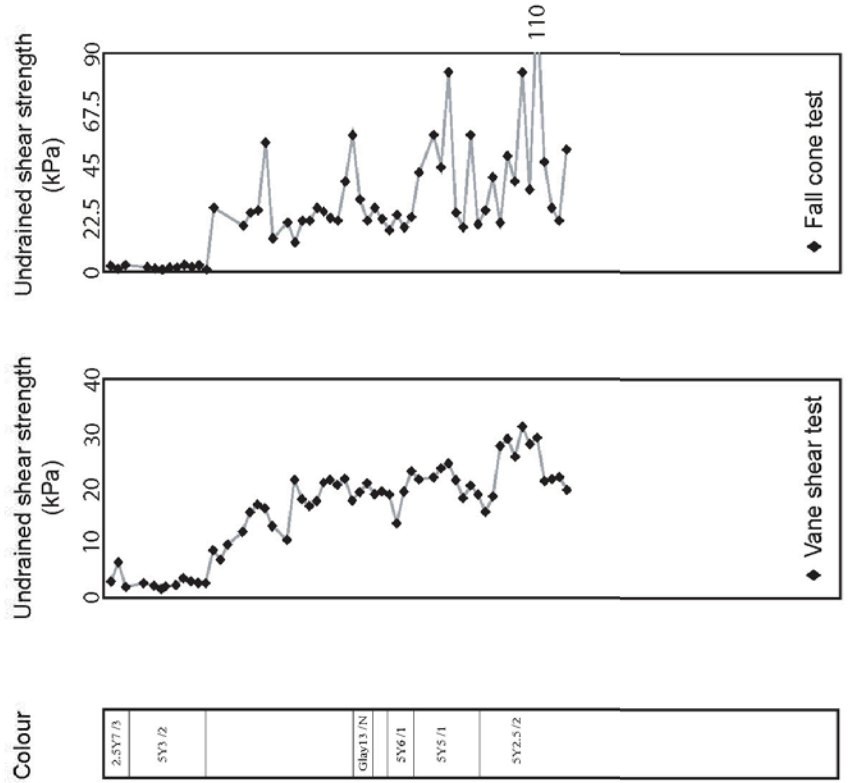
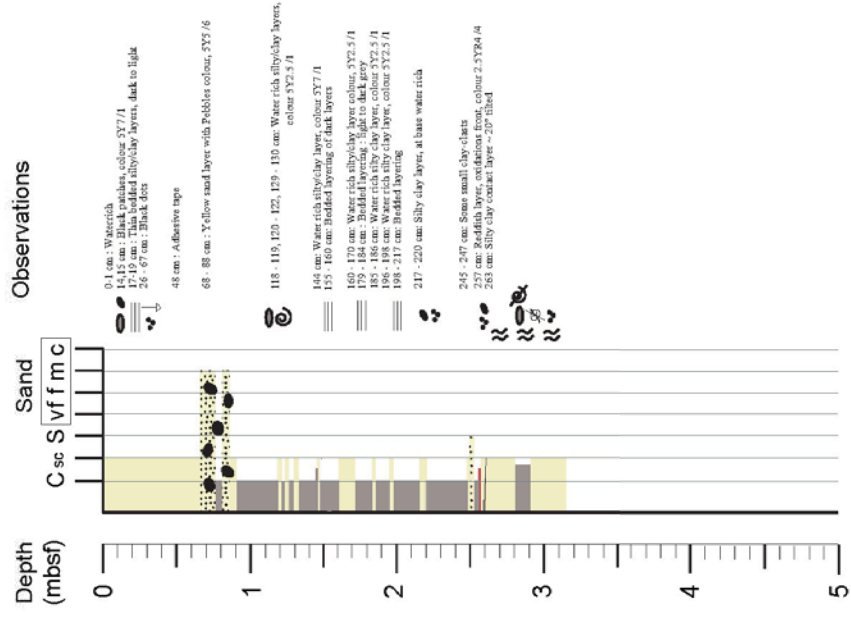
# Core log GeoB13939

Date: 01.07.09  
Station#: GeoB13939  
Time UTC: 07:41

Latitude: 43.64672  
Longitude: 7.21755  
Water depth: 27.7

# Study area: Nice airport

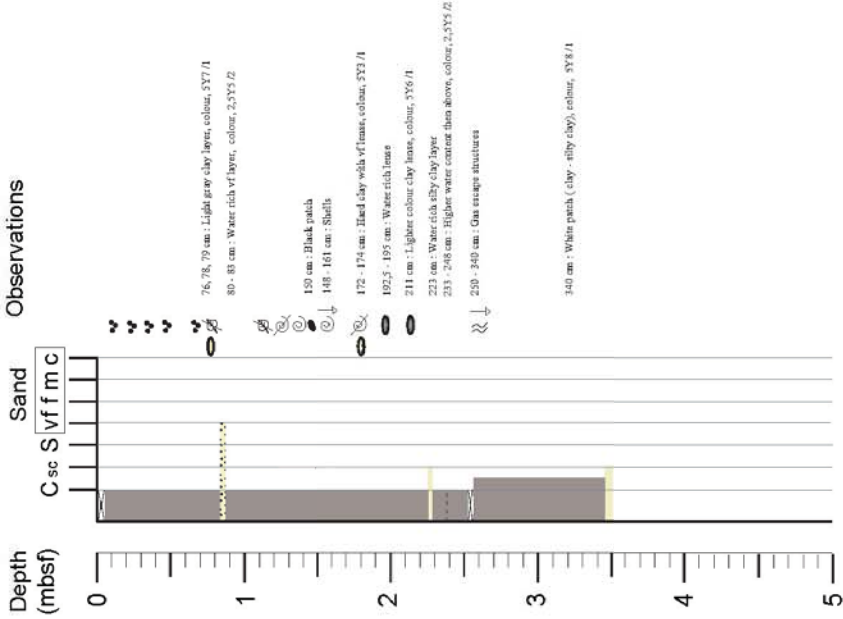
Gravity corer length: 6 m  
Core recovery: 3.19 m



Core log GeoB13940

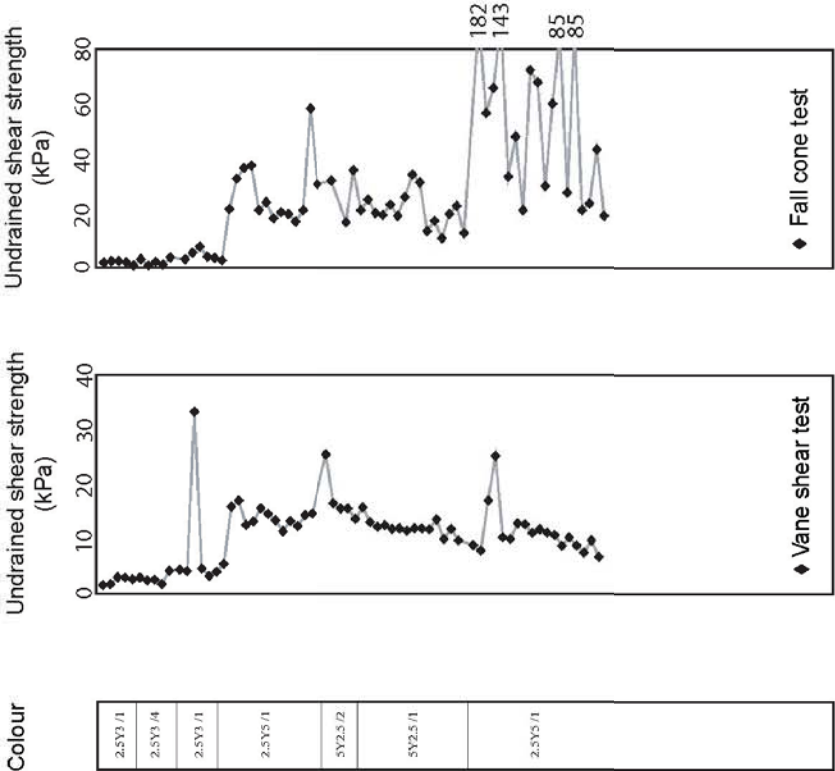
Date: 01.07.09  
Station#: GeoB13940  
Time UTC: 08:25

Latitude: 43.64512  
Longitude: 7.21413  
Water depth: 44.4 m



Study area: Nice airport

Gravity corer length: 6 m  
Core recovery: 3.52 m

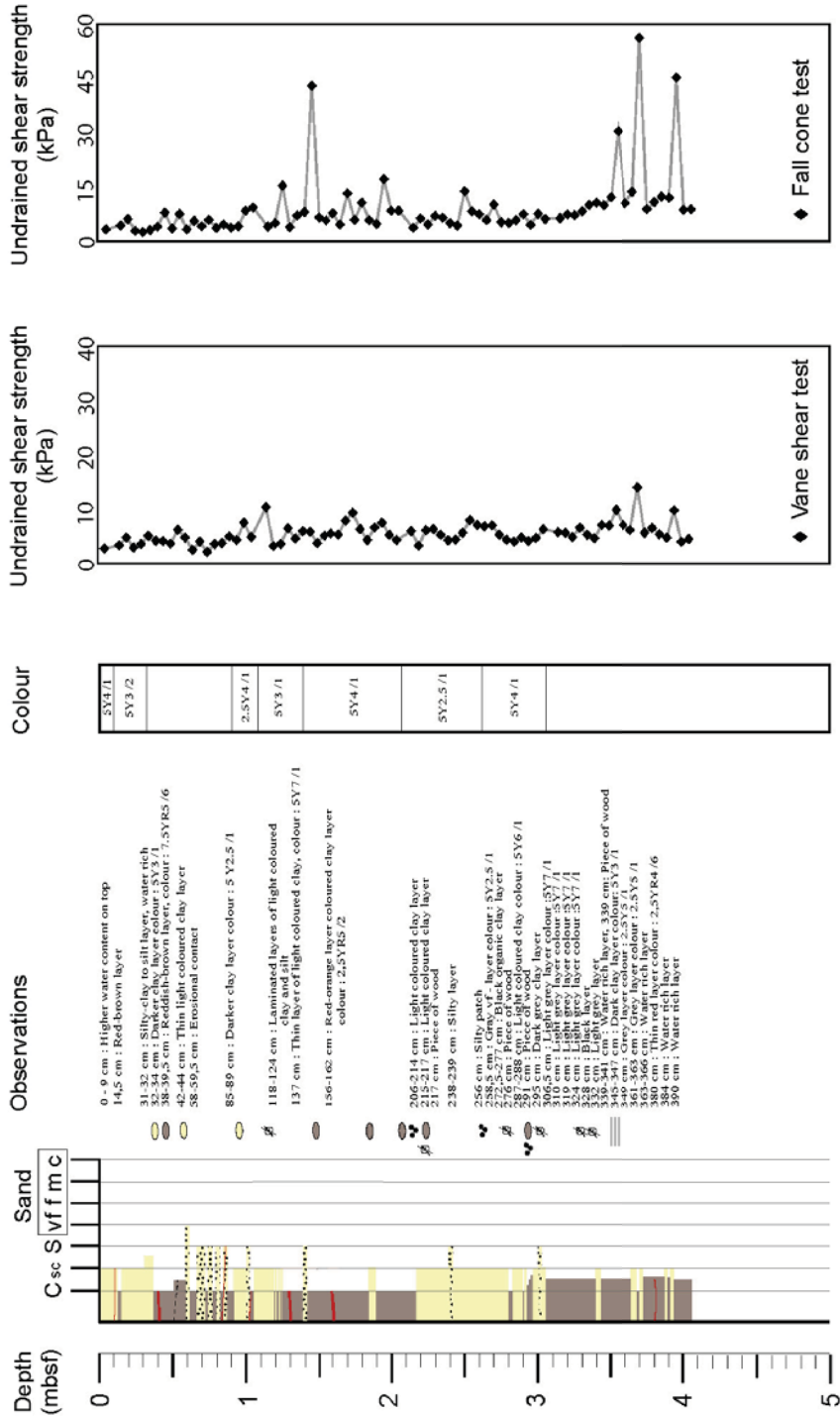


Core log GeoB13946

Date: 02.07.09  
Station#: GeoB13946  
Time UTC: 07:24  
Latitude: 43.64278 N  
Longitude: 7.21100 E  
Water depth: 14.3 m

Study area: Nice airport

Gravity corer length: 6 m  
Core recovery: 4.09 m



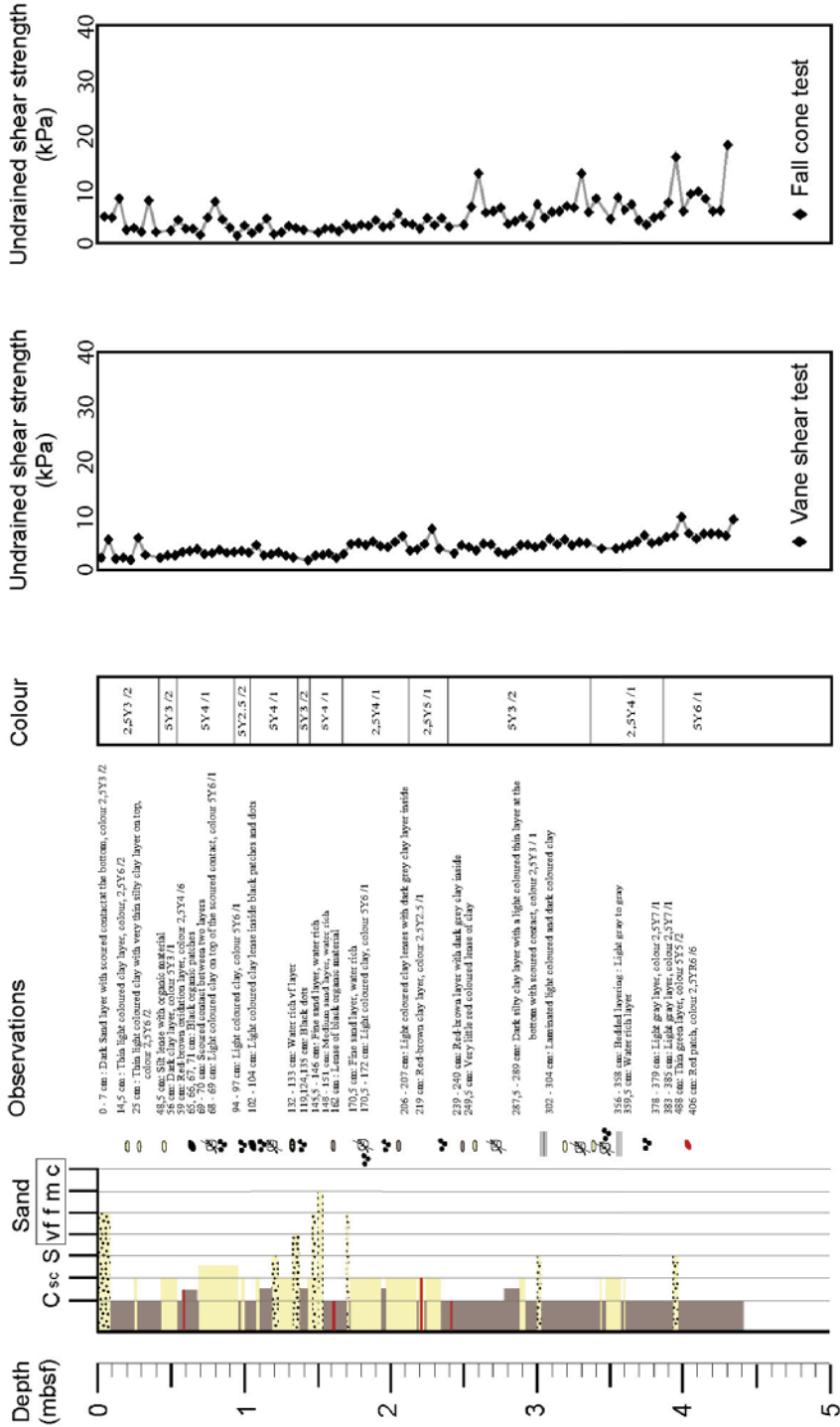
Core log GeoB13952

Date: 03.07.09  
Station#: GeoB13952  
Time UTC: 07:52

Latitude: 43.64380  
Longitude: 7.22225  
Water depth: 25.9

Study area: Nice airport

Gravity corer length: 6 m  
Core recovery: 4.42 m



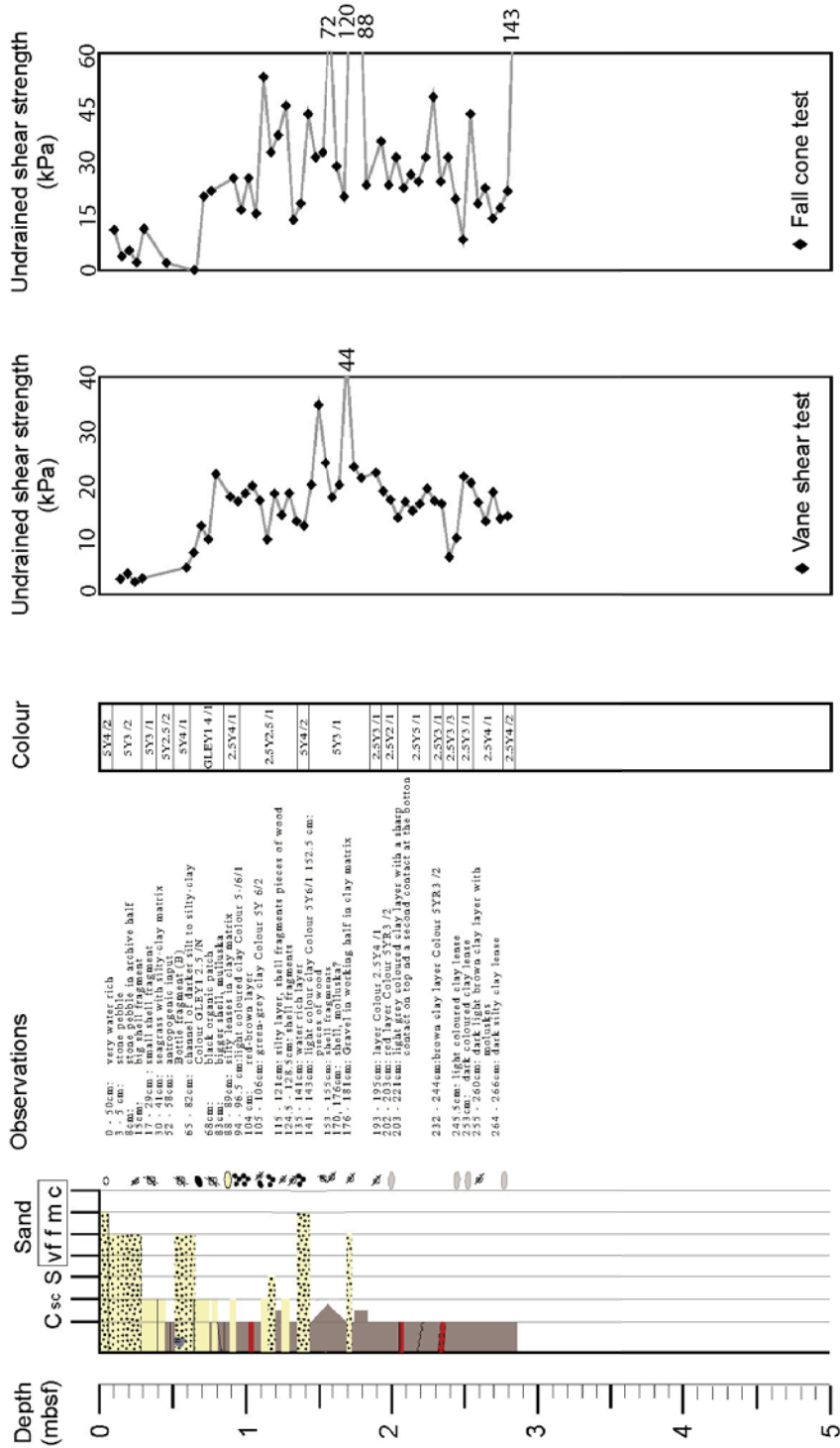
Core log GeoB13953

Date: 03.07.09  
Station#: GeoB13953  
Time UTC: 08:27

Latitude: 43.64750  
Longitude: 7.21677  
Water depth: 19.7 m

Study area: Nice airport

Gravity corer length: 6 m  
Core recovery: 2.85 m





**10.3 MSCL data logs and core photographs**  
**(available in electronic version for cruise participants only)**

**Index of CD-ROM in back pocket  
(for cruise participants only):**

- PDF file of cruise report
- Appendix 10.1 as XLS file
- Appendix 10.2 as PDF files
- Appendix 10.3 as PDF files
- Tables 3 through 6 (Geochemistry) as DOC files

Publications of this series:

- No. 1      Wefer, G., E. Suess and cruise participants**  
Bericht über die POLARSTERN-Fahrt ANT IV/2, Rio de Janeiro - Punta Arenas, 6.11. - 1.12.1985. 60 pages, Bremen, 1986.
- No. 2      Hoffmann, G.**  
Holozänstratigraphie und Küstenlinienverlagerung an der andalusischen Mittelmeerküste. 173 pages, Bremen, 1988. (out of print)
- No. 3      Wefer, G. and cruise participants**  
Bericht über die METEOR-Fahrt M 6/6, Libreville - Las Palmas, 18.2. - 23.3.1988. 97 pages, Bremen, 1988.
- No. 4      Wefer, G., G.F. Lutze, T.J. Müller, O. Pfannkuche, W. Schenke, G. Siedler, W. Zenk**  
Kurzbericht über die METEOR-Expedition No. 6, Hamburg - Hamburg, 28.10.1987 - 19.5.1988. 29 pages, Bremen, 1988. (out of print)
- No. 5      Fischer, G.**  
Stabile Kohlenstoff-Isotope in partikulärer organischer Substanz aus dem Südpolarmeer (Atlantischer Sektor). 161 pages, Bremen, 1989.
- No. 6      Berger, W.H. and G. Wefer**  
Partikelfluß und Kohlenstoffkreislauf im Ozean.  
Bericht und Kurzfassungen über den Workshop vom 3.-4. Juli 1989 in Bremen. 57 pages, Bremen, 1989.
- No. 7      Wefer, G. and cruise participants**  
Bericht über die METEOR - Fahrt M 9/4, Dakar - Santa Cruz, 19.2. - 16.3.1989. 103 pages, Bremen, 1989.
- No. 8      Kölling, M.**  
Modellierung geochemischer Prozesse im Sickerwasser und Grundwasser. 135 pages, Bremen, 1990.
- No. 9      Heinze, P.-M.**  
Das Auftriebsgeschehen vor Peru im Spätquartär. 204 pages, Bremen, 1990. (out of print)
- No. 10      Willems, H., G. Wefer, M. Rinski, B. Donner, H.-J. Bellmann, L. Eißmann, A. Müller, B.W. Flemming, H.-C. Höfle, J. Merkt, H. Streif, G. Hertweck, H. Kuntze, J. Schwaar, W. Schäfer, M.-G. Schulz, F. Grube, B. Menke**  
Beiträge zur Geologie und Paläontologie Norddeutschlands: Exkursionsführer. 202 pages, Bremen, 1990.
- No. 11      Wefer, G. and cruise participants**  
Bericht über die METEOR-Fahrt M 12/1, Kapstadt - Funchal, 13.3.1990 - 14.4.1990. 66 pages, Bremen, 1990.
- No. 12      Dahmke, A., H.D. Schulz, A. Kölling, F. Kracht, A. Lücke**  
Schwermetallspuren und geochemische Gleichgewichte zwischen Porenlösung und Sediment im Wesermündungsgebiet. BMFT-Projekt MFU 0562, Abschlußbericht. 121 pages, Bremen, 1991.
- No. 13      Rostek, F.**  
Physikalische Strukturen von Tiefseesedimenten des Südatlantiks und ihre Erfassung in Echolotregistrierungen. 209 pages, Bremen, 1991.
- No. 14      Baumann, M.**  
Die Ablagerung von Tschernobyl-Radiocäsium in der Norwegischen See und in der Nordsee. 133 pages, Bremen, 1991. (out of print)
- No. 15      Kölling, A.**  
Frühdiaagenetische Prozesse und Stoff-Flüsse in marinen und ästuarinen Sedimenten. 140 pages, Bremen, 1991.
- No. 16      SFB 261 (ed.)**  
1. Kolloquium des Sonderforschungsbereichs 261 der Universität Bremen (14.Juni 1991): Der Südatlantik im Spätquartär: Rekonstruktion von Stoffhaushalt und Stromsystemen. Kurzfassungen der Vorträge und Poster. 66 pages, Bremen, 1991.
- No. 17      Pätzold, J. and cruise participants**  
Bericht und erste Ergebnisse über die METEOR-Fahrt M 15/2, Rio de Janeiro - Vitoria, 18.1. - 7.2.1991. 46 pages, Bremen, 1993.
- No. 18      Wefer, G. and cruise participants**  
Bericht und erste Ergebnisse über die METEOR-Fahrt M 16/1, Pointe Noire - Recife, 27.3. - 25.4.1991. 120 pages, Bremen, 1991.

- No. 19 Schulz, H.D. and cruise participants**  
Bericht und erste Ergebnisse über die METEOR-Fahrt M 16/2, Recife - Belem, 28.4. - 20.5.1991. 149 pages, Bremen, 1991.
- No. 20 Berner, H.**  
Mechanismen der Sedimentbildung in der Fram-Straße, im Arktischen Ozean und in der Norwegischen See. 167 pages, Bremen, 1991.
- No. 21 Schneider, R.**  
Spätquartäre Produktivitätsänderungen im östlichen Angola-Becken: Reaktion auf Variationen im Passat-Monsun-Windsystem und in der Advektion des Benguela-Küstenstroms. 198 pages, Bremen, 1991. (out of print)
- No. 22 Hebbeln, D.**  
Spätquartäre Stratigraphie und Paläozooanographie in der Fram-Straße. 174 pages, Bremen, 1991.
- No. 23 Lücke, A.**  
Umsetzungsprozesse organischer Substanz während der Frühdiagenese in ästuarinen Sedimenten. 137 pages, Bremen, 1991.
- No. 24 Wefer, G. and cruise participants**  
Bericht und erste Ergebnisse der METEOR-Fahrt M 20/1, Bremen - Abidjan, 18.11.- 22.12.1991. 74 pages, Bremen, 1992.
- No. 25 Schulz, H.D. and cruise participants**  
Bericht und erste Ergebnisse der METEOR-Fahrt M 20/2, Abidjan - Dakar, 27.12.1991 - 3.2.1992. 173 pages, Bremen, 1992.
- No. 26 Gingele, F.**  
Zur klimaabhängigen Bildung biogener und terrigener Sedimente und ihrer Veränderung durch die Frühdiagenese im zentralen und östlichen Südatlantik. 202 pages, Bremen, 1992.
- No. 27 Bickert, T.**  
Rekonstruktion der spätquartären Bodenwasserzirkulation im östlichen Südatlantik über stabile Isotope benthischer Foraminiferen. 205 pages, Bremen, 1992. (out of print)
- No. 28 Schmidt, H.**  
Der Benguela-Strom im Bereich des Walfisch-Rückens im Spätquartär. 172 pages, Bremen, 1992.
- No. 29 Meinecke, G.**  
Spätquartäre Oberflächenwassertemperaturen im östlichen äquatorialen Atlantik. 181 pages, Bremen, 1992.
- No. 30 Bathmann, U., U. Bleil, A. Dahmke, P. Müller, A. Nehr Korn, E.-M. Nöthig, M. Olesch, J. Pätzold, H.D. Schulz, V. Smetacek, V. Spieß, G. Wefer, H. Willems**  
Bericht des Graduierten Kollegs. Stoff-Flüsse in marinen Geosystemen. Berichtszeitraum Oktober 1990 - Dezember 1992. 396 pages, Bremen, 1992.
- No. 31 Damm, E.**  
Frühdiagenetische Verteilung von Schwermetallen in Schlicksedimenten der westlichen Ostsee. 115 pages, Bremen, 1992.
- No. 32 Antia, E.E.**  
Sedimentology, Morphodynamics and Facies Association of a mesotidal Barrier Island Shoreface (Spiekeroog, Southern North Sea). 370 pages, Bremen, 1993.
- No. 33 Duinker, J. and G. Wefer (ed.)**  
Bericht über den 1. JGOFS-Workshop. 1./2. Dezember 1992 in Bremen. 83 pages, Bremen, 1993.
- No. 34 Kasten, S.**  
Die Verteilung von Schwermetallen in den Sedimenten eines stadtbremischen Hafenbeckens. 103 pages, Bremen, 1993.
- No. 35 Spieß, V.**  
Digitale Sedimentographie. Neue Wege zu einer hochauflösenden Akustostratigraphie. 199 pages, Bremen, 1993.
- No. 36 Schinzel, U.**  
Laborversuche zu frühdiagenetischen Reaktionen von Eisen (III) - Oxidhydraten in marinen Sedimenten. 189 pages, Bremen, 1993.
- No. 37 Sieger, R.**  
CoTAM - ein Modell zur Modellierung des Schwermetalltransports in Grundwasserleitern. 56 pages, Bremen, 1993. (out of print)

- No. 38 Willems, H. (ed.)**  
Geoscientific Investigations in the Tethyan Himalayas. 183 pages, Bremen, 1993.
- No. 39 Hamer, K.**  
Entwicklung von Laborversuchen als Grundlage für die Modellierung des Transportverhaltens von Arsenat, Blei, Cadmium und Kupfer in wassergesättigten Säulen. 147 pages, Bremen, 1993.
- No. 40 Sieger, R.**  
Modellierung des Stofftransports in porösen Medien unter Ankopplung kinetisch gesteuerter Sorptions- und Redoxprozesse sowie thermischer Gleichgewichte. 158 pages, Bremen, 1993.
- No. 41 Thießen, W.**  
Magnetische Eigenschaften von Sedimenten des östlichen Südatlantiks und ihre paläozeanographische Relevanz. 170 pages, Bremen, 1993.
- No. 42 Spieß, V. and cruise participants**  
Report and preliminary results of METEOR-Cruise M 23/1, Kapstadt - Rio de Janeiro, 4.-25.2.1993. 139 pages, Bremen, 1994.
- No. 43 Bleil, U. and cruise participants**  
Report and preliminary results of METEOR-Cruise M 23/2, Rio de Janeiro - Recife, 27.2.-19.3.1993. 133 pages, Bremen, 1994.
- No. 44 Wefer, G. and cruise participants**  
Report and preliminary results of METEOR-Cruise M 23/3, Recife - Las Palmas, 21.3. - 12.4.1993. 71 pages, Bremen, 1994.
- No. 45 Giese, M. and G. Wefer (ed.)**  
Bericht über den 2. JGOFS-Workshop. 18./19. November 1993 in Bremen. 93 pages, Bremen, 1994.
- No. 46 Balzer, W. and cruise participants**  
Report and preliminary results of METEOR-Cruise M 22/1, Hamburg - Recife, 22.9. - 21.10.1992. 24 pages, Bremen, 1994.
- No. 47 Stax, R.**  
Zyklische Sedimentation von organischem Kohlenstoff in der Japan See: Anzeiger für Änderungen von Paläoozeanographie und Paläoklima im Spätkänozoikum. 150 pages, Bremen, 1994.
- No. 48 Skowronek, F.**  
Frühdiagenetische Stoff-Flüsse gelöster Schwermetalle an der Oberfläche von Sedimenten des Weser Ästuars. 107 pages, Bremen, 1994.
- No. 49 Dersch-Hansmann, M.**  
Zur Klimaentwicklung in Ostasien während der letzten 5 Millionen Jahre: Terrigener Sedimenteintrag in die Japan See (ODP Ausfahrt 128). 149 pages, Bremen, 1994.
- No. 50 Zabel, M.**  
Frühdiagenetische Stoff-Flüsse in Oberflächen-Sedimenten des äquatorialen und östlichen Südatlantik. 129 pages, Bremen, 1994.
- No. 51 Bleil, U. and cruise participants**  
Report and preliminary results of SONNE-Cruise SO 86, Buenos Aires - Capetown, 22.4. - 31.5.93. 116 pages, Bremen, 1994.
- No. 52 Symposium: The South Atlantic: Present and Past Circulation.**  
Bremen, Germany, 15 - 19 August 1994. Abstracts. 167 pages, Bremen, 1994.
- No. 53 Kretzmann, U.B.**  
57Fe-Mössbauer-Spektroskopie an Sedimenten - Möglichkeiten und Grenzen. 183 pages, Bremen, 1994.
- No. 54 Bachmann, M.**  
Die Karbonatrampe von Organyà im oberen Oberapt und unteren Unterapt (NE-Spanien, Prov. Lerida): Fazies, Zyklus- und Sequenzstratigraphie. 147 pages, Bremen, 1994. (out of print)
- No. 55 Kemle-von Mücke, S.**  
Oberflächenwasserstruktur und -zirkulation des Südostatlantiks im Spätquartär. 151 pages, Bremen, 1994.
- No. 56 Petermann, H.**  
Magnetotaktische Bakterien und ihre Magnetosome in Oberflächensedimenten des Südatlantiks. 134 pages, Bremen, 1994.
- No. 57 Mulitza, S.**  
Spätquartäre Variationen der oberflächennahen Hydrographie im westlichen äquatorialen Atlantik. 97 pages, Bremen, 1994.

- No. 58 Segl, M. and cruise participants**  
Report and preliminary results of METEOR-Cruise M 29/1, Buenos-Aires - Montevideo, 17.6. - 13.7.1994 94 pages, Bremen, 1994.
- No. 59 Bleil, U. and cruise participants**  
Report and preliminary results of METEOR-Cruise M 29/2, Montevideo - Rio de Janeiro 15.7. - 8.8.1994. 153 pages, Bremen, 1994.
- No. 60 Henrich, R. and cruise participants**  
Report and preliminary results of METEOR-Cruise M 29/3, Rio de Janeiro - Las Palmas 11.8. - 5.9.1994. Bremen, 1994. (out of print)
- No. 61 Sagemann, J.**  
Saisonale Variationen von Porenwasserprofilen, Nährstoff-Flüssen und Reaktionen in intertidalen Sedimenten des Weser-Ästuars. 110 pages, Bremen, 1994. (out of print)
- No. 62 Giese, M. and G. Wefer**  
Bericht über den 3. JGOFS-Workshop. 5./6. Dezember 1994 in Bremen. 84 pages, Bremen, 1995.
- No. 63 Mann, U.**  
Genese kretazischer Schwarzschiefer in Kolumbien: Globale vs. regionale/lokale Prozesse. 153 pages, Bremen, 1995. (out of print)
- No. 64 Willems, H., Wan X., Yin J., Dongdui L., Liu G., S. Dürr, K.-U. Gräfe**  
The Mesozoic development of the N-Indian passive margin and of the Xigaze Forearc Basin in southern Tibet, China. – Excursion Guide to IGCP 362 Working-Group Meeting "Integrated Stratigraphy". 113 pages, Bremen, 1995. (out of print)
- No. 65 Hünken, U.**  
Liefergebiets - Charakterisierung proterozoischer Goldseifen in Ghana anhand von Fluideinschluß - Untersuchungen. 270 pages, Bremen, 1995.
- No. 66 Nyandwi, N.**  
The Nature of the Sediment Distribution Patterns in the Spiekeroog Backbarrier Area, the East Frisian Islands. 162 pages, Bremen, 1995.
- No. 67 Isenbeck-Schröter, M.**  
Transportverhalten von Schwermetallkationen und Oxoanionen in wassergesättigten Sanden. - Laborversuche in Säulen und ihre Modellierung -. 182 pages, Bremen, 1995.
- No. 68 Hebbeln, D. and cruise participants**  
Report and preliminary results of SONNE-Cruise SO 102, Valparaiso - Valparaiso, 95. 134 pages, Bremen, 1995.
- No. 69 Willems, H. (Sprecher), U. Bathmann, U. Bleil, T. v. Dobeneck, K. Herterich, B.B. Jorgensen, E.-M. Nöthig, M. Olesch, J. Pätzold, H.D. Schulz, V. Smetacek, V. Speiß, G. Wefer**  
Bericht des Graduierten-Kollegs Stoff-Flüsse in marine Geosystemen. Berichtszeitraum Januar 1993 - Dezember 1995. 45 & 468 pages, Bremen, 1995.
- No. 70 Giese, M. and G. Wefer**  
Bericht über den 4. JGOFS-Workshop. 20./21. November 1995 in Bremen. 60 pages, Bremen, 1996. (out of print)
- No. 71 Meggers, H.**  
Pliozän-quartäre Karbonatsedimentation und Paläozeanographie des Nordatlantiks und des Europäischen Nordmeeres - Hinweise aus planktischen Foraminiferengemeinschaften. 143 pages, Bremen, 1996. (out of print)
- No. 72 Teske, A.**  
Phylogenetische und ökologische Untersuchungen an Bakterien des oxidativen und reduktiven marinen Schwefelkreislaufs mittels ribosomaler RNA. 220 pages, Bremen, 1996. (out of print)
- No. 73 Andersen, N.**  
Biogeochemische Charakterisierung von Sinkstoffen und Sedimenten aus ostatlantischen Produktions-Systemen mit Hilfe von Biomarkern. 215 pages, Bremen, 1996.
- No. 74 Treppke, U.**  
Saisonalität im Diatomeen- und Silikoflagellatenfluß im östlichen tropischen und subtropischen Atlantik. 200 pages, Bremen, 1996.
- No. 75 Schüring, J.**  
Die Verwendung von Steinkohlebergematerialien im Deponiebau im Hinblick auf die Pyritverwitterung und die Eignung als geochemische Barriere. 110 pages, Bremen, 1996.



- No. 76**      **Pätzold, J. and cruise participants**  
Report and preliminary results of VICTOR HENSEN cruise JOPS II, Leg 6, Fortaleza - Recife, 10.3. - 26.3. 1995 and Leg 8, Vitória - Vitória, 10.4. - 23.4.1995. 87 pages, Bremen, 1996.
- No. 77**      **Bleil, U. and cruise participants**  
Report and preliminary results of METEOR-Cruise M 34/1, Cape Town - Walvis Bay, 3.-26.1.1996. 129 pages, Bremen, 1996.
- No. 78**      **Schulz, H.D. and cruise participants**  
Report and preliminary results of METEOR-Cruise M 34/2, Walvis Bay - Walvis Bay, 29.1.-18.2.96. 133 pages, Bremen, 1996.
- No. 79**      **Wefer, G. and cruise participants**  
Report and preliminary results of METEOR-Cruise M 34/3, Walvis Bay - Recife, 21.2.-17.3.1996. 168 pages, Bremen, 1996.
- No. 80**      **Fischer, G. and cruise participants**  
Report and preliminary results of METEOR-Cruise M 34/4, Recife - Bridgetown, 19.3.-15.4.1996. 105 pages, Bremen, 1996.
- No. 81**      **Kulbrok, F.**  
Biostratigraphie, Fazies und Sequenzstratigraphie einer Karbonatrampe in den Schichten der Oberkreide und des Alttertiärs Nordost-Ägyptens (Eastern Desert, N'Golf von Suez, Sinai). 153 pages, Bremen, 1996.
- No. 82**      **Kasten, S.**  
Early Diagenetic Metal Enrichments in Marine Sediments as Documents of Nonsteady-State Depositional Conditions. Bremen, 1996.
- No. 83**      **Holmes, M.E.**  
Reconstruction of Surface Ocean Nitrate Utilization in the Southeast Atlantic Ocean Based on Stable Nitrogen Isotopes. 113 pages, Bremen, 1996.
- No. 84**      **Rühlemann, C.**  
Akkumulation von Carbonat und organischem Kohlenstoff im tropischen Atlantik: Spätquartäre Produktivitäts-Variationen und ihre Steuerungsmechanismen. 139 pages, Bremen, 1996.
- No. 85**      **Ratmeyer, V.**  
Untersuchungen zum Eintrag und Transport lithogener und organischer partikulärer Substanz im östlichen subtropischen Nordatlantik. 154 pages, Bremen, 1996.
- No. 86**      **Cepek, M.**  
Zeitliche und räumliche Variationen von Coccolithophoriden-Gemeinschaften im subtropischen Ost-Atlantik: Untersuchungen an Plankton, Sinkstoffen und Sedimenten. 156 pages, Bremen, 1996.
- No. 87**      **Otto, S.**  
Die Bedeutung von gelöstem organischen Kohlenstoff (DOC) für den Kohlenstofffluß im Ozean. 150 pages, Bremen, 1996.
- No. 88**      **Hensen, C.**  
Frühdiaagenetische Prozesse und Quantifizierung benthischer Stoff-Flüsse in Oberflächen-sedimenten des Südatlantiks. 132 pages, Bremen, 1996.
- No. 89**      **Giese, M. and G. Wefer**  
Bericht über den 5. JGOFS-Workshop. 27./28. November 1996 in Bremen. 73 pages, Bremen, 1997.
- No. 90**      **Wefer, G. and cruise participants**  
Report and preliminary results of METEOR-Cruise M 37/1, Lisbon - Las Palmas, 4.-23.12.1996. 79 pages, Bremen, 1997.
- No. 91**      **Isenbeck-Schröter, M., E. Bedbur, M. Kofod, B. König, T. Schramm & G. Mattheß**  
Occurrence of Pesticide Residues in Water - Assessment of the Current Situation in Selected EU Countries. 65 pages, Bremen 1997.
- No. 92**      **Kühn, M.**  
Geochemische Folgereaktionen bei der hydrogeothermalen Energiegewinnung. 129 pages, Bremen 1997.
- No. 93**      **Determann, S. & K. Herterich**  
JGOFS-A6 "Daten und Modelle": Sammlung JGOFS-relevanter Modelle in Deutschland. 26 pages, Bremen, 1997.

- No. 94**      **Fischer, G. and cruise participants**  
Report and preliminary results of METEOR-Cruise M 38/1, Las Palmas - Recife, 25.1.-1.3.1997, with Appendix: Core Descriptions from METEOR Cruise M 37/1. Bremen, 1997.
- No. 95**      **Bleil, U. and cruise participants**  
Report and preliminary results of METEOR-Cruise M 38/2, Recife - Las Palmas, 4.3.-14.4.1997. 126 pages, Bremen, 1997.
- No. 96**      **Neuer, S. and cruise participants**  
Report and preliminary results of VICTOR HENSEN-Cruise 96/1. Bremen, 1997.
- No. 97**      **Villinger, H. and cruise participants**  
Fahrtbericht SO 111, 20.8. - 16.9.1996. 115 pages, Bremen, 1997.
- No. 98**      **Lüning, S.**  
Late Cretaceous - Early Tertiary sequence stratigraphy, paleoecology and geodynamics of Eastern Sinai, Egypt. 218 pages, Bremen, 1997.
- No. 99**      **Haese, R.R.**  
Beschreibung und Quantifizierung frühdiagenetischer Reaktionen des Eisens in Sedimenten des Südatlantiks. 118 pages, Bremen, 1997.
- No. 100**     **Lührte, R. von**  
Verwertung von Bremer Baggergut als Material zur Oberflächenabdichtung von Deponien - Geochemisches Langzeitverhalten und Schwermetall-Mobilität (Cd, Cu, Ni, Pb, Zn). Bremen, 1997.
- No. 101**     **Ebert, M.**  
Der Einfluß des Redoxmilieus auf die Mobilität von Chrom im durchströmten Aquifer. 135 pages, Bremen, 1997.
- No. 102**     **Krögel, F.**  
Einfluß von Viskosität und Dichte des Seewassers auf Transport und Ablagerung von Wattsedimenten (Langeooger Rückseitenwatt, südliche Nordsee). 168 pages, Bremen, 1997.
- No. 103**     **Kerntopf, B.**  
Dinoflagellate Distribution Patterns and Preservation in the Equatorial Atlantic and Offshore North-West Africa. 137 pages, Bremen, 1997.
- No. 104**     **Breitzke, M.**  
Elastische Wellenausbreitung in marinen Sedimenten - Neue Entwicklungen der Ultraschall Sedimentphysik und Sedimentechographie. 298 pages, Bremen, 1997.
- No. 105**     **Marchant, M.**  
Rezente und spätquartäre Sedimentation planktischer Foraminiferen im Peru-Chile Strom. 115 pages, Bremen, 1997.
- No. 106**     **Habicht, K.S.**  
Sulfur isotope fractionation in marine sediments and bacterial cultures. 125 pages, Bremen, 1997.
- No. 107**     **Hamer, K., R.v. Lührte, G. Becker, T. Felis, S. Keffel, B. Strotmann, C. Waschowitz, M. Kölling, M. Isenbeck-Schröter, H.D. Schulz**  
Endbericht zum Forschungsvorhaben 060 des Landes Bremen: Baggergut der Hafengruppe Bremen-Stadt: Modelluntersuchungen zur Schwermetallmobilität und Möglichkeiten der Verwertung von Hafenschlick aus Bremischen Häfen. 98 pages, Bremen, 1997.
- No. 108**     **Greeff, O.W.**  
Entwicklung und Erprobung eines benthischen Landersystemes zur in situ-Bestimmung von Sulfatreduktionsraten mariner Sedimente. 121 pages, Bremen, 1997.
- No. 109**     **Pätzold, M. und G. Wefer**  
Bericht über den 6. JGOFS-Workshop am 4./5.12.1997 in Bremen. Im Anhang: Publikationen zum deutschen Beitrag zur Joint Global Ocean Flux Study (JGOFS), Stand 1/1998. 122 pages, Bremen, 1998.
- No. 110**     **Landenberger, H.**  
CoTRem, ein Multi-Komponenten Transport- und Reaktions-Modell. 142 pages, Bremen, 1998.
- No. 111**     **Villinger, H. und Fahrtteilnehmer**  
Fahrtbericht SO 124, 4.10. - 16.10.199. 90 pages, Bremen, 1997.
- No. 112**     **Gietl, R.**  
Biostratigraphie und Sedimentationsmuster einer nordostägyptischen Karbonatrampe unter Berücksichtigung der Alveolinen-Faunen. 142 pages, Bremen, 1998.
- No. 113**     **Ziebis, W.**  
The Impact of the Thalassinidean Shrimp *Callinassa truncata* on the Geochemistry of permeable, coastal Sediments. 158 pages, Bremen 1998.

- No. 114 Schulz, H.D. and cruise participants**  
Report and preliminary results of METEOR-Cruise M 41/1, Málaga - Libreville, 13.2.-15.3.1998. Bremen, 1998.
- No. 115 Völker, D.J.**  
Untersuchungen an strömungsbeeinflussten Sedimentationsmustern im Südozean. Interpretation sedimentechographischer Daten und numerische Modellierung. 152 pages, Bremen, 1998.
- No. 116 Schlünz, B.**  
Riverine Organic Carbon Input into the Ocean in Relation to Late Quaternary Climate Change. 136 pages, Bremen, 1998.
- No. 117 Kuhnert, H.**  
Aufzeichnung des Klimas vor Westaustralien in stabilen Isotopen in Korallenskeletten. 109 pages, Bremen, 1998.
- No. 118 Kirst, G.**  
Rekonstruktion von Oberflächenwassertemperaturen im östlichen Südatlantik anhand von Alkenonen. 130 pages, Bremen, 1998.
- No. 119 Dürkoop, A.**  
Der Brasil-Strom im Spätquartär: Rekonstruktion der oberflächennahen Hydrographie während der letzten 400 000 Jahre. 121 pages, Bremen, 1998.
- No. 120 Lamy, F.**  
Spätquartäre Variationen des terrigenen Sedimenteintrags entlang des chilenischen Kontinentalhangs als Abbild von Klimavariabilität im Milanković- und Sub-Milanković-Zeitbereich. 141 pages, Bremen, 1998.
- No. 121 Neuer, S. and cruise participants**  
Report and preliminary results of POSEIDON-Cruise Pos 237/2, Vigo – Las Palmas, 18.3.-31.3.1998. 39 pages, Bremen, 1998
- No. 122 Romero, O.E.**  
Marine planktonic diatoms from the tropical and equatorial Atlantic: temporal flux patterns and the sediment record. 205 pages, Bremen, 1998.
- No. 123 Spiess, V. und Fahrtteilnehmer**  
Report and preliminary results of RV SONNE Cruise 125, Cochín – Chittagong, 17.10.-17.11.1997. 128 pages, Bremen, 1998.
- No. 124 Arz, H.W.**  
Dokumentation von kurzfristigen Klimaschwankungen des Spätquartärs in Sedimenten des westlichen äquatorialen Atlantiks. 96 pages, Bremen, 1998.
- No. 125 Wolff, T.**  
Mixed layer characteristics in the equatorial Atlantic during the late Quaternary as deduced from planktonic foraminifera. 132 pages, Bremen, 1998.
- No. 126 Dittert, N.**  
Late Quaternary Planktic Foraminifera Assemblages in the South Atlantic Ocean: Quantitative Determination and Preservation Aspects. 165 pages, Bremen, 1998.
- No. 127 Höll, C.**  
Kalkige und organisch-wandige Dinoflagellaten-Zysten in Spätquartären Sedimenten des tropischen Atlantiks und ihre palökologische Auswertbarkeit. 121 pages, Bremen, 1998.
- No. 128 Hencke, J.**  
Redoxreaktionen im Grundwasser: Etablierung und Verlagerung von Reaktionsfronten und ihre Bedeutung für die Spurenelement-Mobilität. 122 pages, Bremen 1998.
- No. 129 Pätzold, J. and cruise participants**  
Report and preliminary results of METEOR-Cruise M 41/3, Vitória, Brasil – Salvador de Bahia, Brasil, 18.4. - 15.5.1998. Bremen, 1999.
- No. 130 Fischer, G. and cruise participants**  
Report and preliminary results of METEOR-Cruise M 41/4, Salvador de Bahia, Brasil – Las Palmas, Spain, 18.5. – 13.6.1998. Bremen, 1999.
- No. 131 Schlünz, B. und G. Wefer**  
Bericht über den 7. JGOFS-Workshop am 3. und 4.12.1998 in Bremen. Im Anhang: Publikationen zum deutschen Beitrag zur Joint Global Ocean Flux Study (JGOFS), Stand 1/ 1999. 100 pages, Bremen, 1999.
- No. 132 Wefer, G. and cruise participants**  
Report and preliminary results of METEOR-Cruise M 42/4, Las Palmas - Las Palmas - Viana do Castelo; 26.09.1998 - 26.10.1998. 104 pages, Bremen, 1999.

- No. 133**     **Felis, T.**  
Climate and ocean variability reconstructed from stable isotope records of modern subtropical corals (Northern Red Sea). 111 pages, Bremen, 1999.
- No. 134**     **Draschba, S.**  
North Atlantic climate variability recorded in reef corals from Bermuda. 108 pages, Bremen, 1999.
- No. 135**     **Schmieder, F.**  
Magnetic Cyclostratigraphy of South Atlantic Sediments. 82 pages, Bremen, 1999.
- No. 136**     **Rieß, W.**  
In situ measurements of respiration and mineralisation processes – Interaction between fauna and geochemical fluxes at active interfaces. 68 pages, Bremen, 1999.
- No. 137**     **Devey, C.W. and cruise participants**  
Report and shipboard results from METEOR-cruise M 41/2, Libreville – Vitoria, 18.3. – 15.4.98. 59 pages, Bremen, 1999.
- No. 138**     **Wenzhöfer, F.**  
Biogeochemical processes at the sediment water interface and quantification of metabolically driven calcite dissolution in deep sea sediments. 103 pages, Bremen, 1999.
- No. 139**     **Klump, J.**  
Biogenic barite as a proxy of paleoproductivity variations in the Southern Peru-Chile Current. 107 pages, Bremen, 1999.
- No. 140**     **Huber, R.**  
Carbonate sedimentation in the northern Northatlantic since the late pliocene. 103 pages, Bremen, 1999.
- No. 141**     **Schulz, H.**  
Nitrate-storing sulfur bacteria in sediments of coastal upwelling. 94 pages, Bremen, 1999.
- No. 142**     **Mai, S.**  
Die Sedimentverteilung im Wattenmeer: ein Simulationsmodell. 114 pages, Bremen, 1999.
- No. 143**     **Neuer, S. and cruise participants**  
Report and preliminary results of Poseidon Cruise 248, Las Palmas - Las Palmas, 15.2.-26.2.1999. 45 pages, Bremen, 1999.
- No. 144**     **Weber, A.**  
Schwefelkreislauf in marinen Sedimenten und Messung von in situ Sulfatreduktionsraten. 122 pages, Bremen, 1999.
- No. 145**     **Hadeler, A.**  
Sorptionenreaktionen im Grundwasser: Unterschiedliche Aspekte bei der Modellierung des Transportverhaltens von Zink. 122 pages, 1999.
- No. 146**     **Dierßen, H.**  
Zum Kreislauf ausgewählter Spurenmetalle im Südatlantik: Vertikaltransport und Wechselwirkung zwischen Partikeln und Lösung. 167 pages, Bremen, 1999.
- No. 147**     **Zühlsdorff, L.**  
High resolution multi-frequency seismic surveys at the Eastern Juan de Fuca Ridge Flank and the Cascadia Margin – Evidence for thermally and tectonically driven fluid upflow in marine sediments. 118 pages, Bremen 1999.
- No. 148**     **Kinkel, H.**  
Living and late Quaternary Coccolithophores in the equatorial Atlantic Ocean: response of distribution and productivity patterns to changing surface water circulation. 183 pages, Bremen, 2000.
- No. 149**     **Pätzold, J. and cruise participants**  
Report and preliminary results of METEOR Cruise M 44/3, Aqaba (Jordan) - Safaga (Egypt) – Dubá (Saudi Arabia) – Suez (Egypt) - Haifa (Israel), 12.3.-26.3.-2.4.-4.4.1999. 135 pages, Bremen, 2000.
- No. 150**     **Schlünz, B. and G. Wefer**  
Bericht über den 8. JGOFS-Workshop am 2. und 3.12.1999 in Bremen. Im Anhang: Publikationen zum deutschen Beitrag zur Joint Global Ocean Flux Study (JGOFS), Stand 1/ 2000. 95 pages, Bremen, 2000.
- No. 151**     **Schnack, K.**  
Biostratigraphie und fazielle Entwicklung in der Oberkreide und im Alttertiär im Bereich der Kharga Schwelle, Westliche Wüste, SW-Ägypten. 142 pages, Bremen, 2000.

- No. 152 Karwath, B.**  
Ecological studies on living and fossil calcareous dinoflagellates of the equatorial and tropical Atlantic Ocean. 175 pages, Bremen, 2000.
- No. 153 Moustafa, Y.**  
Paleoclimatic reconstructions of the Northern Red Sea during the Holocene inferred from stable isotope records of modern and fossil corals and molluscs. 102 pages, Bremen, 2000.
- No. 154 Villinger, H. and cruise participants**  
Report and preliminary results of SONNE-cruise 145-1 Balboa – Talcahuana, 21.12.1999 – 28.01.2000. 147 pages, Bremen, 2000.
- No. 155 Rusch, A.**  
Dynamik der Feinfraktion im Oberflächenhorizont permeabler Schelfsedimente. 102 pages, Bremen, 2000.
- No. 156 Moos, C.**  
Reconstruction of upwelling intensity and paleo-nutrient gradients in the northwest Arabian Sea derived from stable carbon and oxygen isotopes of planktic foraminifera. 103 pages, Bremen, 2000.
- No. 157 Xu, W.**  
Mass physical sediment properties and trends in a Wadden Sea tidal basin. 127 pages, Bremen, 2000.
- No. 158 Meinecke, G. and cruise participants**  
Report and preliminary results of METEOR Cruise M 45/1, Malaga (Spain) - Lissabon (Portugal), 19.05. - 08.06.1999. 39 pages, Bremen, 2000.
- No. 159 Vink, A.**  
Reconstruction of recent and late Quaternary surface water masses of the western subtropical Atlantic Ocean based on calcareous and organic-walled dinoflagellate cysts. 160 pages, Bremen, 2000.
- No. 160 Willems, H. (Sprecher), U. Bleil, R. Henrich, K. Herterich, B.B. Jørgensen, H.-J. Kuß, M. Olesch, H.D. Schulz, V. Spieß, G. Wefer**  
Abschlußbericht des Graduierten-Kollegs Stoff-Flüsse in marine Geosystemen. Zusammenfassung und Berichtszeitraum Januar 1996 - Dezember 2000. 340 pages, Bremen, 2000.
- No. 161 Sprengel, C.**  
Untersuchungen zur Sedimentation und Ökologie von Coccolithophoriden im Bereich der Kanarischen Inseln: Saisonale Flussmuster und Karbonatexport. 165 pages, Bremen, 2000.
- No. 162 Donner, B. and G. Wefer**  
Bericht über den JGOFS-Workshop am 18.-21.9.2000 in Bremen: Biogeochemical Cycles: German Contributions to the International Joint Global Ocean Flux Study. 87 pages, Bremen, 2000.
- No. 163 Neuer, S. and cruise participants**  
Report and preliminary results of Meteor Cruise M 45/5, Bremen – Las Palmas, October 1 – November 3, 1999. 93 pages, Bremen, 2000.
- No. 164 Devey, C. and cruise participants**  
Report and preliminary results of Sonne Cruise SO 145/2, Talcahuano (Chile) - Arica (Chile), February 4 – February 29, 2000. 63 pages, Bremen, 2000.
- No. 165 Freudenthal, T.**  
Reconstruction of productivity gradients in the Canary Islands region off Morocco by means of sinking particles and sediments. 147 pages, Bremen, 2000.
- No. 166 Adler, M.**  
Modeling of one-dimensional transport in porous media with respect to simultaneous geochemical reactions in CoTreM. 147 pages, Bremen, 2000.
- No. 167 Santamarina Cuneo, P.**  
Fluxes of suspended particulate matter through a tidal inlet of the East Frisian Wadden Sea (southern North Sea). 91 pages, Bremen, 2000.
- No. 168 Benthien, A.**  
Effects of CO<sub>2</sub> and nutrient concentration on the stable carbon isotope composition of C<sub>37:2</sub> alkenones in sediments of the South Atlantic Ocean. 104 pages, Bremen, 2001.
- No. 169 Lavik, G.**  
Nitrogen isotopes of sinking matter and sediments in the South Atlantic. 140 pages, Bremen, 2001.



- No. 170 Budziak, D.**  
Late Quaternary monsoonal climate and related variations in paleoproductivity and alkenone-derived sea-surface temperatures in the western Arabian Sea. 114 pages, Bremen, 2001.
- No. 171 Gerhardt, S.**  
Late Quaternary water mass variability derived from the pteropod preservation state in sediments of the western South Atlantic Ocean and the Caribbean Sea. 109 pages, Bremen, 2001.
- No. 172 Bleil, U. and cruise participants**  
Report and preliminary results of Meteor Cruise M 46/3, Montevideo (Uruguay) – Mar del Plata (Argentina), January 4 – February 7, 2000. Bremen, 2001.
- No. 173 Wefer, G. and cruise participants**  
Report and preliminary results of Meteor Cruise M 46/4, Mar del Plata (Argentina) – Salvador da Bahia (Brazil), February 10 – March 13, 2000. With partial results of METEOR cruise M 46/2. 136 pages, Bremen, 2001.
- No. 174 Schulz, H.D. and cruise participants**  
Report and preliminary results of Meteor Cruise M 46/2, Recife (Brazil) – Montevideo (Uruguay), December 2 – December 29, 1999. 107 pages, Bremen, 2001.
- No. 175 Schmidt, A.**  
Magnetic mineral fluxes in the Quaternary South Atlantic: Implications for the paleoenvironment. 97 pages, Bremen, 2001.
- No. 176 Bruhns, P.**  
Crystal chemical characterization of heavy metal incorporation in brick burning processes. 93 pages, Bremen, 2001.
- No. 177 Karius, V.**  
Baggergut der Hafengruppe Bremen-Stadt in der Ziegelherstellung. 131 pages, Bremen, 2001.
- No. 178 Adegbe, A. T.**  
Reconstruction of paleoenvironmental conditions in Equatorial Atlantic and the Gulf of Guinea Basins for the last 245,000 years. 113 pages, Bremen, 2001.
- No. 179 Spieß, V. and cruise participants**  
Report and preliminary results of R/V Sonne Cruise SO 149, Victoria - Victoria, 16.8. - 16.9.2000. 100 pages, Bremen, 2001.
- No. 180 Kim, J.-H.**  
Reconstruction of past sea-surface temperatures in the eastern South Atlantic and the eastern South Pacific across Termination I based on the Alkenone Method. 114 pages, Bremen, 2001.
- No. 181 von Lom-Keil, H.**  
Sedimentary waves on the Namibian continental margin and in the Argentine Basin – Bottom flow reconstructions based on high resolution echosounder data. 126 pages, Bremen, 2001.
- No. 182 Hebbeln, D. and cruise participants**  
PUCK: Report and preliminary results of R/V Sonne Cruise SO 156, Valparaiso (Chile) - Talcahuano (Chile), March 29 - May 14, 2001. 195 pages, Bremen, 2001.
- No. 183 Wendler, J.**  
Reconstruction of astronomically-forced cyclic and abrupt paleoecological changes in the Upper Cretaceous Boreal Realm based on calcareous dinoflagellate cysts. 149 pages, Bremen, 2001.
- No. 184 Volbers, A.**  
Planktic foraminifera as paleoceanographic indicators: production, preservation, and reconstruction of upwelling intensity. Implications from late Quaternary South Atlantic sediments. 122 pages, Bremen, 2001.
- No. 185 Bleil, U. and cruise participants**  
Report and preliminary results of R/V METEOR Cruise M 49/3, Montevideo (Uruguay) - Salvador (Brasil), March 9 - April 1, 2001. 99 pages, Bremen, 2001.
- No. 186 Scheibner, C.**  
Architecture of a carbonate platform-to-basin transition on a structural high (Campanian-early Eocene, Eastern Desert, Egypt) – classical and modelling approaches combined. 173 pages, Bremen, 2001.
- No. 187 Schneider, S.**  
Quartäre Schwankungen in Strömungsintensität und Produktivität als Abbild der Wassermassen-Variabilität im äquatorialen Atlantik (ODP Sites 959 und 663): Ergebnisse aus Siltkorn-Analysen. 134 pages, Bremen, 2001.
- No. 188 Uliana, E.**  
Late Quaternary biogenic opal sedimentation in diatom assemblages in Kongo Fan sediments. 96 pages, Bremen, 2002.



- No. 189** **Esper, O.**  
Reconstruction of Recent and Late Quaternary oceanographic conditions in the eastern South Atlantic Ocean based on calcareous- and organic-walled dinoflagellate cysts. 130 pages, Bremen, 2001.
- No. 190** **Wendler, I.**  
Production and preservation of calcareous dinoflagellate cysts in the modern Arabian Sea. 117 pages, Bremen, 2002.
- No. 191** **Bauer, J.**  
Late Cenomanian – Santonian carbonate platform evolution of Sinai (Egypt): stratigraphy, facies, and sequence architecture. 178 pages, Bremen, 2002.
- No. 192** **Hildebrand-Habel, T.**  
Die Entwicklung kalkiger Dinoflagellaten im Südatlantik seit der höheren Oberkreide. 152 pages, Bremen, 2002.
- No. 193** **Hecht, H.**  
Sauerstoff-Optopoden zur Quantifizierung von Pyritverwitterungsprozessen im Labor- und Langzeit-in-situ-Einsatz. Entwicklung - Anwendung – Modellierung. 130 pages, Bremen, 2002.
- No. 194** **Fischer, G. and cruise participants**  
Report and Preliminary Results of RV METEOR-Cruise M49/4, Salvador da Bahia – Halifax, 4.4.-5.5.2001. 84 pages, Bremen, 2002.
- No. 195** **Gröger, M.**  
Deep-water circulation in the western equatorial Atlantic: inferences from carbonate preservation studies and silt grain-size analysis. 95 pages, Bremen, 2002.
- No. 196** **Meinecke, G. and cruise participants**  
Report of RV POSEIDON Cruise POS 271, Las Palmas - Las Palmas, 19.3.-29.3.2001. 19 pages, Bremen, 2002.
- No. 197** **Meggers, H. and cruise participants**  
Report of RV POSEIDON Cruise POS 272, Las Palmas - Las Palmas, 1.4.-14.4.2001. 19 pages, Bremen, 2002.
- No. 198** **Gräfe, K.-U.**  
Stratigraphische Korrelation und Steuerungsfaktoren Sedimentärer Zyklen in ausgewählten Borealen und Tethyalen Becken des Cenoman/Turon (Oberkreide) Europas und Nordwestafrikas. 197 pages, Bremen, 2002.
- No. 199** **Jahn, B.**  
Mid to Late Pleistocene Variations of Marine Productivity in and Terrigenous Input to the Southeast Atlantic. 97 pages, Bremen, 2002.
- No. 200** **Al-Rousan, S.**  
Ocean and climate history recorded in stable isotopes of coral and foraminifers from the northern Gulf of Aqaba. 116 pages, Bremen, 2002.
- No. 201** **Azouzi, B.**  
Regionalisierung hydraulischer und hydrogeochemischer Daten mit geostatistischen Methoden. 108 pages, Bremen, 2002.
- No. 202** **Spieß, V. and cruise participants**  
Report and preliminary results of METEOR Cruise M 47/3, Libreville (Gabun) - Walvis Bay (Namibia), 01.06 - 03.07.2000. 70 pages, Bremen 2002.
- No. 203** **Spieß, V. and cruise participants**  
Report and preliminary results of METEOR Cruise M 49/2, Montevideo (Uruguay) - Montevideo, 13.02 - 07.03.2001. 84 pages, Bremen 2002.
- No. 204** **Mollenhauer, G.**  
Organic carbon accumulation in the South Atlantic Ocean: Sedimentary processes and glacial/interglacial Budgets. 139 pages, Bremen 2002.
- No. 205** **Spieß, V. and cruise participants**  
Report and preliminary results of METEOR Cruise M49/1, Cape Town (South Africa) - Montevideo (Uruguay), 04.01.2001 - 10.02.2001. 57 pages, Bremen, 2003.
- No. 206** **Meier, K.J.S.**  
Calcareous dinoflagellates from the Mediterranean Sea: taxonomy, ecology and palaeoenvironmental application. 126 pages, Bremen, 2003.
- No. 207** **Rakic, S.**  
Untersuchungen zur Polymorphie und Kristallchemie von Silikaten der Zusammensetzung  $\text{Me}_2\text{Si}_2\text{O}_5$  (Me:Na, K). 139 pages, Bremen, 2003.

- No. 208 Pfeifer, K.**  
Auswirkungen frühdiagenetischer Prozesse auf Calcit- und Barytgehalte in marinen Oberflächen- sedimenten. 110 pages, Bremen, 2003.
- No. 209 Heuer, V.**  
Spurenelemente in Sedimenten des Südatlantik. Primärer Eintrag und frühdiagenetische Überprägung. 136 pages, Bremen, 2003.
- No. 210 Streng, M.**  
Phylogenetic Aspects and Taxonomy of Calcareous Dinoflagellates. 157 pages, Bremen 2003.
- No. 211 Boeckel, B.**  
Present and past coccolith assemblages in the South Atlantic: implications for species ecology, carbonate contribution and palaeoceanographic applicability. 157 pages, Bremen, 2003.
- No. 212 Precht, E.**  
Advective interfacial exchange in permeable sediments driven by surface gravity waves and its ecological consequences. 131 pages, Bremen, 2003.
- No. 213 Frenz, M.**  
Grain-size composition of Quaternary South Atlantic sediments and its paleoceanographic significance. 123 pages, Bremen, 2003.
- No. 214 Meggers, H. and cruise participants**  
Report and preliminary results of METEOR Cruise M 53/1, Limassol - Las Palmas – Mindelo, 30.03.2002 - 03.05.2002. 81 pages, Bremen, 2003.
- No. 215 Schulz, H.D. and cruise participants**  
Report and preliminary results of METEOR Cruise M 58/1, Dakar – Las Palmas, 15.04..2003 – 12.05.2003. Bremen, 2003.
- No. 216 Schneider, R. and cruise participants**  
Report and preliminary results of METEOR Cruise M 57/1, Cape Town – Walvis Bay, 20.01. – 08.02.2003. 123 pages, Bremen, 2003.
- No. 217 Kallmeyer, J.**  
Sulfate reduction in the deep Biosphere. 157 pages, Bremen, 2003.
- No. 218 Røy, H.**  
Dynamic Structure and Function of the Diffusive Boundary Layer at the Seafloor. 149 pages, Bremen, 2003.
- No. 219 Pätzold, J., C. Hübscher and cruise participants**  
Report and preliminary results of METEOR Cruise M 52/2&3, Istanbul – Limassol – Limassol, 04.02. – 27.03.2002. Bremen, 2003.
- No. 220 Zabel, M. and cruise participants**  
Report and preliminary results of METEOR Cruise M 57/2, Walvis Bay – Walvis Bay, 11.02. – 12.03.2003. 136 pages, Bremen 2003.
- No. 221 Salem, M.**  
Geophysical investigations of submarine prolongations of alluvial fans on the western side of the Gulf of Aqaba-Red Sea. 100 pages, Bremen, 2003.
- No. 222 Tilch, E.**  
Oszillation von Wattflächen und deren fossiles Erhaltungspotential (Spiekerooger Rückseitenwatt, südliche Nordsee). 137 pages, Bremen, 2003.
- No. 223 Frisch, U. and F. Kockel**  
Der Bremen-Knoten im Strukturnetz Nordwest-Deutschlands. Stratigraphie, Paläogeographie, Strukturgeologie. 379 pages, Bremen, 2004.
- No. 224 Kolonic, S.**  
Mechanisms and biogeochemical implications of Cenomanian/Turonian black shale formation in North Africa: An integrated geochemical, millennial-scale study from the Tarfaya-LaAyoune Basin in SW Morocco. 174 pages, Bremen, 2004. Report online available only.
- No. 225 Panteleit, B.**  
Geochemische Prozesse in der Salz- Süßwasser Übergangszone. 106 pages, Bremen, 2004.
- No. 226 Seiter, K.**  
Regionalisierung und Quantifizierung benthischer Mineralisationsprozesse. 135 pages, Bremen, 2004.
- No. 227 Bleil, U. and cruise participants**  
Report and preliminary results of METEOR Cruise M 58/2, Las Palmas – Las Palmas (Canary Islands, Spain), 15.05. – 08.06.2003. 123 pages, Bremen, 2004.

- No. 228 Kopf, A. and cruise participants**  
Report and preliminary results of SONNE Cruise SO175, Miami - Bremerhaven, 12.11 - 30.12.2003. 218 pages, Bremen, 2004.
- No. 229 Fabian, M.**  
Near Surface Tilt and Pore Pressure Changes Induced by Pumping in Multi-Layered Poroelastic Half-Spaces. 121 pages, Bremen, 2004.
- No. 230 Segl, M. , and cruise participants**  
Report and preliminary results of POSEIDON cruise 304 Galway – Lisbon, 5. – 22. Oct. 2004. 27 pages, Bremen 2004
- No. 231 Meinecke, G. and cruise participants**  
Report and preliminary results of POSEIDON Cruise 296, Las Palmas – Las Palmas, 04.04 – 14.04.2003. 42 pages, Bremen 2005.
- No. 232 Meinecke, G. and cruise participants**  
Report and preliminary results of POSEIDON Cruise 310, Las Palmas – Las Palmas, 12.04 – 26.04.2004. 49 pages, Bremen 2005.
- No. 233 Meinecke, G. and cruise participants**  
Report and preliminary results of METEOR Cruise 58/3, Las Palmas - Ponta Delgada, 11.06 - 24.06.2003. 50 pages, Bremen 2005.
- No. 234 Feseker, T.**  
Numerical Studies on Groundwater Flow in Coastal Aquifers. 219 pages. Bremen 2004.
- No. 235 Sahling, H. and cruise participants**  
Report and preliminary results of R/V POSEIDON Cruise P317/4, Istanbul-Istanbul , 16 October - 4 November 2004. 92 pages, Bremen 2004.
- No. 236 Meinecke, G. und Fahrtteilnehmer**  
Report and preliminary results of POSEIDON Cruise 305, Las Palmas (Spain) - Lisbon (Portugal), October 28th – November 6th, 2004. 43 pages, Bremen 2005.
- No. 237 Ruhland, G. and cruise participants**  
Report and preliminary results of POSEIDON Cruise 319, Las Palmas (Spain) - Las Palmas (Spain), December 6th – December 17th, 2004. 50 pages, Bremen 2005.
- No. 238 Chang, T.S.**  
Dynamics of fine-grained sediments and stratigraphic evolution of a back-barrier tidal basin of the German Wadden Sea (southern North Sea). 102 pages, Bremen 2005.
- No. 239 Lager, T.**  
Predicting the source strength of recycling materials within the scope of a seepage water prognosis by means of standardized laboratory methods. 141 pages, Bremen 2005.
- No. 240 Meinecke, G.**  
DOLAN - Operationelle Datenübertragung im Ozean und Laterales Akustisches Netzwerk in der Tiefsee. Abschlußbericht. 42 pages, Bremen 2005.
- No. 241 Guasti, E.**  
Early Paleogene environmental turnover in the southern Tethys as recorded by foraminiferal and organic-walled dinoflagellate cysts assemblages. 203 pages, Bremen 2005.
- No. 242 Riedinger, N.**  
Preservation and diagenetic overprint of geochemical and geophysical signals in ocean margin sediments related to depositional dynamics. 91 pages, Bremen 2005.
- No. 243 Ruhland, G. and cruise participants**  
Report and preliminary results of POSEIDON cruise 320, Las Palmas (Spain) - Las Palmas (Spain), March 08th - March 18th, 2005. 57 pages, Bremen 2005.
- No. 244 Inthorn, M.**  
Lateral particle transport in nepheloid layers – a key factor for organic matter distribution and quality in the Benguela high-productivity area. 127 pages, Bremen, 2006.
- No. 245 Aspetsberger, F.**  
Benthic carbon turnover in continental slope and deep sea sediments: importance of organic matter quality at different time scales. 136 pages, Bremen, 2006.
- No. 246 Hebbeln, D. and cruise participants**  
Report and preliminary results of RV SONNE Cruise SO-184, PABESIA, Durban (South Africa) – Cilacap (Indonesia) – Darwin (Australia), July 08th - September 13th, 2005. 142 pages, Bremen 2006.

- No. 247 Ratmeyer, V. and cruise participants**  
Report and preliminary results of RV METEOR Cruise M61/3. Development of Carbonate Mounds on the Celtic Continental Margin, Northeast Atlantic. Cork (Ireland) – Ponta Delgada (Portugal), 04.06. – 21.06.2004. 64 pages, Bremen 2006.
- No. 248 Wien, K.**  
Element Stratigraphy and Age Models for Pelagites and Gravity Mass Flow Deposits based on Shipboard XRF Analysis. 100 pages, Bremen 2006.
- No. 249 Krastel, S. and cruise participants**  
Report and preliminary results of RV METEOR Cruise M65/2, Dakar - Las Palmas, 04.07. – 26.07.2005. 185 pages, Bremen 2006.
- No. 250 Heil, G.M.N.**  
Abrupt Climate Shifts in the Western Tropical to Subtropical Atlantic Region during the Last Glacial. 121 pages, Bremen 2006.
- No. 251 Ruhland, G. and cruise participants**  
Report and preliminary results of POSEIDON Cruise 330, Las Palmas – Las Palmas, November 21th – December 03rd, 2005. 48 pages, Bremen 2006.
- No. 252 Mulitza, S. and cruise participants**  
Report and preliminary results of METEOR Cruise M65/1, Dakar – Dakar, 11.06.- 1.07.2005. 149 pages, Bremen 2006.
- No. 253 Kopf, A. and cruise participants**  
Report and preliminary results of POSEIDON Cruise P336, Heraklion - Heraklion, 28.04. – 17.05.2006. 127 pages, Bremen, 2006.
- No. 254 Wefer, G. and cruise participants**  
Report and preliminary results of R/V METEOR Cruise M65/3, Las Palmas - Las Palmas (Spain), July 31st - August 10th, 2005. 24 pages, Bremen 2006.
- No. 255 Hanebuth, T.J.J. and cruise participants**  
Report and first results of the POSEIDON Cruise P342 GALIOMAR, Vigo – Lisboa (Portugal), August 19th – September 06th, 2006. Distribution Pattern, Residence Times and Export of Sediments on the Pleistocene/Holocene Galician Shelf (NW Iberian Peninsula). 203 pages, Bremen, 2007.
- No. 256 Ahke, A.**  
Composition of molecular organic matter pools, pigments and proteins, in Benguela upwelling and Arctic Sediments. 192 pages, Bremen 2007.
- No. 257 Becker, V.**  
Seeper - Ein Modell für die Praxis der Sickerwasserprognose. 170 pages, Bremen 2007.
- No. 258 Ruhland, G. and cruise participants**  
Report and preliminary results of Poseidon cruise 333, Las Palmas (Spain) – Las Palmas (Spain), March 1st – March 10th, 2006. 32 pages, Bremen 2007.
- No. 259 Fischer, G., G. Ruhland and cruise participants**  
Report and preliminary results of Poseidon cruise 344, leg 1 and leg 2, Las Palmas (Spain) – Las Palmas (Spain), Oct. 20th – Nov 2nd & Nov. 4th – Nov 13th, 2006. 46 pages, Bremen 2007.
- No. 260 Westphal, H. and cruise participants**  
Report and preliminary results of Poseidon cruise 346, MACUMA. Las Palmas (Spain) – Las Palmas (Spain), 28.12.2006 – 15.1.2007. 49 pages, Bremen 2007.
- No. 261 Bohrmann, G., T. Pape, and cruise participants**  
Report and preliminary results of R/V METEOR Cruise M72/3, Istanbul – Trabzon – Istanbul, March 17th – April 23rd, 2007. Marine gas hydrates of the Eastern Black Sea. 130 pages, Bremen 2007.
- No. 262 Bohrmann, G., and cruise participants**  
Report and preliminary results of R/V METEOR Cruise M70/3, Iraklion – Iraklion, 21 November – 8 December 2006. Cold Seeps of the Anaximander Mountains / Eastern Mediterranean. 75 pages, Bremen 2008.
- No. 263 Bohrmann, G., Spiess, V., and cruise participants**  
Report and preliminary results of R/V Meteor Cruise M67/2a and 2b, Balboa -- Tampico -- Bridgetown, 15 March -- 24 April, 2006. Fluid seepage in the Gulf of Mexico. Bremen 2008.

- No. 264 Kopf, A., and cruise participants**  
Report and preliminary results of Meteor Cruise M73/1: LIMA-LAMO (Ligurian Margin Landslide Measurements & Observatory), Cadiz, 22.07.2007 – Genoa, 11.08.2007. 170 pages, Bremen 2008.
- No. 265 Hebbeln, D., and cruise participants**  
Report and preliminary results of RV Pelagia Cruise 64PE284. Cold-water Corals in the Gulf of Cádiz and on Coral Patch Seamount (NE Atlantic). Portimão - Portimão, 18.02. - 09.03.2008. 90 pages, Bremen 2008.
- No. 266 Bohrmann, G. and cruise participants**  
Report and preliminary results of R/V Meteor Cruise M74/3, Fujairah – Male, 30 October - 28 November, 2007. Cold Seeps of the Makran subduction zone (Continental margin of Pakistan). 161 pages, Bremen 2008.
- No. 267 Sachs, O.**  
Benthic organic carbon fluxes in the Southern Ocean: Regional differences and links to surface primary production and carbon export. 143 pages, Bremen, 2008.
- No. 268 Zonneveld, K. and cruise participants**  
Report and preliminary results of R/V POSEIDON Cruise P339, Piräus - Messina, 16 June - 2 July 2006. CAPPUCCINO - Calabrian and Adriatic palaeoproductivity and climatic variability in the last two millenia. 61 pages, Bremen, 2008.
- No. 269 Ruhland, G. and cruise participants**  
Report and preliminary results of R/V POSEIDON Cruise P360, Las Palmas (Spain) - Las Palmas (Spain), Oct. 29th - Nov. 6th, 2007. 27 pages, Bremen, 2008.
- No. 270 Ruhland, G. , G. Fischer and cruise participants**  
Report and preliminary results of R/V POSEIDON Cruise 365 (Leg 1+2). Leg 1: Las Palmas - Las Palmas, 13.4. - 16.4.2008. Leg 2: Las Palmas - Las Palmas, 18.4. - 29.4.2008. 40 pages, Bremen, 2009.
- No. 271 Kopf, A. and cruise participants**  
Report and preliminary results of R/V POSEIDON Cruise P386: NAIL (Nice Airport Landslide), La Seyne sur Mer, 20.06.2009 – La Seyne sur Mer, 06.07.2009. 161 pages, Bremen, 2009.
- No. 272 Freudenthal, T., G. Fischer and cruise participants**  
Report and preliminary results of Maria S. Merian Cruise MSM04/4 a & b, Las Palmas (Spain) - Las Palmas (Spain), Feb 27th – Mar 16th & Mar 19th – Apr 1st, 2007. 117 pages, Bremen 2009.
- No. 273 Hebbeln, D., C. Wienberg, L. Beuck, A. Freiwald, P. Wintersteller and cruise participants**  
Report and preliminary results of R/V POSEIDON Cruise POS 385 « Cold-Water Corals of the Alboran Sea (western Mediterranean Sea) », Faro – Toulon, May 29 – June 16, 2009. 79 pages, Bremen 2009